INFLUENCE OF GEOCHEMICAL, MORPHOLOGICAL, AND HYDROLOGICAL FACTORS ON GROUNDWATER ARSENIC DISTRIBUTION IN A COMPLEX TERRAIN

Implications for targeting safe aquifers for sustainable drinking water supply

Submitted in Partial Fulfilment of the Requirement
for the Degree of
DOCTOR OF PHILOSOPHY

By

RUNTI CHOUDHURY

DEPARTMENT OF CIVIL ENGINEERING

INDIAN INSTITUTE OF TECHNOLOGY GUWAHATI

GUWAHATI – 781039, INDIA

AUGUST, 2017

Statement of Originality

I hereby declare that the work presented in this thesis entitled "***Influence of Geochemical, Morphological, and Hydrological factors on Groundwater Arsenic Distribution in a Complex Terrain***" is to the best of my knowledge, original, except as acknowledged in the text. This material has not been submitted, either in whole or in part, for degree at any university.

Runti Choudhury

Research Scholar

Department of Civil Engineering

Indian Institute of Technology Guwahati

Certificate

This is to certify that the thesis entitled "***Influence of Geochemical, Morphological, and Hydrological factors on Groundwater Arsenic Distribution in a Complex Terrain***" submitted by Runti Choudhury (Registration No. 126104015) to the Indian Institute of Technology Guwahati for the degree of Doctor of Philosophy is a record of bonafide research work carried out by her under my supervision and guidance. The thesis work, in my opinion has reached the requisite standards fulfilling the requirement for the award of the degree of Doctor of Philosophy. This work has not been submitted earlier for the award of any degree or diploma to the best of my knowledge and belief.

(Supervisor)

Chandan Mahanta

Professor

Department of Civil Engineering

Indian Institute of Technology Guwahati

Acknowledgement

I am indebted to many people who have over the past several years helped and motivated me in this research. It is my privilege to acknowledge these people.

First and foremost, I would like to express my sincere gratitude to my supervisor Prof. Chandan Mahanta at the Department of Civil Engineering, IIT. Without his support, encouragement and guidance it was not possible to complete my doctoral study at IIT Guwahati. I would also like to thank my Doctoral Committee members Dr. Gautam Barua, Dr. Utpal Bora and Dr. Shreeja P. for their time, commitment and helpful suggestions all throughout.

I also would like to thank the other faculty members in the Department of Civil Engineering for being very inspirational to me. Special thanks to Dr. Arup Kumar Sharma. I would like to express my heart felt gratitude to Dr. Lex van Geen (Columbia University). I am indebted to him for all his generosity and support during my visit at Lamont Doherty Earth Institute of Columbia University. Heartfelt thanks to Dr. Bibhash Nath (Columbia University) and Dr. Abhijit Mukherjee (Department of Geology and Geophysics, IIT Kharagpur for their guidance at different stages of my research.

I acknowledge the analytical support from Central Instrumentation Facility (CIF) IIT Guwahati; Department of Geology and Geophysics IIT Kharagpur, Department of Nano Technology; Department of Physics; SIAF, Gauhati University; Department of Geological Sciences; Gauhati University. Heartfelt thanks to Jonali Saikia and Priyadhar Phatak for their support throughout. Without their support it would have been impossible to complete my experimental work. The consistent support from Dr. Jayanta Laskar, Department of Geological Sciences, Gauhati University is duly acknowledged.

I am thankful to the Public health Engineering Department, Assam for all their support during my field work. Special thanks to Abdur Rahim, Ubadur Rahman Neog and Dilip Kakati for their relentless support during my field work in Jorhat, Golaghat, Darrang and Udalguri. Thanks to Mr. Somorjit Singh from North East Space Application Centre (NESAC) for his guidance during the geomorphological mapping.

I would like to extend my sincere gratitude to my friends especially Pallavi and Sushant. I am thankful to my lab mates Shashi, Arvind, Vinay, Sachin, Sophia and others for providing me

technical and moral support during different stages of my graduate study. I wholeheartedly thank Kruti Jajuriya and Shayan Shafiq for their help and support during my field work in Jorhat.

Most importantly, I wish to thank and express my devotion to my parents, my aunt's, my beloved sisters and brother for their support and inspiration all throughout. I also extend my heartfelt thanks to my extended family for all their support and patience during my graduate study. Lastly, but most lovingly, I would like to thank my husband, for his enormous sacrifice and I greatly recognize his support and inspiration in every step of my research and graduate study. Finally, I dedicate this thesis to my beloved parents and dearest husband.

This list would be incomplete without acknowledging the funding authorities. I would like to acknowledge IIIT Guwahati for providing the Institute Research Fellowship for conducting the research. I whole heartedly acknowledge United States India Educational foundation (USIEF) for providing me the Fulbright Nehru Doctoral Research Fellowship 2014-15 for conducting a part of my research work in Lamont Doherty Earth Observatory, Columbia University, New York. This was a lifetime opportunity and the experience gained has not just made me grow academically but also personally.

Last but not the least, I would like to thank the "***Almighty***" for blessing me and providing me the unseen moral support that directed me through my good as well as hard times.

Runti Choudhury

Abstract

Contamination of groundwater by Arsenic (*As*), a known carcinogen, is a major drinking water concern affecting millions globally including South and South East Asia. Often associated with iron (III) hydroxides within soils and sediments, arsenic gets released into groundwater through multiple hydrogeochemical processes. Nearly three decades of research has led to our understanding that reductive dissolution of Fe (III) oxyhydroxides is the primary mechanism of arsenic release into aquifers. Yet, mechanisms of release and accumulation both still remain elusive in terms of effects of local geological and hydrological conditions. The interest to unravel the unknowns has escalated particularly with recent revelation of more new areas discovered to host groundwater arsenic contaminated aquifers.

Large unguarded rural populations are vulnerable due to recent revelation of arsenic contamination of groundwater in the upper Brahmaputra Floodplains aquifers in Assam, India. This has led to scattered interventions to understand the processes, mechanism, spatial distribution and factors contributing to local arsenic release mechanism into groundwater. However, the enormity and natural complexity of the region calls for more intensive research to understand the groundwater arsenic contamination issue within the region and to find possible remediation measure to alleviate the problem.

The mechanism of arsenic release have been investigated along two selected transects in the unperturbed, pristine, upper Brahmaputra River Basin in Assam, India. The work is based on the recent revelation of groundwater arsenic contamination scenario in Assam. Two different tectono-sedimentary sites located on the northern and southern banks of the Brahmaputra River were selected for the study based on the results of a large scale field monitoring program by UNICEF-IITG-PHED. Sediment and groundwater samples collected along the two selected transects were analyzed to examine the spatial variation and the factors controlling arsenic distribution in the study sites. Samples from both public and private utilities were collected following standard protocols and analyzed for their major ions and from arsenic enrichment.

A total of 247 groundwater samples were analyzed for seventeen different parameters viz. pH, EC. Temperature, Dissolved Oxygen, Oxidation-reduction potential (E_h), Na^+, K^+, Mg^{2+}, Ca^{2+}, HCO_3^-, SO_4^{2-}, NO_3^-, Cl^-, PO_4^{3-}, As, Fe and Mn were analyzed to examine the role of hydrogeochemistry in controlling arsenic distribution in the pristine river floodplain. Results

revealed the dominance of water rock interactions in controlling groundwater evolution in the study area. Hydrochemical data from shallow wells revealed a predominantly reducing characteristic in the aquifers, with low NO_3^- and SO_4^{2-} characteristics and high HCO_3^- concentrations. Groundwater occurrence with similar characteristics indicated reductive dissolution of Fe(III) oxyhydroxides as the mechanism of arsenic release into groundwater, however, the low to moderate interrelationship of arsenic with other redox parameters viz. Mn, Fe etc. indicate that As release into groundwater along both the transect is an interplay of more complex mechanisms. Competition by anions viz. PO_4^- was observed to have played some role in arsenic release.

One of the major causes of concerns regarding the growing arsenic crises around the world is the bewildering degree of spatial Arsenic variability. These contrasts have been evidently linked by different studies to the redox state of the underlying sediments, primarily, an association of low groundwater arsenic with relatively oxic, uplifted Pleistocene aquifers, and high groundwater arsenic concentrations in anoxic Holocene aquifers. To understand the factors controlling spatial distribution of arsenic in the study area, and the factors contributing to the variability were studied indepth. Results revealed an interesting pattern along the 35 km southern transect, where arsenic concentrations gradually increased with distance away from the river.

To evaluate the role of sediments in naturally attenuating arsenic, batch studies were conducted using selected sediment samples from the northern transect. Results revealed that oxidized brown sediments, with high solid phase iron concentrations, have higher arsenic adsorption capacity in contrasts to the grey sand and greyish brown sand. Isotherm study revealed that sediments followed Freundlich isotherm model, indicating the dominance of multilayer adsorption on the sediment samples.

Considering the complexity of the study transects, bounded by the Eastern Himalayas and the Brahmaputra River in the northern transect and the Naga Patkai Hill ranges and the Brahmaputra River in the southern transect; the role of geology, geomorphology and hydrology in controlling arsenic enrichment was another vital aspect investigated in the study. With spatial distribution patterns different from those observed in the Bengal Basin, where elevated groundwater arsenic concentrations along the banks of the lower Brahmaputra River in Bangladesh attributed to the effects of a regular supply of fresh, fine-grained sediments, along the southern transect, elevated arsenic concentrations increase with distance from the

river. The role of aquifer flushing as an important hydrological control was attributed to be controlling the pattern of distribution along the transect. Hydrological factors including topographic gradients and slope were observed to be major controls on the distribution patterns along the northern transect.

Contents

List of Figures

List of Tables

Abbreviations and Acronyms

µg/L	Micrograms per liter
As	Arsenic
AAS	Atomic Absorption Spectrophotometer
APHA	American Public Health Association
BIS	Bureau of Indian Standards
bdl	below detection level
CGWB	Central Groundwater Board
C_o	Initial Concentration
C_e	Equilibrium Concentration
EC	Electrical Conductivity
DDL	Diffuse Double Layer
EDX	Energy Dispersive X-Ray
Eh	reducing potential (mV)
F	Faraday constant ($9.65x10^{-4}$ coulomb /mole)
FESEM	Field Emission Scanning Electron Microscope
FTK	Field Test Kit
GBM	Ganges Brahmaputra Meghna
GIS	Geographic Information System
Hfo	Hydrous Ferric Oxide
Hfo_s	Ferrihydrite phase for strong site
Hfo_w	Ferrihydrite phase for weak site
IIT	Indian Institute of Technology Guwahati
LOI	Loss of Ignition
mg/kg	milligrams per kilogram
mg/L	milligrams per liter
NOM	Natural Organic Matter
pH	Hydrogen ion concentration
PHED	Public Health Engineering Department
R	Universal Gas Constant (8.314 J/mol K)
SCM	Surface Complexation Modeling
SI	Saturation Index
SSA	Specific Surface Area

SSE	Selective Sequential Extractions
T	Absolute Temperature (K)
WHO	World Health Organization
VGA	Vapor Generation Assembly
XRD	X-Ray Diffraction
XRF	X-Ray Fluorescence
USIEF	United States India Educational Foundation
UNICEF	United Nations Children's Emergency Fund
µg/L	microgram per litre
ψ_o	Surface potential in volts

Chapter 1

Introduction

1.1 Statement of Purpose

Groundwater Arsenic (As) contamination is an established public health issue for estimated 100 million people across the globe. Some major affected areas are the low lying, topographically flat floodplains of rivers draining the Himalayas (Nriagu et al, 2007; Winkel et al., 2008; Ravenscroft et al., 2009). Although much got to be known from nearly three decades of research around the globe, uncertain terrain of upper Brahmaputra floodplains in Assam remained a gap, making delineation of safe aquifers unsuccessful and unpredictable in this tectonically unstable part of the world. The upper Brahmaputra Floodplain being sandwiched between two active tectono-sedimentary regimes viz. Eastern Himalayas and the Indo Burma Ranges, adds elevated complexity to the overall groundwater aquifer dynamics.

A recent study involving testing of over 56,180 public sources across Assam, revealed 29 % sources exhibiting concentrations above WHO limits of 10 ppb, underlining the urgent need of understanding the processes and factors contributing to arsenic mobilization and transport. As of now most initiatives to install wells in safe aquifers have been jeopardized by the lack of necessary scientific understanding of the aquifer characteristics in the region. Studies are urgently needed for in-depth understanding of the aquifer geometry, sediment architecture and solid-liquid phase partitioning of arsenic.

1.2 Objectives and Hypotheses

The relatively new found natural regime of upper Brahmaputra was found to be an ideal ground for examining some of the emerging global hypotheses. With the revelation of a IITG-UNICEF study revealing out of 56, 180 water sources 8 % sources having arsenic concentrations above 50 ppb and 29% sources above WHO values of 10 ppb, the affected areas were found spread over several geological and geomorphological units within the catchment of the braided channel of the Brahmaputra River. The proposed study thus aims to evaluate the cause(s), extent, estimate, and process (es) of arsenic occurrence in the study area to understand the problem in-depth and to explore mitigation measures. A comprehensive analysis of the water and sediment samples was performed to understand the hydrogeochemical and mineralogical factors contributing to arsenic occurrence and their

possible interconnections in focusing upon realistic and practicable mitigation measures. The primary goal of the study is accomplished through five inter-connected objectives described below:

- Objective 1: Examining the underlying causes of spatial and temporal variability of dissolved arsenic concentrations in alluvial aquifers of the Brahmaputra River Valley
  Hypothesis: Arsenic distribution in the Brahmaputra River Valley is highly variable both spatially and temporarily
- Objective 2: Evaluating arsenic geochemistry in aquifers of the study transect
  Hypothesis: Geochemical factors viz. aquifer redox conditions control arsenic distribution
  Objective 3: Examining arsenic levels and other lithological properties of sediments in the study sites
  Hypothesis: Aquifer depth, sediment color, grain size, and the mineralogy of aquifer material impacts depth wise arsenic distribution in the groundwater
- Objective 4: Determining hydrogeochemical characteristics of groundwater and sediments to develop a conceptual model of arsenic release
  Hypothesis: Although there is a deep consensus that reductive dissolution hypothesis is the prime mechanism of arsenic release into groundwater aquifers, local scale factors viz. depositional history, sedimentation pattern and hydrological factors contributes to arsenic release in the upper Brahmaputra River Floodplains
- Objective 5: Assessment of arsenic kinetics towards developing arsenic-remediation models
  Hypothesis: High solid and aqueous phase iron creates increased adsorption sites leading to efficient as removal

1.3 Significance of the Research Work

Despite three decades of research uncertainties with groundwater arsenic persists. Since most arsenic affected areas around the world are in human perturbed systems, the need and benefits of studying groundwater arsenic in a less disturbed, pristine system, where large scale pumping effect is comparatively less always appear attractive and rewarding scientifically. Besides verifying generic theories, the effects of local scale hydrologic and geologic factors on spatial distribution of arsenic can be better examined. Such improved understanding can help local, regional and global policy makers as well as National and

International donor agencies to develop mitigation strategies thereby fulfilling Sustainable Development Goal 4 of provisioning safe drinking water.

In order to achieve the objectives, a well laid out field and laboratory plan was formulated and adequate groundwater and sediment samples were collected and analyzed. Where necessary, secondary data were used to reinforce primary findings of government departments and private organizations. Findings of this work are expected to make a contribution in the field of and provide practical knowledge to facilitate future groundwater development and management in the rather unique Brahmaputra Valley in Assam.

1.4 Thesis Structure

Chapter 1 is the introductory chapter which forms the background of the study and the need for seeking new insights for understanding the groundwater arsenic contamination in the upper Brahmaputra Basin, a relatively less explored region. The statement of purpose, objectives and hypothesis of the research work are elaborated along with highlighting the significance of the research work.

Chapter 2 presents the reviews from the plethora of existing literature on groundwater arsenic contamination. The key literature and latest breakthrough in arsenic research is presented to provide an insight on how As research has evolved. A synthesis of chemistry of arsenic, its toxicity, occurrence, its sources- both geogenic and natural, mobilization and immobilization mechanisms, natural attenuation mechanism along with hydrologic, geologic and geomorphic controls on spatial distribution of arsenic is presented. The chapter ends with an elaboration on the status of current and emerging arsenic mitigation strategies adopted in different arsenic affected areas around the globe. .

Chapter 3 provides a detailed description of the Brahmaputra River Basin along with the two specific study transects, from along the northern and southern bank of the upper Brahmaputra in Assam, where the current research work is focused. Detailed description of the unique set up of the basin and its complexity manifested by the north-eastward movement of the Indian plate along the Himalayan arc and the east –west convergence along the Indo – Burma fold thrust Schuppen is elaborated. The environmental conditions, geology, drainage and hydrogeology of study transects are lucidly presented. The chapter concludes with a thorough description of previous investigation to unravel the groundwater arsenic contamination issue in the upper Brahmaputra Basin in Assam.

Chapter 4 outlines the comprehensive methodology used for groundwater and sediment sample collection, preservation and analysis. The chapter starts with a description on the rationale for selection of the study transects. The experimental conditions, instruments used, tools and procedures followed to arrive at the results and findings are presented in an elaborative manner.

In **Chapter 5**, efforts have been made to present in a logical and organized way the main findings of the investigations. The findings are presented section wise for aqueous and solid phase hydro-geochemistry for both transects. The chapter started with detailed description of groundwater characteristics along the elected transects followed by a comparison of the hydrochemistry of the study transects with those of other arsenic contaminated areas in South and South East Asia. Temporal variability of water level and arsenic, monitored for over six months along the southern transect are presented to gain an insight on the temporal arsenic variability. Sediment geochemistry which includes sediment mineral characterization using Fourier Transform Scanning Electron Microscopy (FESEM) analysis, Petrographic study, bulk metal analysis, total metal extractions and sequential extractions from borehole sediments are elaborated for both the transects. Geologic and hydrologic controls on spatial arsenic distribution along the study transects are presented, with an elaboration of site specific factors controlling arsenic distribution. The chapter concluded with detailed description of arsenic attenuation study conducted on selected aquifer sediments along with the results of simulations using PHREEQC Surface Complexation Model to predict arsenic adsorption on sediment samples.

Chapter 6 provides the summary and conclusion of the research work, highlighting the salient findings of the research work.

Chapter 2

Literature Review

2.1 Key Literature and Latest Breakthrough in Arsenic Research

Toxicological implication of high arsenic groundwaters was first revealed more than a decade back by Smith et al., (2000). Current research are mostly focused on establishing the critical linkage between arsenic with other health implications viz. renal failures, cancers, hematuria etc. (Ferreccio et al., 2013; Hopenhayn- Rich et al., 1998; Hsueh et al., 2009; Huang et al., 2011; Yuan et al., 2010). Implications of arsenic exposure from drinking water has been strongly linked with development of bladder cancer (Kurttio et al., 1999; Marshall et al., 2007; Steinmaus et al., 2013). A National Health and Nutrition Examination Survey (NHANES) cross-sectional study of 1253 participants with age range between 12–30 years conducted during 2009–2012 with available urinary arsenic and eGFR measures demonstrated an association between urinary tract arsenic with glomerular filtration rate (eGFR) indicating that critical role of arsenic in contributing to renal diseases (Weidemann et al., 2015). Under the Health Effects of Arsenic Longitudinal Study (HEALS) project, McClintock et al., 2014, for the first time investigated and established a link been arsenic exposure and presence of haematuria.

Nearly three decades of research on the groundwater arsenic contamination issue has led to a deeper understanding of the problem (Smedley and Kinniburgh, 2002; Chakraborti et al., 2003; Nriagu et al, 2007; Winkel et al., 2008; Halim et al., 2009; Ravenscroft et al., 2009; Bundschuh et al., 2012; Biswas et al., 2013; Bundschuh et al., 2012; Biswas et al., 2013, Datta, 2015; Podgorski et al., 2017). Yet, with more new areas discovered to host groundwater aquifers contaminated with arsenic and with interplay of conditions varying from local to regional scales, the elusiveness regarding the issue still persists. Researchers worldwide thus are focused on unraveling the unknowns. Current research are now focused on understanding the role of different factors viz. hydrology, groundwater flow, geochemistry, microbiology, tectonics on controlling the fate of arsenic in aquifers (Mukherjee et al., 2014, Guo et al., 2014, Michael and Khan, 2016). Latest breakthrough research on arsenic has been aimed at reducing the gaps between the known and unknowns. Current research are focused on improving sampling methods, for extracting matched samples of uncompromised groundwater and aquifer sediments from specific depth interval for detailed analysis and incubation. The International Core Drilling Program (ICDP) is an

initiative, where a joint effort involving representatives from arsenic affected areas from around the world is made for collecting undisturbed sediment cores from boreholes drilled several meters below ground surface (van Geen et al., 2011; van Geen et al., 2013).

Arsenic research has now escalated; with process oriented research now been driven more toward technology oriented one, in order to unravel the arsenic mystery and develop sustainable mitigation solutions. From a stop gap approach there has been a shift towards devising mechanisms on how safe aquifer sustainability can be enhanced. While, once believed that shallow groundwater aquifers are highly contaminated, leading to reverting to deeper groundwaters as potential safe sources, the revelation by Mukherjee et al., (2007) based on a holistic groundwater aquifer mapping using lithologs in West Bengal that deeper sources are contaminated have led to increased concerns. Recent work by Michael and Khan (2016) have modelled out the implications of intensive irrigation work in the fluvio-deltaic aquifer system of Bangladesh, indicating that under conditions of intensive pumping deeper, aquifers are vulnerable to contamination. Knappett et al., (2016) studied the vulnerability of low arsenic aquifers to municipal pumping in Dhaka, and reported that under condition of continuous Dhaka pumping, accessibility to low As drinking water would be constrained. Berg et al., (2008) have indicated the detrimental effects of Hanoi pumping on the otherwise safe Pleistocene aquifers.

Current research are now more focused on understanding the role of different factors viz. hydrology, groundwater flow, geochemistry and microbiology in arsenic mobilization into groundwater aquifers. Although there is a deep consensus that reductive dissolution of Fe(III) oxy-hydroxides are the primary mechanism of arsenic release into groundwater aquifers, research now show that this mechanism alone cannot explain the arsenic release into groundwaters Local factors along with aquifer conditions concurrently play a role (Biswas et al., 2014). Furthermore, the diverse source of organic matter in aquifers driving the dissolution of Fe-oxyhydroxides still remains controversial (Harvey et al., 2002; Mailloux et al., 2013).

In terms of provenance of arsenic in the GBM basin, recent research have attributed the source of this metalloid, present ubiquitously in the earth's environment to the larger tectonic framework. Mukherjee et al., (2014) attributed arsenic enrichment in groundwater of foreland basin aquifers to crustal evolution processes related to plate tectonics. Under conditions conducive, arsenic enrichment magmatic rocks transported from depth to surficial deposits release arsenic to groundwater (Mukherjee et al., 2014).

2.2 Global Arsenic Knowledge Generation and Application

Most floodplains and delta plain environments around the world are reported to have arsenic levels in groundwater beyond permissible limits (Nriagu et al. 2007). The noteworthy occurrences are in parts of Argentina, Bangladesh, Chile, China, Hungary, India (West Bengal), Mexico, Romania, Taiwan, Cambodia, Vietnam and many parts of the USA, particularly the SW (Figure 2.1). While most of these occurrences are of geogenic origin, anthropogenic activities viz. mining and smelting related activities also control arsenic distribution in groundwater (Rodriguez et al., 2000) (Table 1).

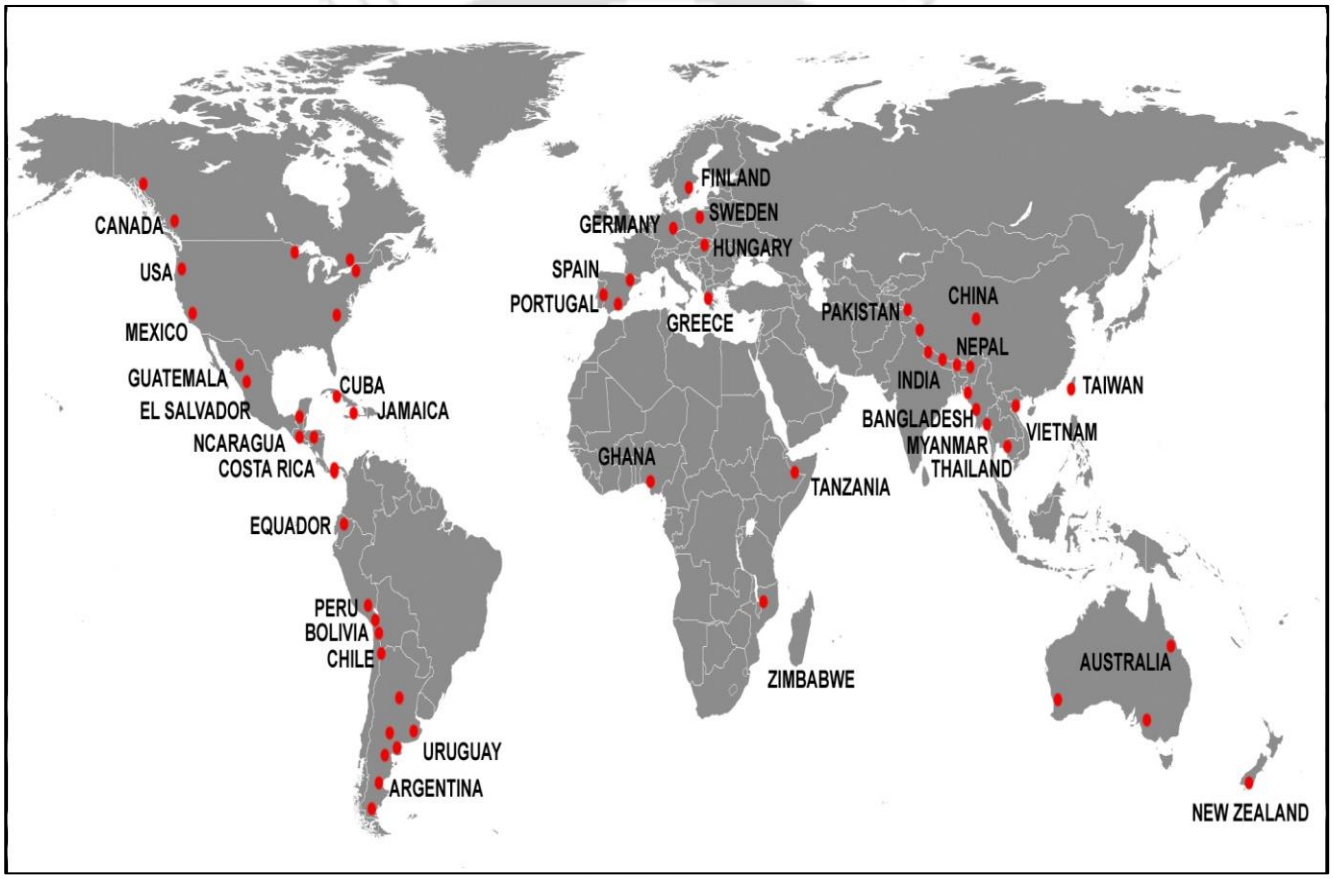

Figure 2.1 World map showing know occurrences of groundwater with elevated concentrations of geogenic arsenic (Adapted from Nriagu et al., 2007)

Table 1 Summary of documented cases of groundwater arsenic contamination along with their mobilization mechanism in some of the Arsenic affected areas around the world

Country	Region/Area Affected	As conc. Range (µg/L)	Source of Contamination	Mechanism of As Release	Reference
Bangladesh	Munshiganj	< 0.5 to 2500	Geogenic	Reductive dissolution of Fe(III) oxyhydroxides	BGS , DPHE 2001
	Araihazar	bdl-900	Geogenic	Reductive dissolution of Fe(III) oxyhydroxides	Metral et al., 2008; van Weinman et al., 2008
India	West Bengal	< 10 to 4600	Geogenic	Reductive dissolution of Fe(III) oxyhydroxides	Bhattacharyya et al., 1997; Chowdhury et al., 1999; Datta et al., 2011
	Assam	< 10 to 1000	Geogenic	Reductive dissolution of Fe(III) oxyhydroxides	Mahanta et al., 2015
	Uttar Pradesh	bdl to 468	Geogenic	Reductive dissolution of Fe(III) oxyhydroxides	Chauhan et al., 2009
	Bihar	bdl to > 300	Geogenic	Reductive dissolution of Fe(III) oxyhydroxides	Chakraborti et al., 2003
China	Yinchuan Basin	< 10 to 105	Geogenic	Competitive desorption of As, Reductive dissolution of Fe-oxyhydroxides	Guo et al., 2014
	Xinjiang	<10 to 185	Geogenic	Desorption under relatively high pH conditions; reductive dissolution of Fe(III)oxides	Zhou et al., 2016
	Songnen basin, P.R. China	< 0.1 to 338	Geogenic	Dissimilatory Fe(III) reduction Coupled with microbial degradation of dissolved organic carbon	Guo et al., 2014
	Datong Basin	<1–1160	Geogenic	Reductive dissolution of Fe (III)-oxyhydroxides	Luo et al., 2012

Pakistan	Indus River Valley	> 200		Elevated pH dissolution	Podgorski et al., 2017
Cambodia	Kendal Province	1 - 1340	Geogenic	Reductive dissolution of metal oxides	Buschmann et al., 2007
	Red River Delta	<1-3050	Geogenic	Reductive dissolution of Fe (III)-oxyhydroxides	Berg et al., 2001
Vietnam	Mekong Delta	<1-1470	Geogenic	Reductive dissolution of Fe (III)-oxyhydroxides (shallow aquifers) Pumping induced release (deeper aquifers)	Erban et al., 2013
Nepal	Nawalparasi	> 500	Geogenic	Reductive dissolution of Fe (III)-oxyhydroxides	Brikowski et al., 2015
Mongolia	Hetao Plain	<1–804	Geogenic	Reductive dissolution of Fe (III)-oxyhydroxides; Competing ion exchange	Luo et al., 2012
Argentina	La Pampa Province; Chaco Pampean		Geogenic (Volcanic ash with 90 % Rhyolitic glass)	Desorption of As from metal oxyhydroxides at high pH (>8); Oxidation of sulfide minerals	Smedley et al., 1998; Bundschuh et al., 2012
Myanmar	Lower Ayeyarwady Basin	< 10 to 630	Geogenic	Reductive dissolution of Fe-oxyhydroxides	van Geen et al., 2013
Mexico		Chihuahua, Coahuila, Durango, and Sonora	Geogenic , Mine Tailings	Reductive dissolution of Fe-oxyhydroxides ; Hydrothermal release	Armienta et al., 1995; Armienta and Segovia (2008); Rodriguez et al., 2000; Nicolli et al., 2012
SW Taiwan	Chianan Plain	50–700	Geogenic	Desorption from clay and dissolution of iron oxyhydroxide	Yang et al., 2016
USA	Maryland, USA,	bdl to 80;	Geogenic	Dissimilatory Fe (III) reduction driven by suboxic, non-sulfidogenic groundwater	Haque et al., 2008; Johannesson et al., 2009; Yang et al., 2013
	Louisiana	10 to 100			

2.3 Geochemistry of arsenic in the environment

Present ubiquitously in the earth's environment arsenic is the twentieth most abundant element in the earth's crust, with the average arsenic content in the continental crust generally varying from 2 mg to 3 mg/kg (Cullen and Reimer, 1989). Several naturally occurring minerals with varying concentrations of solid phase arsenic act as primary sources of arsenic in the environment (Smedley and Kinniburgh, 2002, Savage et al. 2005). Among different rock types, considerable variation in solid phase arsenic concentrations is observed, of which sedimentary rocks host a higher arsenic concentration range (Smedley and Kinniburgh, 2002). While geogenic sources of arsenic contributes largely to the arsenic pool in ground water systems, anthropogenic activities viz. mining, smelting etc. is reported to have arsenic concentrations orders of magnitude higher than under natural conditions (Smedley and Kinniburgh, 2002).

In terms of occurrence in the environment, among the different oxidation states of arsenic (As), As(III) and As(V) are the mostly encountered in soil and water environments. As(V) is the dominant species in an oxidative environment whereas, As(III) is the dominant one in the reducing environment. The occurrence of these different oxidation states in the environment is in turn controlled by the pH and the redox state of groundwater (Welch et al., 1988).

Depending on field measurements of solution pH and Eh, the Eh –pH diagram provides view of the stability area of metal/metalloid species in the solution (Figure 2.2). Positive values of Eh indicate a more oxidising condition while a negative value indicates strong reducing condition. Eh-pH diagram for aqueous solution of arsenic suggests that at pH < 6.9, $H_2AsO_4^-$ species dominates, $HAsO_4$ dominates at higher pH (>6.9), at extreme acidic and alkaline conditions, H_3AsO_4 and AsO_4 predominates (Fig. 2). At the same time, due to slow kinetics, both arsenite and arsenate can coexist in either redox condition (Hendricks, 2006). Among arsenites, $H_3AsO_3^0$ exists at a wide range of pH from very low to about 9.2. High alkaline conditions support the existence of $HAsO_3$¼ and AsO_3^{3-} in water (Smedley and Kinniburgh, 2002). However, presence of extremely high concentrations of reduced sulphur, can lead to significant occurrence of dissolved arsenic sulphide species, thus favouring formation and precipitation of the sulfides of arsenic like As_2S_3, As_4S_4, As_4S_3, etc. Therefore, free sulfur-containing water is not expected to have high arsenic content (Moore et al., 1988).

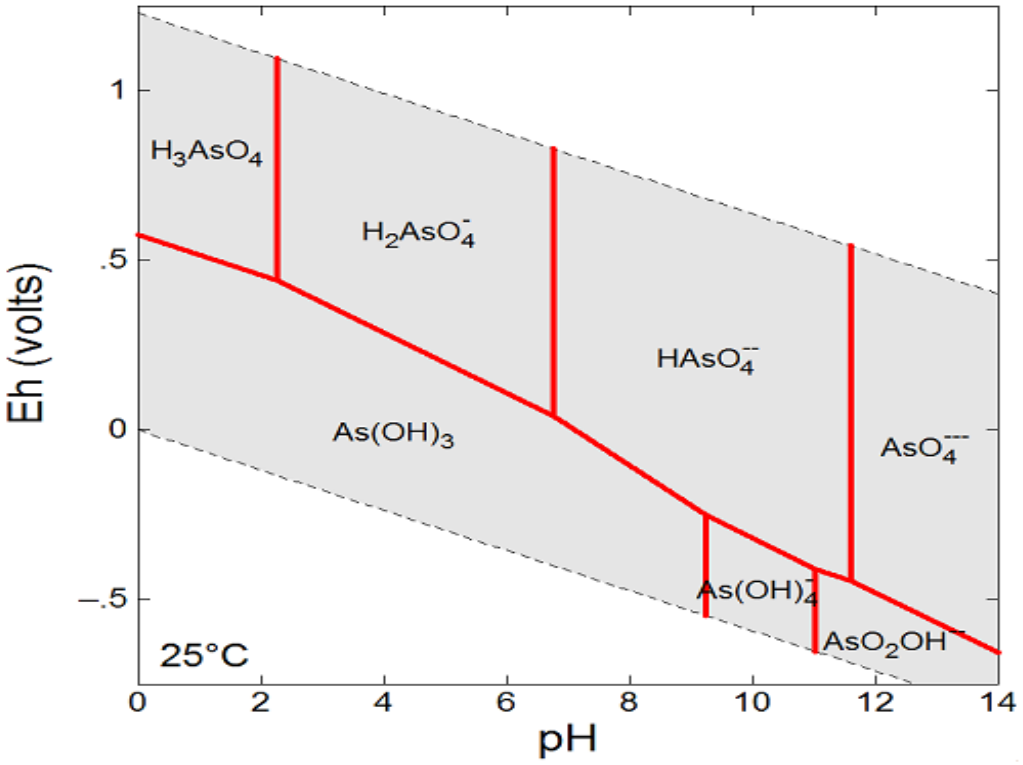

Figure 2.2 Stability fields of dissolved arsenic in water with respect to water pH and Eh at 25°C temperature and 1 atmospheric pressure (Welch et al., 1988; Smedley and Kinniburgh, 2001)

2.4 Geochemical processes in aquifers involving Arsenic

For nearly three decades, geochemical process controlling arsenic release has been intensively studied (Nickson et al., 2000; Smedley and Kinniburgh, 2002; Dowling et al., 2002; Horneman et al., 2004; Islam et al., 2004, Halim et al., 2009; Nath et al., 2008; He et al., 2010; Biswas et al., 2014, Kumar et al., 2016). Aquifer redox condition, pH, water –rock interaction and surface reaction on solid particles are the controlling factors in the aqueous distribution of arsenic (Stumm and Morgan, 1996).

The mineral-water interaction which control the arsenic in the aquifer systems are broadly divided into four types from geochemical point of view:

- Adsorption-Desorption,
- Oxidation-Reduction,
- Precipitation-Dissolution,
- Natural Organic Matter (NOM) facilitated complexation or dissolution

2.4.1 Adsorption Desorption

Adsorption of arsenic onto Fe, As and Mn oxides, clay minerals and organic matter is critical in controlling As mobility (Ravenscroft et al., 2009). Two types of surface complex models have been recognized, Outer-sphere surface complexes formed through nonspecific adsorption, involving the adsorption of anions by simple coulombic (electrostatic) interactions with positive charges. Inner-sphere surface complexes formed through specific adsorption, involving the incorporation of anions as a ligand in the coordination shell of an adsorbent. Outer-sphere complexes contain one or more water molecules between the surface functional group and the adsorbed ion, whereas inner-sphere complexes contain no water molecules between the surface functional group and the adsorbed ion. Inner-sphere complex bonds are much stronger than outer sphere complex bonds, and the inner-spherically adsorbed arsenic anions are not considered to be readily exchangeable.

2.4.1.1 Iron oxides

Iron oxides, identified as one of the most important arsenic adsorbents in natural systems, are common phases found in soil and sediments, either as discrete particles or as coatings on other mineral solids (Wang and Mulligan, 2008). They have an excellent ability to sorb cations and anions to their surfaces thereby decreasing the mobility of many trace elements in the environment (Dzombak and Morel, 1990; Stumm, 1992). The adsorption of arsenic on Fe(III) bearing minerals in natural soil and sediment surfaces have been reported by many researchers (Manning and Goldberg, 1996; Thronton, 1996; Wilkie and Hering, 1996; Fendorf et al., 1997; Raven et al., 1998; Dixit and Hering, 2003; Arai et al., 2005). Adsorption of arsenic species onto Fe-oxides is more highly dependent on its oxidation state than on pH in the range of 5.5-7.5 (Dixit and Hering, 2003). Adsorption of As(III) on both ferrihydrite and goethite is virtually constant between pH 5 and 9, and at all initial concentrations, while As(V) adsorption onto minerals varies with both pH and initial concentration (Dixit and Hering, 2003). Adsorption of arsenite onto magnetite differs significantly from adsorption onto ferrihydrite and goethite, with As(III) adsorption rising to a maximum at about pH 9.5 (Dixit and Hering , 2003). Gimenez et al., 2007 demonstrated that the sorption capacity for both As (III) and As (V) on both natural and synthetic haematite decreases with increasing pH, and at pH < 7, haematite has higher sorption capacities for both As(III) and As(V) than either goethite or magnetite, although at higher pH the difference for As(III) are small. On the contrary, Gimenez et al. (2007) indicated that goethite and

magnetite followed similar trends in sorption capacity with increasing pH for both As(III) and As(V).

The degree of crystallinity and surface area of (hydro) oxides have demonstrated significant effects on their sorption capacity (Wang and Mulligan, 2006). Generally, poorly crystalline hydroxides with a higher surface area show a higher As sorption capacity by providing more active sorption sites; viz, the adsorption of As(III) and As(V) was two or three times greater (on a surface area basis) on ferrihydrite than on goethite (Grafe et al., 2001). On the contrary, adsorption of As(III), As(V), MMA, and DMA by hematite was about half as much as goethite which has a larger surface area (Wang and Mulligan, 2006).

2.4.1.2 Mn Oxides

Manganese oxides in natural systems are often complex minerals of poor crystallinity and mixed oxidation states, showing the capacity to adsorb arsenic and to oxidize As(III) into As(V) (Oscarson et al., 1980; Manning et al., 2002; Foster et al., 2003; Ouvrard et al., 2005). As(III) oxidization by Mn oxide may cause a surface alternation, creating fresh reactive sites for As(V) sorption on the oxide surface (Oscarson et al., 1980; Nesbitt et al., 1998; Manning et al., 2002).

2.4.1.3 Al (hydro) oxides

Al (hydro) oxides are ubiquitous in acidic soils and aquatic environments (Wang and Mulligan, 2006). Amorphous $Al(OH)_3$ has an isoelectric point of 8.5, and thus is an extremely efficient adsorbent to immobilize As. Both outer and inner sphere complexes are formed on Al oxide (γ-Al_2O_3) and gibbsite ($Al_2O_3 \cdot 3H_2O$) (Wang and Mulligan, 2004). It has been reported that the adsorption of As(V), $CH_3AsO(OH)_2$, and $(CH_3)_2AsOOH$ increases up to pH 7 by amorphous $Al(OH)_3$, crystalline $Al(OH)_3$ (gibbsite), α- Al_2O_3, and γ-Al_2O_3, and decreases significantly at higher pH values (Voegelin and Hug., 2003; Lin et al., 2000), while As(III) can be strongly adsorbed from pH 6 to 9.5 and decreases at higher pH values (Lin and Puls, 2000).

2.4.1.4 Sorption to Clay minerals

Ubiquitous in the terrestrial environment, clay minerals largely consist of alumino silicates with alternating layers of Si and Al oxides (Wang and Mulligan, 2006). However, compared with Si and Al oxides, alumino silicates are distinct with high surface charge density and

diverse acid behavior of the edge hydroxyl groups due to the three-dimensional chemical structure (Yang and Mulligan, 2004). As(V) adsorption to kaolinite, montmorillonite, illite, halloysite, and chlorite occurs up to pH 7, then decreases with a pH increase (Lin and Puls, 2000) while As(III) adsorption by the same clay minerals is minimal at low pH and increases with increasing pH. As(V) is adsorbed to a greater extent than As(III) on all clay minerals at a pH below 7 (Wang and Mulligan, 2006).

2.4.1.5 Enhanced sorption by cations

Certain cations, such as Ca^{2+} and Fe^{2+}, has the potential to increase arsenic adsorption by increasing the amount of positive charge on the oxide surface and/or forming a positively charged surface (Wang and Mulligan, 2006). The adsorption of As(V) onto Al oxides was observed to be enhanced in the presence of Ca^{2+} at a pH above 8 (Ghosh and Teoh, 1985). Wilkie and Hering, (1996) reported that the addition of Ca^{2+} also increased the As(V) adsorption onto ferrihydrite at pH 9. The addition of Ca^{2+} and Mg^{2+} to the suspension of ferrihydrite negated part of the competitive effect of silicate on As adsorption. The formation of $CaCO_3$ minerals can restrict the development of high pH, thus inhibiting the As(V) release from the oxides and clays (Meng et al., 2000). Moreover, the formation of $Ca_3(AsO_4)_2$ and $CaHAsO_3$ precipitates has been observed in contaminated soils (Dutre et al., 1995), which contributes to As immobilization.

2.4.1.6 Competing sorption by anions

Competition for adsorption sites induced by the presence of other adsorbing anions or cations can significantly influence adsorption and mobility of As(III) and As(V) (Wilkie and Hering, 1996; Appelo et al., 2002; Dixit and Hering, 2003; Kent and Fox, 2004; Swartz et al.,2004; Anawar et al., 2004; Stollenwerk et al., 2007; Stachowicz et al. 2008). The competitive adsorption by phosphate is the most studied because of its significant role in affecting the arsenic sorption (Ravenscroft et al., 2009). It has been demonstrated that phosphate can suppress the adsorption of both As(V) and As(III), while As(V) is much more strongly affected than As(III) (Smedley and Kinniburgh 2002). Phosphate reduces As(III) adsorption onto ferrihydrite but the effect becomes insignificant at pH 0 (Jain and Loeppert, 2000). Dixit and Hering (2003), however showed that in the presence phosphate, As(III) is sorbed preferentially to As(V)over the pH range of 4 -10.

Carbonates, generally is seen have no significant effect on As(III) and As(V) adsorption (Stollenwerk et al., 2007); but the presence of bicarbonate (HCO_3^-) can facilitate arsenic mobilization from As-containing sulfides such as orpiment in both oxic and anoxic environments (Kim et al., 2000; Anwar et al., 2004). Arsenic mobilization increases with increasing HCO_3^- concentrations and pH while silicate reduces the adsorption of As(III) and As(V) on ferrihydrite at pH 6.8. Adsorption of As(III) on ferrihydrite is decreased between pH 4 and 10 by the presence of silica, by as much as 35% and also decreases the adsorption of As(V) above pH 6 by as much as 60 % (Swedlund and Webster, 1999). However, in natural waters these effects are partly counteracted by magnesium and calcium, which increases As(V) adsorption on ferrihydrite at pH 9 (Wilkie and Hering, 1996; Smith et al., 2000). Increasing the silica concentrations from 1 to 10 ppm, Meng et al. (2000) reported that adsorption of both As(III) and As(V) were reduced from 90 % to 45 %, although the presence of Ca and Mg reduced the Si effect on As(V) but not on As(III).

Apart from the above, sulphate, nitrate, chloride, calcium and magnesium are some of the other ions that affect arsenic sorption. Sulphate ion is reported to have no effect on As(V) adsorption any pH, but reduces As(III) adsorption between pH 2 and pH 6, with negligible effect between pH 7 to pH 10 (Jain and Loeppert, 2000). Similar to sulphate, both chloride and nitrate are reported to have insignificant effect on As(V) adsorption (Naidu et al., 2002).

2.4.2 Oxidation Reduction

Redox potential is another important factor controlling arsenic retention and remobilization in sediments (Bostick et al., 2004; O'Day et al., 2004). After entering water environments, geochemical processes such as adsorption/desorption, precipitation or co-precipitation, and oxidation/reduction (Smedley and Kinniburgh, 2002; Xu et al., 2011) change the form of arsenic within the environment, thus resulting in fixation or migration because different forms of arsenic have different stabilities in water (Burton et al., 2011).

The key redox couples possibly involved in the redox speciation of arsenic are: O_2/H_2O, Mn(IV)/Mn(II), NO_3^-/N_2, NO_3^-/NO_2^-, Fe(III)/Fe(II), SO_4^{2-}/HS^- and CO_2/CH_4 (Gorny et al., 2015). Redox process in groundwater typically occur through the addition of an oxidant, like O_2 , Fe^{3+}, SO_4^{2-} and NO_3^- to an aquifer containing reductant (Apello and Postma, 2005). Redox reactions involving Fe are most important as they can directly or indirectly affect arsenic mobility into groundwater. The sequence of redox processes begins with consumption of O_2 and an increase in CO_2 from decomposition of organic matter (OM). Arsenic bound to

organic matter in then released on degradation of OM. This is followed by denitrification reactions, where, the reduction of NO_3^- to NO_2^- to NO and finally to gaseous N_2O and N_2 occurs. Denitrification is followed by manganese reduction, leading to increase in dissolved Mn^{2+} concentrations. Sorbed As on Mn oxides may be subsequently released as a result of Mn reduction. Reduction of Fe(III) to Fe(II) occurs post Mn reduction, thus increasing the concentrations of dissolved Fe(II). Sorbed As on Fe oxides subsequently gets released into groundwater, as reduction of Fe oxide to Fe(II) lowers the overall net positive charge of the oxide producing weaker electrostatic bonds between sorbed anions and the oxide surface, leading to desorption of the anions. This is followed by SO_4^{2-} reduction to sulfide (S^{2-}) and CH4 production from fermentation and methanogenesis and finally reduction of N_2 to NH_4^+.

The redox reactions controlling As release in groundwater of Bengal Basin are (Bhattacharyya et al., 2002) (Figure 2.3);

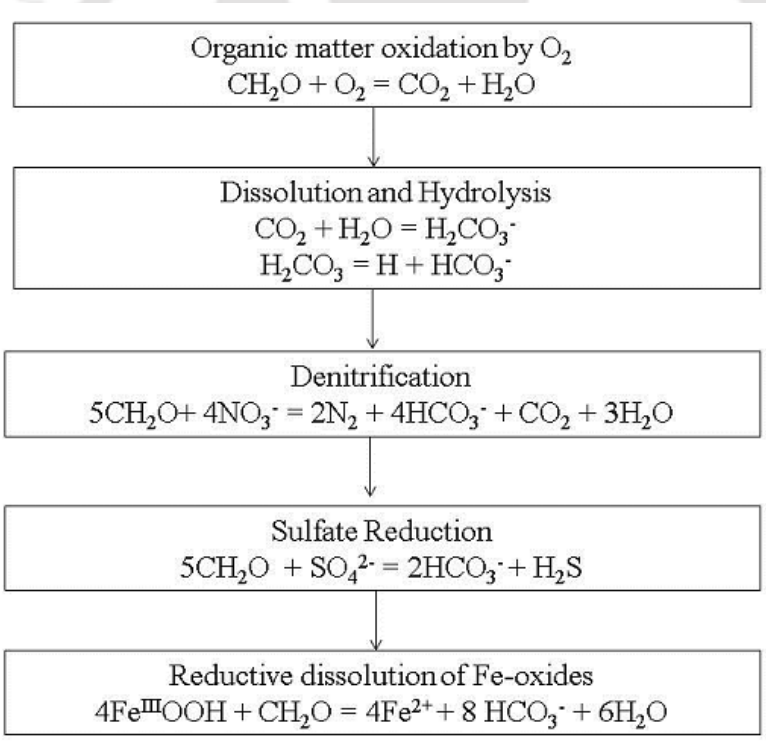

Figure 2.3 Schematic showing sequence of geochemical reactions for dissolution of arsenic in groundwater of Bengal Basin (Bhattacharyya et al., 2002)

2.4.3 Precipitation Dissolution

Reductive dissolution of Fe, with the participation of microbes, plays an important role in managing the migration and transformation of arsenic (Smedley and Kinniburgh, 2002; Islam

et al., 2004). It is generally thought that the microbially mediated reductive dissolution of iron-bearing minerals in water environments leads to the release of arsenic. The amount released depends on the valence state of arsenic and the mineralogical characteristics of Fe within the environment (Islam et al., 2004; Campbell et al., 2006). (Smedley and Kinniburgh, 2002; Drahota et al., 2009; Mandal and Suzuki, 2002) have extensively studied the role of sulfur, alkaline and transition metals precipitates in controlling the solubility of arsenic in porewaters.

The solubility of both As(V) and As(III) are strongly influenced by the redox potential variations in the subsurface environments (Ye et al., 2013). Under oxic conditions (+200 to +500 mV), As(V) is the dominant species, and it is efficiently adsorbed and/or (co)-precipitated with various minerals, particularly iron and manganese (hydr)-oxides. Reduction of these (hydr)-oxides under moderately reducing conditions (0 to +100 mV) results in the partial dissolution of As(V) in porewaters. However, with the reversal of the redox potential to strongly anoxic (0 to −200 mV), reduction of As(V) into As(III) occurs, combined with the production of sulfides.

2.4.4 Natural Organic Matter

The role of dissolved organic carbon and/or Fe-oxyhydroxide solids on arsenic mobility in natural groundwater has been extensively reported (e.g., Charlet and Polya, 2006). Microbial activity controls redox conditions and the phases in which arsenic occurs, thereby directly or indirectly affecting diagenetic reactions involving arsenic speciation in shallow sediments (Stumm and Morgan, 1996; Anwar et al., 2002).

Organic matter plays a key role in many microbial reactions in sediments and the type of organic matter present affects its reactivity and hence bioavailability (Smedley and Kinniburgh, 2002). It is presumed to be carrier of arsenic and to control the mobility, digenetic cycling, transport, aggregation and deposition of arsenic and other trace elements in soils, sediments, biogenic deposits and groundwater of most delta plain (McArthur et al., 2001; Bauer et al., 2008). Organic matter derived from decomposition of terrestrial plants can act as an arsenic sink forming insoluble complexes and through metal bridged ternary complexation (Redman et al., 2002; Lin et al., 2004).

2.4.5 Bacterial Reduction

The role of microbes in arsenic speciation and mobilization has become increasingly clear (Smedley and Kinniburgh, 2002). Microbes play a significant catalytic role in the oxidation of arsenite, respiration of arsenates and reactions involving methylation and volatilization (Lloyd and Oremland 2006; Oremland and Stolz; 2005; Oremland et al. 2004). The microbial transformations either act as sources of energy or as detoxifying mechanisms. While a number of chemoautotrophs oxidize As(III) by using oxygen, nitrate or ferric iron as a terminal electron acceptor and CO_2 as their sole carbon source, certain heterotrophs are also capable of As(III) oxidation using organic carbon (Smedley and Kinniburgh, 2002). On the other hand, many prokaryotes (e.g. Bacillus selentireducens and Bacillus arsenicoselantis) are capable of As(V) respiration or As(III) oxidation (Oremland et al. 2002; Oremland and Stolz 2003; Pederick et al. 2007).

Microbially induced redox reactions viz. the dissimilatory Fe-reducing bacterium Shewanella alga reduces Fe(III) to Fe(II) in scorodite ($FeAsO_4.2H_2O$), releasing As(V) and Fe(III)-reducing bacteria Geobacter and Geothrix have also been shown to affect arsenic cycling in reduced aquifer sediments (Cummings et al. 1999; Islam et al. 2005).

2.5 Arsenic Mobilization Processes

Three different mechanisms viz. Oxidation of sulphides, reductive dissolution mechanism and competitive exchange mechanism have been proposed to control arsenic release and accumulation in ground water (Das et al., 1995; Chowdhury et al., 1999; Acharyya et al., 2000); of which the most accepted mechanism is the reductive dissolution of Fe (III) oxy(hydroxides).

2.5.1 Oxidation of sulphide minerals

Numerous primary sulphide minerals like Fe sulphides such as pyrite and arsenopyrite, complex copper sulphides such as enargite and tennantite, as well as the As sulphides orpiment and realgar, occur in association with gold and base-metal deposits in mineralized zones (Smedley , 2008). Oxidation of arsenic bearing pyrites present in aquifer sediments have been proposed to be mechanism of arsenic release (Das et al., 1996; Chowdhury et al., 1999; Mandal et al., 1996; Mallick and Rajagopal, 1996). Mechanism of pyrite oxidation in aquifer in the unsaturated zone is presented in Fig 4. However, due to the lack of substantial pyrite in the sediments (Umitsu, 1993), strongly reducing conditions prevalent in the contaminated aquifers (von Brömssen et al., 2007), and lack of dissolved sulfate present in

groundwater (Acharyya et al., 1999) this mechanism has been discarded. The mechanism of oxidative release of arsenic from sulphide minerals is illustrated below (Figure 2.4),

In the unsaturated zone: FeS_2 (+As) + $15/4O_2$ + $7/2\ H_2O \rightarrow 2SO_4^{2-} + 4H^+ + Fe(OH)_3$ + As

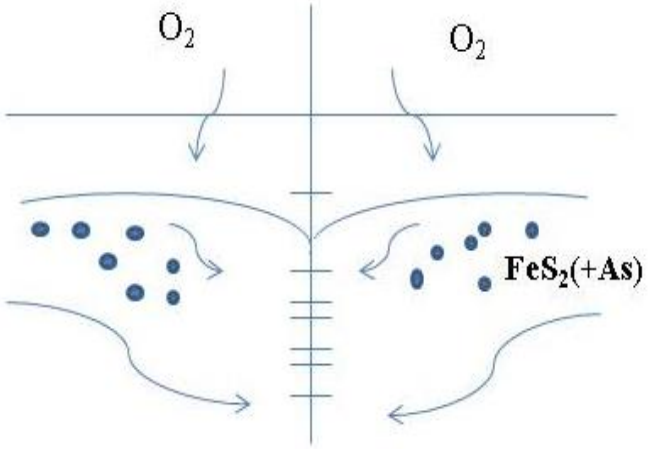

Figure 2.4 Mechanism explaining release of arsenic from sediment into groundwater by oxidation of sulphide minerals. Groundwater drawdown facilitates access of oxygen to pyrite that contains As which dissolves (adapted from Appelo and Postma, 2005)

2.5.2 Release from iron oxides under reducing conditions

The reductive dissolution of Fe-oxyhydroxides onto which arsenic was adsorbed or co-precipitated during sediment deposition, coupled to the mineralization of organic matter, (Bhattacharya et al., 1997; Nickson et al., 2000, McArthur et al., 2001; Bhattacharya et al., 2002; Harvey et al., 2002, Stuben et al., 2003, McArthur et al., 2004) is currently the widely accepted mechanism of arsenic release into of the reduced sedimentary aquifers (Fendorf et al., 2010) (Figure 2.5). Ferric oxides and hydroxides which ubiquitously adsorbs arsenic and other trace elements, release arsenic when they are reduced to the ferrous state under the presence of sedimentary organic matter as the redox driver as per the reaction below (Ravenscroft et al., 2009). However, the source of organic matter in the aquifers driving the dissolution of Fe-oxyhydroxides still remain controversial (Harvey et al., 2002, 2006; Rowland et al., 2006; Farooq et al., 2010; Neumann et al., 2010; Datta et al., 2011; McArthur et al., 2012; Lawson et al., 2013; Mailloux et al., 2013).

Mechanism of reductive dissolution can be represented by the flowing reaction (Appelo and Postma, 2005)

In aquifer: $CH2O + H_2O \rightarrow CO_2 + 4H^+ + 4e^-$

$Fe(OH)_3As + 3H^+ + e^- \rightarrow Fe^{2+} + 3H_2O$ +As

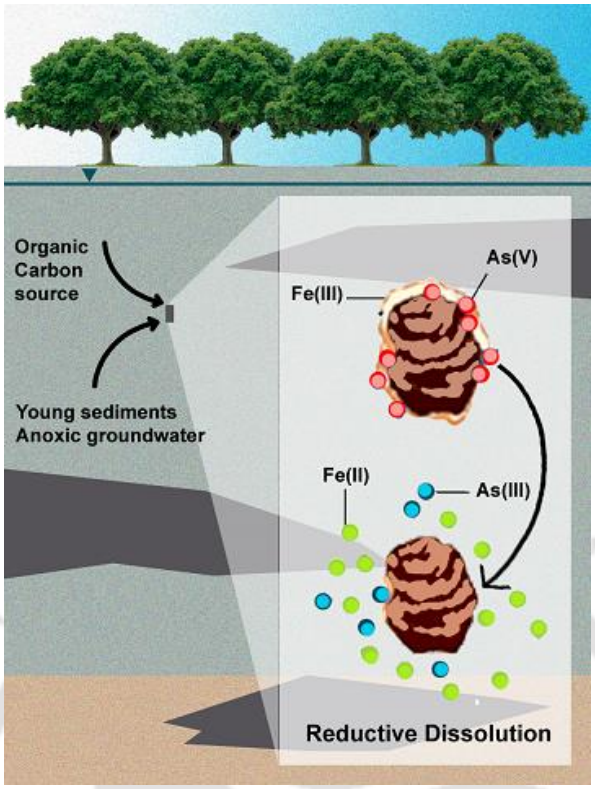

Figure 2.5 Schematic explaining release of arsenic from sediment into groundwater by reductive dissolution of Fe(III) oxyhydroxides (adapted from Michael, 2013)

2.5.3 Competitive exchange mechanism

The role of competitive sorption has been widely reported (Smedley, 2008; Swedlund and Webster, 1998; Rochette et al., 2000). The competitive sorption between arsenic and the anions can inhibit arsenic sorption and then increase As mobility, which hinders arsenic immobilization (Smedley and Kinniburgh, 2002). Phosphate is a well-known competitor for arsenate on Fe-oxide binding sites (Manning and Goldberg, 1996) and is often present at relatively high concentrations in reducing high-As groundwaters such as those in Bangladesh (BGS and DPHE, 2001), West Bengal (McArthur et al., 2004) and China (Smedley et al., 2003). Bicarbonate, also often present at very high concentrations in high-As groundwaters, has likewise been implicated as a potential competitor for As (Appelo et al., 2002; Charlet et al., 2007). Silica may exert a control on the sorption of As(V) and As(III) (Swedlund and Webster, 1998; Rochette et al., 2000) although its effect was considered less significant for groundwaters in West Bengal by Charlet et al. (2007).

Competitive exchange of As for P, where in P introduced from fertilizer and organic matter decomposition, competes for same site as As, releases arsenic. However, the quantities of P required to mobilize the amount of arsenic observed is unrealistic, given the depth of aquifers and the relative non-mobility of P through sediments (Bose and Sharma, 2002), indicating that arsenic release into groundwater is controlled by a combination of different mechanism.

2.6 Spatial and Temporal variability of As

One of the major causes of concerns regarding the growing arsenic crises around the world is the bewildering degree of spatial variability of groundwater arsenic concentrations (Radloff et al., 2016). Arsenic concentrations in groundwater may vary laterally from unsafe to safe within scales of 10 to 100 m, limiting identification of As safe aquifers (van Geen et al., 2003). Attempts to unravel the cause of this variability in the Bengal Basin has led to the understanding that local scale flows, influenced by massive groundwater withdrawal largely influence the spatial and vertical heterogeneity of arsenic distribution within shallow aquifers (Harvey et al., 2005; Harvey et al., 2006). Introduction of surface derived Organic Matter (OM) is also reported to be exacerbated by the extensive pumping of groundwaters in this region, resulting in the drawdown of increased volumes of organic rich recharge waters from the surface, thus preserving reducing condition in shallow aquifers (Harvey et al., 2002, 2005; Lawson et al., 2013, 2016). van Geen et al., (2008) have attributed the spatial variation of As to the differential flushing histories of aquifers.

The temporal variation of arsenic have been studied by several authors (Chatterjee et al., 1995; BGS and DPHE, 2001; Cheng et al., 2005,2006; van Geen et al., 2007; Farooq et al., 2011, Bhattacharyya et al., 2011). The seasonal variation in arsenic concentrations has been primarily attributed to the dilution differences during monsoon and post-monsoon (Farooq et al., 2011), although the findings often differ regarding the time period and change in arsenic concentrations, aquifer depths experiencing maximum variation and processes regulating seasonal cycling of arsenic in aquifer (Chatterjee et al., 1995; BGS and DPHE, 2001; Cheng et al., 2005, 2006; van Geen et al., 2007; Farooq et al., 2011).

2.7 Hydrological factors influencing arsenic mobilization

Geochemical triggers are not the sole controls of arsenic release into groundwater. Hydrological controls also plays a major role in influencing arsenic mobilization in groundwater aquifers (Stute et al., 2007). Groundwater flow patterns, residence time,

seasonal changes in recharge and pumping rates are reported to influence arsenic concentration. Smedley and Kinniburgh (2002) pointed out that whether released arsenic remains at problematic levels in groundwater depends not only on whether there are biogeochemical reactions that retard the transport of arsenic, but also upon the hydrologic and hydrogeologic properties of the aquifer, such as flow velocity and dispersion. Older rock bodies draining younger groundwater and younger rocks holding older groundwater both may have high concentrations of arsenic in groundwater. It is only when the geochemical trigger to mobilize arsenic and the hydrogeological regime to preserve it are both operating that we see high groundwater arsenic concentrations on a regional scale (Smedley and Kinniburgh, 2002).

In BDP various stable and radioactive isotopic compositions in groundwater have been studied to understand its geochemical behavior and recharge processes, particularly with reference to As-enrichment (Shivanna et al., 1999, Agarwal et al., 2000; Harvey et al., 2002, Sikdar and Sahu, 2009 and Sengupta et al., 2008). Stute et al. 2007, documented the most systematic relationship reported to date between dissolved arsenic concentrations and age, for the Araihazar area in Bangladesh. He demonstrated an increase of dissolved arsenic concentrations with the age of groundwater determined by ^{3}H-^{3}He dating at a rate of approximately 20 µg/L As per year.

Based on an integrated hydrologic-biogeochemical study in Vietnam, Postma et al. (2007) documented steep gradients in arsenic concentrations along flow paths in the upper 10 m of the aquifer and detailed biogeochemical changes along inferred flow paths. Subsequently, Benner et al., (2007) provided one of the most holistic view of subsurface flow using an extensive hydrologic measurements and groundwater simulations to illustrate flowpaths in a relatively unperturbed (little extraction of groundwater) Cambodian aquifer. Their measurements, along with aqueous chemistry (Polizzotto et al., 2008), indicated that on an annual basis, groundwater flows from wetlands toward the Mekong River, and transports arsenic along inferred flow lines.

van Geen et al in 2008 reported the influence of flushing histories on groundwater arsenic concentrations. Using a one dimensional advection dispersion model to show flushing history, combined with a linear isotherm dictating the equilibration of arsenic between the dissolved and particulate phases, the regional as well as local patterns in arenic distribution in shallow aquifers was explained.

The influence of pumping and the subsequent migration of the contaminant plume in deeper aquifers have been demonstrated by many authors (von Brömssen et al., 2007, Erban et al., 2013). These studies have modeled how groundwater extraction is causing interbedded clays to compact and expel water containing dissolved arsenic or arsenic-mobilizing solutes (e.g., dissolved organic carbon and competing ions) to deep aquifers over decades, in Bengal and Mekong delta plain, Vietnam.

Controls of hydraulic gradient in promoting arsenic enrichment has been clearly demonstrated by previous researchers (Nordstrom and Archer, 2003; Fendorf et al., 2010; Smedley et al., 2002) and more recently by Zhang et al., (2013); Guo et al., (2016); Zhu et al., (2015). These studies have shown that high arsenic groundwater usually corresponds to low hydraulic gradients. Zhang et al., (2013) developed an empirical relation for As concentration and hydraulic gradients for recharge and runoff flow regimes, showing that the hydraulic gradient of groundwater is less than 0.79‰, the concentrations of arsenic are usually more than 10 μg/l.

Sengupta et al., 2014 based on their studies in the Chianan Plain, SW Taiwan reported that arsenic concentrations, especially in the proximal zones, are spatially varied. Most of the proximal zone aquifer is As-safe, possibly due to recharge of oxic water and also insufficient residence time for water–rock interaction, as evident by high ^{3}H concentration. On the other hand, the arsenic enrichment in proximal groundwater seems to be controlled by local factors (i.e., presence of impermeable layer inhibiting vertical and lateral groundwater flow and subsequently releasing arsenic through strong water–rock interaction) as evident by low 3H concentration and existence of thick clay layer around those wells. A recent study in Terai hills in Nepal, have shown how thick clay layers impeding vertical recharge to aquifers have led to increased concentrations of arsenic in shallow aquifers (Brikowski et al., 2016).

2.8 Geologic factors influencing arsenic mobilization

While redox behavior in aquifers and hydrology controls arsenic concentrations in groundwater, local geology/stratigraphy is also seen to play considerable role in controlling arsenic distribution (Stanger, 2005; Saunders et al., 2005; Shamsuddha et al., 2008, Mukherjee et al., 2013). Stanger (2005) gave a paleo-hydrogeological model for arsenic contamination in southern and South East Asia. He argued that the Proto-Himalayan uplift of the Paleo Tethys created the palaeo-drainage systems of the Ganges – Brahmaputra, Irrawaddy, Mekong, and Red Rivers, with consequent headwater erosion of arsenic-rich

sediments. The downstream deposition of immature and easily redistributed Neogene sandstones, silts, and iron-rich clays has created secondary and tertiary reservoirs of adsorbed and authigenic arsenic, from which the current arsenic-rich groundwaters have evolved. Saunders et al. (2005) further proposed that As-enriched groundwater is a product of interactions between tectonic, geochemical and biological processes. The geochemical processes are linked to chemical weathering of a variety of bedrock types, as noted by analyses of surficial material in major parts of continental crust (e.g. Ahmed et al., 2004; Grosz et al., 2004; Saunders et al., 2005; Mukherjee et al., 2012), which re-emphasized the existence of some regional-scale geochemical process.

More recently, Mukherjee et al., 2015, studied the known global arsenic distribution pattern and suggested the occurrence of a large scale geological process linked to the origin of arsenic. They hypothesized that hydrothermal-genic deposits in orogenic belts may act as primary provenance for the As-laden sediments that are transported into foreland basins by wind, glacial erosion, and/or streams, which serve as modern-day aquifers, where the sediments release arsenic into groundwater by water–rock interaction during various biogeochemical processes under conducive hydrogeochemical conditions.

Verma et al. (2016) proposed a generic model of geologic controls on arsenic distribution for the upper Brahmaputra Basin and attributed the high arsenic concentration to the crustal evolution process through which arsenic is subsequently mobilized from aquifer matrix to groundwater through water –sediment reactions under favorable biogeochemical conditions.

2.9 Geomorphic controls on spatial distribution of As

Geomorphic controls on arsenic distribution in the Bengal Delta Plain has been widely reported (Weinman et al., 2008; McArthur et al., 2004; Sahu and Sukhla, 2013; Sahu and Saha, 2015). Studies in the Middle Ganga Plains and elsewhere in the Mekong and the Bengal basin have demonstrated specific links link between geomorphic features and the arsenic (Papacostas et al., 2008; Sahu and Saha, 2015; Stahl et al., 2016;). The bewildering degree of spatial variability observed from a few meters to several hundred meters have been linked to localized geomorphic units and near surface geology (Khan and Hoque, 2002; Hoque et al., 2009; Sahu and Saha, 2015). Of the different geomorphic units discernable in a fluvio deltaic set up, natural levees and bars, which represent elevated parts of the floodplains, are reported to host arsenic safe aquifers while, meandering thin levees with low

elevation and lithologies dominated by fines are reported to host high arsenic groundwater (Weinman et al., 2008; Sahu and Saha, 2015).

Weinman et al., (2008) demonstrated that spatial arsenic heterogeneity in the shallow aquifer of Araihazar, Bangladesh is associated with floodplain evolution. They reported that depositional features viz. bars and levees formed under high energy braided channel conditions host low As aquifers while features viz. levees formed under low energy meandering stream conditions host high arsenic aquifers, owing to their thicker and fine-grained floodplain cap. Weinman et al., (2008) further emphasized that the relationships between arsenic in shallow and near-surface geology and geomorphology indicate a level of predictability that is relevant at the village scale.

McArthur et al. (2011) suggested that lateral heterogeneity exists because As is confined to Holocene aquifers of paleo-channels while it is absent in Pleistocene aquifers of paleo-interfluves. The formation of these geomorphic features was linked to sea level changes during the Late Quaternary period and because of that Pleistocene aquifers were flushed extensively of their dissolved constituents while Holocene aquifers were not (BGS/DPHE, 2001).

Sahu and Saha, (2015) associated arsenic variability in the Middle Ganga Plains to the different sediment types in the floodplain of the meandering Ganges River. Donselaar et al., (2017) recently produced a generic spatial aquifer architecture model for the release and accumulation of arsenic in fluvial flood basins. They concluded that the anoxic hypolimnion waters and the clay plugs are the loci of microbial respiration that triggers reductive dissolution of iron oxy-hydroxides and the release of arsenic. Juxtaposed point bars in fluvial setting accumulate arsenic by permeability contrast and poor aquifer-flushing efficiency.

2.10 Immobilization of Arsenic in the Environment

Arsenic sorption to solid phases has been proposed as a principal control on its mobility which can transfer soluble or mobile arsenic to particulate phases, thus immobilizing it (Wang and Mulligan, 2006). Sorption behavior of natural and experimentally developed minerals has been extensively studied to elucidate their arsenic attenuation potential (Stollenwerk et al. 2007, Dousova et al., 2012). It has been established that immobilization of arsenic in natural solids depends on the presence of hydrated oxides and/or hydroxides of Al, Mn, and especially Fe (Manning et al., 1998; Randall et al., 2001; Sherman and Randall,

2003). Adsorption behavior of arsenic on naturally available solids and laboratory generated adsorbents has been extensively studied to see their capacity for arsenic retardation and natural attenuation (Chakraborty et al., 2014). In Bangladesh, Radloff et al. (2011) have shown that arsenic migration from shallow to deeper aquifers can be significantly influenced by adsorption on aquifer sediments. Measurements of distribution coefficients (K_d) of arsenic on aquifer sediments has been made by several researchers to see the potential arsenic mobilization in aquifers (Stollenwerk et al., 2007; Nath et al., 2009; Itai et al., 2010; Jessen et al., 2012, Robinson et al., 2011; Sharif et al., 2011, Rajapaksha et al.,2011).

2.11 Isotherm studies

The two empirical models most frequently used to describe heavy metal adsorption in soils and on soil components are Freundlich and Langmuir isotherms models (Mouni et al., 2009). Simplicity and easy interpretability are some of the reasons for extensive use of these models (Hafeznezami et al, 2016). The Langmuir equation is based on the assumption that only monolayer surface layer exists, adsorption takes place at independent sites and adsorption sites are equivalent, while Freundlich equation assumes a multilayer adsorption (Hafeznezami et al, 2016). Isotherms are of limited use in describing geochemical systems as they do not include any information on the structure of adsorbed species, which is one of the important aspects determining species reactivity (Koretsky, 2000; Apello and Psotma, 2005).

2.12 Kinetics of As adsorption

The rate of metal sorption is affected by the type of soil components (Sparks, 1999). Sorption reaction can involve physical sorption, outer sphere complexation (electrostatic attraction), inner sphere complexation (ligand exchange) and surface precipitation and can occur on time scales of microseconds to months (Sparks, 1999; Apello and Postma, 2005).

Various kinetic models viz. Pseudo First Order kinetic model, Pseudo second order kinetic model, inter particle diffusion models have been used to test their validity with the experimental adsorption data.

2.13 Surface Complexation Model (SCM)

In Surface Complexation, ions are drawn near and held at the mineral surface by electrostatic forces (Miller, 2001). The ions can be held electrostatically, surrounded by water molecules in a diffuse layer near the oxide surface (outer-sphere complex), or lose the water molecules

and covalently bond with the oxide directly, or through a ligand exchange process (inner-sphere complex) (Hemond, 1995). As^{3+} and As^{5+} ions form inner sphere complexes (Manning and Goldberg, 1996; Manning and Goldberg, 1997; Manning et al., 1998). Sorption reactions at metal oxide surfaces, which ubiquitously dominate aquifer geochemistry, are fully describable using surface complexation theory (Manning and Goldberg, 1997; Manning et al., 1998, Goldberg, S. 1998; Smith and Jaffe, 1998). Therefore, quantification of aquifer geochemistry depends on quantification of surface complexation reactions.

Surface complexation model (SCM) are used widely as equilibrium based approach to describe and predict metal cation and anion sorption reactions on surfaces of reactive phases in soils such as oxide and clay minerals (Stumm, 1992; Appelo and Postma, 2005). Electrostatic forces draw ions to a solid where they may chemically bond to the surface (Stumm, 1992; Davis et al., 1998). Fundamental sorption reactions that take place at the metal oxide surface are fully describable by surface complexation theory (Dzombak and Morel, 1990; Goldberg, 1988; Koretsky, 2000; Sposito, 1989). The most prominent As attenuation reaction is surface complexation reaction with hydrous metal oxides (Langmuir, 1997; Miller, 2001; Sracek et al., 2004; Robinson et al., 2011; Sharif et al., 2011). The complexity of soil materials and their surface site heterogeneity hinder the direct identification of the most active mineralogical and organic components. Thus, the determination of "intrinsic" stability constants for molecular-scale metal sorption reactions and estimation of surface site densities for sorption site is problematic (Davis et al., 1998).

SCM are fundamentally based on chemical and physical principles that are controlled by measurable parameters such as specific surface area, surface site-density, electrical and chemical potentials of the surface, and intrinsic surface constants associated with reactive surface sites and adsorbate ions etc. (Davis et al., 1998; Miller, 2001). Component additivity (CA) approach is used in SCM, where it is assumed that the surface of adsorbent is composed of a mixture of mineral phase whose properties are known from studies of the individual phases (Davis et al., 1998; Sracek et al., 2004; Sharif et al., 2011). CA approach assumed that one mineral phase dominates adsorption, which facilitate a direct equilibrium calculation if the exposed surface area and surface-site density of the particular mineral phase in the soil or sediment can be quantified (Davis et al., 1998).

Surface complexation models (SCM) use the law of mass action, expressed as an equilibrium constant, to define protonation (Ks+), deprotonation (Ks-) and ion-specific sorption to a

surface (K_{int}). To implement SCM in PHREEQC the sorption constants must be known for each mineral phase and ion modeled. Central of SCM approach is that protonation and disassociation reactions and ion-specific complexation constants are reversible and apply over a range of pH and ionic strength conditions. The equilibrium constants Ks^+ and Ks^- are determined for protonation-deprotonation reactions at the oxide surface. The protonation reaction with surface, S, are described by two steps reversible process below:

$$K_{S^+} = \frac{[SOH_2^+]}{[SOH][H^+]} exp \frac{(F\psi_\circ)}{RT}$$

$$K_{S^-} = \frac{[SO^-][H^+]}{[SOH]} exp \frac{(-F\psi_\circ)}{RT}$$

where *F* is the Faraday constant ($9.65x10^{-4}$ coulomb/mole), ψ_o is the surface potential in volts, R is the universal gas constant, and T is the absolute temperature. This exponential electrostatic term appended to the standard form of the equilibrium mass-action equation is used to account for the change in surface potential because of the adsorption of the modeled ion.

With changing pH, K_{S+} and K_S-, the equilibrium constants, allow surface sorbing properties to change. Constants for specific sorbing ions that meet these constraints are referred to as "intrinsic constant" or K_{int}. In order to apply these models to SCM, K_{int} for surface reactions must be known for each surface to be used, each sorbing ion, and each site defined on the surface.

Each protonation state of an oxyanion has a unique K_{int}. For example, K_{int} for Diffuse Layer Model (DLM) surface complexation models have the following forms for arsenate sorbing to a single site:

$$K^1_{As_{int}} = \frac{[SH_2AsO_4]}{[SOH][H_3AsO_4]}$$

$$K^2_{As_{int}} = \frac{[SHAsO_4^-][H^+]}{[SOH][H_3AsO_4]} exp \frac{(-F\psi_\circ)}{RT}$$

$$K^3_{As_{int}} = \frac{[SAsO_4^{2-}][H^+]^2}{[SOH][H_3AsO_4]} exp \frac{(-F\psi_\circ)}{RT}$$

The electrical layer geometries of the model differ, but they all reduce to mass action equations that are solved numerically. With respect to broad multicomponent modeling proposed here, the most important part of the commonality and formulation among the SC models is the universal application of the mass law constraint. Mass law formulation allows the sorption reactions to be used in existing theoretical and mathematical framework of thermodynamic equilibrium models. Surface complexation reaction become part of the general mathematical solution of an equilibrium state between an aqueous solution and a solid sorbing phase.

2.14 Current and Emerging status of different mitigation strategies

Mitigation initiatives to ensure safe drinking water supply among affected communities are designed largely based on understanding gained from previous studies. Mitigation strategies undertaken largely include piped water supply schemes, rain water harvesting, installation of dug wells, installation of deep tube wells and distribution of community based filters (Jakariya et al., 2007**;** Biswas et al., 2013). However, the success of these strategies are largely jeopardized because of lack of community acceptance triggered by technical , economic and social constraints (Ahmed et al., 2006; Jakariya et al., 2007, Nath et al., 2008; Johnston et al., 2010, Biswas et al., 2014). Being culturally linked to using groundwater from tubewells in premises, the use of alternative drinking water sources viz. water from community based deep tubewells and piped water supply from community distribution points are often seen to be compromised (Johnston et al., 2010). Furthermore, it is worth to note that in rural areas, collection of water of domestic purpose is a gender concern, with water being collected primarily by the women (Singh et al., 2005). Collection of water from deep tube wells thus adds immensely to the workload of the women folks (von Brömssen, 2012). These facets largely alter the affects. Thus, to achieve sustainable safe drinking water worldwide and meet the global Sustainable Development Goals (SDG) goal 7, it becomes important to delineate the sustainability of arsenic free safe aquifers and to see how locally available practices can be promoted for achieving safe drinking water.

Few recent studies have scrutinized the ongoing indigenous drilling practice by local drillers in rural Bengal and attempted to correlate aquifer sediment color with the occurrence of As in groundwater (van Geen et al., 2003; von Brömssen et al., 2007; Pal and Mukherjee, 2008;

McArthur et al., 2011; Pal and Mukherjee, 2009; Bundschuh et al., 2010). It is reported that grey sand aquifers (GSA) are mostly contaminated with dissolved As (>10 µg/L), whereas brown sand aquifers (BSA) maybe safe (<10µg/L) (eg. von Brömssen et al., 2007; McArthur et al., 2008, 2011). Consequently this BSA has been proposed as an alternative drinking water source, which can be targeted by locally available cheap drilling technology (von Brömssen et al., 2007; McArthur et al., 2011). With an aim to facilitate targeting low-arsenic aquifers, Bromsson et al., 2007, studied sediment colors and redox conditions of the aquifer sediments. Their study suggested that low-As groundwater from the oxidized unit were either because the redox status of the studied sediments were higher, hence reductive dissolution of Fe(III)-oxyhydroxides did not yet result in super saturation of adsorption sites for As or because the As content in the reducible fraction is low. To evaluate the sustainability of oxidized reddish sediments as potential source of low dissolved arsenic, Bromsson et al., 2008 further, described the lithofacies and genesis of the sediments within 60 m depth and established a relationship between aqueous and solid phase geochemistry. Equilibrium modeling based on saturation indices suggested that the concentrations of dissolved Fe, Mn and PO_4^{3-} total in groundwater was influenced by secondary mineral phases in addition to redox processes. Simulating As(III) adsorption on hydro ferric oxides using the Diffuse Layer Model and analytical data gave realistic concentrations of dissolved and adsorbed As(III) for the reducing aquifer and they speculated that the presence of high PO_4^{3-} tot in combination with reductive dissolution resulted high- arsenic in groundwater.

More recent studies have recommended sediment color tool developed on the basis of perception of the sediment color by the local driller's and monitoring of water quality for targeting arsenic safe drinking water (SASMIT, 2014; Hossain et al., 2017). However, such initiatives are to be backed with regular surveillance and monitoring along with bringing local driller's under a regulatory framework which will make them more responsible to target safe water sources during tubewell installation practice (Hossain et al., 2017).

Studying the role of subsurface distribution of palaeo-channel sediments (As-polluted groundwater) and palaeo-interfluvial sediments (As-free groundwater) in providing safe drinking water, Hoque et al., (2012) gave the paleosols model of arsenic distribution. The paleo-interfluvial sequence, which occurred as three distinct units that together occupied 20 km of the studied traverse, yielded As-free groundwater from brown sands at depth<100 m. Their study also highlighted that well-color can be used both to successfully predict the

degree of As-pollution in groundwater, and to locate regions of buried palaeo-interfluve that will yield As-free groundwater for the foreseeable future.

In a recent study by van Geen et al (2013), attempts have been made to study the effects of retardation on arsenic transport through a Pleistocene aquifer in Vietnam and hence its sustainability. Pleistocene aquifers are increasingly being used as a safe source of drinking water; therefore the need to understand the conditions under which the low arsenic can be maintained is important. Reconstructing the initial phase of contamination of a Pleistocene aquifer near Hanoi, the group demonstrated that changes in groundwater flow conditions and redox state of aquifer sands induced by groundwater pumping caused lateral intrusion of arsenic contamination more than 120 m from a Holocene aquifer (with high arsenic concentrations) into a previously uncontaminated Pleistocene aquifer. However, the group also reported that due to the adsorption of arsenic on the aquifer sands, there is 16 to 20 fold retardation in the extent of the contamination relative to the reconstructed lateral movement of groundwater over the same period.

Deeper aquifers which were once believed to be viable source of safe drinking water (Mukherjee et al., 2008) are now reported to be under threat due to intensive pumping (Erban et al., 2013) . To study the sustainability of deeper aquifers, Radloff et al., 2011 studied the influence of adsorption behavior and water demand on arsenic migration into deeper aquifers. Simulations using present and future scenarios of water use suggested that arsenic adsorption significantly retards arsenic transport, thereby extending the area over which deep groundwater can be used with low risk of arsenic contamination. Based on their study, Radloff et al., 2011suggested that based on vulnerabilities to arsenic intrusion, monitoring for sustaining the deeper low arsenic aquifers are to be prioritized.

Studying the long term viability of deeper aquifers, Erban et al., 2013, have linked arsenic release to deeper aquifers to pumping-induced land subsidence. Analyzing a large area (>1,000 km^2) of the Mekong Delta, Vietnam, in which arsenic is found pervasively in deep, Pliocene–Miocene-age aquifers, where nearly 900 wells at depths of 200–500 m are contaminated, they have linked the contamination to abstraction induced land subsidence. They have reported that deep groundwater extraction has caused interbeded clays to compact and expel water containing dissolved arsenic or arsenic-mobilizing solutes (e.g., dissolved organic carbon and competing ions) to deep aquifers over decades thus posting a severe threat to the long term sustainability of the deeper safe aquifers.

Hence, before advocating for targeting safe aquifers it is necessary to investigate regional distribution and subsurface geologic architecture at different geographic locations. It is important to develop site specific strategies to ensure safe and sustainable and affordable solutions to affected communities. Natural options with little to no maintenance costs should be preferably explored. With some exceptions, deep aquifers (below 120 m) could supply almost As-free (<10 µg/L) water (Ahmed et al., 2004; Michael and Voss, 2008). However, the safety, sustainability and sufficiency of these aquifers have not yet been rigorously assessed. Aquifers composed of oxidized sediments have been reported to naturally attenuate As and thereby produce safe water (Stollenwerk et al., 2007; Robinson et al., 2011). It is thus necessary to undertake detailed hydrogeochemical investigation along with solid liquid phase partitioning behavior to constrain the underlying reason for the occurrence of low dissolved As in groundwater of brown sand aquifers that can highlight its long term sustainability for safe drinking water supply.

Chapter 3

Study Area, Hydrogeology, Geology, Environmental Condition

3.1 Brahmaputra Basin: Tectonic Setting

The study area being sandwiched between two important tectono-sedimentary regimes, i.e Himalayan foreland and the Indo Burma Ranges (Figure 3.1), brief knowledge of various stratigraphic sequences and tectonic features of Brahmaputra Basin is a prerequisite to understand the geological setting of the study area which could have a strong influence on the groundwater quality of the area. The complex tectonic setting of the region is manifested by the north-eastward movement of the Indian plate along the Himalayan arc and the east –west convergence along the Indo – Burma fold thrust Schuppen belt (Nandy, 2000). Major tectonic discontinuities that mark the Himalayas include the Tsangpo Suture (TS), main Central Thrust (MCT) and the Main Boundary Fault (MBF). Six longitudinal lithotectonic units juxtaposed along generally north-dipping thrust faults mark the Himalayas (Le Fort, 1996), which from north to south, are: (1) Trans-Himalayas consisting of calc-alkaline plutons; (2) Indus suture zone, exposing ophiolitic bands representing the zone of collision between India and Eurasia; (3) Tibetan Himalayas, represented by fossiliferous Cambrian to Eocene sediments; (4) Higher Himalayas, located north of the Main Central Thrust, composed of schists, gneisses, and leucogranites; (5) Lower or Lesser Himalayas, composed of unfossiliferous Precambrian and Palaeozoic sedimentary rocks, and crystalline rocks; and (6) Sub-Himalayas, representing Miocene to Pleistocene molasse-type deposits of the Siwaliks (Uddin et al., 2007). Early tertiary synorogenic sediments, with turbidites and schists along with the Naga Opiolite belts mark the north-south trending Indo-Burman Ranges. Apart from the Himalayas and the Indo-Burma thrust belt, other important tectonic features that mark the Brahmaputra River Basin in Assam and dominated by crustal materials of pre-Gondwana landmass are the Mikir Hills, the Shillong Plateau and the Mishmi Hills (Uddin et al., 2007). These tectonic features in turn adds uniqueness to the upper Brahmaputra Basin in Assam.

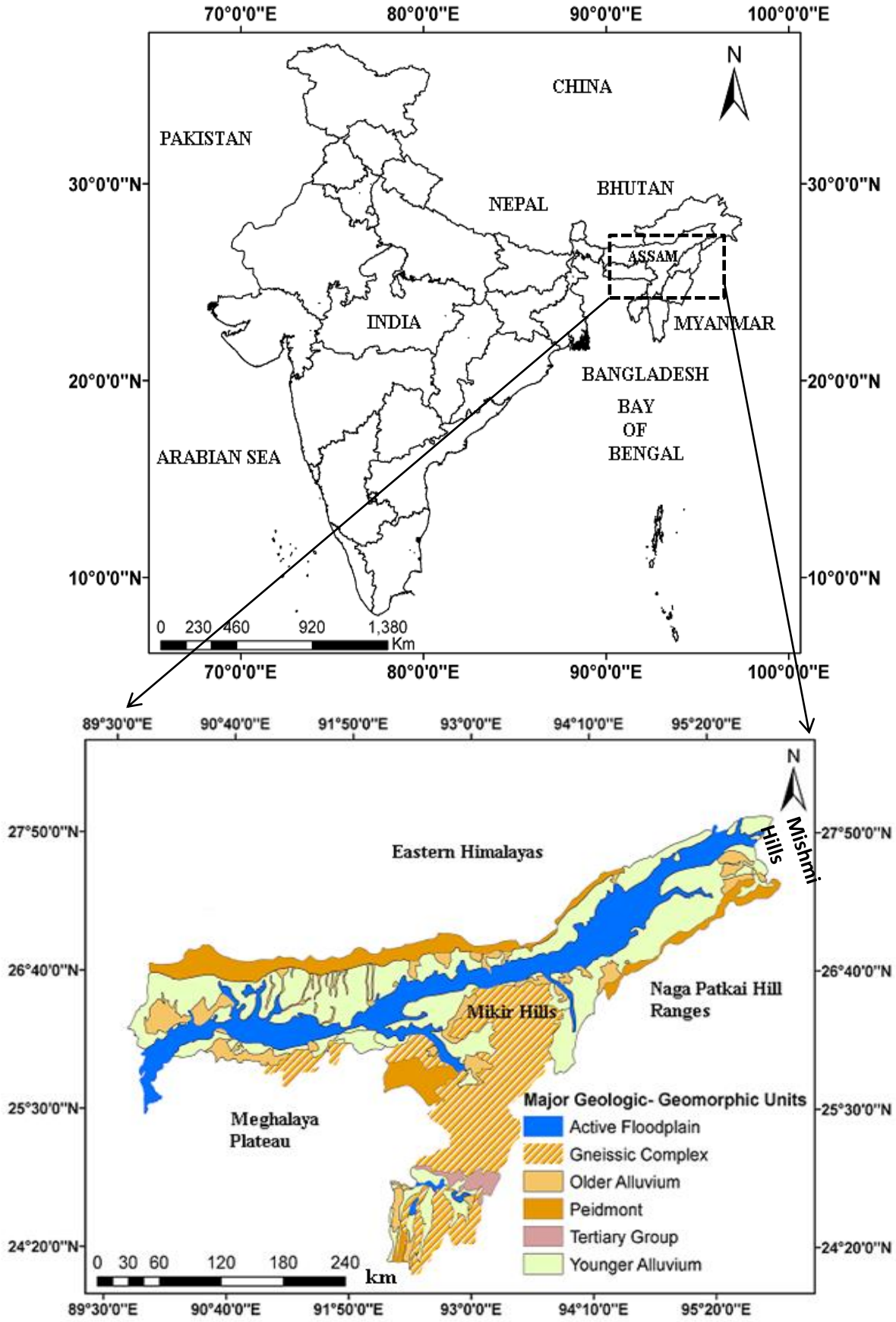

Figure 3.1 Geological base map of Assam showing the different geological formations (modified from Geological Survey of India)

3.2 Geology and Hydrology

Several workers have reported the evolution, morphology, sedimentology, channel change and related hydraulic processes of the Brahmaputra Basin and the Brahmaputra River in particular (Bristow 1987; Goswami, 1985; Goswami, 1988a; Goswami, 1988b; Coleman, 1969; Galy and France-Lanord, 2001; Garzanti et al., 2004). Geologically, the Brahmaputra Basin in Assam is bordered by the eastern Himalayas on the north and east, the Naga Patkai Hill ranges on the northeast and the Precambrian rocks dominated Mikir Hills and Shillong Plateau on the south (Sharma, 2005). The alluvial plain of Assam abuts against the Siwaliks of the Himalayas on the northern side, while the southeastern side of the alluvial plain abuts against the Tertiary rock sequences occurring in Naga Patkai Hill ranges consisting of dark grey shales, sandstones and shales with coal seams, thin conglomerates, ferruginous sandstones and mottled clays, soft sandstones, clays and conglomerates, thick pebble beds, thin clays and sand (Figure 3.2) (Sharma, 2005). Sandwiched between the eastern syntaxis of the Himalayas and the northern end of the Indo-Burman Ranges, the basin received synorogenic sediments of several kilometers thick from these orogenic belts, which preserves a more or less continuous record of the orogenic events (Uddin et al., 2007). Alluvial and floodplain sediments carried by the Brahmaputra main channel and its tributaries from adjoining Himalayan and Naga Patkai Range provenance, described as younger sediments dot the plains along with the older alluvium of Quaternary and Tertiary ages (Evans, 1932 and Mathur and Evans, 1964).

Globally, the Brahmaputra is the main carrier of the erosion products of the central and eastern Himalayas, its current erosion rates estimated to be ˷ 2.9 mm/ year (Galy and France, 2010; Galy and France Lanord , 2001). The numerous tributaries that drain the key tectonic features discussed above are the provenance source of these sediments. Northern tributaries of the Brahmaputra primarily drain the Himalayan metamorphic rocks, while a few major tributaries (vz. Subansiri, Kuru) have their headwaters in the Tethyan Himalayan sedimentary zone of south Tibet (Garzanti et al 2004). The eastern tributaries of the Brahmaputra (Lohit, Dibang) drain the Mishmi Hills, which include a calc-alkaline diorite-tonalite-granodiorite complex and tholeiitic metavolcanic rocks of island arc affinity, along with further cutting through the Tidding suture which includes chlorite-schists, amphibolites, serpentinites and metacarbonates, and finally across the easternmost continuation of the Himalayan belt (Grazanti et al., 2004; Kumar, 1997). Two extremities exists in the sediments carried by the eastern rivers, the plagioclase-rich Lohit sand consisting of metapsammite, metabasite, and

limestone grains, along with blue-green hornblende and epidote, indicating provenance chiefly from Mishmi arc plutons and amphibolites, and the feldspar-poor Dhansiri sand largely consisting of shale/siltstone to slate/metasiltstone grains from accreted turbidites of the Indo- Burman Ranges (Grazanti et al., 2004). Southern tributaries of the Brahmaputra (Buri Dihing, Dhansiri, Kopili) drain the outer part of the northern Indo-Burman Ranges which includes Cretaceous/Eocene pelagic sediments overlain by thick Eocene/Oligocene turbidites associated with ophiolitic allochthons (Sengupta et al., 1990).

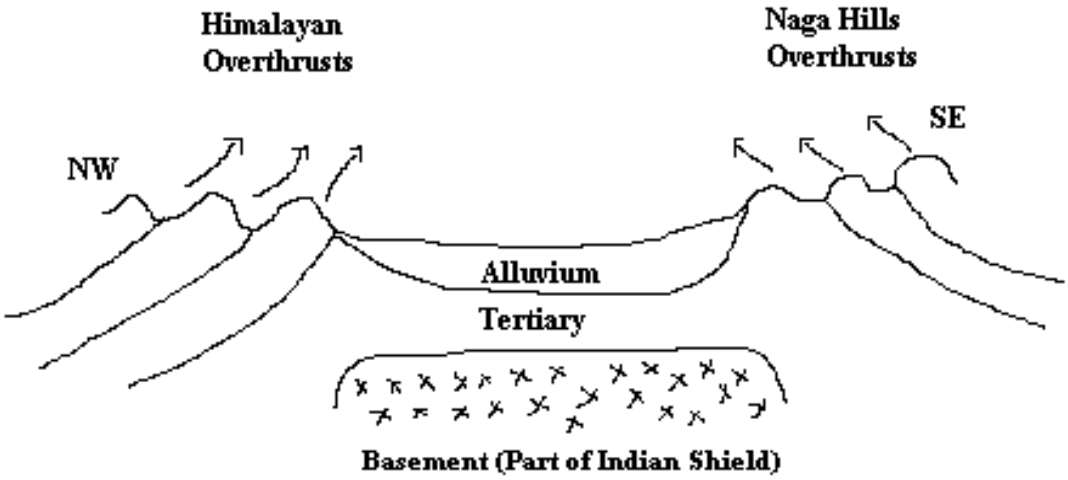

Figure 3.2 Sketch section across Upper Assam (modified from Mathur and Evans, 1964)

3.3 Geomorphology

Geomorphologically, three different geomorphic units dominate the Basin: depositional, denudational and structural, of which the depositional unit, which is of fluvial origin, includes floodplain deposits, younger alluvial plains, older alluvial plains, upper piedmont plain, lower piedmont plain and valley-fill areas. The Brahmaputra main channel undergoes changes in response to variations in the flow regime, pattern of sediment transport, and neotectonics. Continuous shifting of the thalweg from one location to another takes place within the banklines and the river exhibits a braided channel pattern with temporal changes in bankline location as well as channel configuration (Sharma, 2005). Recently, Lahiri et al., (2014) reported significant difference in fluvial dynamics of the tributaries of the Brahmaputra River in upper Assam valley, with northern tributaries being marked by frequent avulsions (mostly westward) and meander migration being more frequent in the southern tributaries.

3.4 Sedimentology of the alluvial aquifers

The Brahmaputra basin in Assam is underlain by a 200 – 300 m thickness of recent alluvium (Mahanta and Subramanian, 2004). The alluvial soils can be divided into two main sub types- young alluvial and old alluvial soils (Talukdar et al, 2004). The alluvial sediments of the Brahmaputra comprise of silt, clay, sand and gravels (CGWB, 1995). The recent alluvial soils carried by the rivers are light grey to dark grey in colour and are confined to the flood plain area adjacent to the Brahmaputra River and its tributaries. The older alluvial soil is sandy loam to silty and clay-loam characterized by light yellowish brown to light brown colour (CGWB, 2008). These alluvial soils are characterized by organic matter and available phosphorus and low potash. The soils in the southern part are residual in origin, derived from the semi-consolidated rocks underlying these areas. Brought down by the Brahmaputra and its numerous tributaries draining the Himalayas, these materials act as arsenic sink in the floodplain areas (Singh, 2004). Similar lithologic set up of the Brahmaputra Floodplain in Bangladesh comprising of alluvial silt and clay, peat and clay units have been reported to be some of the highly arsenic affected areas in Bangladesh (Reza et al., 2010). The dominant hue of the colour of the soils of the Brahmaputra basin is 10YR, with a change of greyness of the soils of the eastern part of the basin to yellowish brown along with reddish mottles in the western part of the basin (a characteristic feature of the soil colour of the Brahmaputra Basin) (Talukdar et al., 2004). Based on the characteristic features of drainage, wetness and chemical processes associated, soil colour may vary within locations (Talukdar et al., 2004).

3.5 Study Transects

To seek answers to the proposed objectives, a transect based approach was adopted, where two representative transects, viz. the northern transect sandwiched between the Eastern Himalayas and the Brahmaputra River and the southern transect straddled between the Naga Patkai Hill Ranges in the south and the Brahmaputra River in its north were chosen. The study area bears significance being located in a homogeneous alluvial terrain which is the direct pathway of sediment transfer from the Himalayas and the Naga Patkai Hill Ranges to the floodplain of the Brahmaputra River.

3.5.1 Northern transect

The 55 km northern transect (covering the districts viz. Darrang and Udalguri Districts), forms a major part of the northwestern parts of the Brahmaputra river basin in Assam (Figure 3.3). Tectonically, the transect is the eastern continuity of the Indo-Gangetic-Brahmaputra

foreland basin of the Himalayas, and is bounded by the eastern Himalayas in its north and Brahmaputra River to the south (Figure 3.3). The topography is characterized by almost flat plains and higher elevated flat uplands along the foothills of the Himalayas (ARSAC 1990). Sedimentation in the study area occurs through the materials carried down by the northern tributaries of the Brahmaputra viz. Dhansiri, Noa Noi, Noa Nadi etc. and the Brahmaputra main channel. The major tributaries of the Brahmaputra in the study transect flow through the strongly deformed Lesser Himalayan metasediments, composed of Precambrian limestone, dolostones, shale, quartzite and schists, along with gneisses and dolerite sills (Garzanti et al., 2004).

3.5.2 Southern transect

The southern transect is a 35 kms transect covering three districts in Assam viz. Dergaon, Golaghat and Titabor, where a distinct pattern of groundwater arsenic distribution from high to low arsenic concentrations were observed from the outcome of the Arsenic Screening and Surveillance program in Assam (Figure 3.3) (Mahanta et al., 2015). The transect forms a part of the Upper Assam foreland basin. The land surface of the site is characterized by a depression followed by a slight elevated area comprising of sandy loamy soil type characteristic of tea garden areas. A topographic gradient of 10 to 12 m is observed along the 35 mts transect. The Brahmaputra River bounds the northern boundary while the Naga Patkai hill ranges bounds the southern extrimity of the study transect, the two rivers viz. Dhansiri and Bhogdoi flowing from the Naga Hills marking the western and eastern extremities of the study area. The southern tributaries, the Burhi Dihing, the Dhansiri and Kopili drain through turbidites similar to those in Siwaliks, the Indian Plate and ophiolites (Singh et al., 2006).

Geophysical survey conducted by Oil India Limited gives us a detailed account of the structural and depositional history of the basin (Sahoo and Gogoi, 2011). The generalized structure inferred from seismic surveys indicates that the Assam plains form a broad arch at the basement level with its apex in the region of the present Brahmaputra river course and sloping towards the Himalayan foot hills in north and Naga Hills in the south. This arch is dissected by a number of faults with a general strike of NE-SW or ENE-WSW trend parallel to the fault pattern observed in the Mikir hills metamorphic complex and also parallel to Naga thrust (Ray et.al., 1983). Irregularities in the basement surfaces known from gravity survey and differential movement along these faults control the structural pattern in the sedimentary cover.

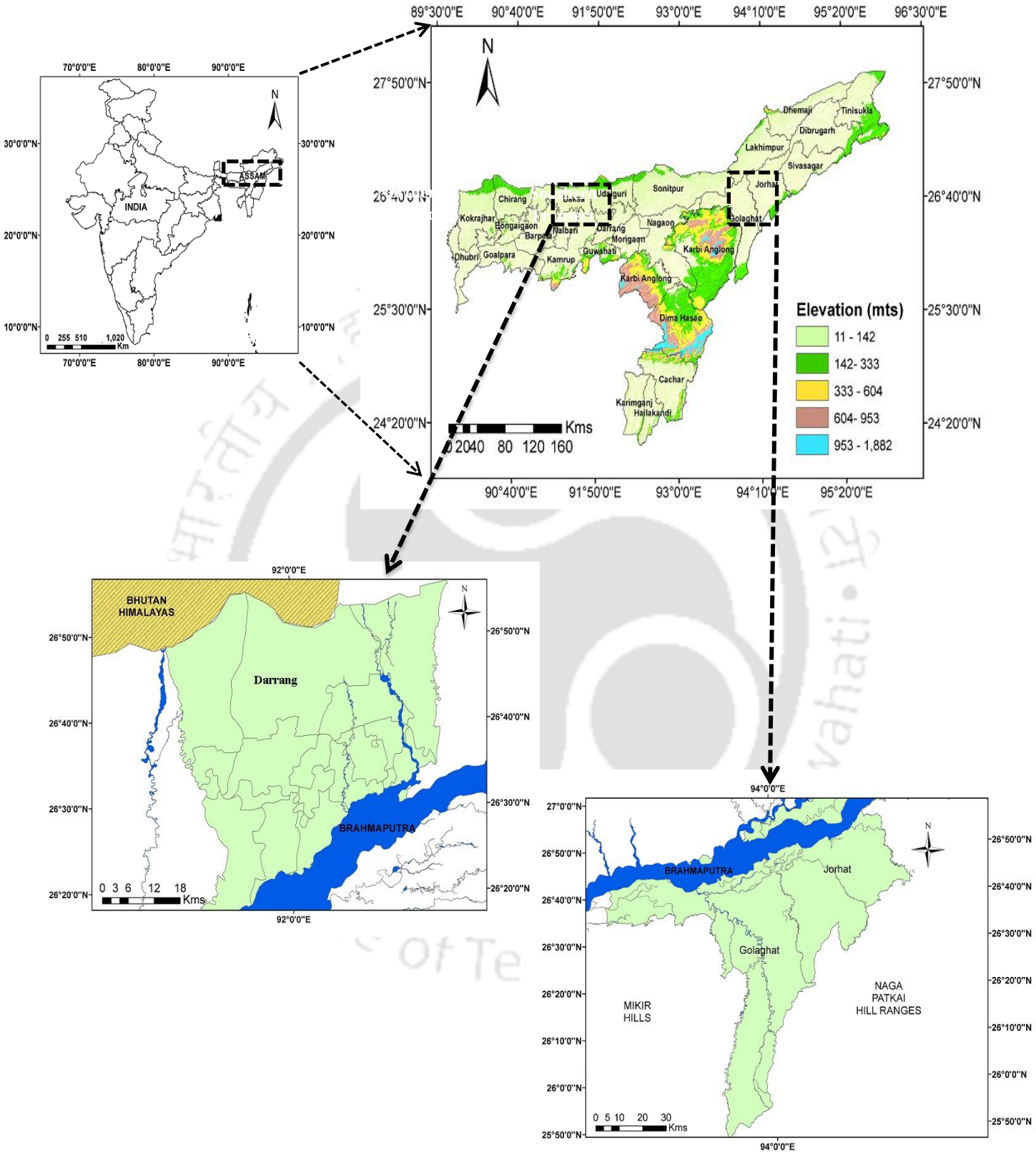

Figure 3.3 Map of the study area showing location of the selected transects, (a) Northern Transect (b) Southern Transect

3.6 Geological setting

Major parts of the northern transect is covered by thick deposits of unconsolidated sediments, except in the south eastern part where few isolated hillocks consisting of gneissic rocks are exposed (Table 2). Both new and old alluvial sediments are found along the transect. The study area lies in the new alluvial plains, which are found in the active floodplains bordering the Brahmaputra River and older alluvium which are found further away from the active floodplains zones (CGWB 2004). The alluvial deposits are more than 200 m to 300 m in thickness except the inselbergs where alluvial thickness ranges between 10 m to 30 m (DGM, 1994). Subsurface geology comprises of beds of unconsolidated aquifer material throughout the district. The eastern part of the district has a thick sand cover ranging between 21 m to 31 m at the top followed by alternate layers of clay sand/gravel zones. The southern part of the district which covers the study area, however, has a thin clay and silt zone present at the top followed by thick sand and gravel zones. Two types of aquifer zones are encountered in the area, (i) Shallow aquifer zone (depth < 50 m below ground level and (ii) Deeper aquifer zones (depth between 50 m to 200 m bgl).

Table 2 Stratigraphic succession of northern transect

Age	Lithostratigraphy	Rock type
Recent	Flood plains	Fine sand, silt and clay
Recent	Alluvial plains	Sand, silt and clay, Gritty sand are present in the north
Quaternary	Piedmont plain	Gravels, pebbles, boulders, sand and silt with minor clay
Mid Miocene	Siwalik group	Boulder conglomerate, sandstone & clay bed. Clay stones and clayed sandstone & hard compacted sandstone
Permo Carboniferous	Gondwana Supergroup	Quartzitic sandstones with coal beds carbonaceous, slate with dolomite boulder, carbonaceous rocks & slate
Precambrian	Duiri group	Boulder slates, slates and some quartzites
Precambrian	Thungsing Quartzite formation	Coarse, gritty feldspathic quartzites with pebbles & conglomerate layers and minor slates and phyllites

The geology along the southern transect can be broadly classified as alluvium except Tiru hills and Disai hills (Table 3). In this area Barail series (Lower Tertiary formation) is found which consist of carbonaceous materials. Crude oil sources are found in association with Barail series in the Borholla region of the district (DGM, 1994b). The geomorphic unit of the study area comprises of younger alluvial plains. It occupies major part of the district and is at slightly higher elevation than the present day flood plain of Brahmaputra River, which is often inundated by floods. The area has gentle slopes towards the north. The soil types mainly consist of sand, silt, clay and gravel. The area is characterized by high recharge, but sometimes clay lenses form aquicludes (ARSAC, 1990).

Table.3 Stratigraphic succession of southern transect

Age	**Lithostratigraphy**	**Unit/ Formations**	**Major Lithological Units**
Recent	Dihing	Alluvium	Unconsolidated sands with clay and lignite sands
Pleistocene	Dhekiajuli		
Pliocene	Dupitila	Namsangs Beds	Poorly consolidated sandstones with clay and lignite sands
		Girujan Clays	Mottled clays with sandstones lenses
Miocene	Tipam	Tipam Sandstones	Arenaceous sequence
	Surma		Arenaceous sequence , sandstones with shale and grit beds
Oligocene	Barail	Not Subdivided	(Upper Part: Mudstone/Shale with sandstone bed and coal bands); (Argillaceous Sequence); (Lower Part: Sandstones with Shale Bands) (Arenaceous sequence)
Eocene	Jaintia	Kopili Alterations	Splintery Shales with sandstone and fine gained sandstones with coal bands
		Sylhet Limestone	Splintery Shales with sandstone and limestone bands
		Therria	Sandstone, calcareous sandstones and limestones
Precambrian	Granitic Basement		Gneisses, schists etc.

Source: Handique et al., 1989

3.7 Hydrogeology

The study areas are located in the younger alluvial plains deposits which covers major portions of the districts. The plain is built by the lower reaches of rivers fanning out from the foothill region, abandon river channel, cut off meanders, natural levees and back swamps (DGM, 1994). Sub surface lithology is mainly dominated by gravel, sand, silt and clay. Groundwater occurs both under confined and unconfined conditions, the water levels varying from 1.1 m to 7.5 m bgl. The floodplains of Brahmaputra occur along the river bank covering 2 km to 7 km from the bank towards the north. The area is inundated during the rainy season and transported materials are deposited all over the area. Groundwater levels in the floodplains vary between 1 m to 3m (Figure 3.4). Older alluvium plains occur as isolated patches in the eastern part of the district, and located at slightly higher elevation.

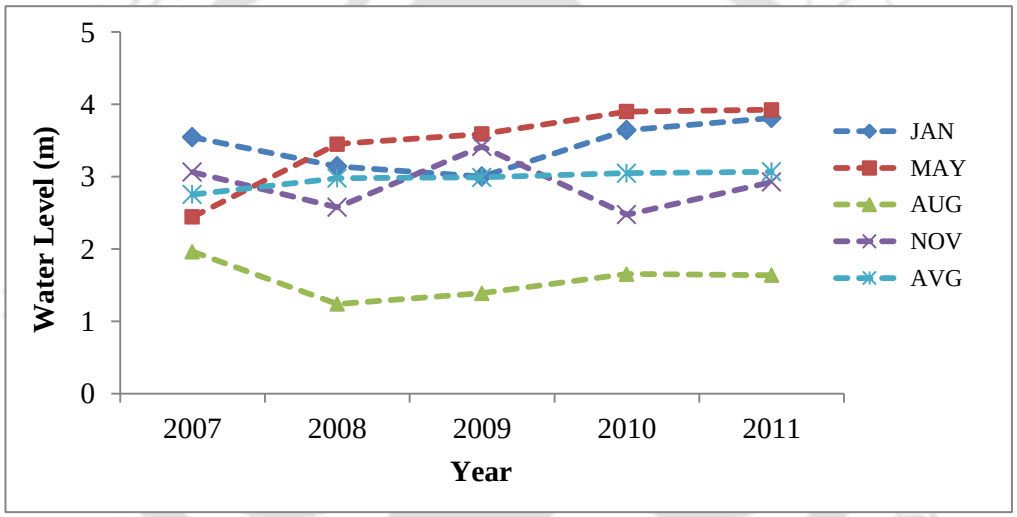

Figure 3.4 Groundwater level fluctuation for CGWB monitored wells in the northern transect (CGWB, 2012)

Along the southern transect, groundwater occurs under both water table to semi confined conditions in the near surface conditions and in the deeper horizons, under semi confined to confined condition. Available sub surface information indicates that three or four prolific system exist down to a explored depth of 300 m, in the central parts. Adjacent to the Brahmaputra River, five to six aquifer systems with limited thickness exist within the depth range of 400 m. In the southern parts, the aquifer system fades out due to mixing of finer particles of sand and clay leading to decrease in thickness of aquifer system. Groundwater levels in areas close to the mountain foothills are observed to vary between 1 m to 2 m, while towards the floodplains the water level fluctuates between 1 m to 4 m (Figure 3.5) (CGWB,

2015). Aquifer geometry varies widely across the district, with increased aquifer thickness and clay sand beds in the northeastern and northwestern parts. Varied thickness of clay beds overlying and underlying the aquifer thickness exists throughout the district. Southwards in Titabor, lying close to the Naga hills, the thickness of the clay beds increases reaching upto a maximum of 103 m (CGWB, 2008).

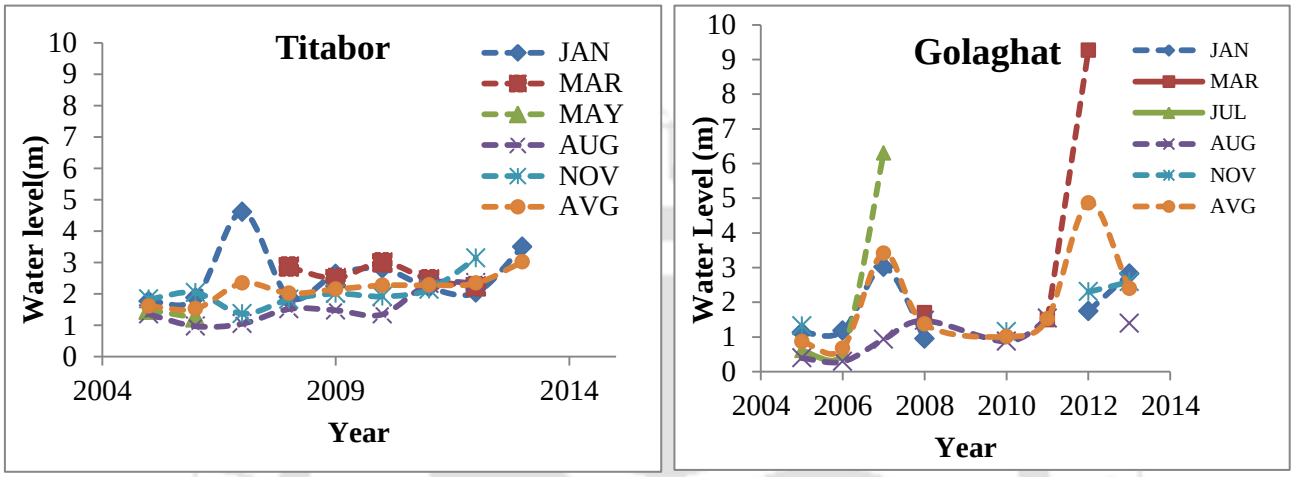

Figure 3.5 Groundwater level fluctuation for CGWB monitored wells in the southern transect (CGWB, 2015)

3.8 Drainage

The mighty Brahmaputra River along with its tributaries controls the drainage system of the entire valley and inundates considerable areas annually. The Brahmaputra River flowing in an east-west direction through the northern extremity of the districts along with its important south bank tributaries viz the Dhansiri, Bhogdoi, Kakodonga drain the districts. These tributaries originating in the Naga Hill ranges flow northwards to reach the Brahmaputra River almost at right angles, giving rise to sub parallel drainage systems.

On the northern bank transect, the Eastern Himalayan tributaries of the Brahmaputra in the Assam Plain drain through granites, gneisses, schists, marbles of the Higher Himalaya; quartzites, dolostones, shales, granites, gneisses and schists of the Lesser Himalaya and the turbidites and Neogene molasses of the Siwaliks. The directions of groundwater flow are strongly influenced by surface topography.

3.9 Landuse and Landcover

Being an agrarian economy, most part of the study transects along both the transect are dominated by agricultural lands. The remaining areas of the district are covered by forest areas and wetlands along with numerous perennial and non-perennial water bodies. Along the southern transect, apart from agricultural crops, tea plantation is a major industry, with several hectares being used for plantation (Figure 3.6-3.7).

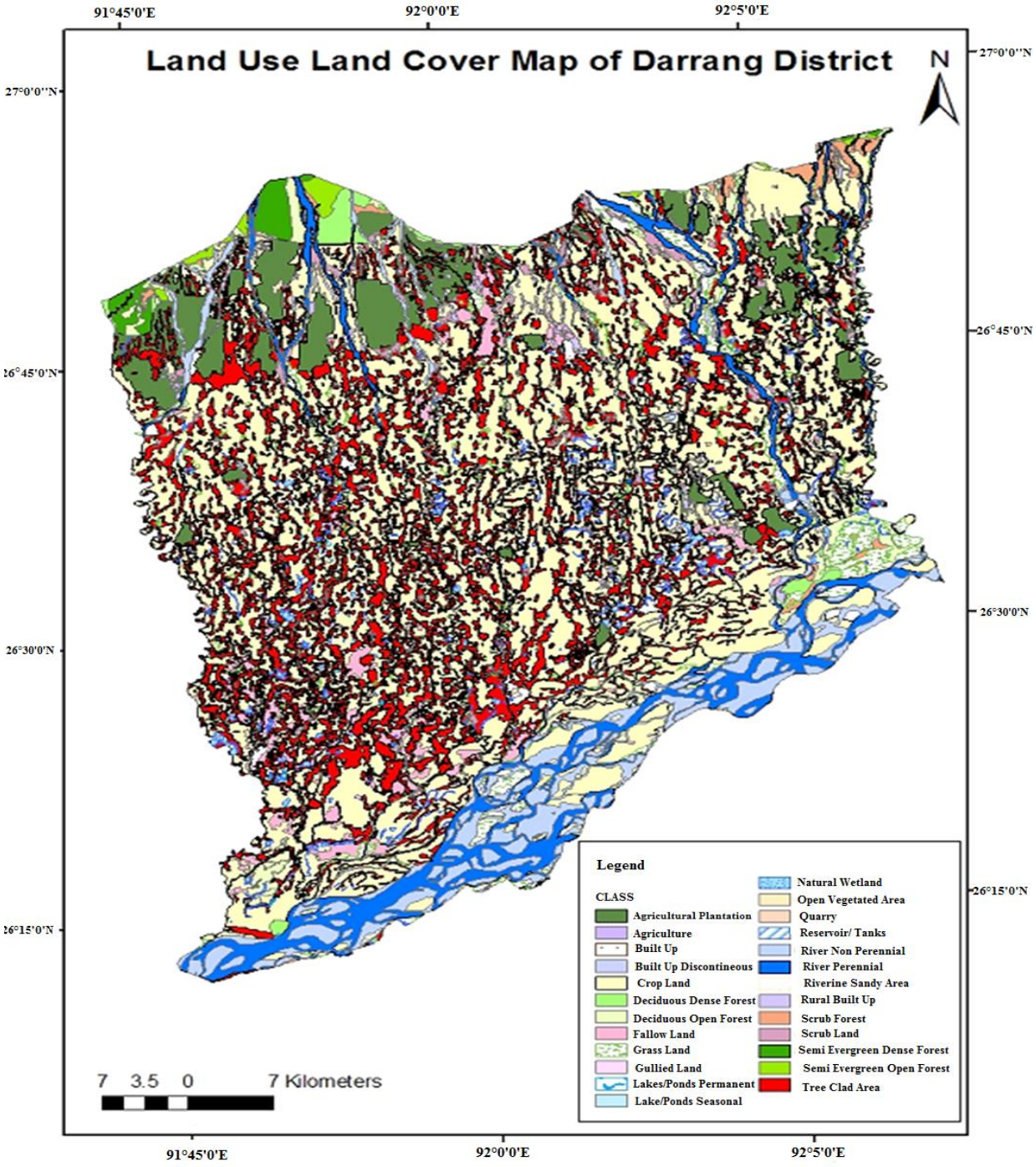

Figure 3.6 Landuse and Landcover along the northern transect

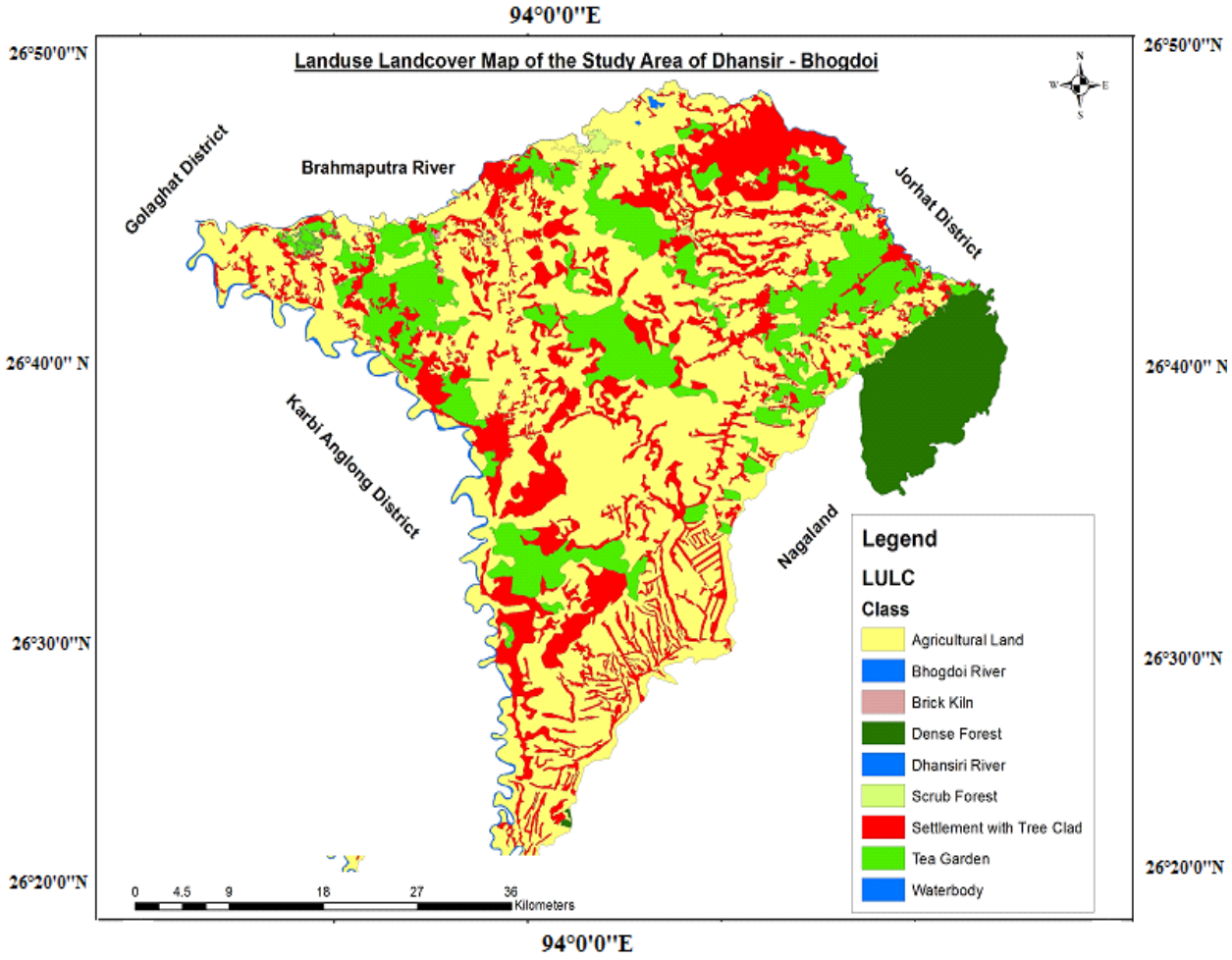

Figure 3.7 Landuse and Landcover along the southern transect

3.10 Previous Investigation

Groundwater As contamination issue in the upper Brahmaputra Basin in Assam is slowly unfolding, and has started gaining serious attention only lately (Table 4). The affected areas are spread over several different geological and geomorphological units. A primary investigation of groundwater arsenic distribution carried out in the previously unexplored upper Brahmaputra river basin revealed large number of areas with elevated groundwater arsenic within the catchment of the braided channel of Brahmaputra River. Primary data revealed that a considerable percentage (29.8%) of the 56,180 sampled wells analyzed have elevated arsenic concentrations above the World Health Organization (WHO) guidelines of 10 µg/L and eight percent of all sampled wells have concentration above the 50 µg/L (Indian permissible drinking water limit) (Figure 3.8) (Mahanta et al., 2015). Accordingly, a large population of more than seven hundred thousand inhabitants of the area, who depends on groundwater for sustenance, are estimated to be exposed to arsenic related health risk. Singh (2004) reported maximum arsenic concentration in Jorhat in the southern bank of the Brahmaputra River in Assam (194-657 µg/L) and in the northern bank (100-200 µg/L), with

varying concentrations in areas like Golaghat (100-200 µg/L) lying in the southern bank and Lakhimpur lying in the northern bank of the Brahmaputra River in Assam (50-550 µg/L). A study conducted by Chakraborti et al (2004) showed that in the two reportedly worst affected districts, Karimganj, in Barak Valley and Dhemaji district in Brahmaputra Valley, 19% of the samples contained higher concentrations than the Indian guideline limit of 50 µg/L, and 2 % samples contained more than 300 µg/L. Based on studies conducted in Darrang and Bongaigaon Districts lying in the northern bank of the Brahmaputra River in Assam, Enmark and Nordborg (2007) reported As concentrations to range between 5 to 606 µg/L. This study for the first time made a comparison between groundwater arsenic concentrations and sediment colour in the upper Brahmaputra Floodplains in Assam. They reported grey sand aquifers hosted arsenic safe groundwater in contrasts to what has been reported from West Bengal, India and Bangladesh, where brown where sediment with red or brown colors generally yield safe As (As <10 µg/L) groundwater (von Brömssen et al., 2007; McArthur et al., 2011). This contrast has been attributed to the dynamics of sediment deposition and flushing rate in the study areas (Mahanta et al., 2015). A study by Chetia et al (2011) in Golaghat District lying in the southern bank of Brahmaputra River reported As concentration ranging between 1 to 128 µg/L in six blocks of the district. Goswami et al., (2013) studied the arsenic mobilization mechanism and health implications in Majuli district, the once largest river island and reported concentrations as high as 100 µg/L. Their study confirmed the presence of As in hair, nail and urine samples and reported the impacts of arsenic manifestations on communities.

A recent study by Baviskar et al., 2015 reported concentration levels as high as 440 µg/L in Jorhat district and reported reductive dissolution of Fe-oxyhydroxides as the key mechanism of arsenic release into groundwater. Subsequently, Choudhury et al. 2015 based on their studies in Nalbari district, lying on the northern bank of the Brahmaputra, reported concentration levels ranging between <10 µg/L to 200 µg/L. Verma et al., 2015 based on their work in three geomorphic terrains in Darrang district reported As concentrations above WHO limits to be mostly concentrated in the older alluvium zones along the runoff zones. High arsenic in older alluvial zones has been suggested to be related to palaeogeomrphology and hydrology, present-day river channel morphology and sediments transportation rates in the Brahmaputra Basin.

Sailo et al., 2015, studied the adsorption capacity of aquifer sediments from one of the highly arsenic affected areas in the southern bank of River Brahmaputra in Assam. Adsorption

capacity of oxidized brown sands with high Fe and Mn were reported to be high and suggested the potential of these sediments as possible mitigation alternatives.

Kumar et al., 2016 studied As and F co-contamination issue in groundwater of Karbi Anglong district, located in the Barak Valley in Assam. Average As concentration values of 2.1 µg/L were reported in groundwater samples, with reductive dissolution mechanism being the release mechanism of arsenic into groundwater. While these recent studies to unravel the groundwater arsenic contamination issue in Assam have helped develop insights, yet these studies, so far have remained spatially restricted and a comprehensive picture is yet to emerge.

Das et al.,(2016), recently reported arsenic concentrations ranging between 0.21– 44.6 µg/L and 0.19–73.0 µg/L from Jorhat district lying along the southern bank of the Brahmaputra, for samples collected during monsoon and pre-monsoon seasons. They attributed pyrite oxidation as one of the probable pathways of arsenic mobilization during the drier periods, especially pre-monsoon. Das et al., (2016) based on their study in the Brahmaputra River Floodplains also attributed high arsenic release to be affected by alkalinity and pH increase, the patchy As concentrations being affected by proximity to rivers.

Khanikar et al., (2017) reported high arsenic groundwater in the northern bank of the Brahmaputra river in Asam and have reinforced that Fe (hydr) oxides are the direct source of As release in the affected region and reductive hydrolysis of such (hydr) oxides release arsenic into groundwater. The study further emphasized the higher probability of arsenic getting into the food chain through tea and other edible plants irrigated with arsenic contaminated water.

Verma et al. (2016) pointed out the greater abundance of clay at a drill site in Jorhat compared to two drill sites on the northern bank of the Brahmaputra but tentatively attributed higher arsenic concentration to the south to differences in tectonic history and sediment provenance. The higher As concentrations were linked to crustal evolution process through which As is subsequently mobilized from aquifer matrix to solution in groundwater by water–sediment reaction under favorable biogeochemical conditions.

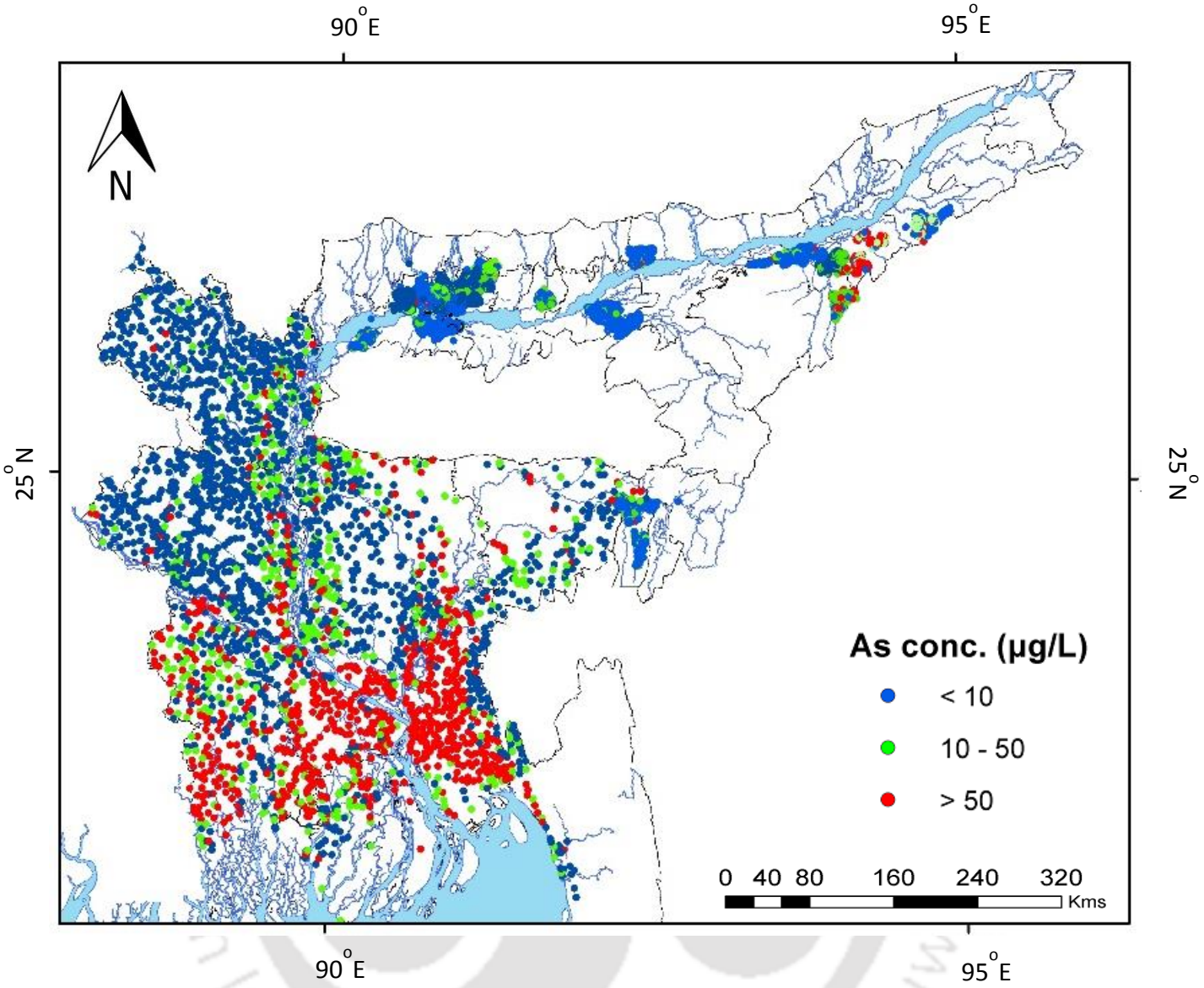

Figure 3.8 Map showing As concentrations in shallow wells (<60 m depth) in the upper Brahmaputra River basin in Assam, NE India (Mahanta et al., 2015), along with As distribution in the lower Brahmaputra River basin in Bangladesh (BGS & DPHE, 2001), Colours in the map indicates As concentration ranges (light blue ≤10 µg/L; green 10–50 µg/L; red >50 µg/L)

Table 4 Studies on groundwater arsenic contamination in the upper Brahmaputra Basin in India along with proposed mechanism of release

Bank with reference to the Brahmaputra River in Assam, India	**Area/Region**	**Arsenic concentration Range (ppb)**	**Mechanism of arsenic release**	**Author**
Both northern and southern bank	Assam	Below detection limit (bdl) to 800	Reductive dissolution of Fe(III) oxyhydroxides	Singh et al., 2004
Northern Bank	Darrang and Bongaigaon		Reductive dissolution of Fe(III) oxyhydroxides	Enmark and Nordborg., 2007
Both northern and southern Bank	18 districts in Assam	bdl to 800	Reductive dissolution of Fe(III) oxyhydroxides	Mahanta et al., 2010
Northern Bank	Nalbari	bdl to 200	Reductive dissolution of Fe(III) oxyhydroxides	Choudhury et al., 2015
Northern Bank	Lakhimpur		Reductive dissolution of Fe(III) oxyhydroxides	Chetia et al., 2009
Northern Bank	Nagaon		Reductive dissolution of Fe(III) oxyhydroxides	Kumar et al., 2016
Southern Bank	Jorhat	bdl to 440	Reductive dissolution of Fe(III) oxyhydroxides	Baviskar et al., 2015
	Majuli	1 to 128	Reductive dissolution of Fe(III) oxyhydroxides	Goswami et al., 2013
Southern Bank	Jorhat	21 to 44; 19 to 73	Reductive dissolution of Fe(III) oxyhydroxides	Das et al., 2016

Chapter 4

Materials and Methods

4.1 Selection of groundwater sampling sites

The outcome of a comprehensive Arsenic Screening and Surveillance Program in Assam valley (Mahanta et al., 2015), revealed groundwater arsenic distributions to be localized at discrete pockets within the Brahmaputra floodplains (Figure 3.8). With this background, a 50 km representative transect was chosen along the northern bank of the Brahmaputra River in Assam, where previous investigation revealed arsenic concentrations above guideline values. While deciding sampling locations, along with the geographical coverage (i.e. spatial distribution), a transect based approach was considered. Groundwater samples (n = 153) along the transect were collected from both private and public tubewells spread along the selected transect during February and November 2013 (Figure 4.1).

Close scrutiny of some of the decipehered hotspot areas, where groundwater arsenic concentration were much above guideline values, demonstrated that within the southern bank of the Brahmaputra River, the spatial arsenic distribution demonstrated a pattern different from that observed in the lower Brahmaputra River in Bangladesh, where, high arsenic groundwater occur close to the river (Figure 3.8). This was followed by testing over 900 wells <50 m deep within a 1,800 km^2 area within the southern bank using field test kit for As. Results demonstrated similar patterns as those observed during the Arsenic Screening and Surveillance Program, where high As concentrations occurred away from the Brahmaputra river (Figure 3.8). Thus, for in-depth study of this spatial variability, a 35 km representative transect perpendicular to the Brahmaputra River was selected for drilling and groundwater sample collection. The elevation difference of 10 to 12 m is observed along the 35-km long transect. A total of 134 groundwater sources were collected for detailed hydrochemical analysis November 2016 (Figure 4.2). The drill site was selected close to sampled groundwater wells for investigation of subsurface sediment profiles.

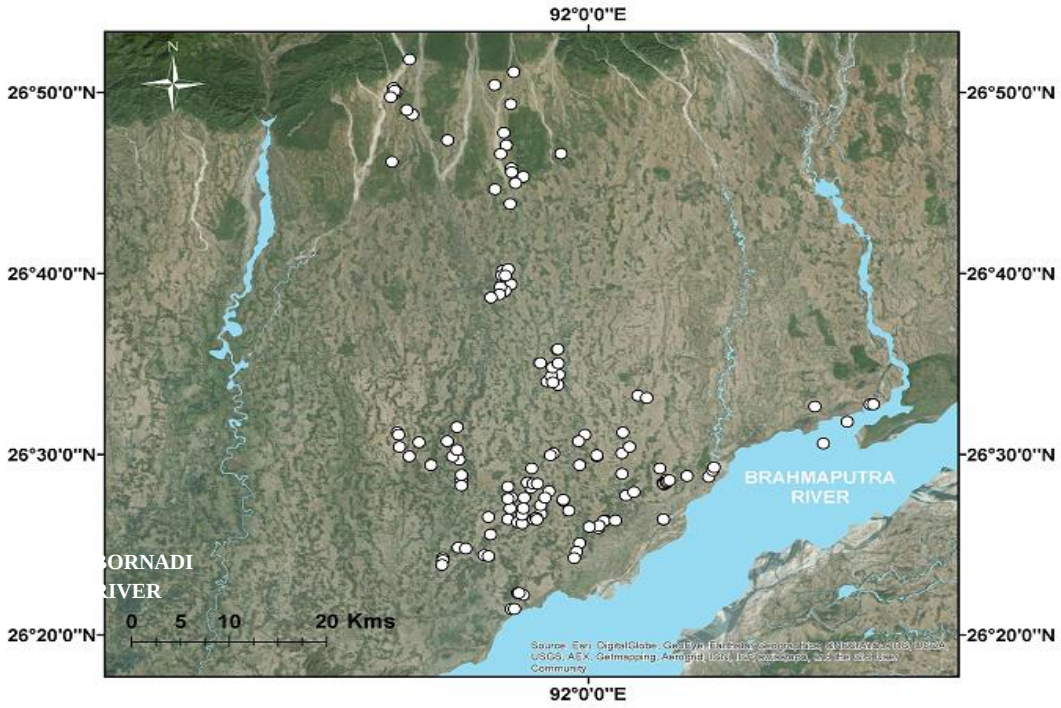

Figure 4.1 Map showing groundwater sampling locations (marked as white circles, n = 153) along the northern transect. The satellite image of the study site acquired from ESRI, World Imagery

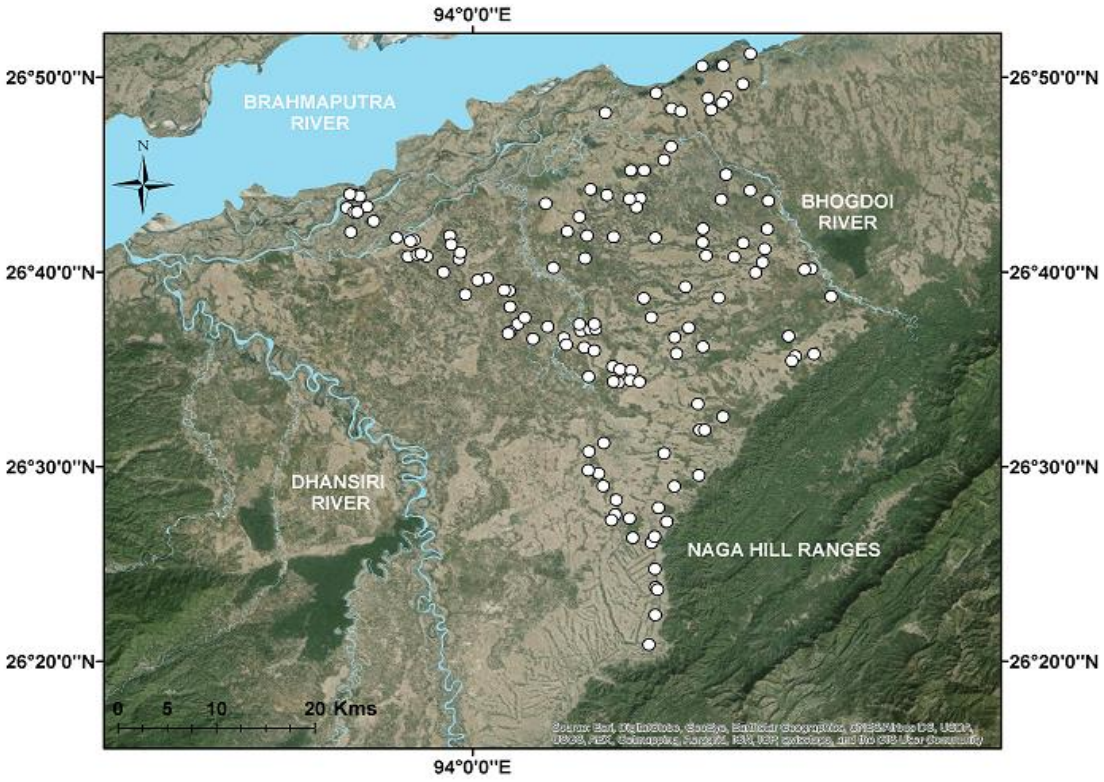

Figure 4.2 Map showing groundwater sampling (marked as white circles, n = 132) locations along the southern transect. Brahmaputra River is flowing from east to west at the bottom. The satellite image of the study site acquired from ESRI, World Imagery

4.2 Groundwater Sampling and analysis

Two hundred and eighty (280) groundwater samples (150 samples from along the northern transect and 133 samples from along the southern transect) were collected from hand-pump and public water supply wells during February 2013 to 2014 and during November 2016. The groundwater samples were collected from depths ranging from 2-60 m below ground level (bgl) but normally <50 m bgl representing the shallow aquifers system in the study area. All sampled wells were purged for several well volumes prior to sample collection to ensure that the water samples represented fresh groundwater from the aquifer. Sample collection commenced only when the specific conductance, pH and temperature measurements were stabilized. Insitu measurements for oxidation-reduction potential (E_H), temperature, pH and dissolved oxygen (DO) were done using a multiparameter probe (Hanna 9282), with a temperature accuracy of ±0.15°C (resolution 0.01°C), pH accuracy of ±0.02 pH (resolution 0.01), E_H accuracy of ±1.0 mV (resolution 0.1 mV), and a DO accuracy of ±0.10 mg/L (resolution 0.01 mg/L). Post collection, all groundwater samples were filtered by 0.45-µm filter paper. Samples for cations (major and trace) were collected and preserved by acidification with 6 N HNO_3 in the field to pH~2. Major anions were measured by ion chromatography (Thermo Scientific "Dionex") in the Hydrogeology Laboratory of Indian Institute of Technology (IIT) Kharagpur and a part of it (n = 60) were analysed at IIT Guwahati. The major cations and trace metal have been measured by inductively coupled plasma with optical emission spectrophotometer (ICP-OES, Thermo Fisher ICAP 6000). Precision for most of the analyses were better than 3% (Verma et al., 2014). Analysis of groundwater quality parameters carried out in environmental engineering laboratory of Indian Institute of Technology (IIT) Guwahati were conducted using American Public Health Association (APHA, 1998) recommended standard methods (Table 5). Major and minor cations viz. Calcium (Ca^{2+}), Sodium (Na^{+}), Potassium (K^{+}) were analyzed in Flame Photometer; Magnesium (Mg^{2+}), Manganese (Mn), Iron (Fe) were measured with atomic absorption spectroscopy using Spectra Duo, Varian BV (AAS). Arsenic was measured using Hydride Generation Technique in AAS with Vapor Generation Assembly (VGA). The instrument was calibrated and the sample concentrations were confirmed using a series of As calibration standards of known concentrations. The calibration standards were prepared from high purity single-element stock solutions. The name of the experiment and analytical instrument used for the analysis of water and soil are summarized and tabulated (Table 5 and 6). The tubewells are at variable depths and the geographical locations of the tube wells were determined using a hand held Global Positioning System (GPS).

4.3 Installation of monitoring wells

A set of three monitoring wells LAN_01, BAT_01 and MAD_01 were installed along the southern transect, at distances of 5, 19, and 41 km from the river at depths of 45, 32, and 57 m from the surface. Along with the installed monitoring wells, four paired shallow wells (LAN_2, BAT_2, BAT_3 and MAD_4), adjacent to each monitoring wells were also measured. The hand flapper method described above was used for drilling. Sampling was done for a period of six months to see the temporal variability in the groundwater As concentration ranges. Samples were acidified and bought to the Environmental Engineering laboratory at IIT Guwahati where analysis for As, Fe and Mn concentrations were done using the Hydride Generation Atomic Absorption Spectrophotometer.

4.3.1 Groundwater level measurements

Groundwater level measurements were taken monthly for a duration of six months from three monitoring wells paired with an existing shallow well using a Solinst 101 P2 Water Level Meter (Figure 4.3) . The measurements were done to estimate groundwater flow velocity and direction of flow and to check for the consistency between hydraulic gradient and groundwater age measurements.

Figure 4.3 Water level measurements conducted using Solinst 101 P2 Water Level Meter.

Table 5 List of the groundwater quality parameters analyzed and name of the experiment or instrument

Parameters	**Name of Instrument/Equipment**
pH	pH meter
Electrical Conductivity (EC)	Conductivity Meter
Alkalinity (HCO_3^-)	Titration Method
Calcium (Ca^{2+})	Flame Photometer
Magnesium (Mg^{2+})	Atomic Absorption Spectroscopy (AAS)
Sodium (Na^+)	Flame Photometer
Potassium (K^+)	Flame Photometer
Chloride (Cl^-)	Argentometric Method
Sulphate ($SO4^{2-}$)	Turbidimetric Method
Phosphate ($PO4^{3-}$)	Ascorbic Method
Nitrate (NO^{3-})	UV Visible Spectrophotometer
Iron (Fe)	Atomic Absorption Spectroscopy (AAS)
Manganese (Mn)	Atomic Absorption Spectroscopy (AAS)
Arsenic (As)	Vapor Generation Assembly (VGA) of AAS

Table 6 List of analytical instruments and their model/manufacturer used for the analysis of groundwater and sediment parameters

Instrument/Equipment	**Model/ Manufacturer**
Pocket ORP Meter	ORP Testr10-Eutech
Pocket TDS Meter	TDS Testr11 – Eutech
Pocket pH Meter	pH Testr10 –Eutech
Pocket Conductivity Meter	EC Testr11-Eutech
GPS	Trimble
Digital pH Meter	µpH system 361, Systronics India
Digital conductivity Meter	VSI 04, India
Microprocessor Based Flame Photo Meter	128 Systronics, Ahmedabad, India
Digital Spectrophotometer	166 Systronics, Ahmedabad, India
UV Visible Spectrophotometer	Cary 50 Bio, Varian
High Speed Research Centrifuge	R24 Remi, Mumbai, India
Analytical Balance	AB304S Metteler Instrument AG, Switzerland
Hot Plate	JSGW, India
Magnetic Stirrer (1/8 HP)	LS 104B
Water Purification System (Milipore)/ (MiliQue)	Merck Milipore
Mechanical Stirrer	LS04B, ELTEK, Mumbai, India
Horizontal shaker	REICO, Calcutta, India
Incubator shaker End over end rotary shaker	Wagner's shaking machine, Reico Pvt. Ltd., Kolkata
Atomic Absorption Spectrophotometer	Spectra Duo, Varian BV, Netherlands
Laser Particle size analyzer	AWM 2000, Malvern instruments, Worcestershire
Scanning Electron Microscopy (SEM)	LEO, 1430 VP, Carl Zeiss, Germany
Water Bath	International Commercial Trader
Field Emission Scanning Electron Microscope (FESEM)	
X-ray Diffraction (XRD)	
Analytical Balance	Model: AB304S, M/S Mettler Instrument AG, Switzerland
Drying Oven	Model: PSI, M/S Mahindra Scientific Instrument Co., India

4.4 Arsenic measurements with field kit

The Arsenic Econo-Quick test kit (Part No. 481298, Industrial Test Systems Inc., Rock Hill, SC, USA) was used to test of total of 777 private and public wells <50 m deep within a 1,800 km^2 area between June and August 2015. The regional pattern inferred from this survey was used to position a transect of drill sites. Groundwater samples were collected after hand-pumping for 3-5 min to purge each well. The kit uses the 19^{th}-century Gutzeit method, which relies on the generation of arsine gas from an acidified sample to which zinc powder is added and the change in color induced by arsine of a test strip impregnated mercuric bromide. The entire procedure requires less than 15 min by excluding the oxidizing reagent ("Reagent 2") provided with the kit. The color of the test strip is compared by eye with a reference chart corresponding to 9 bins of As concentrations in the 0-1000 µg/L range. George et al. (2012) showed that kit measurements were consistent with laboratory measurements for well-water from Bangladesh, provided over-estimation of As concentrations by the kit by a factor of two is taken into account. Well depths recorded while testing are based on the household's recollection, which is typically correct because they witnessed the installation and every section of PVC had to be paid for.

The field kit was also used to estimate the exchangeable fraction of As in aquifer sands. About 0.5 g of freshly collected sand was added to the kit's reaction vessel along with 50 mL of (low As) bottled water. The slurry was processed as a water sample (without Reagent 2) and a visual reading of the strip against the reference chart was obtained after the standard 10 min reaction time.

4.5 Sediment Sampling and analysis

Fifteen boreholes were drilled during Feb 2013 and Dec 2013 along the northern transect and nine borewells during Nov 2016 along the southern transect with the help of local drillers provided by the Public health Engineering Department (PHED) Assam (Figure 4.3-4.4). The borehole samples were collected approximately at every 2 m depth and was drilled to an approximate depth of 30 m. During drilling the color and texture of sediment was noted and samples were collected in clean sealed air tight polythene bags and stored in dark until analysis.

Care was taken in selecting both the transects such that they were representative of any northern and southern bank transect. The northern transect with a total length of 54.5 km had a local gradient of 0.004 m/m, while the southern transect with an approximate length of 35 km had a local gradient of 0.003 m/m (Figure 4.4- 4.5). The transects represent a typical

down gradient section with a systematic change in surface elevation and topographic relief. The directions of groundwater flow are strongly influenced by surface topography.

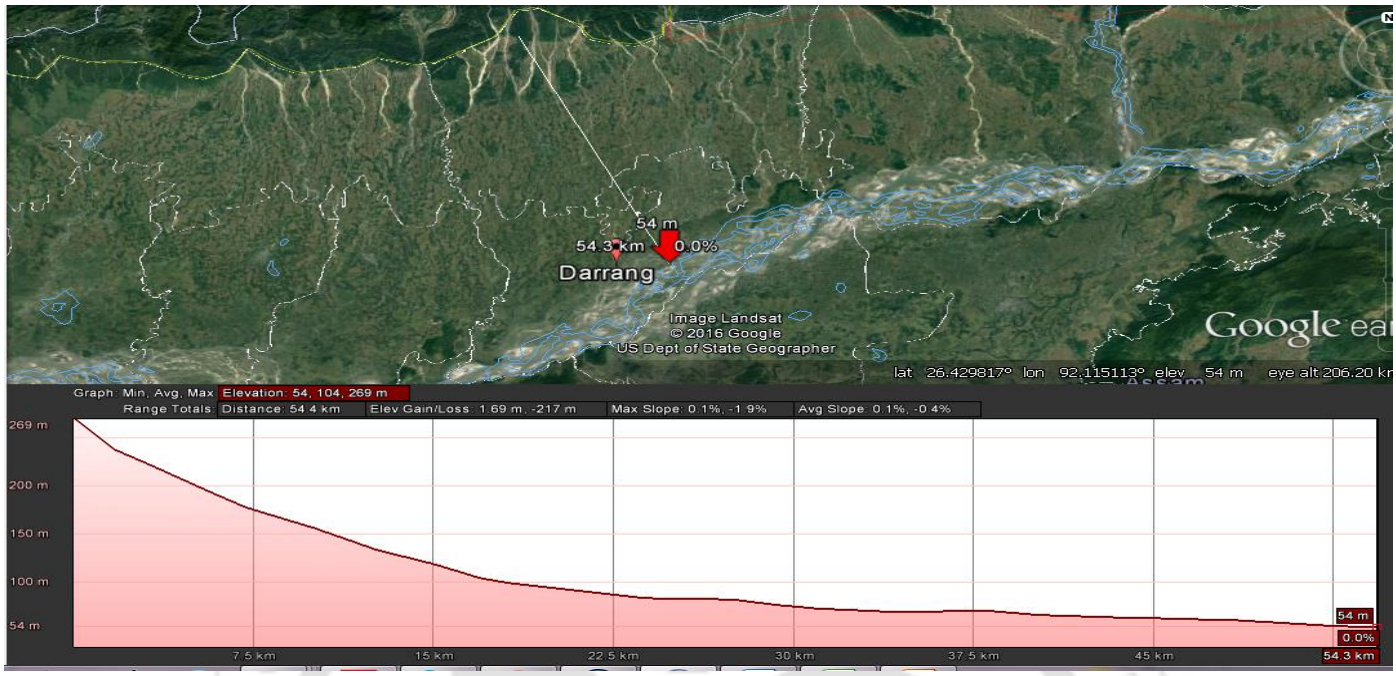

Figure 4.4 Elevation profile of the 55km northern bank transect showing variation in topography

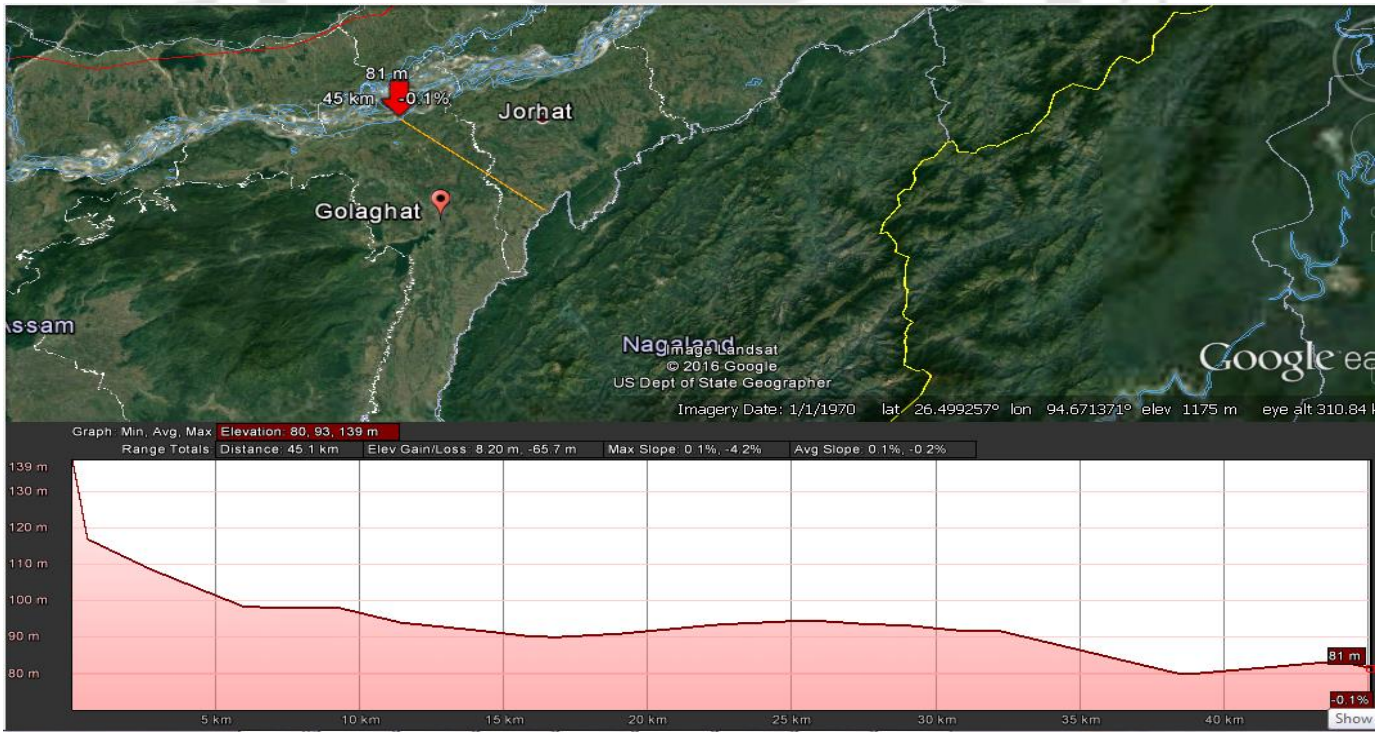

Figure 4.5 Elevation profile of the 35 km southern bank transect showing variation in topography

4.6 Collection of cuttings

Aquifer sediment cuttings for visual and chemical characterization were collected from fifteen drilled wells along the 55 km northern transect and nine drilled wells along the 35 km southern transect by relying on the indigenous method of installing wells, the "hand-flapper" or "sludger" method (Figure 4.6- 4.9). This method is based on the application of suction and release, using the hand as a check valve, to a PVC pipe that is repeatedly lowered and raised to deepen a drill hole (Horneman et al., 2004). The sediment samples were collected from depths ranging up to 60 m. Sediment samples collected were packed in zipped polyethylene bags and put in black polyethylene in order to avoid direct contact with sunlight and oxygen. The collected samples were brought back and stored in the laboratory until analysis.

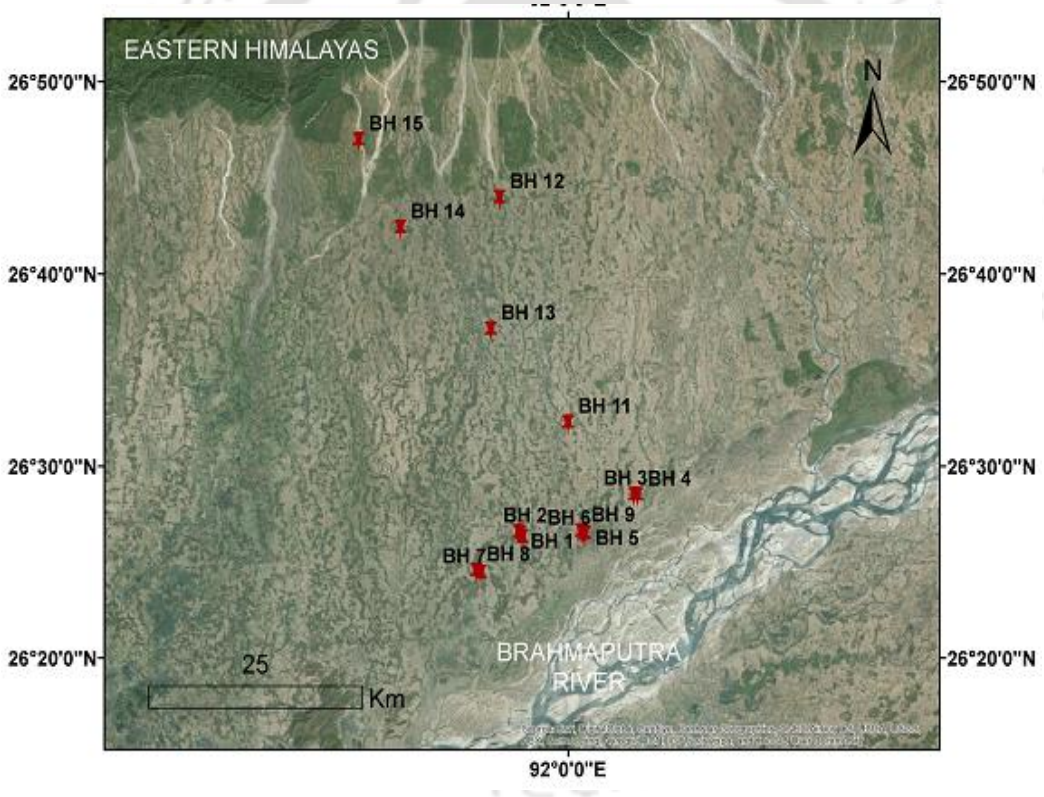

Figure 4.6 Map showing the approximate location of the study transect and the location of drilled borewells (red markers with numbers) on the northern bank of the River Brahmaputra. The satellite image of the study site acquired from Google Earth Pro. Landsat image of the study transect acquired from USGS Earth Explorer

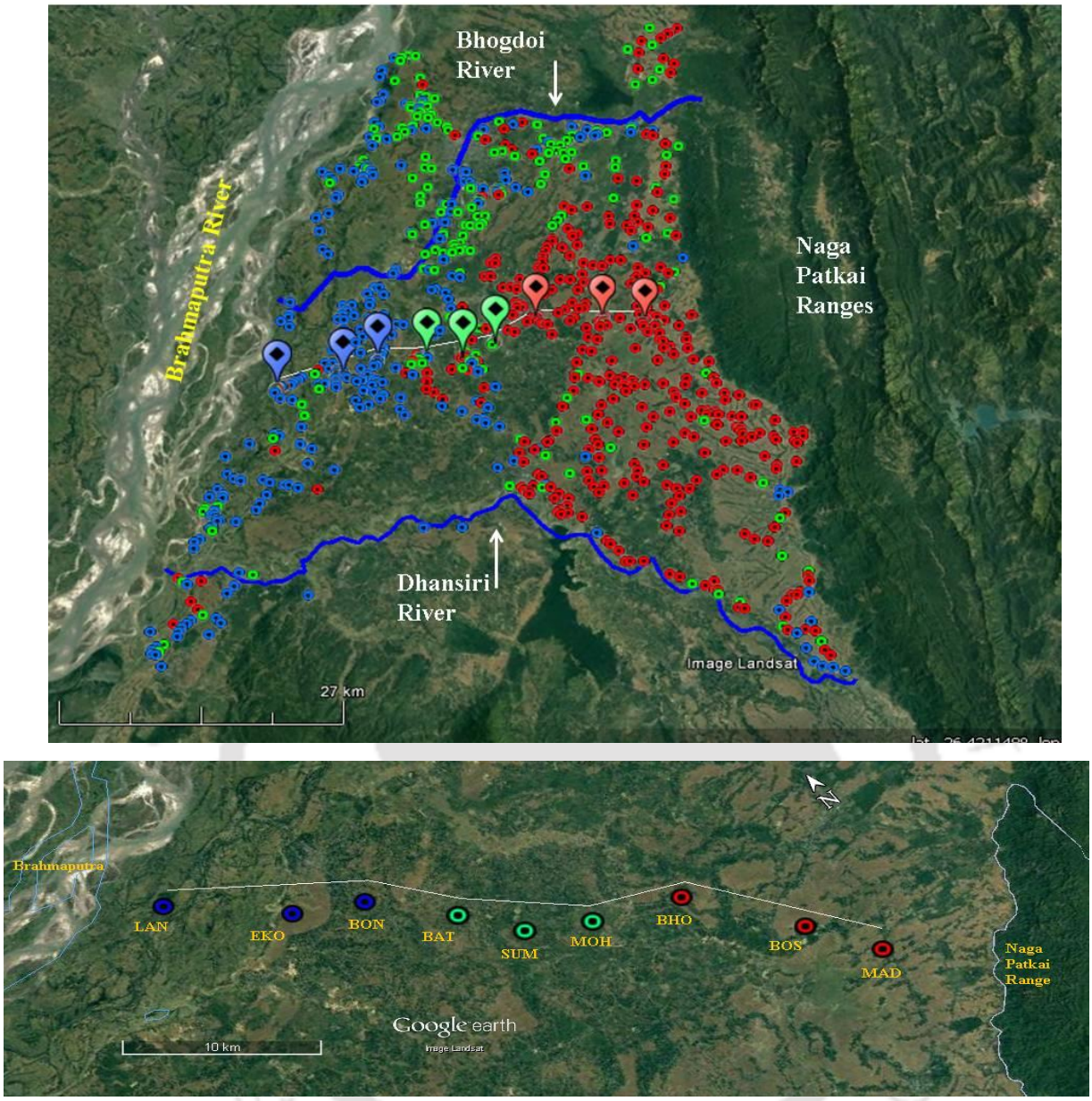

Figure 4.7 Map showing the approximate location of the study transect and the location of drilled borewells (markers with name of borewells, red marker indicates borehole location in zone of high groundwater As, green indicates borehole location in zone of intermediate groundwater As and blue indicates boreholes in low As groundwater) on the southern bank of the River Brahmaputra. The satellite image of the study site acquired from Google Earth Pro. Landsat image of the study transect acquired from USGS Earth Explorer

Figure 4.8 Drillers using Hand Flapping method used for drilling borewells in the study area

Figure 4.9 Sediment cores from drilled borewells

4.7 Solid Phase Analysis

The sediment samples collected from the sampling sites were kept in plastic air tight zipper bags and covered with black polythene bags until analysis. Then the samples were air dried. The air dried samples were then used for the following analyses.

4.8 Chemical Properties

4.8.1 pH

The sediment pH was determined on air dried soil samples in ratio 1: 5 i.e. soil:), 0.01M $CaCl_2$ solution shaken for 30 minutes and measured the pH of supernatant using a pH electrode (Hendershot et al., 2008).

4.8.2Loss on Ignition (LOI)

The samples were oven dried at 105°C for 24 hours after it was brought into laboratory and the resulting loss in weight gives the percentage soil moisture content (MS %) in the sample. The organic carbon content in the sediment samples were determined by loss on ignition (LOI), which measures weight loss after burning at specified temperatures. LOI is then calculated using the following formula (Dean, 1974):

$$LOI_{550} = (DW_{105} - DW_{550})/DW_{105})*100$$

Where LOI_{550} represents LOI at 550°C (as percentage), DW_{105} represents the dry weight of the sample before combustion (g) and DW_{550} the dry weight of the sample after heating to 550°C (g).

4.9 Mineralogical investigations

Mineralogical studies included i) X-ray florescence (XRF) for analysis of the bulk composition of sediments, ii) X-ray diffraction (XRD) for targeting oxide, hydroxide, sulphide, sulfate and carbonate minerals and iii) Field Emission Scanning Electron Microscope (FESEM) with energy dispersive X-ray spectrometer (EDS) for qualitative characterization of grain coatings and authigenic mineral phases.

4.10 X-Ray Diffraction (XRD)

Mineralogical phases presented were identified using X-ray powder diffraction (MAC Science XXP 18) with Cu Kα radiation and a position sensitive detector. The accelerating

voltage was kept at 30 kV and the current at 20 mA. A divergent slit (1°), a scattering slit (1°) and a receiving slit (0.3 mm) were used to produce the best spectrum. Scans were conducted from 5° or 10° to 70° at the rate of 1° to 2Θ/min. Data were digitally recorded, and peak position and intensity were determined either on screen or using the smoothed and peak finder feature in the software (Figure 4.10).

Approximate relative abundance ratios of major minerals were estimated from the relative intensities of the most intense and specific peak of each mineral from the XRD chart. Identification of compounds was made by manual search of the JCPDS- International Centre for Diffraction Data (ICDD) as a reference database.

Figure 4.10 XRD instrument used for mineral phase identification

4.11 X-ray Fluorescence (XRF)

For estimation of the total solid phase, drill cuttings from each of the twelve borewells were analyzed by X-Ray fluorescence for a suite of elements viz. As, Fe and Mn including Ca using an InnovX-Delta instrument. Analysis of NIST reference material SRM 2711 was done at the beginning and end run.

Estimation of major oxides was done using PANalytical AXIOS X-Ray Fluorescence spectrometer using the Pressed Pellet Method. Major oxides were identified using the Super-Q Software for quantative and qualitative analysis.

4.12 Particle Size Analysis

Laser particle size analyzer (Mastersizer 2000) was used to find the specific surface area (SSA) of the soil samples. Malvern software assisted with the instrument showed the particle size distribution. The specific surface area (SSA) was calculated by the Malvern software from the results of laser diffraction measurement using the following equation:

$$SSA = \frac{6\sum \frac{V_i}{d_i}}{\rho \sum V_i} = 6/\rho D[3,2]$$

where v_i is the relative volume in class i with mean class diameter of ρ is the density of the material, and [3, 2] is the surface weighted mean diameter. This was automatically calculated by the laser diffraction system software by assuming that the particles are perfectly smooth, solid spheres.

4.13 Reflectance measurements

A CM700d diffuse reflectance spectrophotometer (Minolta Corp., USA) was used to quantify changes in the color of the freshly collected clay and sand cuttings through the cling-wrap at the drill site. The instrument was calibrated each day with a white barium sulfate place. Readings corresponded to an illuminant source of D65 (daylight-containing ultraviolet component, color temperature 6504K), with the observer angle set to 10°, and excluding the specular component (direct reflection). Previous work has shown that the proportion of Fe(II)/Fe in the acid-leachable fraction of Fe oxides in aquifer sediments is linearly related to the first-derivative transform of the spectrum between 520 and 520 nm (Horneman et al., 2004). Sediment samples were placed in a cut 20 mL scintillation vial (surface diameter 1.75 cm) and covered with clear polyethylene cling-wrap (Glad®, USA). Each reading is the average of a sequence of three measurements made automatically without moving the instrument Three such averaged readings were collected, then the sediment was mixed and another 3 readings obtained. The sequence was then repeated a third time. The reflectance values discussed are, therefore, based on a total of 9 readings. Before analyzing each sample, the white standard was premeasured. The drift in reflectance difference at these wavelengths over the course of the day for the white calibration remained $\leq$0.01%.

4.14 Field Emission Scanning Electron Microscope (FESEM)

Selected sediment samples were analyzed for elemental and morphological compositions of minerals using a Field Emission Scanning Electron Microscope (FESEM) equipped with a JEOL-JSM 5800 LV microscope and combined with an energy dispersive X-ray spectrometer (EDAX) (Figure 4.10).

Powdered samples were first suspended in ethanol and then spread over a thin aluminium foil. The substrate with the suspension was allowed to dry and once the solvent evaporated, a thin film of the sample was formed. This was done to create required surface and uniform sample thickness for analysis. The aluminium foil with the sample was then mounted on a carbon tapes and coated. Finally using FESEM morphological studies were conducted.

Figure 4.11 FESEM used for elemental and morphological mapping of sediment samples

4.15 Petrographic Study

Mineralogy of sediment samples were studied combining optical petrography facility available at Department of Geological Sciences, Gauhati University. Mineral phases of sediment samples were done on polished thin sections, prepared from samples collected at different depths of the drilled borewells. The thin sections were examined for mineral types and textures using a petrographic microscope under both polarized and cross polarized light.

4.16 Sequential Extraction Procedures (SSE)

Metals present in sediments can be associated with several reactive components. The total metal concentration indicating the overall metals in the soils does not provide any information regarding the chemical nature or potential mobility and bioavailability of a particular element.

As a result of sequential extractions, it is possible to (a) obtain detailed information about arsenic distribution among the different solid phases associated with the selected solid matrix and (b) evaluate the relative contribution of these fractions to the concentration values observed in the experiments. These findings in turn can be used in groundwater preservation strategies because they allow understanding dominant roles of the different mineral fractions to adsorb As and the conditions under which As can be released to the groundwater (Molinar et al., 2013).

To characterize the distribution of As in the sediments, all sediment samples were evaluated using a modified sequential extraction method for As described by Wenzel et al., (2001) (Table 7). The procedure is used to examine the arsenic concentrations associated with five "operationally defined phases" within the sediment, including non-specifically bound (outer sphere surface complexed), amorphous bound (inner sphere surface complexed), amorphous hydrous Fe (Mn, Al) oxides (e.g, ferrihydrite), crystalline (hydrous) Fe (Mn, Al) oxides (e.g, goethite, hematite and magnetite) and residual (e.g., aluminosilicates; framework silicates, such as quartz; Wenzel et al., 2001). Moreover, the sequential extraction technique employs reagents that were chosen to selectively attack the specific soil phases with minimal dissolution of non- target phases, and the sequence of reagents is applied from relatively weaker to increasingly stronger to dissolve progressively more refractory mineral phases (Wenzel et al., 2001).

Prior to extraction, all sediment samples were air-dried at ambient temperature. The dried sediments were then passed through a 2-mm sieve and homogenized. Reagents were prepared using ultra-pure Milli-Q water. The volume of all extraction solutions used was 25 mL.

Fraction 1. A 1.0 gm (dry weight) aliquot of each sediment sample was placed into a 50 mL centrifugation tube (Fisher Scientific), along with 25 mL of 0.05 M $(NH_4)_2SO_4$ reagent (Table 1). The mixture was subsequently agitated for 4 hours at 20 °C on a shaker (VWR Mini Shaker), and then centrifuged for 15 minutes at 2000 rpm. The resultant supernates were

filtered (0.4 μm membrane filters), acidified with ultra-pure HNO_3, and stored at 4 °C prior to analysis. The residual soil was used for the subsequent extraction step.

Fraction 2. The residue from fraction 1 was placed in a 50 mL centrifuge tube along with 25 mL of 0.05 M $NH_4H_2PO_4$ solution, and subsequently agitated for 16 hours at 20 °C on the Mini Shaker as described above. The sediment-reagent slurry was then centrifuged, filtered, and acidified as described above.

Fraction 3. The residue from fraction 2 was placed in a 50 mL centrifuge tube along with 25 mL of 0.2 M NH_4-oxalate buffer solution and the pH was adjusted to 3.25 using oxalic acid. The mixture was subsequently shaken for 4 hours at 20 °C in the dark, and then centrifuged, filtered, and acidified as described above. To account for potential carryover to the next extraction steps, we employed a wash step to recover As remaining in the rest of the solution and re-adsorbed onto amorphous metal oxides. The residue from the primary extraction was placed in a 50 mL centrifuge tube along with the same reagents and the wash step solution was subsequently shaken for 10 min in the dark, followed by centrifugation, filtration, and acidification as described above.

Fraction 4. The residual from fraction 3 was placed in a 50 mL centrifuge tube along with a 0.2 M NH_4-oxalate buffer solution and 0.1 M ascorbic acid adjusted to pH 3.25. The centrifuge tube containing the sediment-reagent solution slurry was then placed in a heated water bath (96±3 °C) for 30 minutes. After cooling, the sediment-reagent slurry was then centrifuged, filtered, and acidified as described above. A wash step using the same reagents was employed to recover As remaining in the rest of the solution and re-adsorbed onto crystalline Fe and Al oxide minerals. Here, a 50 mL centrifuge tube containing the residue from the primary extraction along with the same reagents was subsequently shaken for 10 min in the dark, and centrifuged, filtered, and acidified as described above.

Fraction 5. The residue from fraction 4 was subsequently digested using a two-step process. First, the EPA acid digestion method 3050B was used whereby the sediment residue was placed in a 25 mL mixture of 16 N HNO_3 and 30% H_2O_2, which was then placed in a heated water bath (95 °C±5 °C) for 4 hours. After cooling, the sediment reagent solution slurry was centrifuged, filtered, and acidified as described above. Secondly, the remaining residue was subsequently digested in a Teflon® beaker with 20 mL ultrapure HF, and the mixture was evaporated to near dryness, followed by 20 mL of ultrapure 16 N HNO_3, which was again evaporated to near dryness. Subsequently, an additional 20 mL of ultrapure HF was added

and the mixture was evaporated to near dryness. The residue was then re-dissolved with Milli-Q water and diluted up to 25 mL with Milli-Q water. The sediment-reagent solution slurry was subsequently centrifuged, filtered, and acidified as described above. The concentration of total extractable As in the residual phase was then determined by the sum of the combined digestion techniques. All supernatants of the sequential extraction procedure were analysed for As by the VGA mode of Atomic absorption Spectrophotometer (AAS). The instrument was calibrated and the sample concentrations were confirmed using a series of As calibration standards of known concentrations. The calibration standards were prepared from high purity single-element stock solutions.

Table 7 Summary of extraction procedure, along with the "operationally defined" sediment phases targeted by each extractant

Fraction	**Extractant**	**Target phase**	**Possible Mechanism**
1	0.05 M $(NH_4)_2SO_4$; 4 hr shaking (20 °C)	Physisorbed As (outer sphere surface complexes), commonly referred to as labile or reactive As (Hamon et al., 2004)	Anion exchange for SO_4 for As
2	0.05 M $NH_4H_2PO_4$; 16 hr shaking (20 °C)	Chemisorbed As (inner sphere surface complexes; also labile)	Anion exchange of PO_4 for oxyanions As
3	0.2 M NH_4–oxalate buffer, pH 3.25; 4 hr shaking (dark; 20 °C)	Non labile As associated with amorphous and poorly crystallized Fe (Mn, Al) oxide/oxyhydroxides	Ligand-promoted dissolution
4	0.2 M NH_4–oxalate buffer + 0.1 M ascorbic acid (pH 3.25); 30 min in water basin at 96 ± 3 °C	Non-labile As associated with well crystallized Fe (Mn, Al) oxide/ oxyhydroxides	Reduction of Fe(III) and Al(III)
5	a. 16 N HNO_3+ H_2O_2; Acid digestion (EPA method 3050B; see www.epa.gov/SW-846/pdfs/3050b.pdf) b.. 16 N HNO_3+ HF (Tessier et al., 1979; Tang et al., 2004)	a. Liberate As associated with residual minerals such as orpiment (Keon et al., 2001) b. Release As associated within aluminosilicate minerals (Johannesson and Zhou, 1999)	a. Oxidation of sulfides and organic matter b. Dissolution of aluminosilicate

4.17 Radiocarbon dating of sediment and groundwater

Groundwater samples for radiocarbon analysis were collected in 250 ml glass bottles with polyseal caps and were poisoned with 0.2 ml of saturated $HgCl_2$. Analysis of $^{13}C/^{12}C$ and $^{14}C/^{12}C$ in dissolved inorganic carbon (DIC) were performed at the NOSAMS facility at Woods Hole Oceanographic Institution following standard protocols with a precision of 0.1 % (Elder e al., 1998; Radolff et al., 2016).

A total of 13 organic rich clay samples from drilled borewells along the southern transect were collected for ^{14}C age dating. The samples were collected wrapped in thin film and put in airtight polyethylene zipper bags and preserved to minimize bacterial activity, prior to sending sample for analysis. The samples were analyzed within 6 months of collection at the NOSAMS facility at Woods Hole Oceanographic Institution by Accelerator Mass Spectrometer (AMS).

4.18 GIS Software

ESRI ArcGIS 9.3 software was used for preparation of maps and spatial mapping of arsenic and other parameters in the study area. Details of borehole and groundwater sources were put into an attribute table, which was then used for spatial and temporal mapping of sources.

LISS (IV) image with a spatial resolution of 6m, obtained from North East Space Application center (NESAC) was used for image interpretation. The geomorphic units along the southern transect were deciphered by identifying features on their basis of tone, texture, size and arrangements; along with field level studies for ground truthing. ArcGIS 10 was used for preparation of the 1: 50,000 thematic maps of the geomorphic features.

4.19 Geochemical Modeling (PHREEQC)

The geochemical modeling tools PHREEQC version 2.14.2 (Parkhurst and Appelo 1999) and Visual MINTEQ version 2.53 (Dzombak and Morel 1990, Allison et al. 1991) were used for:

i) Calculation of saturation indices with the objective to identify possible mineral phases controlling the aqueous chemical composition. The thermodynamic relationships between species in solution and aquifer solid phases were established through the degree of saturation with respect to minerals. Saturation index (SI) is defined as: $SI = \log (IAP/ K_{sp})$ where IAP is the ion activity product and Ksp is the solubility product for a given temperature. When SI=0 ($IAP= K_{sp}$) the solution is at thermodynamic equilibrium with respect to a specific mineral and when SI >0 the water is supersaturated with respect to a mineral and vice versa. Calculation of SI was done to identify possible sinks and sources of dissolved elements and

for further interpretation of possible reactions controlling the aqueous chemistry (Sracek et al. 2004).

Inverse geochemical modeling is commonly used to reconstruct geochemical evolution of groundwater from one point in an aquifer to another point located in the inverse direction along the groundwater flow path (Plummer, 1992). It attempts to account for the chemical changes that occur as water evolves along a flow path (Plummer et al., 1994). Inverse modeling is used to calculate the moles of minerals and gases that must dissolve or precipitate/degas to account for the difference in composition between initial and final water end members (Parkhrust and Appelo, 1999). Inverse modeling has been applied to determine reactions that lead to convert primary minerals to secondary minerals along with assessing the geochemical evolution of groundwaters (Plummer et al., 1990; Sharif et al., 2008; Peikam et al., 2016). Inverse geochemical model was used to determine the flow path evolution of groundwater and its relation to mobilization of arsenic in groundwater of the aquifer (Sharif et al., 2011). Understanding how arsenic is released to water requires knowledge of not only the source of arsenic but also the dominant geochemical processes that affect its fate. Belkhiri et al, 2010 applied inverse geochemical modeling to define the variation and the genetic origin of chemical parameters of groundwater in the Ain Azel plain, Algeria.

Helgeson (1968) used inverse modeling to simulate the processes of water–rock interaction and the mass transfer based on groundwater chemical data. Accordingly, geochemical processes along the groundwater flow paths can be quantitatively described, in case that groundwater chemistry and possible mineral phases are known (Plummer and Back, 1980). The mineral phases could be gases, minerals and/or ions involved in cation exchange reaction (Parkhurst and Appelo, 1999).

The equilibrium Surface Complexation Model of PHREEQC (Parkhurst and Apello, 1999) was used to predict the difference between sorbed As on HFO phases derived from sequential extraction and modeled simulations. The Diffused Layer Model (DLM) of Dzombak and Morel (1990) was used to simulate surface complexation reactions. Ferrihydrite and Goethite were selected as the model sorbents. Ligand sorption was considered to occur at two sorption sites on ferrihydrite with a density of 0.005 mol/mol Fe for the strong site, and 0.2 mol/mol Fe for the weak site (Dzombak and Morel, 1990). Ligand sorption for goethite was considered to occur at only one sorption site with a density of 0.00000384 mol sites/m^2

(Manning and Goldberg, 1996). Surface areas of Ferrihydrite and Goethite were considered as 600 m^2/g and 43.7 m^2/g, respectively (Dzombak and Morel, 1990; Manning and Goldberg, 1996).

4.20 Attenuation Study

4.20.1 Batch Sorption Study

Natural geochemical processes control arsenic adsorption and desorption. The viability of aquifers to release low-As water depends on the capacity of these sediments to remove As from the groundwater that could infiltrate from the zone of high organic content and strongly reduced sediment. Three different sediment types from boreholes drilled in the northern bank of the Brahmaputra River floodplain in Darrang districts were used for the adsorption experiments. The same sediment samples were also used for the competition experiments.

Stock solutions of 100 µg/L and 200 µg/L were prepared from $NaAsO_2$ (Sigma-Aldrich, USA) and $Na_2HAsO_4 \cdot 7H_2O$. (Sigma-Aldrich, USA), respectively, in deionized water. Effect of solution pH on As adsorption of was studied by performing batch experiments at initial pH values of 6.5, 7 and 7.5. The pH was adjusted using 0.1 M HCl and 0.1 M NaOH. All experiments were conducted in 50-mL polypropylene shaking flasks. A 25-mL aliquot of the appropriate As solution was added to 0.2 g (accurately weighed) of the sediment sample and the flasks were placed in a shaking incubator that was held at 25 °C and shaken at 180 rpm for a specified period of 24 hours.

4.20.2 Kinetic Study

Arsenic removal kinetic tests for As(V) by three selected soil sediment samples from the northern transect, were conducted in 50 ml polyethylene centrifuge tubes at room temperature (26 +/-2 ºC) by taking 2 gram of air dried soil with 40 ml solution (i.e. 1:20 soil/water ratio). The initial As concentration As(V)] of 100 µg/l and 200 µg/l were used which corresponds to the As concentrations in the study area. The pH was set to 6.5 by using 0.1M HCl or 0.1M NaOH prior to the start of the experiment. Blank samples without As were also included in the experiment to verify the desorption of As from the sediments. The samples were gently shaken in horizontal shaker at an rpm of 180 for 1440 minutes (24 hours). The tubes along with its duplicates were withdrawn from the horizontal shaker at predefined time interval i.e. 5, 10, 20, 30, 60, 120, 240, 360, 600, 1440 minutes. The tube was centrifuged at 9000 rpm for 15 minutes and supernatant were collected using a syringe. The amount of As adsorbed per unit mass of soil sediment (µg/g) was calculated from Eq.1and the sorption percentage using

Eq. 2. The different adsorption models viz. pseudo first order kinetic model, pseudo-second order kinetic model and the various linearized forms, were fitted for the As(V) adsorption data. It was done in order to develop an understanding into the actual adsorption processes occurring in the sediment samples. The pH of the solution was set to 6.5. The stock solutions were prepared from reagent grade i.e. As(V) from $Na_2HAsO_4.7H_2O$, PO_4^{3-} from K_2HPO_4, SiO2 (silica) from $Na_2SiO_3.9H_2O$ and HCO_3- from $NaHCO_3$.

The amount of As adsorbed per unit mass of soil sediment (µg/g) was calculated from the difference between the concentration of the supernatant and that of the initial solutions using following equation:

$$(C_i - C_e) * V/m \quad (1)$$

where C_i and C_e and are the arsenic concentration in µg/l at initial and equilibrium respectively, V is the volume of solution in ml, m is the weight of soil sediment in mg. The amount of the adsorbate adsorption was calculated as follows:

$$S(\%) = (C_i - C_f)v/C_i \; X \; 100 \quad (2)$$

where S is the *As* adsorption (%), C_i is the initial concentration of the *As*(µg/l), C_f is the final concentration of *As* (µg/l), and V is the volume of solution in ml.

Adsorption isotherms for As(V) were determined in separate experiments for concentrations ranging between 100 to 800 µg/L As(V) . Adsorbed As(V) was determined by difference between initial and final aqueous concentrations. Adsorption as a function of pH was measured using initial As(V) and As (III) concentrations of 300 µg/L for pH values ranging from 6.5, 7 and 7.5. 0.1 N HCl or NaOH solutions were used to adjust the pH.

4.21 Effects of competing ions

The effect of competing ions on As(V) adsorption on aquifer sediments was examined using PO_4^{3-}, HCO_3^- and SiO_2 as the competing anions. These three anions were selected since they are the common co-existing anionic components in natural waters, which may affect As mobility (Katsoyiannis and Zouboulis, 2002). High concentrations of anionic species have been used in many previous studies (Frau et al., 2008; Guan et al., 2009) that aim to verify

the prevalence of a particular mechanism, thereby minimizing the possible interference of secondary mechanisms. The effects of As adsorption by PO_4^{3-} was demonstrated by increasing the PO_4^{3-} concentration in the solution from 0.5 mg/l to 3 mg/l. Similarly the competing effect of HCO_3^- was studied by increasing the HCO_3^- concentration from 200 mg/Lto 500 mg/L. The effect of SiO_2 was studied by increasing its concentration from 10 mg/l to 30 mg/L. The combined effect of anions was studied with solution containing 250 mg/L of HCO_3^- , 15 mg/L of SiO_2 and the concentration of PO_4^{3-} was increased from 0.5 mg/L to 3 mg/l.

4.22 Validity of the model

The validity of the different adsorption models viz. first order model, second order model and Intra Particle diffusion model, were tested and quantitatively checked using coefficient of determination (R^2) between the actual experimental results and the model output. The coefficient of determination, R^2, to test the best fitting of the kinetic model to the experimental data was calculated using the Eq. 3

$$r^2 = \frac{\sum(q_m - \bar{q}_t)^2}{\sum(q_m - \bar{q}_t)^2 + \sum(q_m - \bar{q}_t)^2} \quad (3)$$

Where q_m is the amount of As adsorbed on the surface of the sediment at any time, t, (µg/mg) obtained from the second order kinetic model; q_t is the amount of As adsorbed on the surface of the sediment at any time t, (µg/mg) obtained from experiment, and $\bar{q}_t$ is the average of q_t (µg/mg).

Chapter 5
Results and Discussion

Keeping in mind the objectives of the research work, groundwater and sediment samples were collected from the two selected transects, the northern and southern transect. Analyzed groundwater samples demonstrated contrasting spatial arsenic variability along both transects, while for aquifer redox conditions, bulk solid phase measurements and sequential extractions for samples along the transects, the observed variations were limited. Detailed results and corresponding discussions for observed trends are presented below.

5.1 Hydrogeochemistry of groundwater along northern transect

pH of groundwater samples collected along the northern transect ranged between 6.08 to 7.83 indicating circum neutral condition, while measured temperature values were almost uniform, ranging from 23.30 to 29.50°C (Table 8).Calcium (Ca^{2+}) dominated the cation chemistry with values ranging between 1.1 to 60.2 mg/L and mean concentration being 11.7 mg/L, median 11.15 mg/L, std.dev. 6.9 mg/L. Concentrations of sodium (Na^{+}) ranged between 0.8 to 46.8 mg/L with a mean concentration of 12.1 mg/L, median 10.96 mg/L, std. dev. 7.4 mg/L and magnesium (Mg^{+}) concentrations ranged between 0.2 to 24.6 mg/L, mean 6.6 mg/L, median 6.24 mg/L, std. dev. 4.4 mg/L (Table 8).

Anions were predominated by bicarbonate (HCO_3^-), with values ranging from, 62.7 mg/L to 268.5 mg/L, mean 129.7 mg/L, median 120 mg/L and std. dev. 43.9 mg/L. Concentrations of chloride (Cl^-) ranged between 0.9 to 30.9 mg/L, mean 5.5 mg/L, median 4.04 mg/L, std. dev. 4.2 mg/L and sulphate (SO_4^{2-}) concentrations ranged between 0.1 to 20.1 mg/L; (mean 5.5, median 3.65 mg/L, std. dev. 4.6 mg/L). With a mean of 2.1 mg/L, median 1.37 mg/L and std. dev. of 2.9 mg/L, NO_3^- concentrations were generally low for all groundwater samples, except for one sample with 31 mg/L located close to the floodplain area. PO_3^- concentrations ranged between 0.1 to 3.5 mg/L with median values of 0.6 mg/L. Field ORP measurements [corrected to standard Hydrogen Electrode, (SHE)] varied from 28.1 to 197.8 mV (mean 85.4 mV) and generally exhibited higher values near the recharge zone (near Bhutan foothills) compared to groundwater samples collected further down slope near the Brahmaputra main channel. Wide variations were observed in field electrical conductivity (EC) values, ranging from 58 to 775 µS/cm, median of 176 µS/cm. Dissolved oxygen (DO) concentrations ranged between 0.1 mg/L to 2.8 mg/L (mean 0.8 mg/L; std. dev. 1.4 mg/L);

with higher DO values observed near the proximal zones and low values along the runoff areas and discharge zones.

Total arsenic concentrations (bdl to 134 µg/L and median value of 14 µg/L) in groundwater along the northern transect showed a wide range with 62 sources meeting the WHO guideline value of 10 µg/L, another 80 sources with As concentrations up to the earlier national standard of 50 µg/L and 11 sources with concentration >50 µg/L As (Table 8). High spatial variability along the transect with a trend of low As concentrations near foothills and an increasing concentrations along the floodplains (Figure 5.1-5.2) was observed. Fe concentration ranged between bdl to 41 mg/L with median concentration of 14.2 mg/L., while concentrations of Mn and SO_4^{2-} ranged between bdl to 5.9 mg/L and 0.2 to 20.1 mg/L respectively. No trend could be established in the concentration of Fe and Mn from the recharge (near foothills) to discharge zone (close to river bank) (Figure 5.3).

Table 8 Groundwater composition along northern transect (n =153) (units mg/L, except pH and EC in µS/cm)

Parameter(s)	Units	Min	Max	Mean	Median	Std. Dev.	Skewness
Eh	**mV**	28.08	197.82	85.39	53.88	52.73	0.75
Temp	**(°C)**	23.30	29.50	25.04	24.99	0.75	1.73
DO	**mg/L**	0.13	2.81	0.80	0.62	0.53	1.38
pH		6.00	7.80	6.81	6.75	0.43	0.23
Na^+	**mg/L**	0.81	46.55	12.11	10.96	7.35	1.09
K^+	**mg/L**	0.02	19.79	3.08	2.27	2.93	2.85
Ca^+	**mg/L**	1.13	60.47	11.73	11.15	6.87	2.79
Mg^+	**mg/L**	0.19	24.59	6.59	6.24	4.42	1.08
Cl^-	**mg/L**	0.89	30.85	5.46	4.04	4.16	2.19
HCO_3^-	**mg/L**	62.70	268.50	129.67	120.00	43.94	1.33
SO_4^{2-}	**mg/L**	0.13	20.11	5.49	3.65	4.59	1.09
NO_3^-	**mg/L**	bdl	31.02	2.06	1.37	2.92	6.86
PO_3^-	**mg/L**	0.11	3.5	1.43	0.55	1.24	0.93
Fe	**mg/L**	0.04	41.02	13.94	14.53	10.27	0.28
Mn	**mg/L**	bdl	5.87	0.94	0.81	0.80	2.62
As	**(µg/L)**	bdl	134.00	18.72	14.60	19.19	2.06

bdl: below detection limit, ** NA Not Available

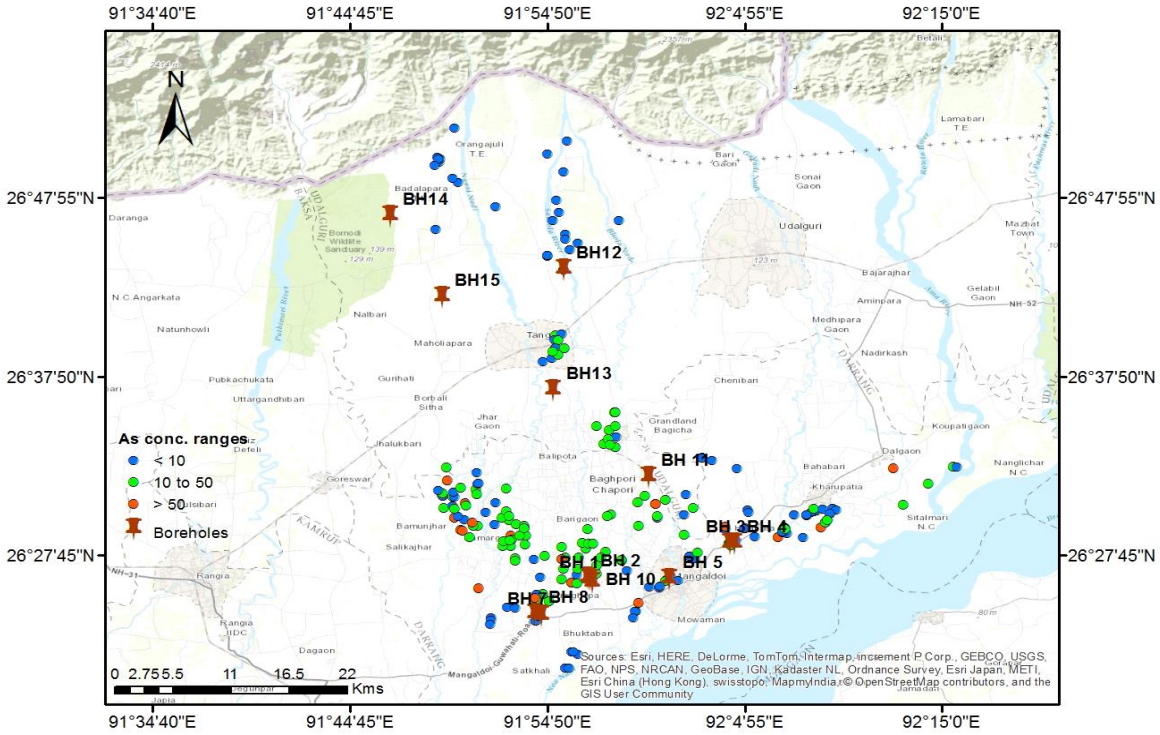

Figure 5.1 Map showing groundwater sampling locations (n=153) along with drilled borehole locations. The symbol colors correspond to As content of groundwater (blue ≤10 µg/L; green 10–50 µg/L; red >50 µg/L)

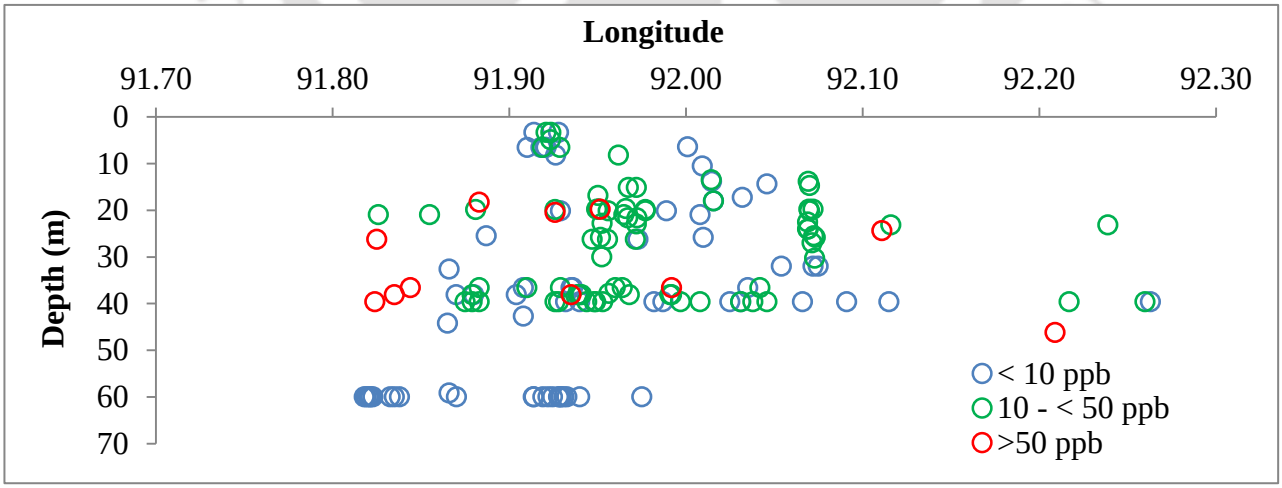

Figure 5.2 As distribution w.r.t depth and longitude, for groundwater along the northern transect. The symbol colors correspond to As content of groundwater (blue ≤10 µg/L; green 10–50 µg/L; red >50 µg/L)

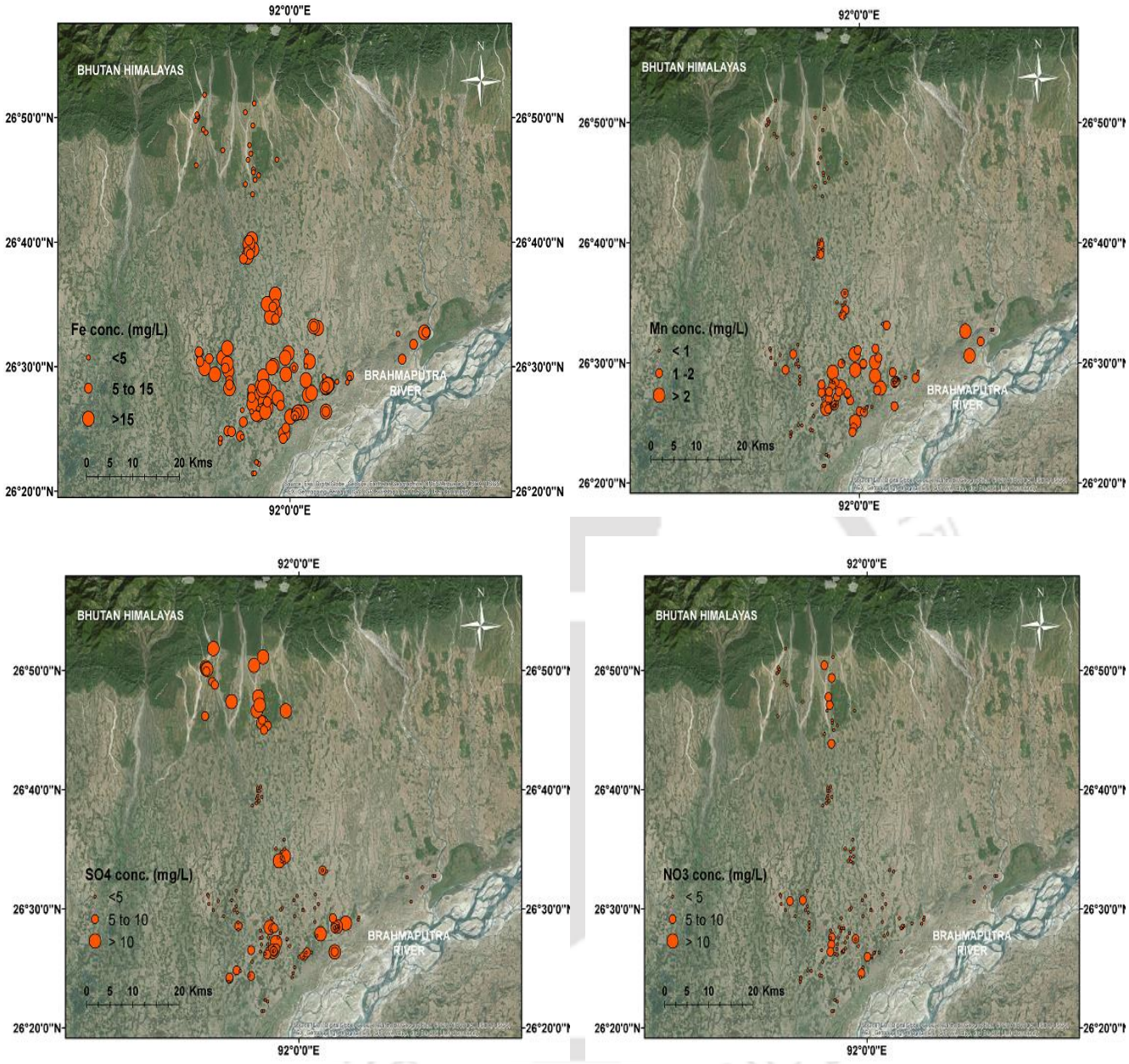

Figure 5.3 Spatial distribution of Fe, Mn, SO_4 and NO_3 along the northern transect. The size of the circles represents relative magnitude of concentration (mg/L)

5.1.1 Hydrogeochemical facies

To classify major ions in groundwater and to summarize major contrasts in hydrogeochemical compositions between water sources, Piper diagrams developed indicated groundwater in the study transect to be broadly divided into three hydrogeochemical facies: (1) Ca^{2+}- HCO_3^-; (2) Ca^{2+}-Na^+-HCO_3; (3) Na^+-Ca^{2+}-HCO_3^-. Most of the groundwater samples

belong to Ca^{2+}-Na^{+}-HCO_3^{-} and Na^{+}-Ca^{2+}-HCO_3^{-} while only few samples belonged to Ca^{2+}-HCO_3^{-} category (Figure 5.4).These results are consistent with previous studies in the study area (Choudhury et al., 2015; Sailo and Mahanta, 2013) which showed similar results for groundwater composition. High HCO_3^{-} in groundwater of downstream Bengal basin or Central Gangetic plain (Zheng et al., 2004; Mukherjee and Fryar, 2008, Mukherjee et al., 2012), reportedly played important role in hydrochemical evolution and trace metal mobilization. High concentrations of Ca^{2+} and HCO_3^{-} is a common feature in South and Southeast Asia floodplain aquifers (Berg, 2001, Bhattacharya et al., 2002, Buschmann et al., 2007, Postma et al., 2007) and this highlights the important role of carbonate dissolution and generation of bicarbonate in the hydrochemical evolution of groundwater facies and subsequent trace metal mobilization (Mukherjee et al., 2008). The anions were dominated more than 80% by HCO_3^{-} . Biodegradation of organic matter vis a vis dissolution of carbonate minerals as well as that of NO_3^{-} and SO_4^{2-} acting as an electron acceptors in the system which allow oxidation of organic matter was believed to be an important contributor to the generation of anoxic conditions that produce high concentration of HCO_3^{-}.

In aquifers, HCO_3^{-} could be released from the dissolution of carbonate minerals via biodegradation of organic matter (Halim et al., 2009)

$$CH_2O \text{ (organic matter)} + O_2 \rightarrow CO_2 + H_2O \quad (1)$$

$$CaMg(CO_3)_2 + CO_2 + H_2O \rightarrow Mg^{2+} + 2HCO_3^{-} + CaCO_3 \quad (2)$$

The reduction of $NO_3^{-}$and SO_4^{2-} through microbial degradation of organic matter to produce HCO_3^{-}can be summarized as,

$$4NO_3^{-} + 5CH_2O = 2N_2 + 5HCO_3^{-} \quad (3)$$

$$SO_4^{2-} + 2CH_2O = 2H_2S + 2HCO_3^{-} \quad (4)$$

The concentrations of NO_3^{-} and SO_4^{2-} in groundwater samples slightly decreased with increasing HCO_3^{-} concentrations (Figure 5.5). A gradually decreasing trend is a clear evidence of microbially mediated reduction in presence organic matter.

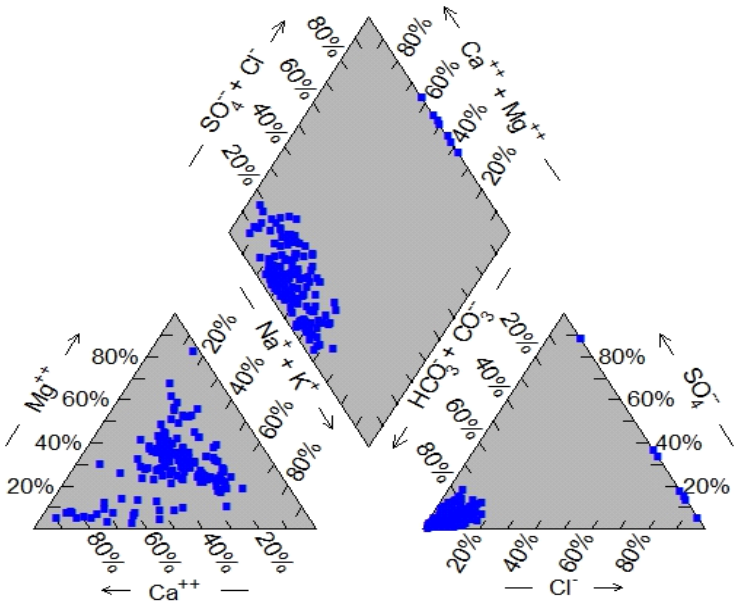

Figure 5.4 Piper Plots of groundwater samples collected from along the northern transect

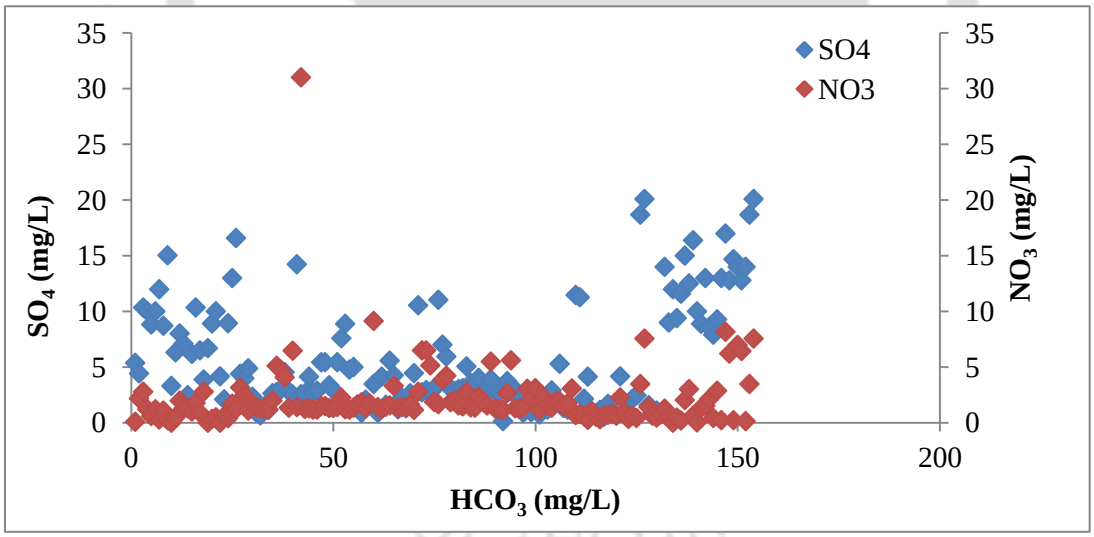

Figure 5.5 Concentrations of NO_3^- and SO_4^{2-} in the groundwater with respect to HCO_3^- concentration.

5.1.2 Evolution of major ion composition in groundwater

Major cations in groundwater viz. Ca^{2+}, Mg^{2+}, Na^+ and K^+ are released from silicate and carbonate mineral weathering enhanced by respired CO_2 from oxic and anoxic organic matter degradation (Halim et al., 2009). Major source of Ca^{2+} in groundwater are often from carbonate minerals such as calcite and dolomite while major source minerals of Mg^{2+} are

biotite and chlorite minerals (Ho et al., 2001). Dissolution of orthoclase and clay minerals supply K^+ ions in groundwater (Ho et al., 2001). The observed positively skewed distribution of different cations is possibly due to the differential rate of carbonate and silicate mineral weathering in the study area. Anions viz. Cl^-, SO_4^{2-} and NO_3^- are major inorganic components deteriorating the quality of groundwater as drinking water (Halim et al., 2009). HCO_3^- in groundwater aquifers could be released by the dissolution of carbonate minerals via biodegradation of organic matter (Ho et al., 2001). High skewness value of 6.86 observed for NO_3^- could be due to agricultural input or other anthropogenic cause which potentially contributes to high NO_3^- concentration in groundwater sample (Raju et al., 2015). Agricultural application of fertilizer may also possibly contribute to high Cl^- concentration in groundwater (Halim et al., 2009). Locally used bleaching powder [$Ca(ClO)_2$] could be another probable cause of high Cl^- into groundwater aquifers (Das et al., 2016) along with local recharge gained from surface contribution as recharge by river or irrigation return flow (Sharif et al., 2008). The southern study transect being an agricultural area, fertilizer use may be a potential source of PO_4^- ion into groundwater samples. Alternatively, PO_4^- ion may be released in groundwater due to microbial mediated reductive dissolution of Fe(III)-oxyhydroxide (McArthur et al., 2004).

Chemistry of recharging water, water-aquifer matrix interaction (eg. Cation exchange, mineral dissolution) available reactive organic matter and groundwater residence time within aquifer primarily control the evolution of major ions compositions in groundwater (Mukherjee et al., 2008). Carbonate mineral dissolution, silicate weathering and ion exchange processes primarily regulates geochemical evolution of major solute compositions in groundwater (Dowling et al., 2003; Mukherjee and Fryar, 2008). These processes in turn depend on the bulk mineralogy of the aquifer sediments and the kinetics of chemical weathering processes (Tardy et al., 1971; Faure, 1998). The concentration of Na^+ and K^+ in groundwater is primarily controlled by silicate mineral weathering and ion exchange, while carbonate mineral dissolution mainly controls $Ca^{2+,}$ Mg^{2+} and HCO_3^- in groundwater. Meybeck (1987) reported that in comparison to silicate weathering, carbonate weathering rates are nearly 12 times faster. Therefore, presence of highly leachable litho-units as well as groundwater residence time significantly influences groundwater chemistry. Solute mass balance approaches have been adopted to demonstrate the extent of different chemical processes occurring and their contributions to the evolution of groundwater in the study area.

The bivariate mixing plots (Figure 5.6) of Na^+-normalized Ca^{2+} versus Na^+-normalized Mg^{2+} and Na^+-normalized HCO_3^-, examine the relative contribution of three major weathering mechanisms (silicate, carbonate, and evaporite) to solute concentration in groundwater (Gaillardet et al., 1999; Mukherjee and Fryar, 2008; Mukherjee et al., 2012). Bivariate plots of Na-normalized (μM/μM) Ca^{2+}versus $Na^+$and HCO_3^- versus Ca^{2+} shows that groundwater samples are clustered between the zone of global average silicate and carbonate weathering (Figure 5.7), indicating that the water chemistry is controlled predominantly by silicate weathering and to some extent by carbonate weathering.

Bivariate plot of HCO_3^- versus Na+K ions indicate that most groundwater samples fall above the 1:2 line, while on the plot of Na+K ions versus total cation , the samples fall below the 1:1 line (Figure 5.7), suggesting that both carbonate and silicate weathering are major processes contributing to the major cation pool of the groundwater samples. The ratio of Na+K ions to total cations ranged between 0.10 to 0.78 with a mean of 0.50, while ratio of Ca+Mg ions to total cations ranged between 0.22 to 0.90 with a mean of 0.49, indicating that Ca and Na ions are the dominant cations, derived from weathering of silicate (Ca-silicates) and carbonate (calcite and dolomite) minerals and silicate mineral weathering and ion exchange.

Soluble ions in natural waters mainly come from rock and soil weathering, anthropogenic input and partly from the atmosphere input (Xing et al., 2013). Gibbs diagrams which are related to ratios of cations (Na+ K)/(Na+K+Ca) and anions ($Cl/Cl+HCO_3$) against TDS (Gibbs, 1970), are generally used to study factors influencing water chemistry (Mamatha and Sudhakar, 2010). Gibbs plot indicates that majority of the samples falls in the zone of rock dominance revealing the interaction between aquifer material and groundwater as the major source of dissolved ions controlling the hydrogeochemistry (Figure 5.8). With limited industrial base in the region, rock water interaction controlling geochemical evolution of groundwater seems relevant for the study transect. Weathering of silicate minerals, viz. albite (soda feldspar), orthoclase, microcline (potash feldspar) etc. and carbonate minerals viz. calcite, dolomite etc. may be the probable mechanisms controlling evolution of groundwater along the southern transect.

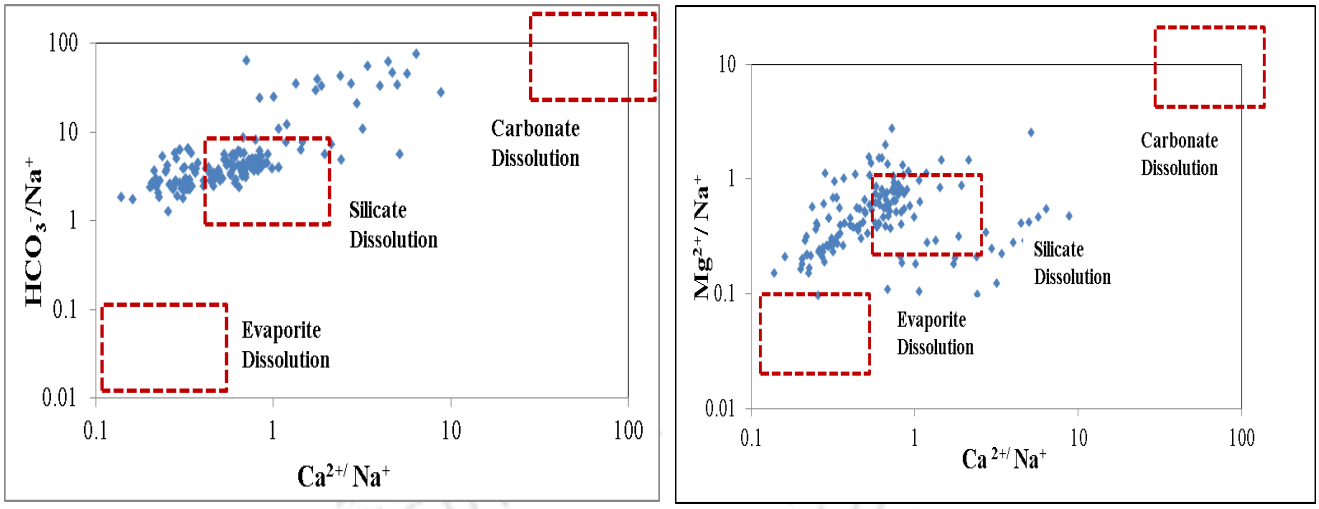

Figure 5.6 Bivariate plots of Na-normalized (µM/µM) Mg ions versus Ca ions and HCO_3 ions versus Ca ions to show trends of weathering. The dashed rectangular areas demonstrate global average compositions of groundwater with respect to evaporite dissolution, silicate weathering, and carbonate dissolution without mixing (following Gaillardet et al., 1999 and Mukherjee et al., 2012)

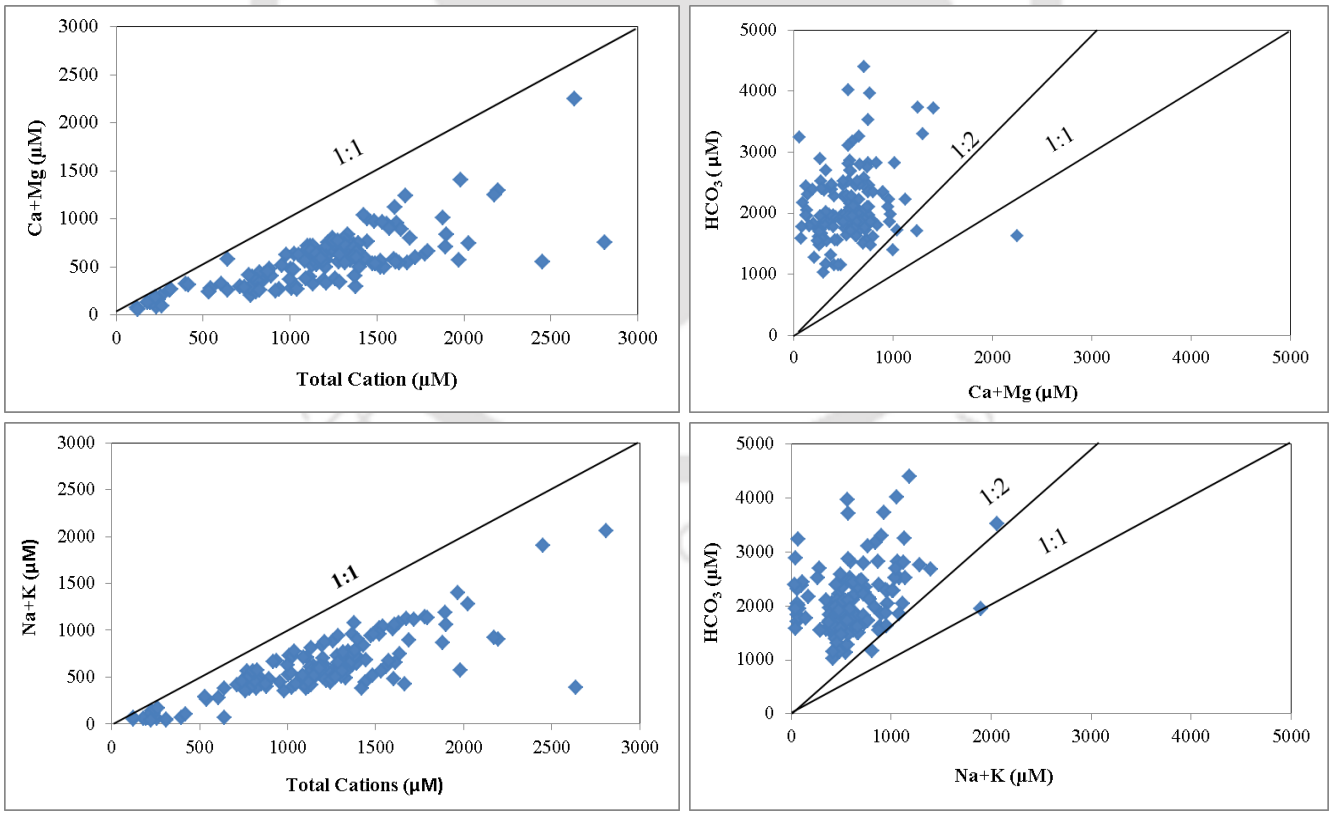

Figure 5.7(a) Bivariate plots of Ca + Mg (µM) ions and Na + K (µM) ions versus total cation (µM) concentration in the groundwater samples; (b) Bivariate plots of HCO_3 ions (µM) versus Ca + Mg ions (µM) and Na + K ions (µM) in the groundwater samples

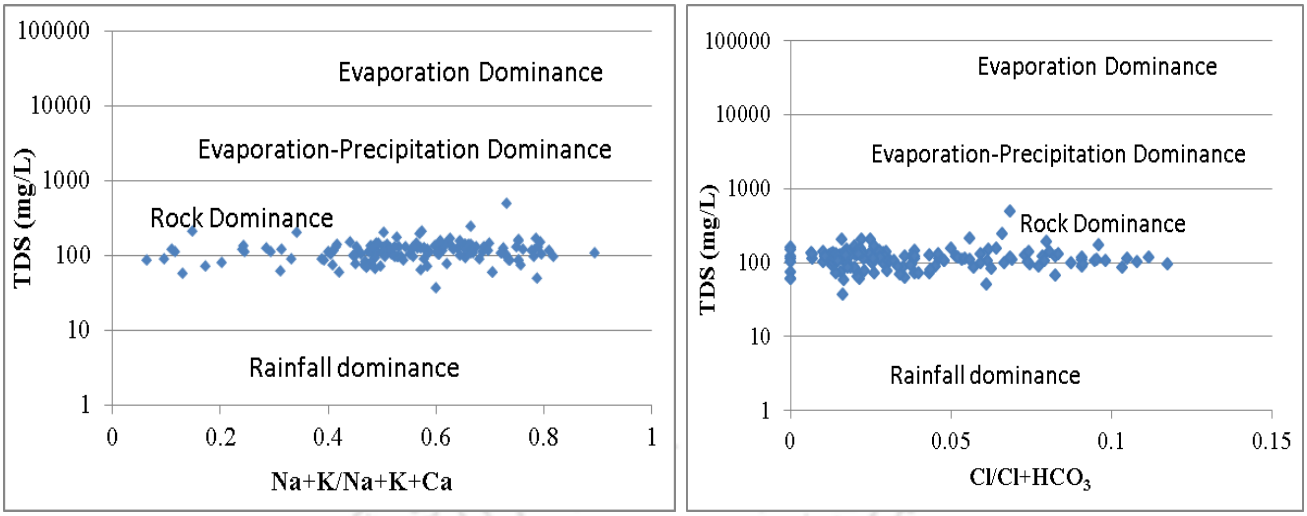

Figure 5.8 Gibbs plot for groundwater (n =153) for the north bank transect

5.1.3 Arsenic and other water quality parameters

Scatter plots to investigate interrelation between As and hydrogeochemical parameters demonstrated no distinctive trends between As with redox sensitive parameters viz. Fe and Mn (Figure 5.9). A strong correlation of As with Fe would indicate that reductive dissolution of Fe oxyhydroxides as a process of arsenic release into groundwater (Nickson et al., 1998; Cummings et al., 1999; McArthur et al., 2001). However, the observed weak correlation between As and Fe could be due to the non-conservative nature of Fe, which has been previously suggested (Mahanta et al., 2015) including the precipitation of dissolved Fe as pyrites and siderite solids ($FeCO_3$), vivianite [$Fe_3(PO_4)_28H_2O$], pyrite (FeS_2) and rhodochrosite ($MnCO_3$) under reducing conditions (Reza et al., 2010, Guo et al., 2014, Sracek et al., 2000; 2004; Mukherjee et al., 2008; Hasan et al., 2010). Repeated cycles of oxidation and reduction in the subsurface in response to water table fluctuations or addition of oxygen during well sampling is also reported to lead to poor As-Fe correlation (Reza et al., 2010). Poor correlation (R^2=0.1) between As and Fe thus suggests that simple breakdown of FeOOH may not be sufficient to explain high levels of dissolved As (Dowling et al., 2002).

Observed weak correlation between As and Mn may be explained by the fact that dissolved manganese concentrations in reducing aquifers are generally controlled by rhodochrosite, $MnCO_3$. Mn can also be implemented as a minor constituent in siderite (Mukherjee and Bhattacharya 2001; Bhattacharya et al. 2001; Sracek et al., 2004; Ahmed et al., 2004). Additionally, possible explanation for the lack of correlation with Mn is that the

adsorption/desorption from manganese oxides/hydroxides play a minor role in controlling the mobility of As in the aquifer (von Brömssen et al., 2007; Hassan et al., 2007; Mukherjee et al., 2008).

Moderate to strong positive correlations between As and HCO_3^- in groundwater indicate that microbially mediated reductive dissolution of As-bearing Fe(III) oxides by organic matter is the main mechanism of As release, where the reductive driving force is derived from organic carbon in aquifers (Nickson et al. 1998; Anawar et al. 2003; Islam et al. 2004). Weak correlation between As and HCO_3^- (R^2=0.2) (Figure 5.9) is suggestive of a complex relation between both parameters, e.g. multiple sources and sinks for HCO_3^- like decomposition of dissolved organic carbon (DOC) and precipitation of carbonates (Mahanta et al., 2015).

Weak to no correlation of As with NO_3^- and SO_4^{2-} suggests that sulphate oxidation is not a probable mechanism of As release into groundwater. It reaffirms that pyrite/sulfide oxidation is not the governing mechanism of As release in groundwater along the northern transect. Studies in downstream Brahmaputra and Bengal basin have reported that correlation between As and redox sensitive parameters may be limited by the occurrence of multiple reactions in heterogeneous sediments (Mukherjee and Fryar, 2008).

Phosphate in particular is known to compete strongly with As for available bonding sites on Fe(III) oxides (Acharyya et al., 2000; Manning and Goldberg, 1996). Phosphate, whose chemical sorption behavior is very similar to that of arsenate, competes for the available sorption sites on metal oxides/hydroxides/clay minerals/ organic matter and may lead to the desorption of As [mostly As (V)] and thus release As into groundwater (Acharyya et al. 1999, 2000). While the competing role of PO_4^- in releasing As into groundwater has been reported (Stollenwerk et al. 2007; Stachowicz et al. 2008; Biswas et al., 2014), with an observed weak correlation between As and PO_4^- concentrations, the possible competing role of PO_4^- in As release in groundwater along the northern transect may be limited.

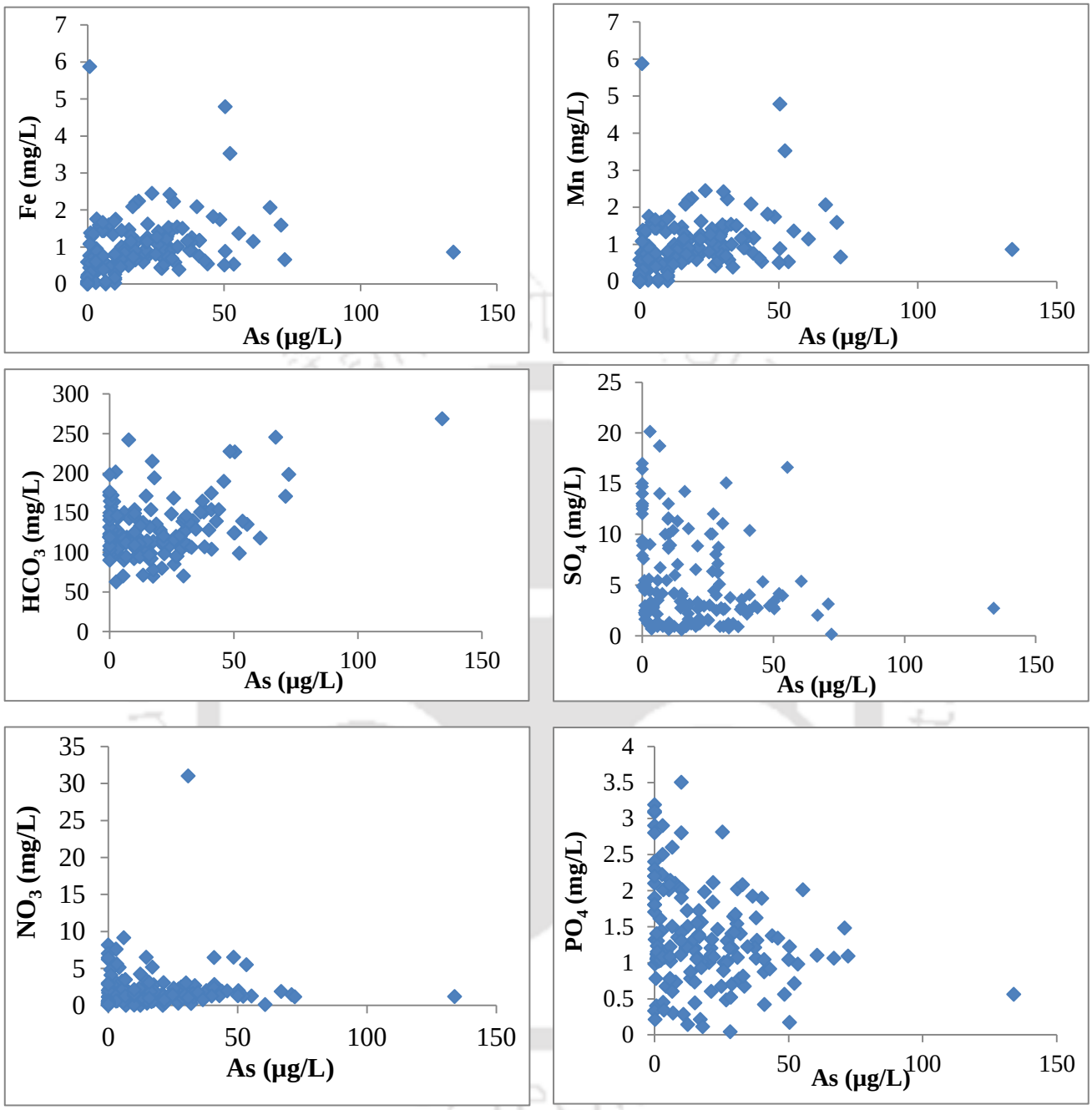

Figure 5.9 Scatter plots showing behavior of (a) As (µg/L) with various parameters: (a) Fe, (b) Mn, (c) HCO_3^- (d) SO_4^{2-}, (e) NO_3^- (f) PO_4^-

5.1.4 Depth profile of As Fe, Mn, SO_4 and HCO_3

Sources with As concentrations above WHO and national limits were mostly concentrated around the shallow depth range, as observed in most arsenic contaminated aquifers in South

and Southeast Asia (BGS and DPHE, 2001; Ahmed et al., 2004; Zheng et al., 2005) (Figure 5.10). Concentrations of As, Fe and Mn in groundwater at similar depths (<50 m depth) suggest that these constituents are derived from similar geochemical processes and most likely from similar mineralogical sources (Shamsudduha et al. 2008).

Depth variation of As, Fe and SO_4^{2-}, indicated that zones of high arsenic could be correlated with high Fe and low SO_4^{2-}concentrations. However, it is intriguing that under a wide range of Fe concentrations, dissolved As concentrations are within moderate ranges, contrary to what is observed in other arsenic affected areas in South and South East Asia. The probable cause of moderate As occurrences may possibly be the higher Fe/As ratios in the area.

Higher dissolved Fe/As ratios along with high levels of dissolved Fe in the study area, indicate that arsenic mobility could possibly be controlled by increased sorption densities on solid phases (Dixit and Hering, 2006) and/or retained by evolving new phases that incorporate arsenic and iron (Herbel and Fendorf, 2006). Neidhardth et al., 2014 introduced an easily degradable carbon source (sucrose) into a shallow aquifer via four nested monitoring wells and distributed by circular pumping to study the role of organic carbon in mobilization of iron, manganese and arsenic into groundwater. Their experimental results showed that although there was an increase in the concentrations of Fe and Mn in the groundwater after the addition of sucrose, the response of the groundwater arsenic to addition of sucrose and successive microbial process were much lower when compared to other major and trace elements. Comparing the large pool of sedimentary Fe-oxydroxides (several g/kg) to the fraction of dissolved Fe (several µM), they assumed that there were always sufficient residual Fe-mineral phases available for adsorption of As (Neidhardth et al., 2014). The observed moderate levels of arsenic concentrations (As > 50 µg/L to As < 100 µg/L) can thus be attributed to the higher sorption densities on solid phases. Consistent with studies in Bengal Basin, Fe and Mn demonstrated similar depth control, with high concentrations being concentrated in shallow depths (Farmer and Lovell, 1986; Mukherjee et al., 2008). The presence of a wide scatter for Fe with respect to Mn suggests that some but not all of the Fe and Mn dissolution may occur in overlapping redox zones (Mukherjee et al., 2008).

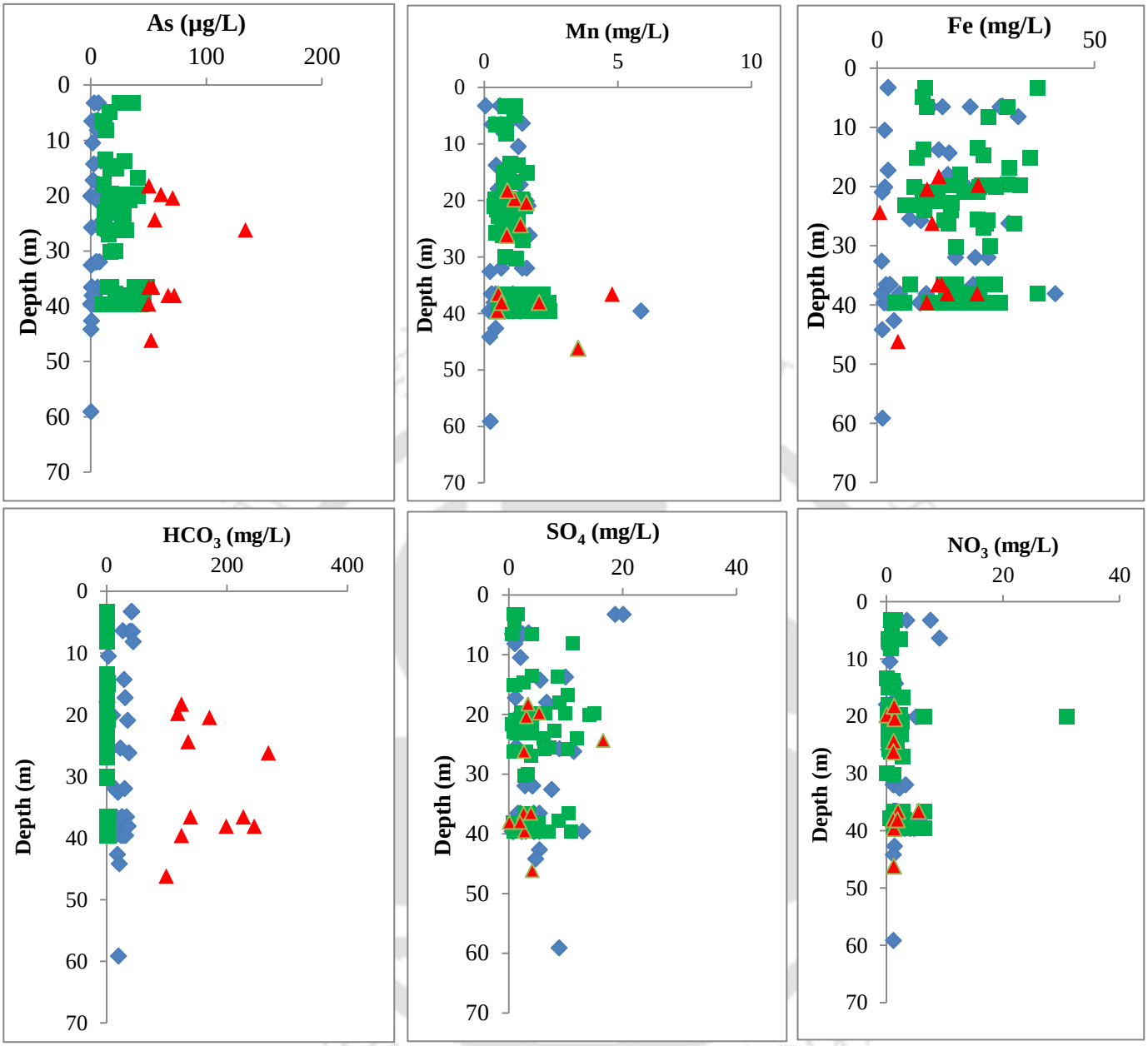

Figure 5.10 Depth distribution of As, Fe, Mn, SO_4 and HCO_3 for groundwater along the northern transect. The same symbol color corresponding to the As content of groundwater (light blue ≤10 µg/L; green 10–50 µg/L; red >50 µg/L) are used for dissolved Fe, Mn, SO_4^{2-}, $NO_3^-$and HCO_3^-

5.1.5 Saturation Indices

Water-rock interaction process such as dissolution and precipitation of minerals facilitates transfer between bedrock and groundwater (Taheri et al., 2017). Dissolution initiates when groundwater tends to move towards equilibrium and continues until groundwater is saturated

with those particular mineral components. Under equilibrium concentrations, the excess mineral components may combine in the solution to form precipitates of that particular mineral, and this reaction is called precipitation (Deutsch, 1997).

Saturation index calculations for groundwater from northern transects were carried out to calculate saturated and under-saturated mineral phases that are thought to be affecting the chemistry of the groundwater. Groundwater along the northern transect is generally highly under-saturated with respect to O_2 and has higher CO_2 than the atmosphere, suggesting a strong input of CO_2 from the degradation of organic matter. SI values < 1 for most northern bank samples indicated groundwater to be highly under-saturated with respect to the major As phases (e.g. arsenolite, As_2O_5, and $FeAsO_4 \cdot 2H_2O$) and Mn oxide phases (e.g. birnessite, bixbyite, manganite, and pyrolusite), representing that when As and Mn enter into solution, they do not precipitate as those phases (Table.9).

Groundwater is supersaturated with respect to Fe (III) (oxyhydr) oxide phases like magnetite, hematite, goethite, indicating that precipitation of Fe(III) phases from groundwater is thermodynamically favorable (Figure 5.11). Saturation indices calculation shows that carbonate mineral phases viz. calcite ($CaCO_3$) and dolomite ($MgCa(CO_3)_2$) are under-saturated and generally gave similar (mean) values. These samples probably come from an environment where calcite and dolomite are impoverished or where Ca^{2+} and Mg^{2+} exist in other forms and have not reached equilibrium with the carbonates due to short residence time. The SI for major mineral phases that may regulate the concentration of Fe(II) and Mn(II) in groundwater are mostly at or close to equilibrium (eg. Rhodochrosite ($MnCO_3$) and siderite ($FeCO_3$). The saturation states of Fe and Mn bearing carbonates, and oxides (eg. Fe(III) oxide/hydroxides such as magnetite, hematite, goethite etc.) in the groundwater indicate favorable conditions for potential As adsorption onto the surfaces of Fe and Mn-bearing oxides and carbonates formed under oxidizing and reducing conditions, respectively.

Table 9 Summary of saturation indices (SI) calculated by PHREEQC for selected phases for the groundwater samples of both transects

Transect	Mineral Phases	Formula	Min	Max	Average
Northern Transect	**Anhydrite**	$CaSO_4$	-5.25	4.18	-3.84
	Arsenolite	As_2O_3	-28.06	-11.28	-16.7
	As_2O_5	As_2O_5	-33.98	-13.72	-30.99
	Birnessite	MnO_2	-21.92	-11.8	-18.28
	Brucite	$Mn(OH)_2$	-21.17	3.09	-7.4
	Calcite	$CaCO_3$	-2.56	0.10	-1.40
	CO_2 (g)	CO_2	-3.70	-0.60	-1.65
	Dolomite	$CaMg(CO_3)_2$	-5.75	0.30	-2.80
	Ferrihydrite	$Fe(OH)_3$	-3.79	-3.82	0.01
	Gypsum	$CaSO_4{:}2H_2O$	-5.03	-1.18	-3.66
	Goethite	FeOOH	2.45	9.69	5.93
	Haematite	Fe_2O_3	6.92	21.40	13.93
	Magnetite	Fe_3O_4	5.21	25.02	15.60
	Rhodochrosite	$MnCO_3$	-2.96	1.57	-0.13
	Siderite	$FeCO_3$	-2.13	2.13	0.63

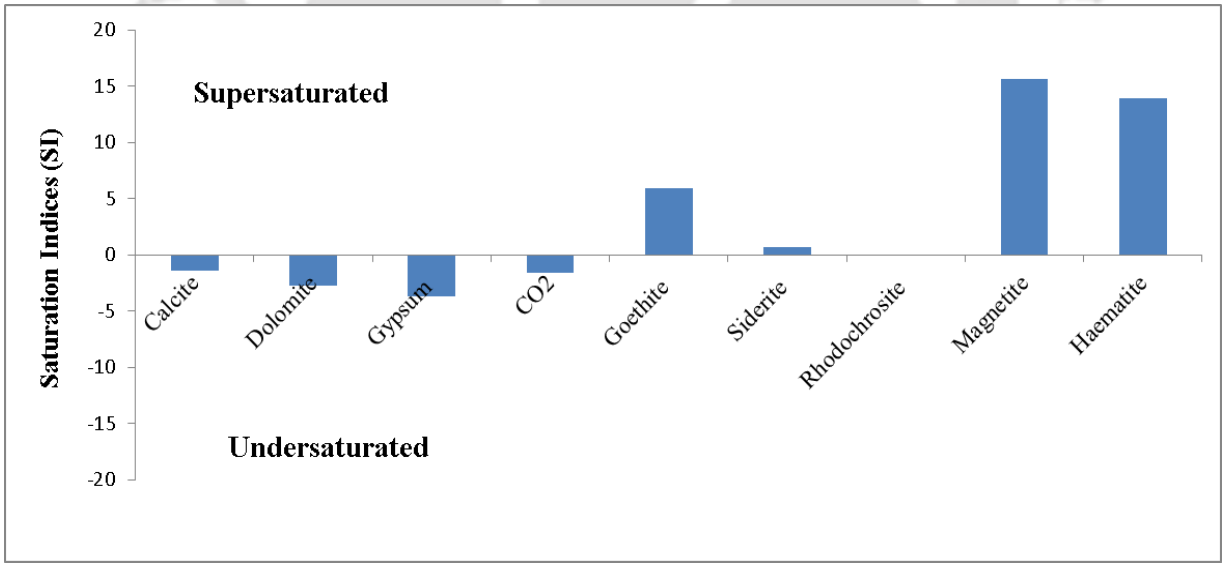

Figure 5.11 Plot of mean saturation index (SI) calculations for groundwater along the northern transect, carried out to calculate saturated, under-saturated and equilibrium mineral phase

5.1.6 Inverse Geochemical Modeling

Hydrogeochemical processes, including dissolution, precipitation, ion-exchange, sorption, and desorption, together with the residence time occurring along the flow path, control the variation in chemical composition of groundwater (Apodaca et al., 2002), which can be modeled by inverse geochemical models. Inverse geochemical modeling was used to determine sets of mole transfers of phases that account for changes in water chemistry between an initial water composition and a final water composition (Parkhurst and Appelo, 1999). In inverse modelling, one aqueous solution (starting solution) is made to mix with other aqueous solution (mixing solution) to solve a set of linear equalities that account for the changes in the moles of each element by the dissolution or precipitation of minerals to produce the observed composition of an end aqueous solution (Parkhurst and Appelo, 1999). Determination of possible mineral phases is vital for inverse modeling, which is based on mineral compositions of aquifer sediments, groundwater chemical constituents and the aquifer conditions (Güler and Thyne, 2004). Potential phases (minerals) for model run were selected from XRD, SEM, and chemical analysis of sediment samples. Potential mineral phases in the inverse modeling were constrained (precipitation/dissolution) using a conceptual model of overall trends in chemical data and saturation indices (logarithm of the quotient of the ion activity product (IAP) and solubility product constant (K_{SP}) data (over-saturated phases were allowed to precipitate) of groundwater of selected water-wells. XRD peak positions and petrographic study revealed that aquifer sediments are mainly composed of quartz, calcite, chlorite, and micas. Mean concentrations of groundwater along a selected flow path from the northern transect was selected to perform the inverse modeling simulation (Table 10). The flow paths were selected on the basis of geographic locations and surface elevations of the point in the catchment (Figure 5.12). The inverse models were formulated so that primary mineral phases viz. quartz, calcite, dolomite, gypsum, were constrained to dissolve until they reached saturation, and calcite was set to precipitate once it reached saturation, while siderite, rhodochrosite, magnetite and hematite were set to precipitate once they reached saturation.

In inverse geochemical modeling, the groundwater flow system and chemical composition of the aquifer were assumed to be steady- state conditions. The modeling approach assumed that initial and final end member waters that were used in the simulations were representative groundwaters from the same, or convergent flow path(s), and accordingly the minerals employed in the model calculations must occur within the aquifer matrix. Further, it was

presumed that the effects of hydrodynamic dispersion along the modelled flow paths are negligible (Plummer et al., 1983; Zhu and Anderson, 2002; Johannesson and Tang, 2009).The following geochemical reactions were hypothesized to proceed during the groundwater flow, and these were simulated with inverse geochemical models:

i. Precipitation or dissolution of calcite, dolomite, and gypsum.

ii. Oxidation of pyrite with precipitation of amorphous iron-oxyhydroxide

iii. Sulfate reduction with the evolution of hydrogen sulfide (H_2S).

Table 10 Mean parameter values of the three principal water groups along northern transect

	pH	EC	Fe	Mn	Na	K	Ca	Mg	HCO_3	SO_4	NO_3	Cl
Recharge Zone (n= 8)	6.85	158	1.37	0.16	3.36	2.00	4.50	1.74	142	13.79	2.54	3.93
Runoff Zone (n = 10)	7.34	181	20.95	0.73	12.67	7.29	5.85	4.28	111	1.55	0.86	9.24
Discharge Zone (n = 16)	6.54	153	17.36	1.67	10.36	3.79	10.95	6.52	98	3.32	1.68	4.83

All values are in mg/l except pH and EC (µSiemens/cm)

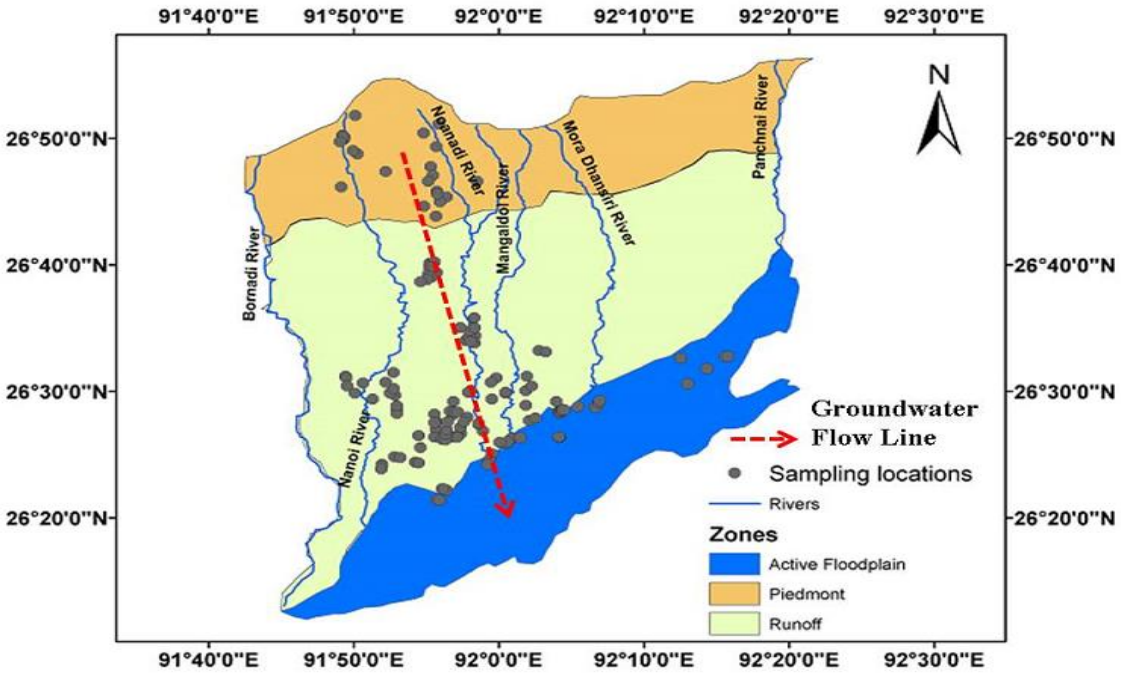

Figure 5.12 Map showing general direction of groundwater flow through the three different zones

To evaluate possible hydrochemical reactions along flow path, inverse mass-balance models were developed using the hydrochemical reaction computer code PHREEQC (Parkhurst and Appelo, 1999). Three primary processes contribute to the generation of solutes in groundwater: evaporation, carbonate dissolution and precipitation, and silicate weathering (Garrels and MacKenzie, 1971). Thus, simulations were performed to demonstrate the groundwater evolution from the recharge (mean value of samples) to the discharge zone (mean value of samples). The models were selected from all the possible models based on the statistical measurements calculated by PHREEQC (sum of residuals and maximum fractional error) and to represent different possible combinations of reactants and products that can account for the change in water chemistry (Table 11).

Inverse geochemical modeling indicates that a relatively few number of phases are required for groundwater evolution along the flow path in the study area. Inverse modeling suggests that dissolution of carbonates and hydroxides are the major processes leading to evolution of groundwater along the flow path.

Inverse geochemical modeling showed carbonate, ferrihydrite and CO_2 are dissolving while gypsum and H_2S are precipitating along the flow path. Calcite and dolomite dissolution is indicated by positive mole balance. Dissolution of calcite is possible as groundwater in the study transect is under-saturated with respect to calcite. Positive phase mole transfer for Fe–oxyhydroxides indicated that Fe precipitated during precipitation of sulphide phases (viz. H_2S) are major geochemical processes in the aquifers along the flow path. Dissolution of $Fe(OH)_3$ phase indicate that microbially mediated reductive dissolution of Fe-oxyhydroxides is a mechanism of arsenic release in groundwater.

Sulfate reduction is indicated from negative phase-mole transfer values (degassing of hydrogen sulfide gas), and by strong hydrogen sulfide (H_2S) odour emanating from the tube wells during sampling. The inverse geochemical modeling confirmed the hypothesized general processes leading to the evolution of groundwater along the flow path. Inverse model calculations were conducted using the computer program PHREEQC v. 2.13.0 (Parkhurst and Appelo, 1999). Thermodynamic database used: phreeqc.dat, values are in mol/kg H_2O. Positive (mass entering water) and negative (mass leaving water) phase mole transfers indicated dissolution and precipitation, respectively.

Tables 11 Summary of species involved in phase transfers in the water groups. Four models were found in simulation 1

Mineral Phases	Phase State	Phase Mole Transfers	Phase Mole Transfers	Phase Mole Transfers	Phase Mole Transfers
Goethite	Dissolution	1.28E+02	4.51E+01	4.51E+01	
$Fe(OH)_3(a)$	Dissolution	1.28E+02	4.51E-01	4.51E+01	
Gypsum	Precipitation	-2.48E-04	-1.28E-04		-1.28E+02
CaX2	Precipitation	-3.46E-04			
NaX	Dissolution	6.93E-04			
Dolomite	Precipitation	-7.77E-05			
H_2S	Precipitation		3.40E-05	3.96E-05	1.28E+02
CH_2O	Dissolution			1.47E-04	2.56E+02
Calcite	Dissolution				1.28E+02
CO_2	Dissolution				1.28E+02

5.1.7 Stable Isotopes

Stable isotopes ($\delta^{18}O$ and $\delta^{2}H$) of groundwater samples from northern transect was analysed to infer the sources of recharge into the aquifers. Assuming that aquifers along the study transect were recharged locally, mechanism of recharge can be explained via mechanism of direct meteoric recharge, surface water infiltration and evaporation influenced recharge. The values of$\delta 1^{8}O$ and$\delta^{2}H$ in the sampled wells varied within -7.66 ‰ VSMOW to -2.68 ‰ VSMOW and -49.09 ‰ VSMOW to -12.70 ‰ VSMOW. Results indicated that groundwater samples fell along the Global Meteoric Water Line (GMWL: $\delta^{2}H = 8\ \delta^{18}O + 10$) of Craig (1961), suggesting some influence of evaporation through recharging water in study area, the trend of samples being $\delta^{2}H= 7.15\delta 1^{8}O + 4.27$ (Figure 5.13).

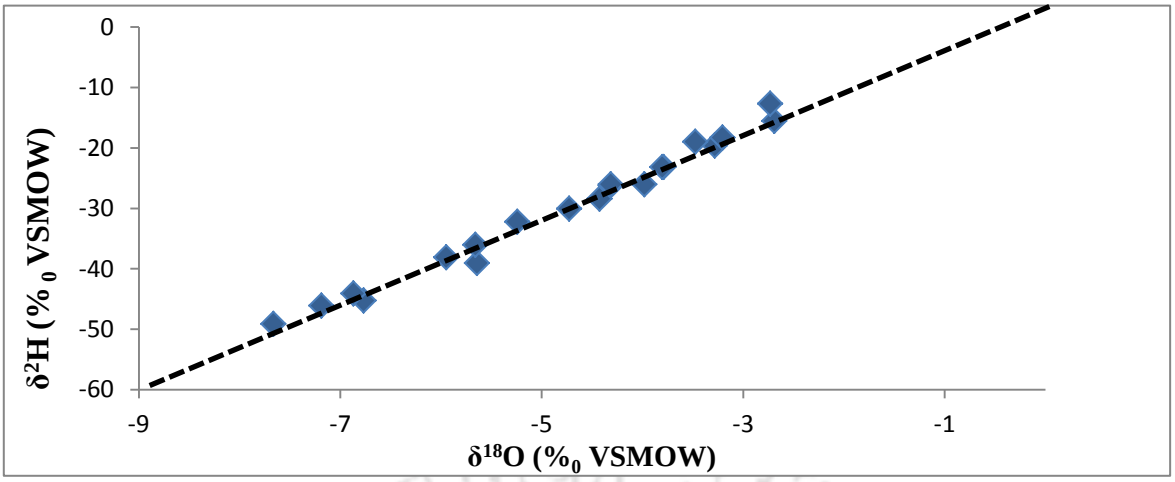

Figure 5.13 Bivariate plot of $\delta^{18}O$ and $\delta^{2}H$ for selected groundwater samples along the northern bank transect. The Global Meteoric Water Line (GMWL) of Craig (1961) is provided for reference

5.2 Hydrogeochemistry of groundwater along southern transect

Major ion composition of groundwater samples (n = 134) collected along the southern transect demonstrated that Sodium (Na^{+}) is the dominant cation, with maximum value 201 mg/L and median of 16 mg/L (Table 9). Concentrations of Ca^{+}, Mg^{2+} and K^{+} ranged as (bdl to157 mg/L), (1 to 24.4 mg/L) and (bdl to 17 mg/L) respectively (Table 12).

Anions were predominated by HCO_3^{-}, with values ranging from, (22.5 mg/L to 438 mg/L, median 135 mg/L) whereas SO_4^{2-} and Cl^{-} showed low concentrations in all groundwater samples along the transect (median: 8.2 mg/L and 6 mg/L respectively). Dissolved NO_3^{-} concentrations (range 0.5 – 20.5 mg/L, median 6 mg/L) and remained relatively low throughout the study area. PO_4^{-}concentrations ranged between 0.2 to 2.8 mg/L with median values of 1.1 mg/L.

Groundwater As measurements showed As concentrations ranging between bdl to 604 µg/L and median value of 40 µg/L. Total arsenic concentrations in groundwater along the transect showed a wide range with 23 % sources that met the WHO guideline for As of 10 µg/L, 32 % sources with As concentrations up to 50 µg/L and 43 % sources with concentration >50 µg/L As. High spatial variability was observed along the transect with a general trend of high As concentrations near the base of the Naga hills and a gradually decreasing concentrations along the floodplains (Figure 5.14). Fe concentration ranged between bdl to 27 mg/L with

median concentration of 9 mg/L., while concentrations of Mn and SO_4^{2-} ranged between bdl to 1.2 mg/L and bdl to 36 mg/L respectively. There are no distinct variation in the concentration of Fe and Mn from the recharge (near foothills) to discharge zone (close to river bank) (Figure 5.15).

Table 12 Groundwater composition along the southern transect (units mg/L, except pH)

Parameter(s)	Units	Min	Max	Mean	Median	Std. Dev	Skewness
pH		6	7.75	7	7.05	0.30	0.30
Na	**mg/L**	3.6	201.4	35.2	15.9	43.6	2.4
Ca	**mg/L**	bdl	157.1	22.0	15.0	24.2	3.0
K	**mg/L**	bdl	17.0	1.9	1.6	1.9	4.4
Mg	**mg/L**	1.0	24.4	11.1	10.0	5.2	0.8
Cl	**mg/L**	bdl	28.0	4.6	3.6	4.5	2.1
HCO_3	**mg/L**	22.5	438.0	142.3	135.0	67.0	1.3
SO_4	**mg/L**	bdl	35.7	10.1	8.2	6.7	1.0
NO_3	**mg/L**	0.5	20.5	6.3	6	3.9	0.8
PO_4	**mg/L**	0.2	2.8	1.1	1.1	0.4	1.3
Fe	**mg/L**	bdl	26.8	10.5	9.0	7.0	0.6
Mn	**mg/L**	0.1	1.2	0.5	0.4	0.3	0.8
As	**(µg/L)**	bdl	604.0	96.9	39.8	122.4	1.7

bdl below detection limit, ** NA Not Available

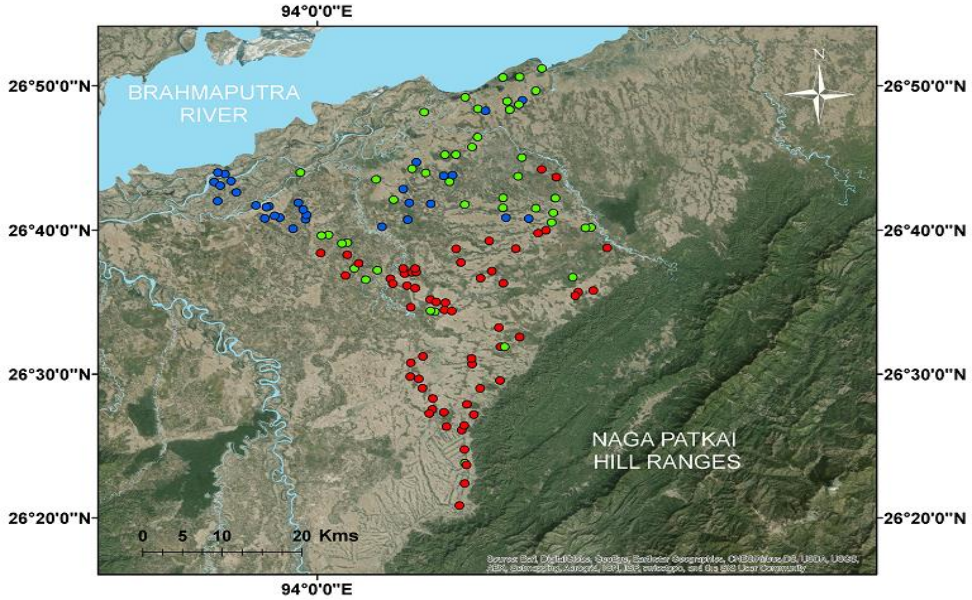

Figure 5.14 Map showing groundwater sampling locations (n=134). The symbol colors correspond to the As content of groundwater (blue <10 µg/L; green 10–50 µg/L; red >50 µg/L)

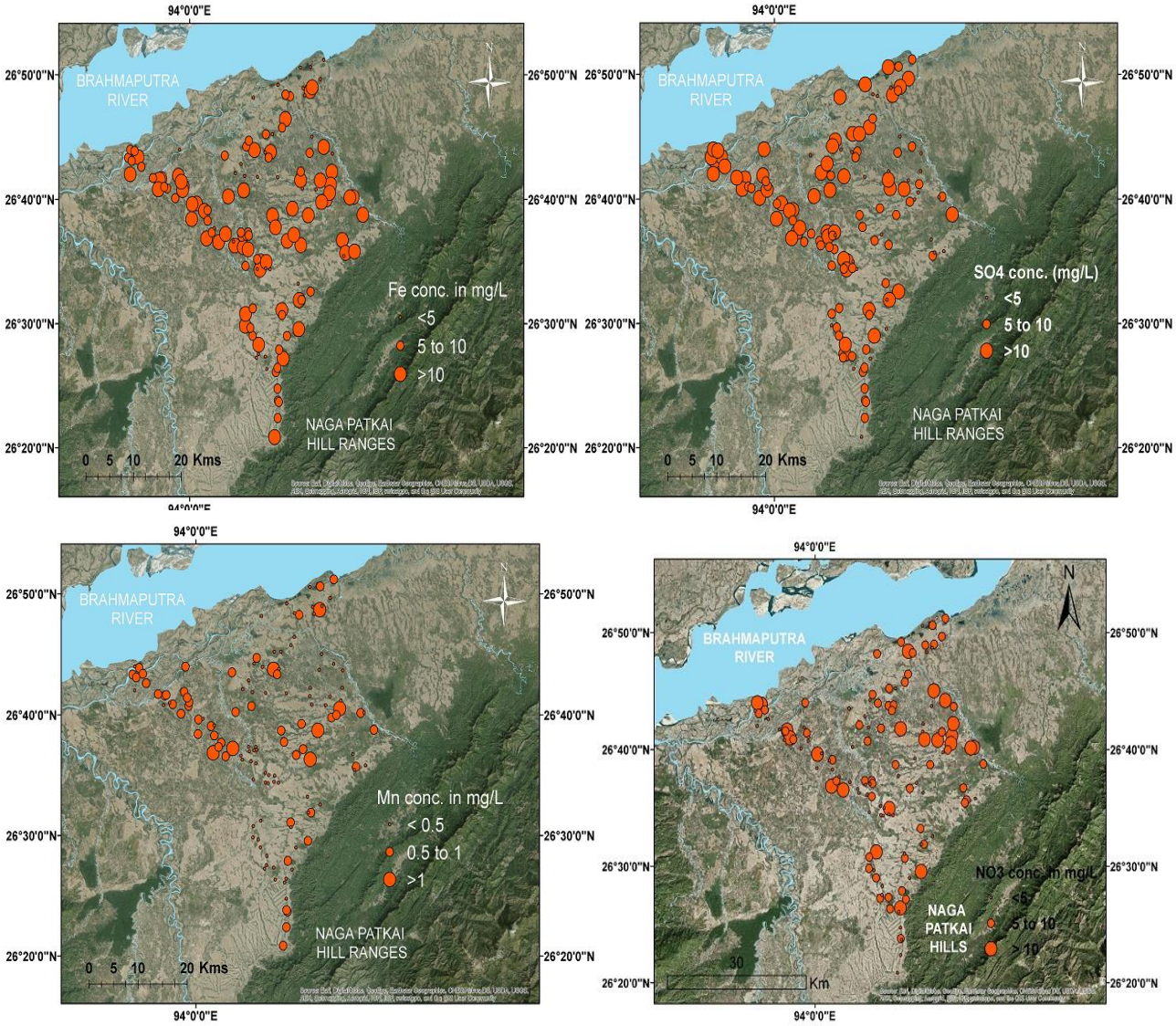

Figure 5.15 Spatial distribution of Fe, Mn, SO_4^{2-} along the southern transect. The size of the circles represents magnitude of concentrations

5.2.1 Hydrogeochemical facies

The aquifers along the southern transect also showed distinct relationship with major solutes in the groundwater. The Piper plot (Figure 5.16) suggests that groundwater of study area were under Na-Ca-HCO_3 hydrogeochemical facies. Previous study (Sailo and Mahanta, 2013) showed almost similar results of groundwater composition in Assam (Titabor). High HCO_3^- in groundwater of downstream Bengal basin or Central Gangetic plain (Zheng et al., 2004; Mukherjee and Fryar, 2008, Mukherjee et al., 2012), is seen to play important role in hydrochemical evolution and trace metal mobilization. The anions are dominated by HCO_3^- accounting to more than 80% of the total anion concentration. Dissolution of carbonate minerals via biodegradation of organic matter as well as the NO_3^- and SO_4^{2-} acting as an electron acceptors in the system to allow oxidation of organic matter was believed to be an

important contributor to the generation of anoxic conditions that produce high concentration of HCO_3^-.Clear evidence of microbially mediated reduction in presence of organic matter was indicated as concentrations of NO_3^- and SO_4^{2-} in groundwater samples decreased with increasing HCO_3^- concentrations (Figure 5.17).

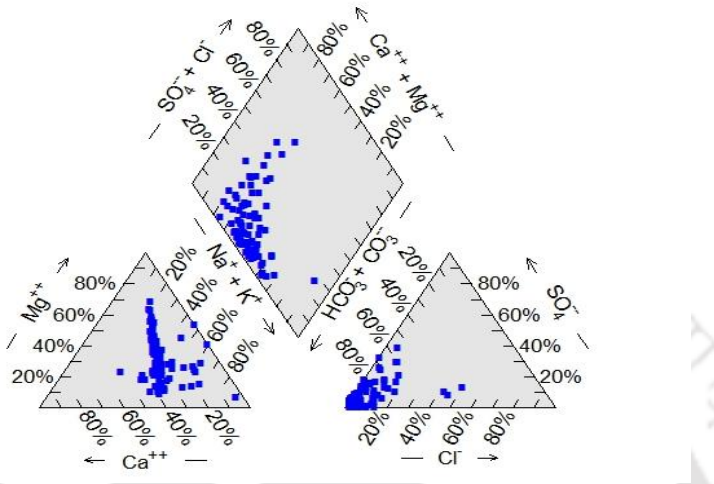

Figure 5.16 Piper Plots of groundwater samples collected along the southern transect

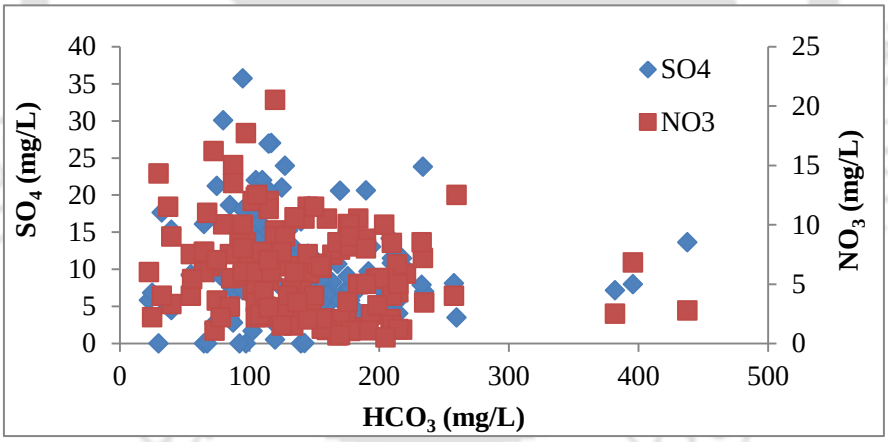

Figure 5.17 Concentrations of NO_3^- and SO_4^{2-} in the groundwater with respect to HCO_3^- concentration

5.2.2 Evolution of major ion composition in groundwater

Na^+ and Ca^{2+} in groundwater can be derived from incongruent dissolution of plagioclase feldspars (Saether et al., 1997), while carbonate minerals like calcite and dolomite contributes to Ca^{2+} and Mg^{2+}(Zheng et al., 2004). K^+ in groundwater may be released from orthoclase and clay minerals (Halim et al., 2009). Observed high NO_3^- concentrations in a few samples could be due to agricultural or other anthropogenic causse which might potentially

contributed to high NO_3^- concentration in the groundwater sample (Raju et al., 2015). The study transect being dominated by agricultural cultivation and tea plantations, fertilizer use may be a potential source of PO_4^- ion into groundwater aquifers along the transect.

Similar to the northern transect, solute mass balance approaches have been adopted to demonstrate the extent of the chemical processes occurring and its contribution to the evolution of groundwater in the study area. The bivariate mixing plots (Figure 5.18) of Na^+ normalized Ca^{2+} versus Na-normalized $Mg^{2+}$and Na-normalized HCO_3^-, examined the relative contribution of three major weathering mechanisms viz. silicate weathering, carbonate weathering, and evaporite dissolution to solute concentration in groundwater (Gaillardet et al., 1999; Mukherjee and Fryar, 2008; Mukherjee et al., 2012). Bivariate plot of Na-normalized (μM/μM) Ca^{2+} versus Na^+ and HCO_3^- versus Ca^{2+} indicated that groundwater samples were clustered in the zone of global average silicate, indicating that water chemistry along southern transect was controlled predominantly by silicate weathering.

Most groundwater samples along the southern transect tend to fall along the 1:2 line on bivariate plot of HCO_3^-versus (Na + K) ions and samples that fall below the 1:1 line on bivariate plot of (Na + K) ions versus total cation suggesting silicate weathering as a dominant process to introduce major ion in groundwater (Figure 5.19). The ratio of Na+K ions to total cations ranged between 0.23 to 0.95 with a mean of 0.54, while ratio of Ca+Mg ions to total cations ranged between 0.05 to 0.77 with a mean of 0.46, indicating that Na and Ca ions were the dominant cations, derived from weathering of silicate (Ca-Na-silicates) minerals. The dominance of Na^+ ion in groundwater along the transect did indicate that pronounced silicate weathering contributed to Na^+ concentrations in groundwater. The cluster along the 1:2 line on the HCO_3^- versus (Na + K) ions plot further suggests that Na and K were primarily derived from dissolution of the reported micas and mafic minerals present in the Naga Patkai hill ranges.

Plots of TDS against Na+K/ Na+K+Ca ions and TDS against Cl/Cl+HCO_3^- ions suggest that rock-water interaction is the natural mechanism controlling the dissolved ions in groundwater of the southern bank transect (Figure 20). With little industrial base in the region, As enrichment being controlled primarily by rock water interaction and the associated processes of weathering and dissolution seems relevant along the study transect. Recent study by Das et al., 2016, in an area close to the study transect reported that weathering and dissolution processes appear to be the dominant processes controlling groundwater evolution along the study transect. With a lower relief and higher residence time of groundwater and sediments in

the southern transect (Singh et al. 2005), water rock interaction reactions involving processes of weathering and dissolution were primary factors controlling the ion balance in groundwater along the southern transect.

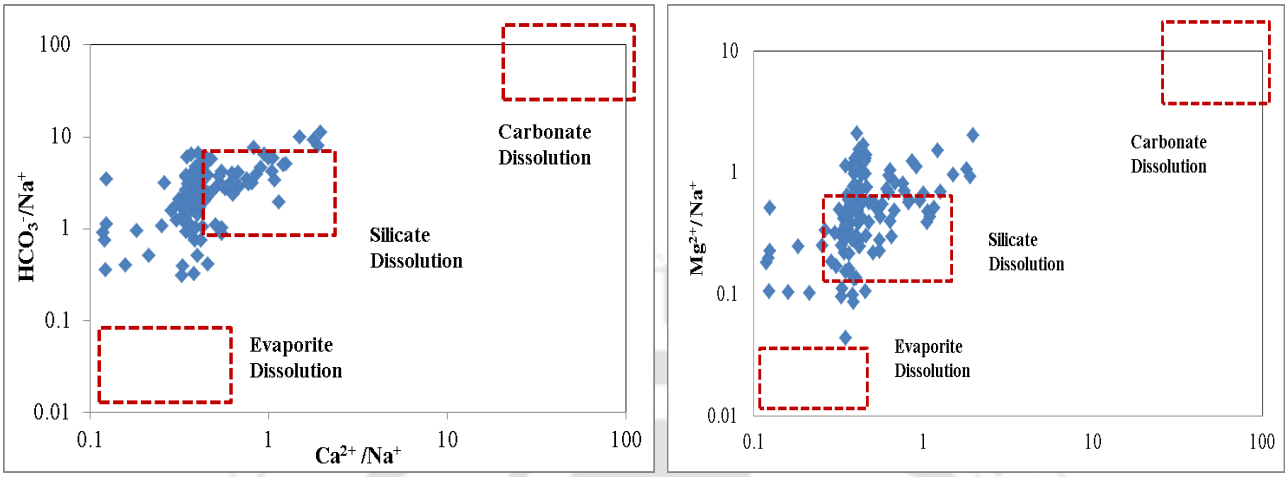

Figure 5.18 Bivariate plots of Na-normalized (µM/µM) Mg^{2+} ion versus Ca^{2+} and HCO_3^- versus Ca^{2+} ion to show trends of weathering. The dashed rectangular zones demonstrate global average compositions of groundwater with respect to evaporite dissolution, silicate weathering, and carbonate dissolution without mixing

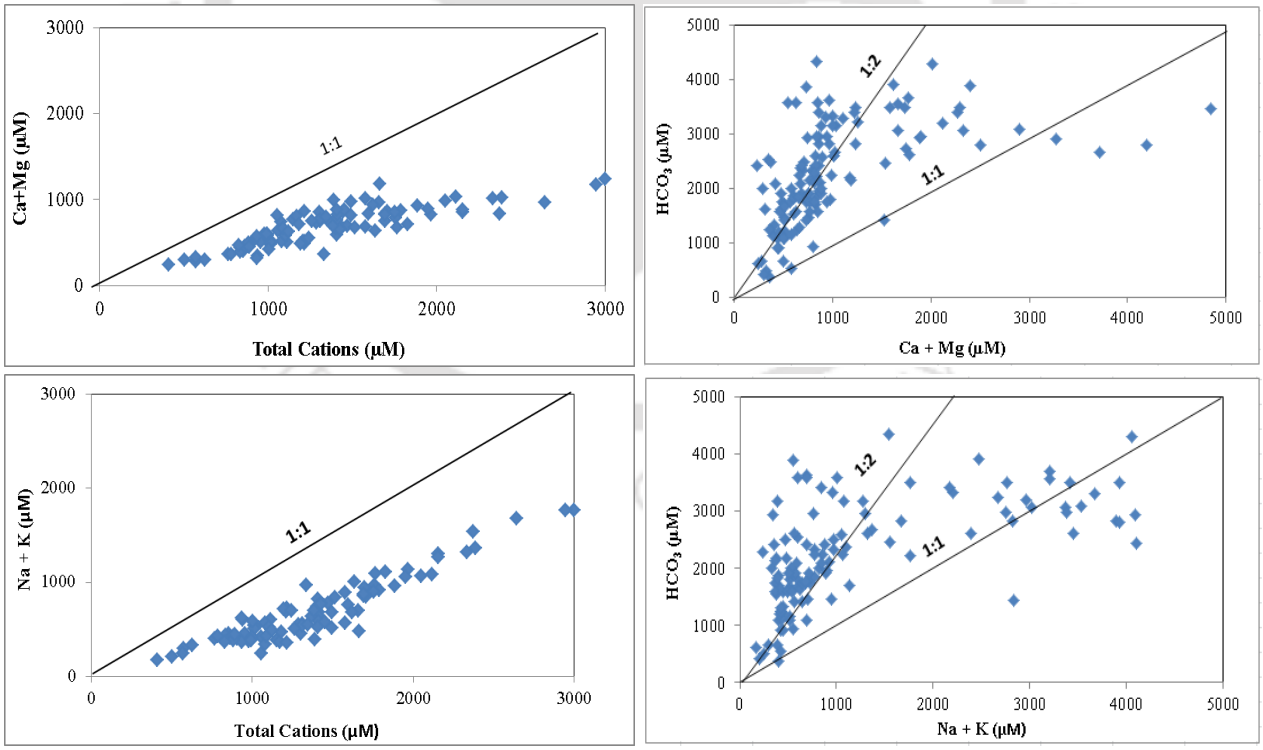

Figure 5.19(a) Bivariate plots of Ca + Mg (µM) and Na + K ions (µM) versus total cation (µM) concentration in groundwater samples; (b) Bivariate plots of HCO_3 (µM) versus Ca + Mg ions (µM) and Na + K ions (µM) in groundwater samples

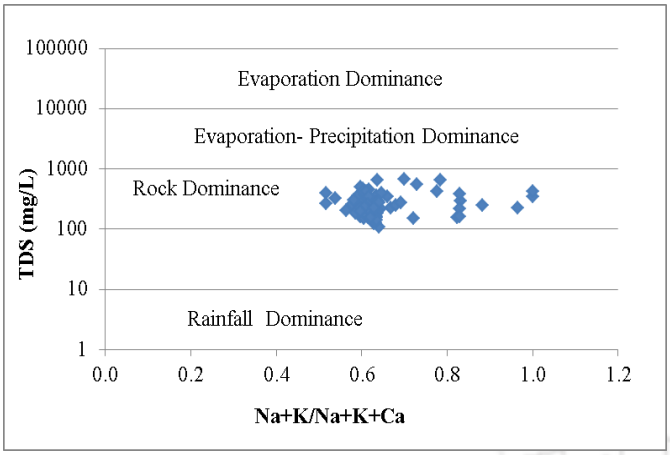

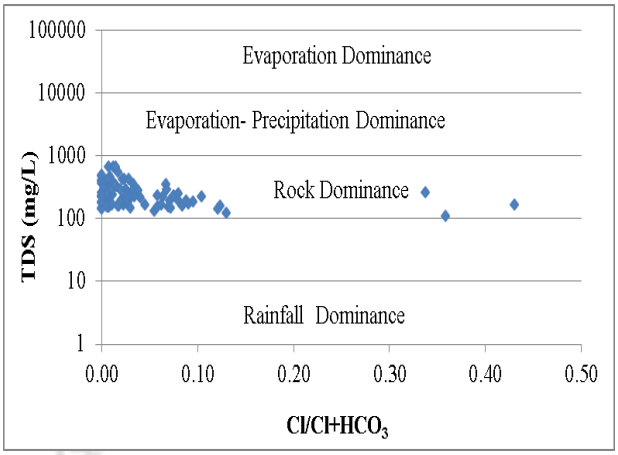

Figure 5.20 Gibbs plot for groundwater (n = 134) for the southern bank transect

5.2.3 Arsenic and other water quality parameters

In most fluvial environments, like the Ganges Brahmaputra Basin, hosting high As groundwater, As is released from iron and manganese (FeOOH, FeS, MnOH) bearing minerals through the process of microbial reduction (Nickson et al., 2000; McArthur et al., 2004) ensuring a significant correlation of As with redox sensitive parameters viz. Mn and Fe. Potential conditions under which low to no correlation exists between As and redox sensitive parameters viz. Fe and Mn has been already discussed in Section 5.1.4. Similar to groundwater along the northern transect, limited correlation was observed between As with redox sensitive parameters viz. Mn and Fe along the southern transect. Such low to no correlations between As and other groundwater parameters were recently reported in groundwater studies from another area adjoining the study transect (Verma et al., 2016; Das et al., 2016), indicating that As release and mobilization in the study transect may possibly be a combination of complex geochemical processes viz. pH dependent desorption, competitive desorption etc., in addition to the generally accepted mechanism of reductive dissolution of Fe(III) oxyhydroxides.

In contrast to that in the northern transect, the observed positive correlation between As and HCO_3^- (R^2 = 0.54) suggests that degradation of organic matter contributes to high HCO_3^- in groundwater (Artenger et al., 2000; Halim et al., 2010). A distinct correlation suggest As mobilization in groundwater in an anoxic environment (Ahmad et al., 2004; Halim et al., 2010; Yadav et al., 2015) (Figure 5.21).

Phosphate in particular is known to compete strongly with As for available binding sites on Fe(III) oxides (Acharyya et al., 2000; Manning and Goldberg, 1996). A moderate correlation observed between As and PO_4^- indicates the possibility of competitive exchange mechanism, where PO_4^- ions possibly compete for adsorption sites with As, thereby releasing As into

groundwater. Weak to no correlation of As with NO_3^- and SO_4^{2-} suggests that sulphate oxidation is not a probable mechanism of As release into groundwater along the southern transect. With no sulphide bearing minerals being observed in sediment samples from boreholes drilled adjacent to sampled groundwater, it can be emphasized that oxidation of sulphide is not a probable mechanism of As release into groundwater of the study area.

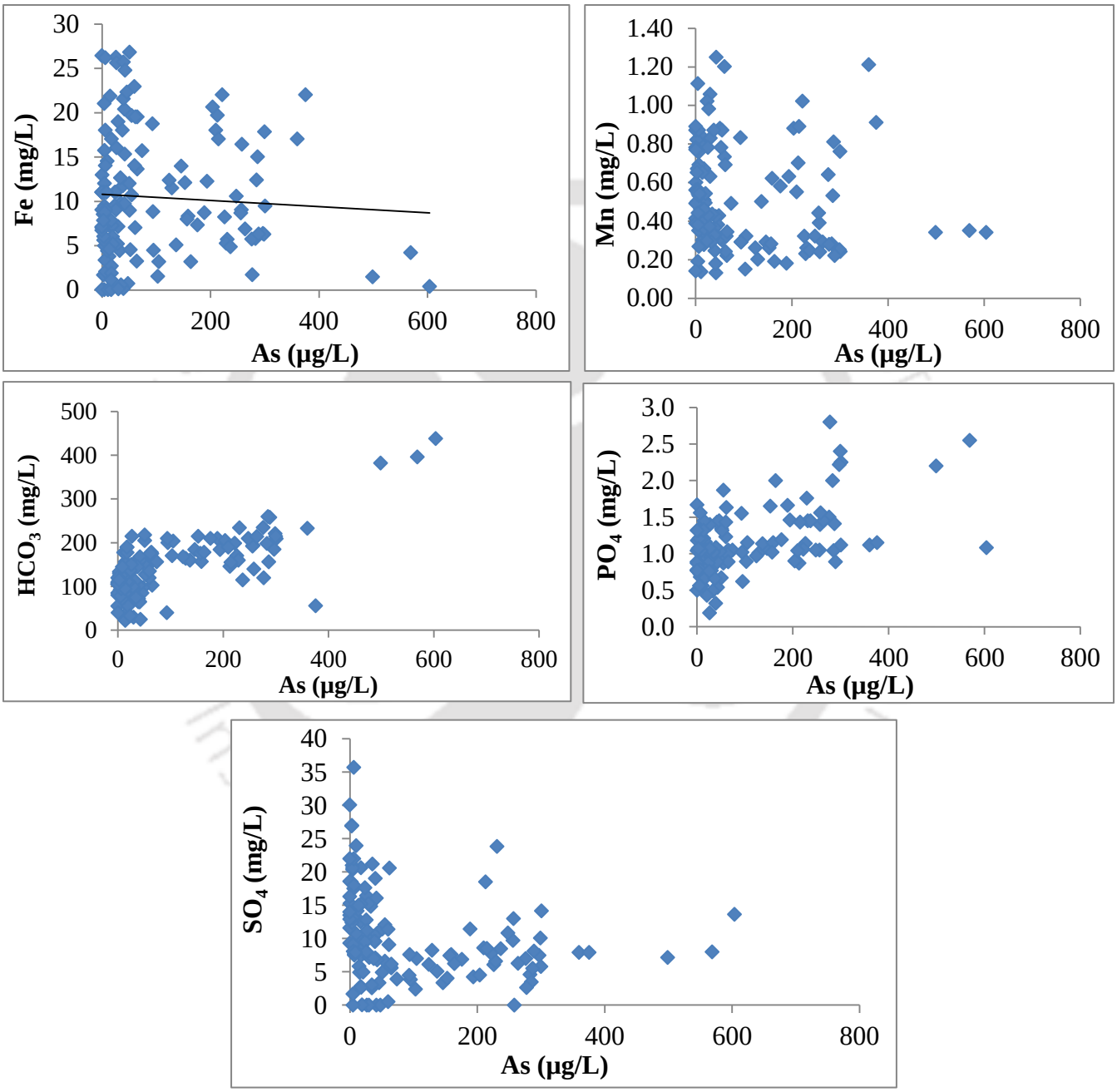

Figure 5.21 Scatter plots showing behavior of (a) As (mg/L) with various parameters: (a) Fe, (b) Mn, (c) SO_4^{2-}, (d) HCO_3^-(e) PO_4^-

5.2.4 Depth profile of As Fe, Mn and SO_4

Depth variation of As, Fe, Mn and SO_4^{2-} for groundwater samples along the southern transect showed no distinct depth correlation between the distribution of As with Fe, Mn and SO_4^{2} (Figure 5.22). High As concentrations (<50 µg/L) did not necessarily correspond to high Fe concentrations and low SO_4^{2-}concentrations. As concentrations above WHO guideline values are mostly concentrated within the depth range varying between 20 to 70 m. The variability in occurrence of As, Fe and Mn is probably due to complex precipitation-dissolution processes combined with biodegradation of organic matter (Bhattacharyya et al., 2006).

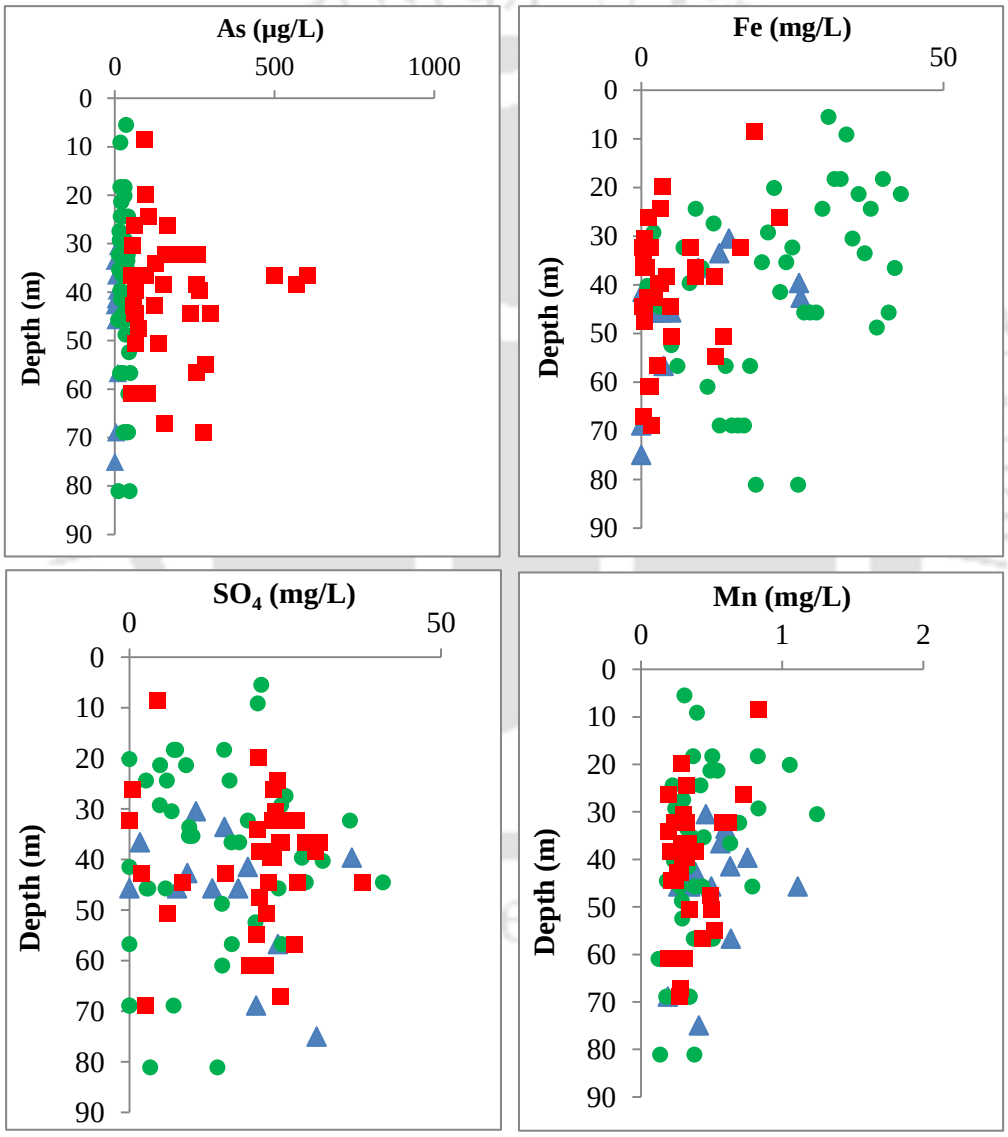

Figure 5.22 Depth distribution of As, Fe, Mn and SO_4^{2-} for groundwater along the southern transect. The same symbol color corresponding to the As content of groundwater (light blue ≤10 µg/L; green 10–50 µg/L; red >50 µg/L) are used for dissolved Fe, Mn and SO_4^{2-} concentrations

5.2.5 Saturation Indices

SI values <1 for most southern bank samples indicate groundwater to be highly under-saturated with respect to the major As phases (e.g. arsenolite, As_2O_5, and $FeAsO_4 \cdot 2H_2O$) and Mn oxide phases (e.g. birnessite, bixbyite, manganite, and pyrolusite), representing that when As and Mn enter into solution, they do not precipitate as those phases (Table.13).

Groundwater along southern transect is supersaturated with respect to Fe (III) (oxy)hydroxide phases like magnetite, hematite, goethite, indicating that precipitation of Fe(III) phases from groundwater is thermodynamically favorable. Saturation indices calculation show that carbonate mineral phases viz. calcite ($CaCO_3$) and dolomite ($MgCa(CO_3)_2$) are under-saturated. These samples probably come from an environment where calcite and dolomite are impoverished or where Ca^{2+} and Mg^{2+} exist in other forms and have not reached equilibrium with the carbonates due to short residence time. This is in good agreement with higher concentration of Ca, Mg and bicarbonate ions in the groundwater samples. The SI for major mineral phases that may regulate the concentration of Fe(II) and Mn(II) in groundwater are mostly at or close to equilibrium (eg. Rhodochrosite ($MnCO_3$) and siderite ($FeCO_3$). The saturation states of Fe- and Mn-bearing carbonates, and oxides (eg. Fe(III) oxide/hydroxides such as magnetite, hematite, goethite etc.) in the groundwater indicate favorable conditions for potential As adsorption onto the surfaces of Fe and Mn-bearing oxides and carbonates formed under oxidizing and reducing conditions, respectively.

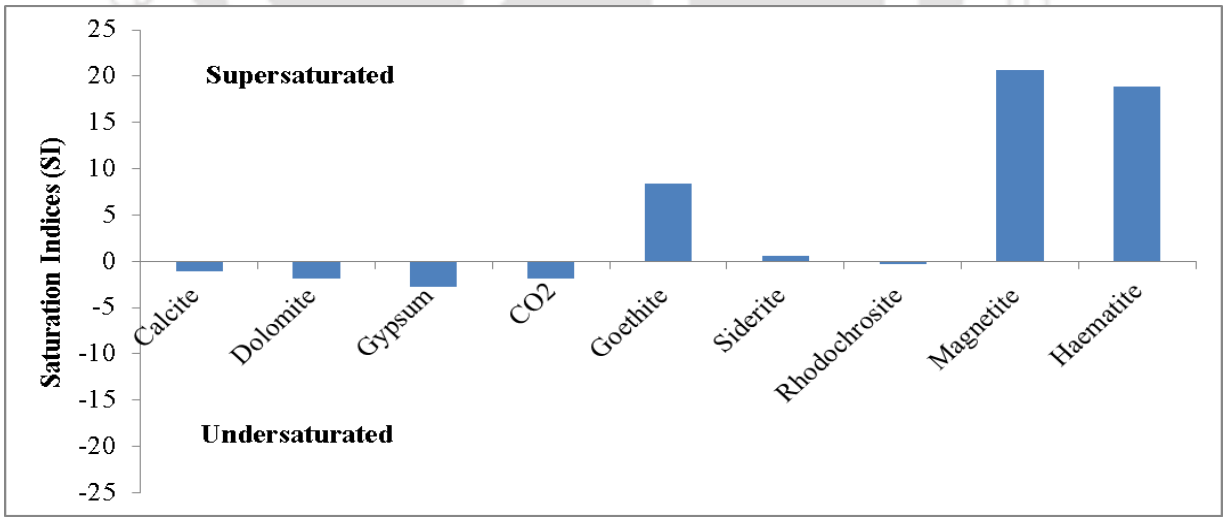

Figure 5.23 Plot of mean saturation index (SI) calculations for groundwater along the southern transect, carried out to calculate saturated, under-saturated and equilibrium mineral phase

Table 13 Summary of saturation indices (SI) calculated by PHREEQC for selected phases for the groundwater samples for the southern transect

Transect	Mineral Phases	Formula	Min	Max	Average
Southern Transect	**Anhydrite**	$CaSO_4$	-5.09	-1.83	-3.41
	Arsenolite	As_2O_3	-25.77	-12.11	-24.94
	As_2O_5	As_2O_5	-30.08	-28.44	-29.47
	Birnessite	MnO_2	-18.13	-12.24	-13.07
	Calcite	$CaCO_3$	-2.45	0.06	-1.04
	CO_2	CO_2	-4	0	-1.86
	Dolomite	$CaMg(CO_3)_2$	-4.32	0	-2.77
	Ferrihydrite	$Fe(OH)_3$	1.04	3.5	2.82
	Gypsum	$CaSO_4{:}2H_2O$	-4.87	0	-2.77
	Goethite	FeOOH	0	9.39	8.44
	Haematite	Fe_2O_3	0	22.17	18.87
	Magnetite	Fe_3O_4	0	23.45	20.71
	Rhodochrosite	$MnCO_3$	-2.12	1.06	-0.26
	Siderite	$FeCO_3$	-1.23	1.39	0.63

5.2.6 Stable Isotopes

Aquifer recharge along the southern bank transect are inferred based on isotope measurements by Verma et al., (2016), who recently reported that groundwater samples from the southern bank analysed for stable isotopes ($\delta^{18}O$ and $\delta^{2}H$) show similar trend and fall along the Global Meteoric Water Line (GMWL: $\delta^{2}H=8\ \delta^{18}O+10$) of Craig (1961) suggesting that some evaporation might have taken place through recharging water in the study area, the reported trend for southern samples being $\delta^{2}H=6.8\ \delta^{18}O+2.7$ respectively. In summary, the isotope results provided tentative evidence about sources of recharge and possible mobilization As enrichment mechanisms as follows:

1. Precipitation from rain water is a major source of recharge into groundwater aquifers along both the transects.

2. Samples from both the transects demonstrated the effect of evaporation. This might have a potential contribution to As enrichment with increased concentrations of dissolved species.

5.2.7 Spatio-Temporal Variability of As

To study the spatio- temporal variability of As, monthly monitoring of seven wells (which includes three installed monitoring wells viz. LAN_1, BAT_1 and MAD_1 and paired shallow wells viz. LAN_2, BAT_2, BAT_3 and MAD_3) along the southern transect perpendicular to the River Brahmaputra showed clear variability of As concentrations for the monitoring well close to the Brahmaputra River (LAN_2), while for the wells further away (MAD_2), towards the base of the Naga Hills, As concentrations remained relatively stable (Figure 5.24). Concentrations of Fe and Mn followed similar trend as that of As for all the monitoring wells, while pH showed little variability.

Water level measurements demonstrated wide variability for the monitoring well LAN_2 adjacent to the floodplain areas and MAD_2 closer to the high As zone, at the base of the Naga Patkai Hills. Studies to understand the temporal variability of As in the Bengal Basin have earlier attributed the variability to the flushing of aquifer, by infiltration of groundwater from low arsenic aquifers, seasonal fluctuations in groundwater recharge and the impact of irrigation drawdown (McArthur et al., 2010, Bhattacharyya et al., 2011). The seasonal recharge pulses, coupled with the annual cycle of precipitation and recharge were also reported to influence groundwater flow patterns as a function of water level changes (Cheng et al., 2005).

As variability in the study transect can be attributed to the combined effect of aquifer flushing and lithology. Variability in wells closer to the Brahmaputra River is possibly due to the flushing effect caused due to the seasonal recharge pulses, while the presence of thick impermeable clay layers inhibited active recharge into the aquifers close to the hills.

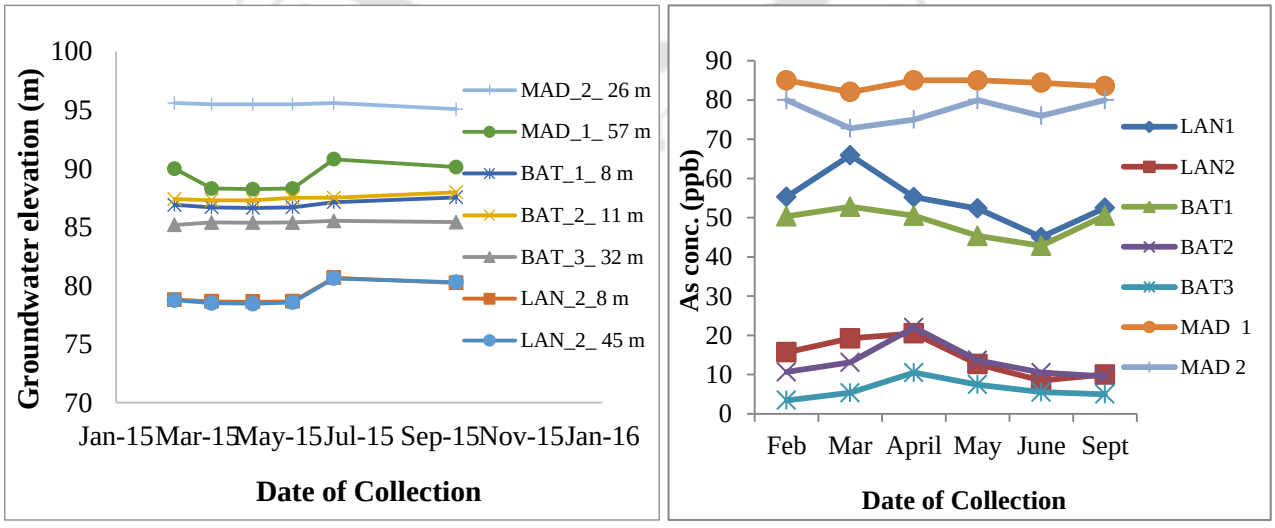

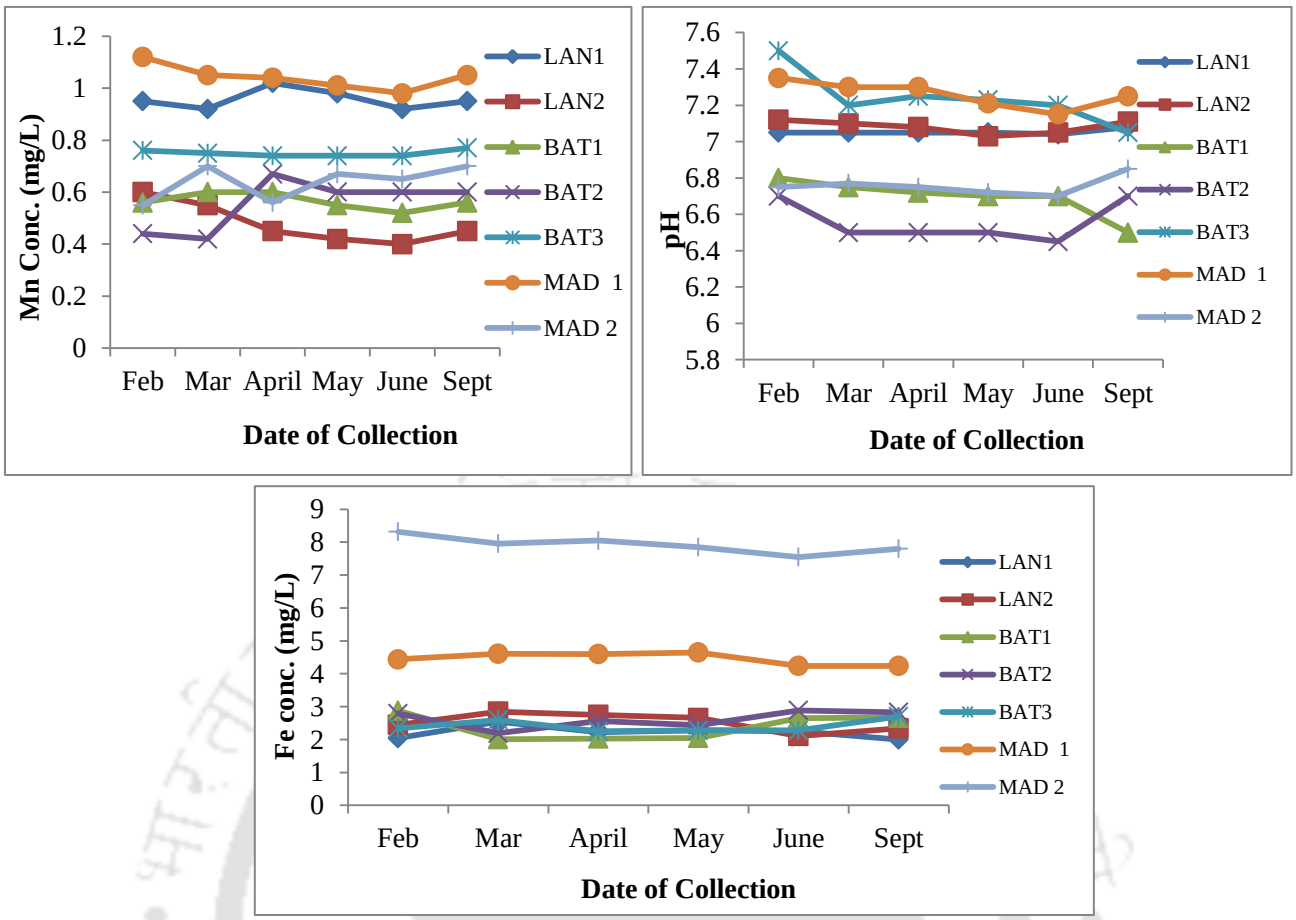

Figure 5.24 Temporal variability of As and groundwater heads for the seven monitoring wells along the southern bank transect

5.3 Aquifer sediment chemistry

Physical and chemical properties of sediment samples collected from drilled boreholes along both transect are discussed below:

5.3.1 Sediment pH

pH of selected sediment samples from borewells drilled along the study transects indicated acidic pH with values ranging between 4.15 to 5.02 (Figure 5.25). Microbial oxidation of organic matter releasing carbon dioxide (CO_2) into groundwater and subsequently forming carbonic acid (H_2CO_3) contributes to acidic pH in sediments. Among other factors leading to acidic pH of sediments are organic acids, respiration of plant roots, hydrolysis of Al, nitrification, oxidation of sulfide, fertilizers etc. (Tan, 2011).

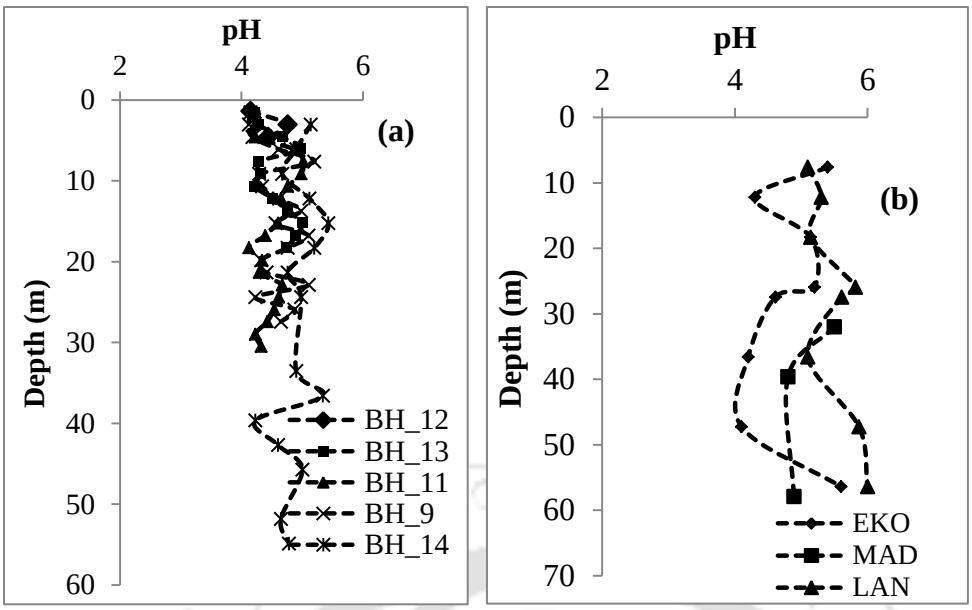

Figure 5.25 pH variation of selected sediment samples from boreholes along (a) the northern and (b) southern transect

5.3.2 Organic Matter

The organic content in aquifer sediments was represented by the loss on ignition (LOI). LOI defines the percentage of weight of volatile organic solids at a high temperature (i.e. 550°C). Depth profile of LOI showed heterogeneity along each drilled borewell (Figure 5.26). The organic matter present in sediments was degraded by micro-organisms, depleting the oxygen in water, thus creating reducing conditions.

CH_2O (organic matter) + O2 $\longrightarrow$ CO_2 + H_2O

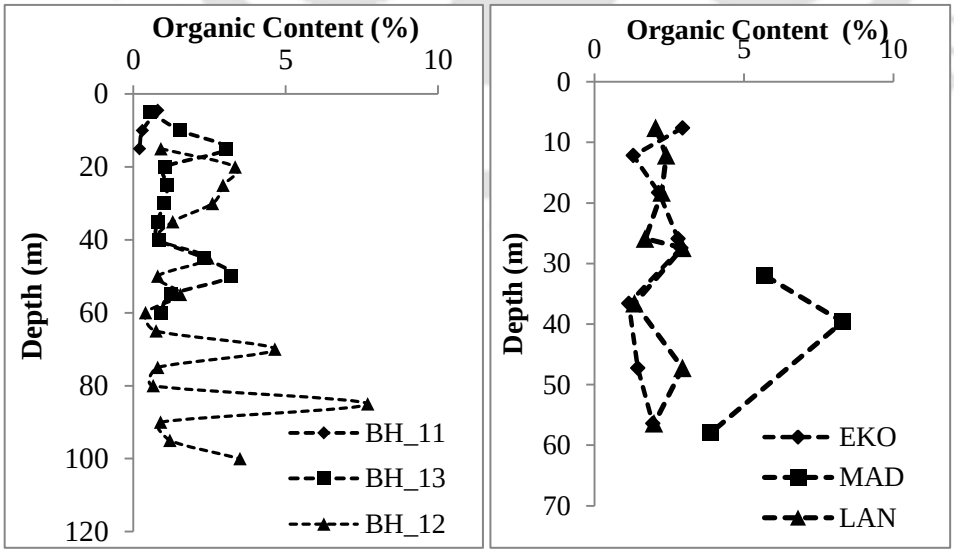

Figure 5.26 Organic Content variation of selected sediment samples from boreholes along the northern and southern transects

5.3.3 Lithology

A vertical lithofacies sequence of the sediments for both the study transects was prepared from the set of drilled boreholes along both transects. Based on the texture and lithology, the sediments could be categorized into three broad lithotypes viz. Clay, Sand and Gravels. Aquifer sands primarily consisted of fine, medium to coarse grained sands with varying proportions of clays and sharp litho-boundaries.

Lithological profile from drilled borewells along the northern transect revealed presence of coarse sands, gravels and rock fragments in the proximal zone, while clays and sands dominate aquifers in the distal zone (Figure 5.27-5.28). Along the southern transect, towards the surface, the aquifers are covered by a clay-rich aquitard mostly in the wells in the proximal zone, close to the base of the Naga hills, while sandy aquifers dominated the distal zone. Grain size profiles and fining upward sequence of aquifer sediments represents the fluvial origin of the aquifer sediments which are primarily carried by the Brahmaputra River and its numerous tributaries draining the eastern Himalayas and the Naga Hill Ranges (Tucker, 1991; Robinson et al., 2009). Presence of several clay and silty clay layers interbedded with sand close to the floodplain areas suggests a typical floodplain alluvial deposit formed by a meandering river.

The cutting recovered during drilling show a marked increase in the thickness of a surface clay layer starting from none to <5 m at the 3 sites closest to the river to 60 m of almost continuous clay at the most distant site near the base of the Naga foothills (Figure 5.28). Near the river, fine to medium grain sands clearly dominate the lithology, while only thinner lenses of sands were encountered in boreholes closer to the hills. No sand was recovered during drilling to 25 m depth at the third closest site to the Naga Hills.

Borehole sediment colour varied from gray (chemically reduced) to orange-brown (chemically oxidized) as discerned in many other As affected fluvial-deltaic sedimentary sequences (e.g., Bengal Basin; BGS and DPHE, 2001). Most groundwater aquifers along the northern transect, close to the river, are dominated by gray clays and sands. In contrast, aquifers close to the Brahmaputra river in the southern transect are mostly dominated by sands. Most of the sand across the transect was grey, with the exception of the site closest to the river where brown sand was recovered between 20 and 45 m depth and the next closest with brown sand extending from 5 to 45 m depth. The lithological variations observed in the

bore wells along both the transects indicates the different depositional regimes of the transects. The flashy northern tributaries of the northern tributaries of Brahmaputra carries much of the sediment loads and deposits the same along its much avulsed floodplains while the much sluggish southern tributaries, with its distinct meandering characteristics deposit its sediment loads in its meandered floodplains. Orange-Brown colour sediment observed at the top part of the borehole close to the floodplains suggested that this particular part of the sedimentary column was perhaps exposed to oxidation, and would naturally mean a period of non-deposition, interspersed by events of intermittent flooding (Umitsu, 1993).

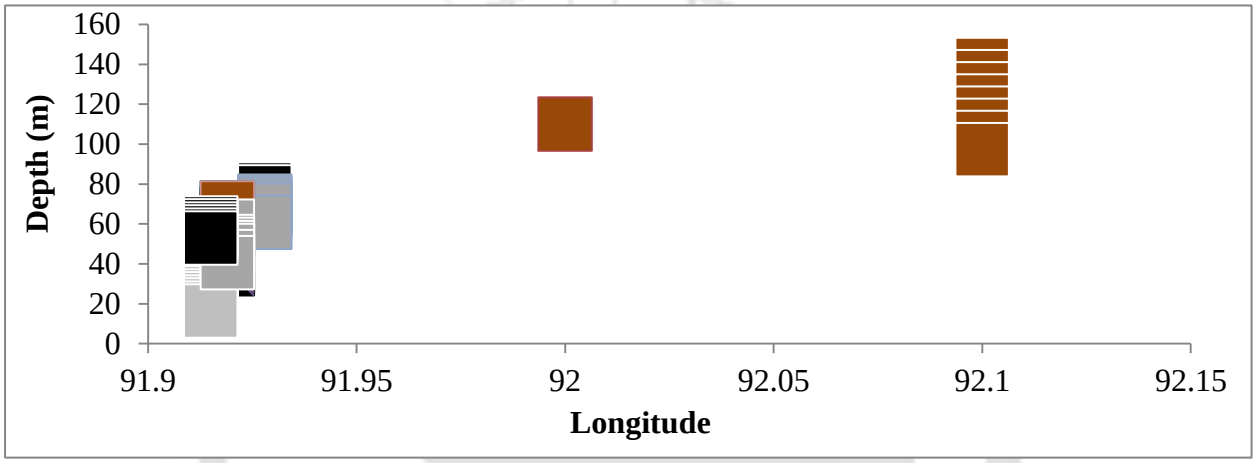

Figure 5.27 Lithological profile of transect (N-S) based on lithologs collected from drilled wells along southern transect. Grey colour indicates grey sands; Brown colour indicates brown sands; Black indicates clay

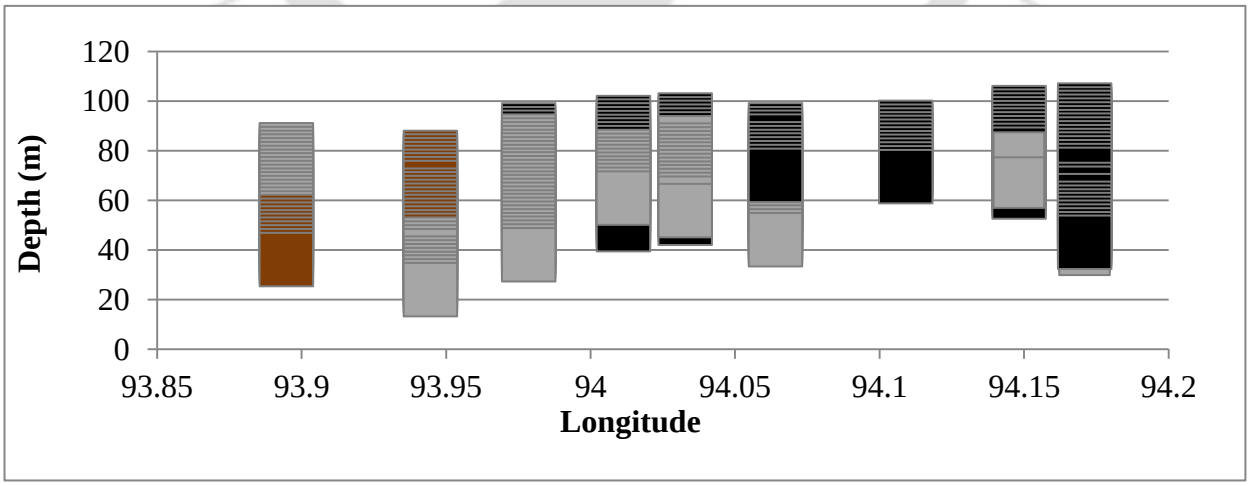

Figure 5.28 Lithological profile of transect (N-S) based on lithologs collected from drilled wells along southern transect. Grey colour indicates grey sands; Brown colour indicates brown sands; Black indicates clays

5.3.4 Particle size distribution of sediments

Specific Surface Area (SSA) is the measure of the solid or particles per unit volume per unit weight. Depth wise measurements of sediment samples from bore wells along both transects was made using Malvern Laser Particle Size Analyzer. SSA measurements demonstrated the heterogeneous distribution of aquifer sediments in the study transects, which corresponds well to the aquifer lithologies (Figure 5.29-5.30). Plots of bulk As vs. SSA demonstrated that high solid phase As corresponds well with high SSA owing to high adsorption capacity (Anwar et al., 2003). Also, Fe, Mn and Al oxides and hydroxides are the major components of fine grained particles with high SSA and thus was believed to retain high As under specific pH conditions (Pierce and Moore, 1982; Anawar et al., 2003; Reza et al., 2010).

Grain size distribution of depth wise sediment samples along both transects were analysed for understanding the lithological characteristics of aquifer sediments. d_{60} value , which means that 60% of samples are finer than this sieve size (Masch and Denny 1966), was used to represents sediment grain-size characteristics. d_{60} and d_{50} values have been earlier used by several authors to demonstrate grain size distribution in sediment samples (Ni et al., 2016; van Geen et al., 2008). The d_{60} values were observed to be lower for clays and gradually increased to sand sized particles for borewells along both transects (Figure 5.31). Sediments with small grain size are likely to have more surface sites available for As adsorption, which perhaps is a controlling factor for the observed high As contents in samples with low d_{60} values. At shallow depths, d_{60} values were observed to be lower compared to sediments at deeper depths (Figure 5.31). Dark grey clays, observed in boreholes drilled at the base of the Naga Hills were dominated with lower d_{60} values, compared to other borewells along the southern transect. Lower d_{60} values correspond to high As (Figure 5.31).

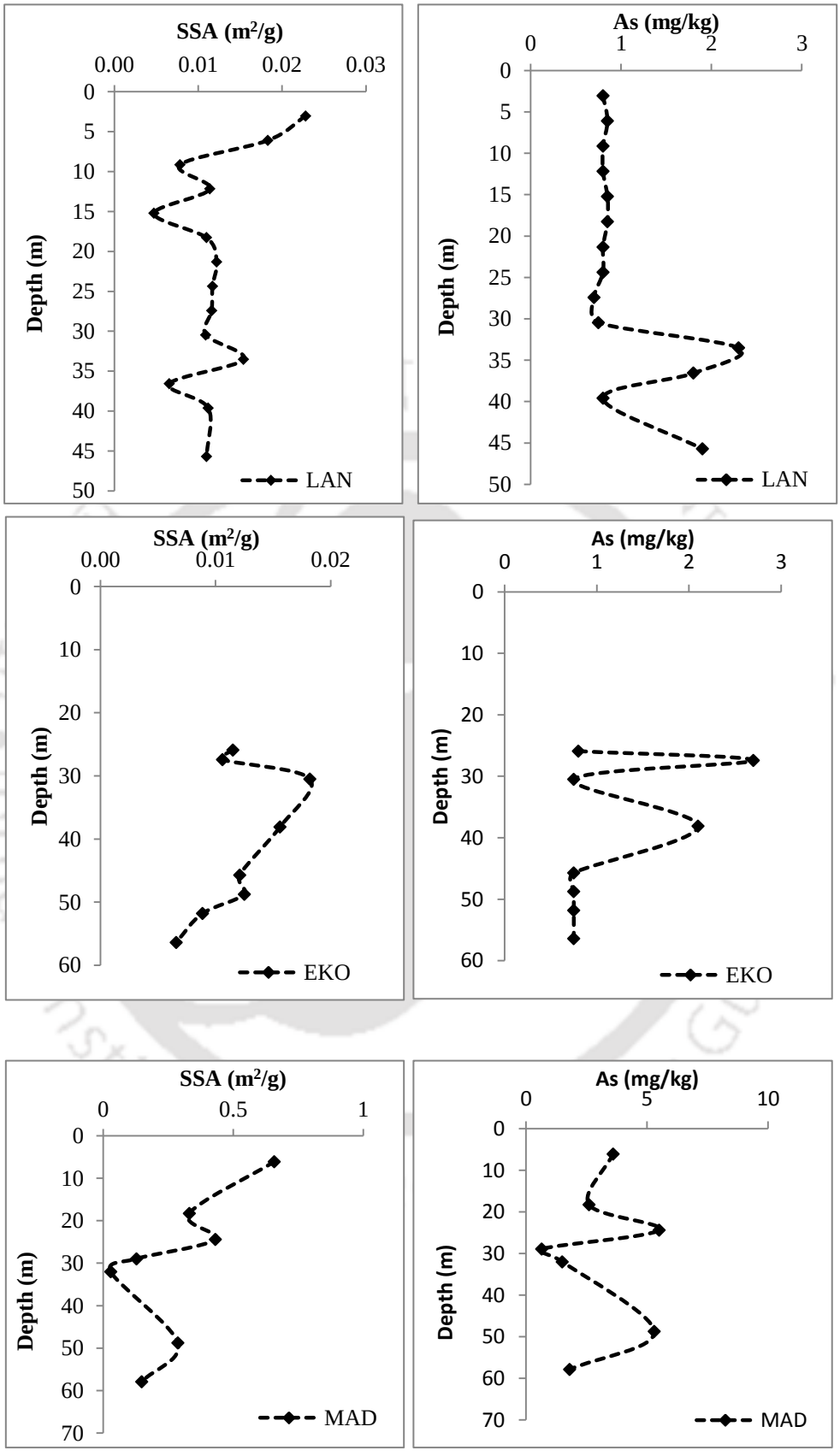

Figure 5.29 Specific Surface Area (SSA) and As (mg/kg) distribution along depth for sediment samples collected along southern transect

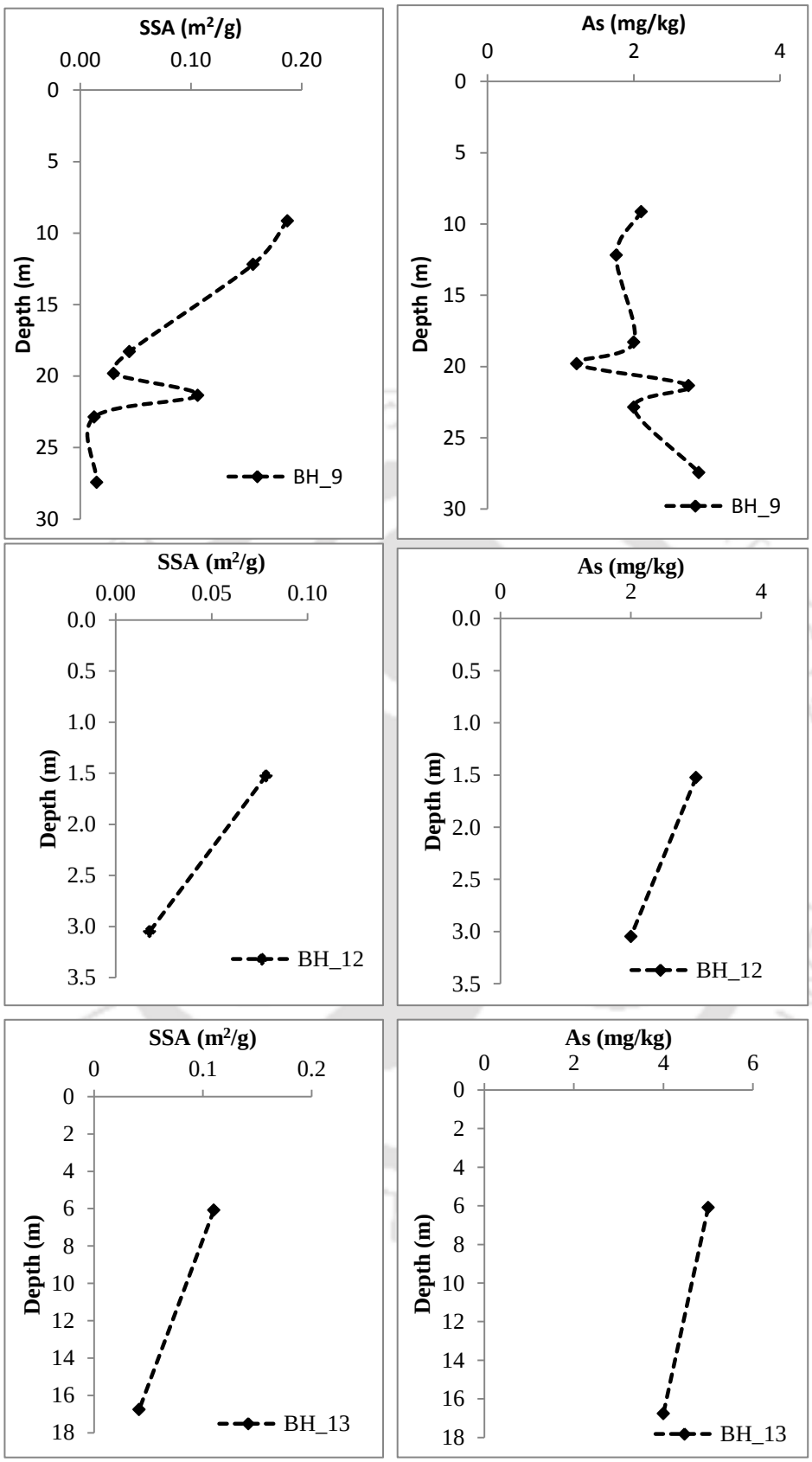

Figure 5.30 Specific Surface Area (SSA) and As (mg/kg) distribution along depth for sediment samples collected along northern transect

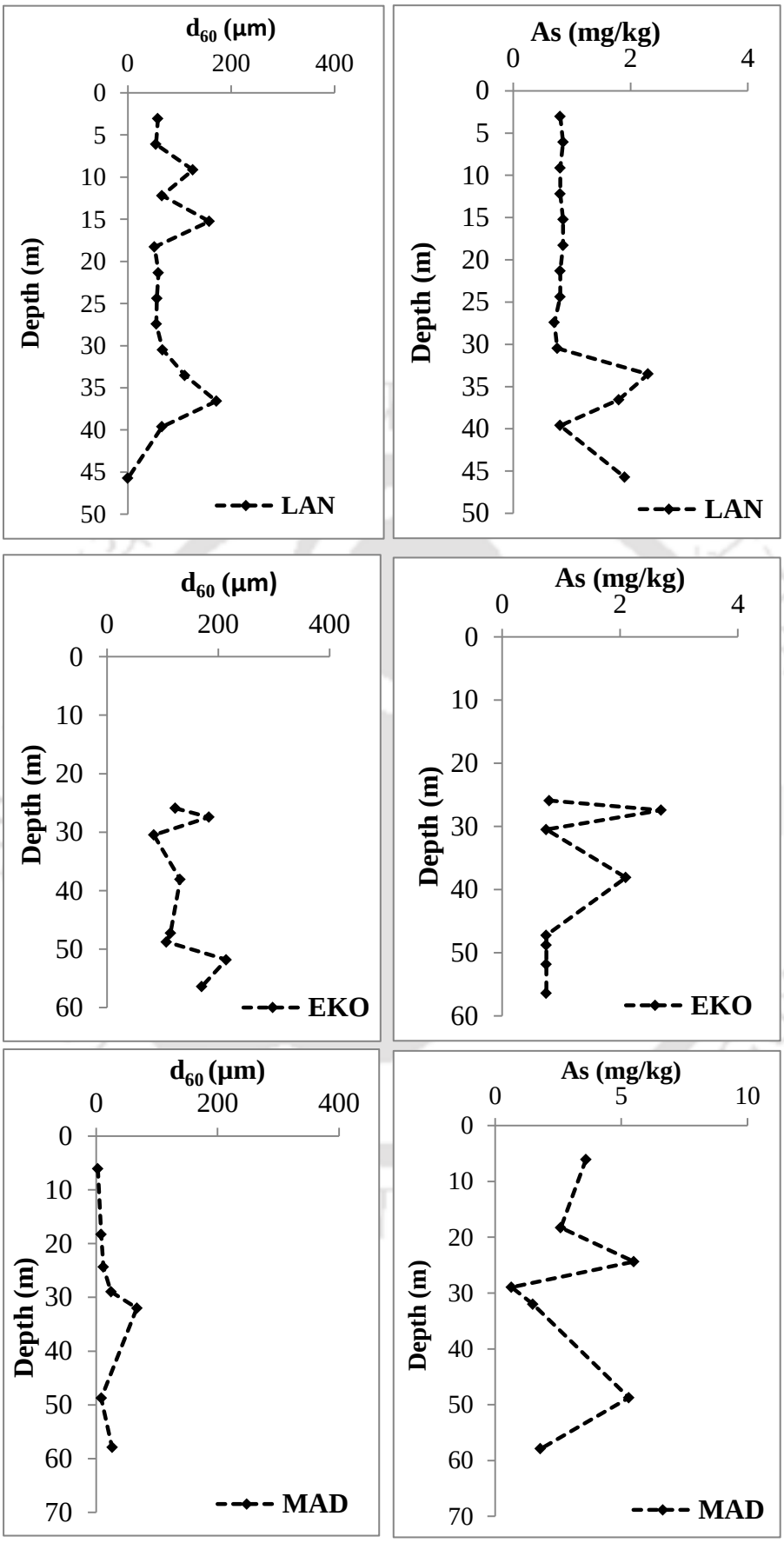

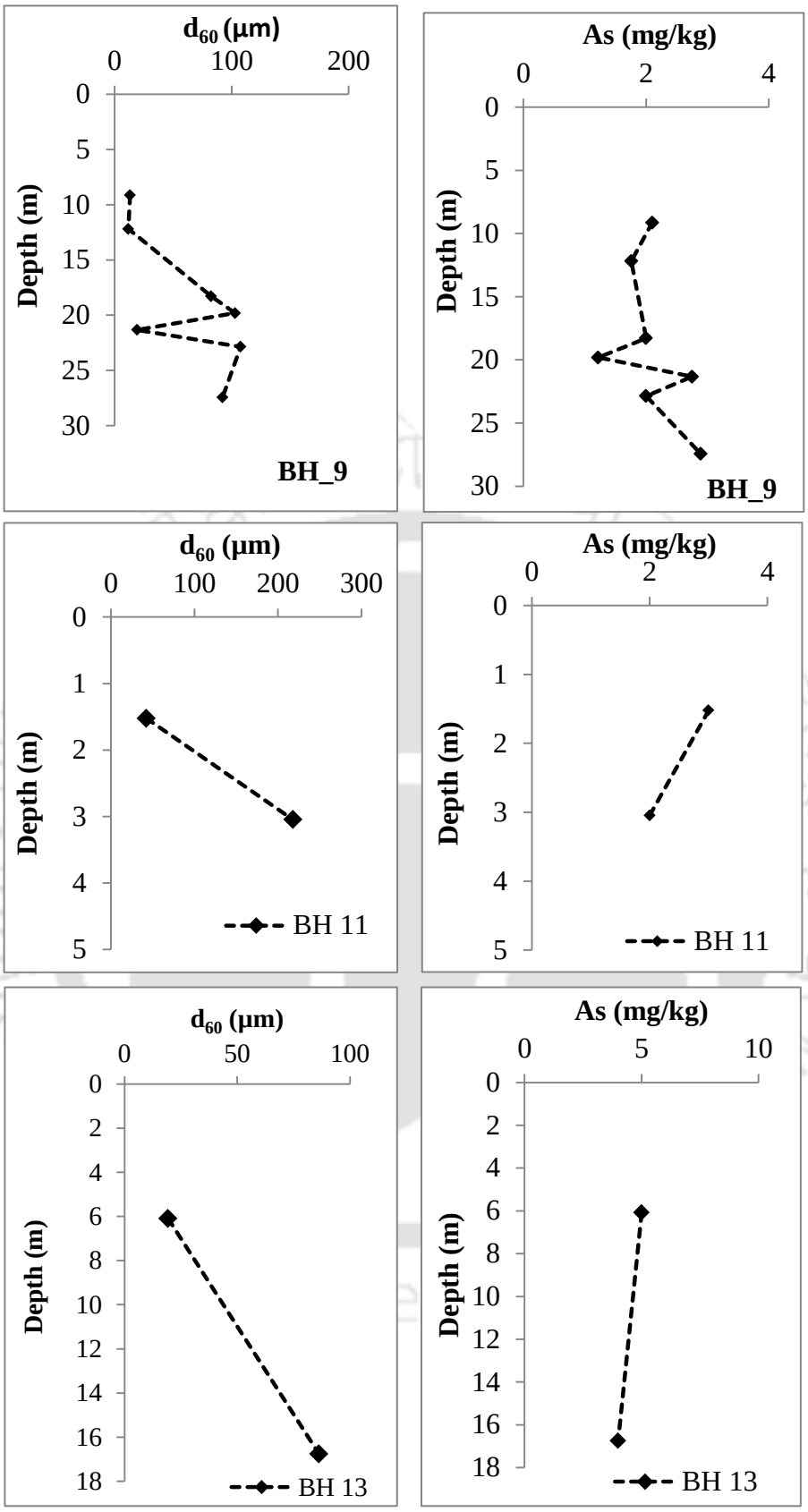

Figure 5.31 Vertical profiles of d_{60} and total As (mg/kg) content in sediment samples collected along the northern (BH_9, BH_11, BH_13) and southern (LAN, EKO, MAD) transects

5.3.5 Mineralogical composition

Morphological study on selected sediment samples (BH_9 from northern transect and BH_LAN and BH_EKO from southern transect) from the transects revealed sub angular to sub rounded grains with well crystalline particles and platy mineral phases suggesting transport over distance before deposition and source not local, hinting the Bhutan Himalayas and the Naga Hill ranges as possible provenance (Figure 5.32a-5.32c). Well defined crystalline phases in aquifer sediments indicated silicates and Fe-Mn hydroxides like quartz, microcline, plagioclase, goethite etc., while flaky mineral phases were indicative of phyllosilicates like biotite and muscovite. Phyllosilicates are composed of tetrahedral and octahedral nets, which may offer available reactive surfaces for arsenic adsorption, potentially via iron hydroxide molecular bonding on the edge of unit layers of the minerals (Nakano et al., 2014). The bulk mineralogical composition of the sediment at both transects were similar, with dominant mineral suites being quartz, mica, feldspars and kaolinite with varying relative proportions. Arsenic is reported to be adsorbed on iron oxide-coated feldspar, mica and quartz grains in the Ganges plain sediments (e.g., Breit et al., 2001; Kent and Fox, 2004; Lowers et al., 2007). Verma et al. (2016) reported similar presence of feldspar (K-feldspar and plagioclase), mica (biotite and muscovite), ferromagnesian minerals, i.e., amphibole, highly altered pyroxene along with some heavy minerals, i.e., monazite, and rutile in aquifers of the Brahmaputra River floodplain aquifer sediments.

Similar mineralogical suites in sediment samples from areas of high and low dissolved As are reported from Vietnam and elsewhere, indicating that these mineral phases can potentially be the sources and sinks for As release into groundwater (Berg et al., 2008, Biswas et al., 2014). Arsenic peak pattern observed in the EDX spectra suggested that solid phase As occur as adsorbed and/or co-precipitated phases associated with Fe- Mn –oxide coatings and aluminosilicates. EDX profiles of the aquifer sediments showed the mineralogy being dominated by aluminosilicates of Na, K, Mg as well as that of Al and Fe bounded with silicates (Figure5.32a-5.32c). These mineral phases are potential sites that could serve as adsorbing surfaces for As (Tuutijärvi et al. 2012; Waltham and Eick 2002).

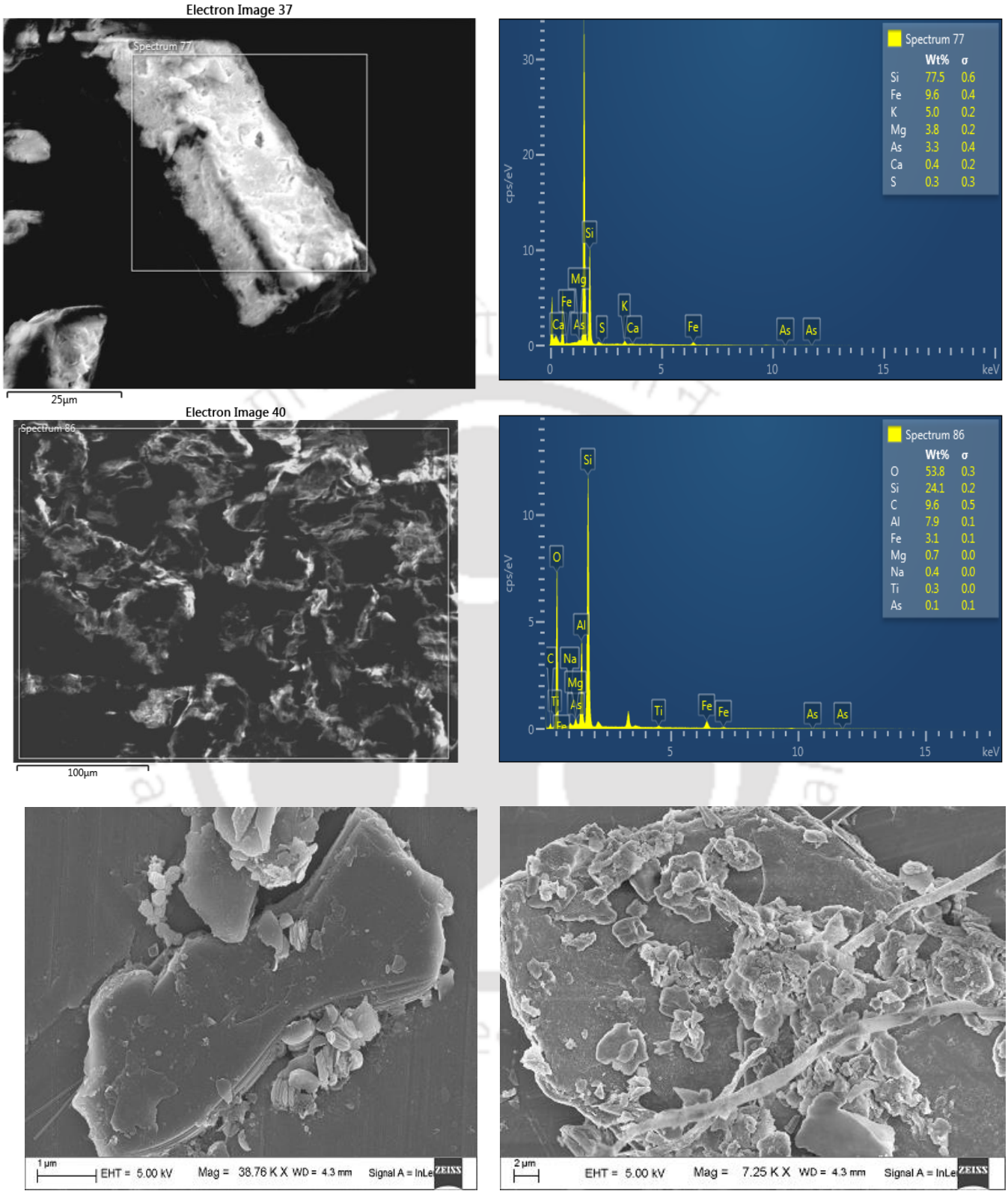

Figure 5.32(a) FESEM images of sediment samples from northern transect (BH_9)

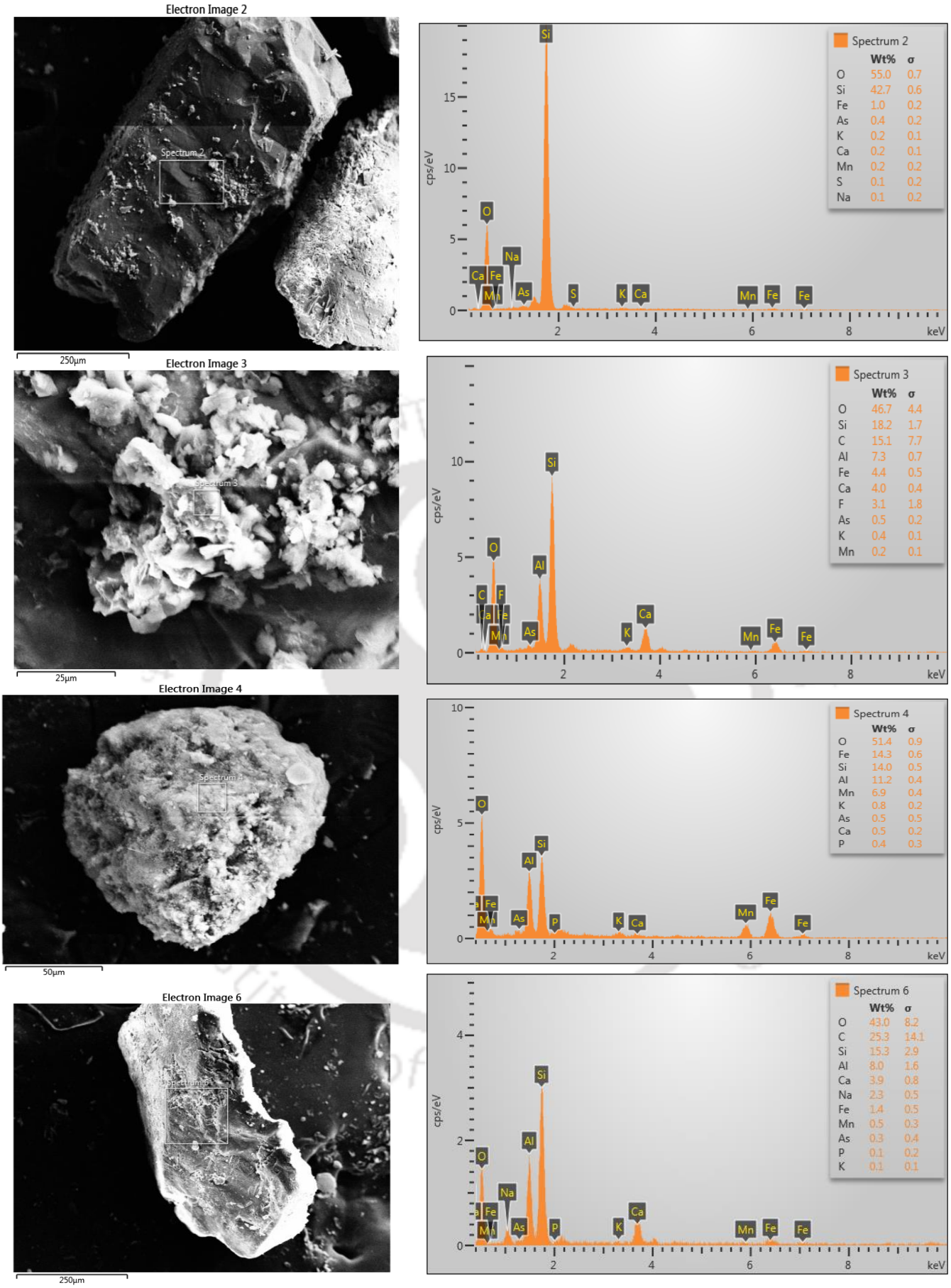

Figure 5.32(b) FESEM images of sediment samples from southern bank transect (LAN)

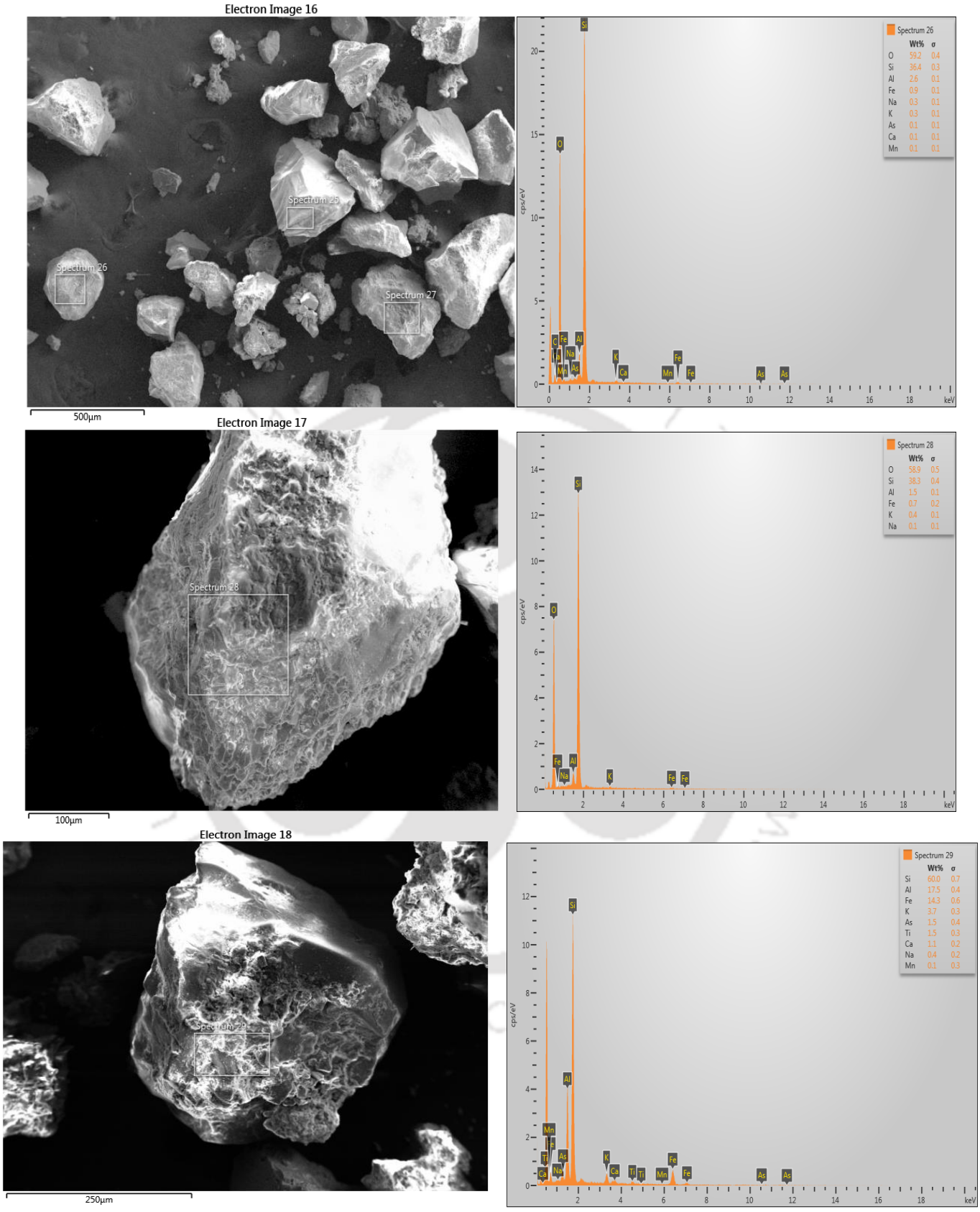

Figure 5.32(c) FESEM images of sediment samples from southern bank transect (EKO)

5.3.6 Petrography

14 thin sections were studied for petrographic analysis (Figure 5.33a-5.33b). Samples along northern transect indicated presence of quartz, feldspar, mica and clay minerals. The occurrence of chert, altered feldspar, chloritized biotite and chlorite indicated the sands to be derived from sedimentary and meta-sedimentary terrains. Additionally thin section petrography indicated presence of immature detritus comprising of quartz, feldspar (microcline and orthoclase), lithic grains, mica (biotite, muscovite), hornblende, chlorite and sericite. Ferruginous grain coatings were mostly common on the framework detrital grains. Intrlocking framework of angular, slightly fractured quartz grains and prismatic laths of feldspars were observed. The feldspars showed cloudy appearance under polarized light indicating partial alteration to secondary minerals like sericite (in the case of weathered plagioclase feldspars) and kaolin (in the case of microcline). Presence of cross hatched and polysynthetic twinning indicated presence of microcline and plagioclase feldspars. The intergranular grains are filled up by fine rock fragments and brownish or opaque hydrated iron hydroxides. Weathering of pre-existing ferromagnesian minerals like biotite has probably led to formation of some of chlorite. In the Bengal Basin, similar mineral phases were reported to be key arsenic bearing phases in aquifer sediments, with As concentration in biotite, chlorite and iron hydroxide coatings ranging between 9mg/kg and <1 mg/kg, 5 and 50 mg/kg and 30 mg/kg, respectively (Sengupta et al. 2004). These arsenic bearing mineral phases act as key repositories of solid phase As, which under redox conditions conducive to mobilization of arsenic, release arsenic into groundwater.

Along the southern transect, close to the Naga Ophiolite belt, major mineral phases included quartz, plagioclase feldspars, hornblende, epidote and garnet. Presence of mafic minerals like hornblende and epidote indicated that aquifer sediments had been derived directly from the Indo-Burma Ranges comprising of Cretaceous to Eocene pelagic sediments overlain by Eocene to Oligocene flysch, upper Miocene to Pleistocene mollasse, and ophiolitic suites that were scraped off an oceanic part of the Indian plate (Curray et al., 1979; Sengupta et al., 1990; Kumar, 2004).Verma et al., (2016) observed presence of pyroxene and other mafic minerals in sediment samples collected from the upper Brahmaputra basin and attributed the same to be derived from weathering of gabbroic complex (ophiolite) and basalt.

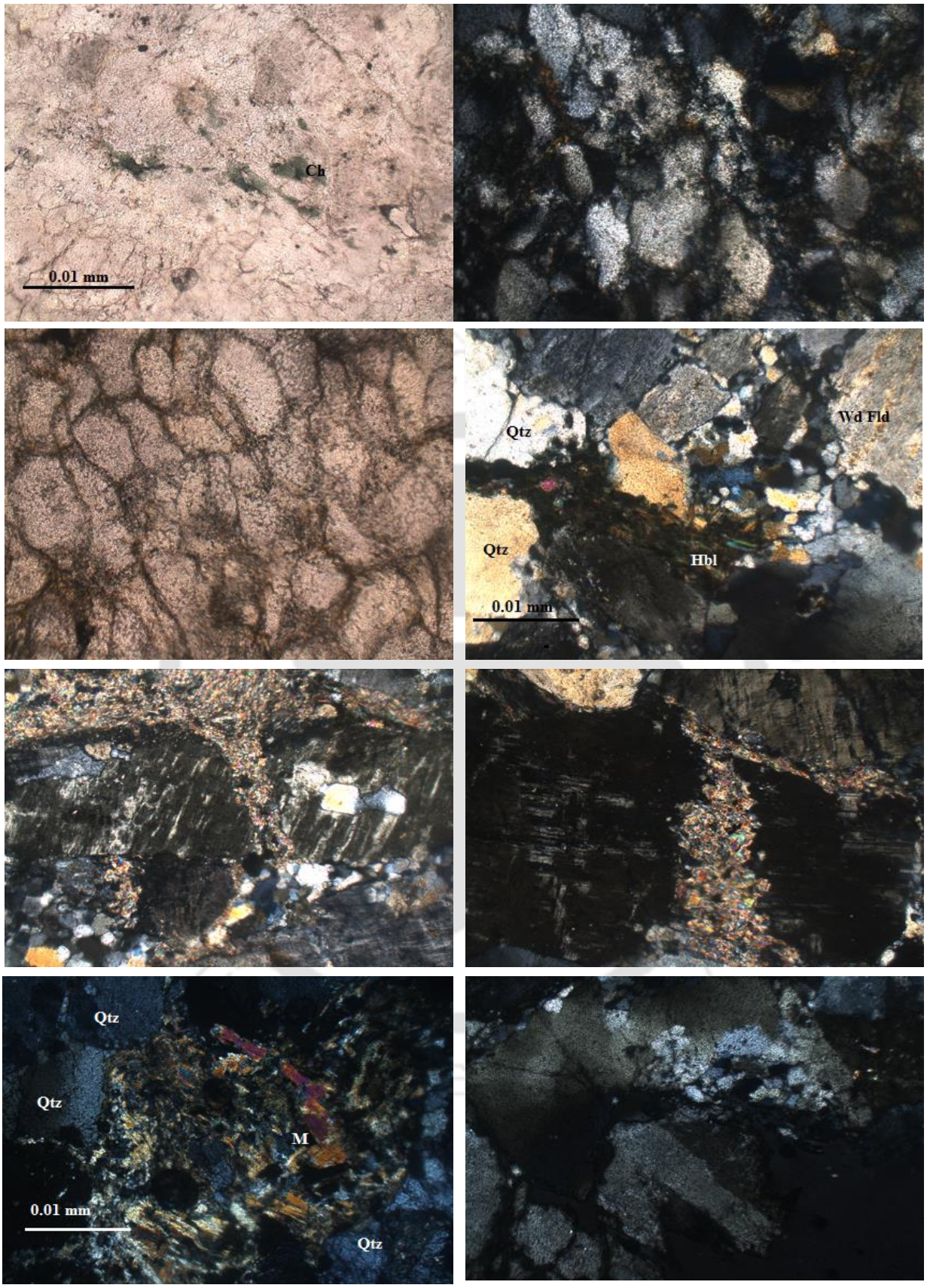

Figure 5.33(a) Representative photomicrographs of As-enriched aquifer sands from northern transect. Abbreviations: ct: coating; qtz: quartz; M: muscovite; ch: chlorite (under polarized light); hlb: hornblende; Wd Fld: Weathered Feldspars

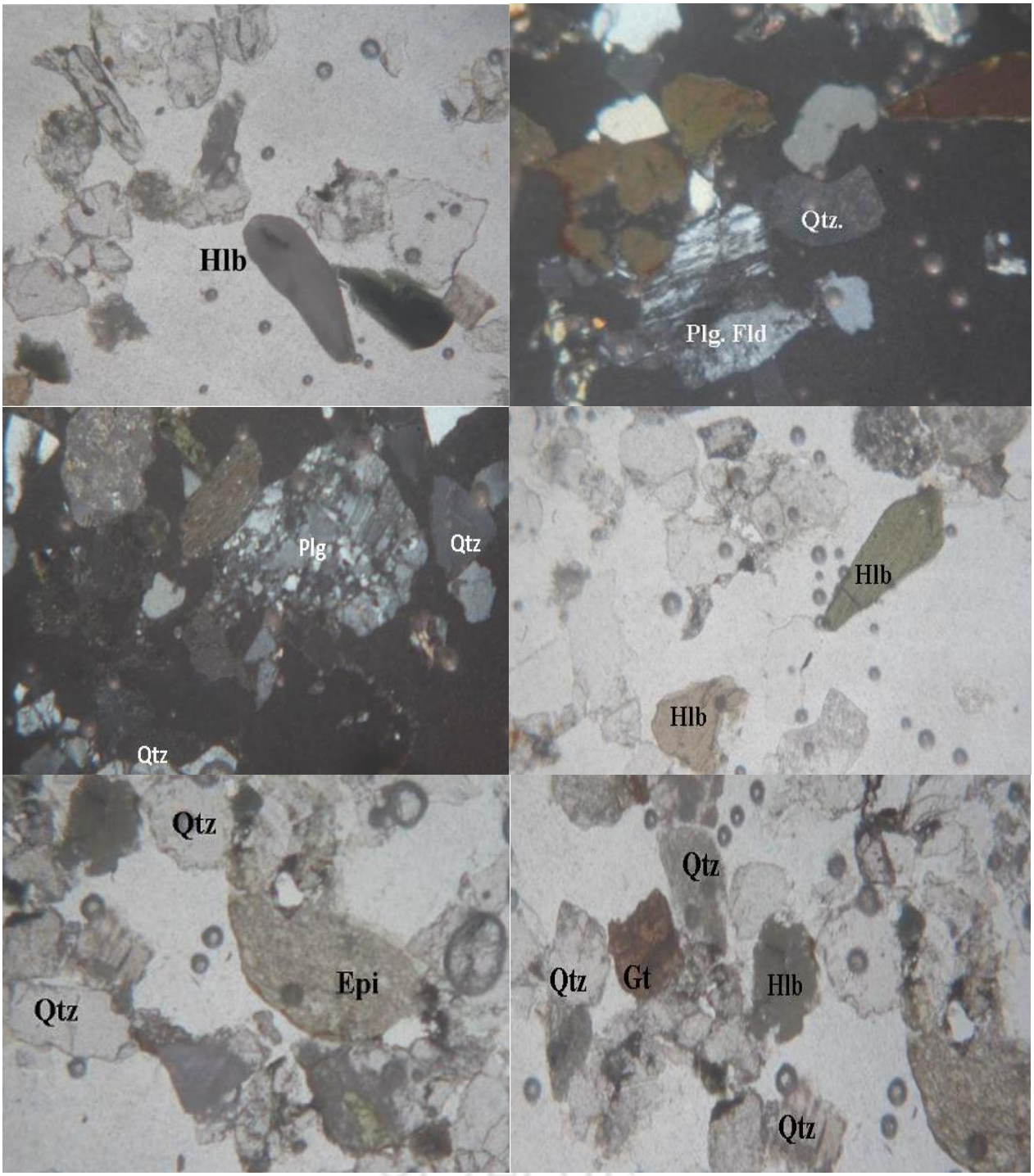

Figure 5.33(b) Representative photomicrographs of As-enriched aquifer sands from southern transect. Abbreviations: qtz: quartz; hlb: hornblende; Plg. Fld: Plagioclase Feldspars; Gt. Garnet; Epi: Epidote

5.3.7 XRD

XRD analyses of depth wise aquifer sediments from select boreholes revealed similar occurrence of minerals along both transects. XRD peak patterns confirmed presence of

phyllosilicates (2Θ spacing: 17-20-30), quartz (2Θ spacing: 26.95, 26.85, 27), feldspar (2Θ spacing: 20-30, 27.5) and clay minerals (Illite), with bulk composition being dominated by quartz, phyllosilicates, feldspars and clay minerals. Phyllosilicates are composed of tetrahedral and octahedral nets, which might offer available reactive surfaces for arsenic adsorption, potentially via iron hydroxide molecular bonding on the edge of unit layers of the minerals (Nakano et al., 2014).At certain depths, peak patterns revealed presence of Iron arsenate, Gypsum, Orpiment, Arsenopyrite XRD peak patterns of sediments from southern transect revealed the dominance of clay minerals viz. kaolinite and illite (Figure 5.34a-5.34b).

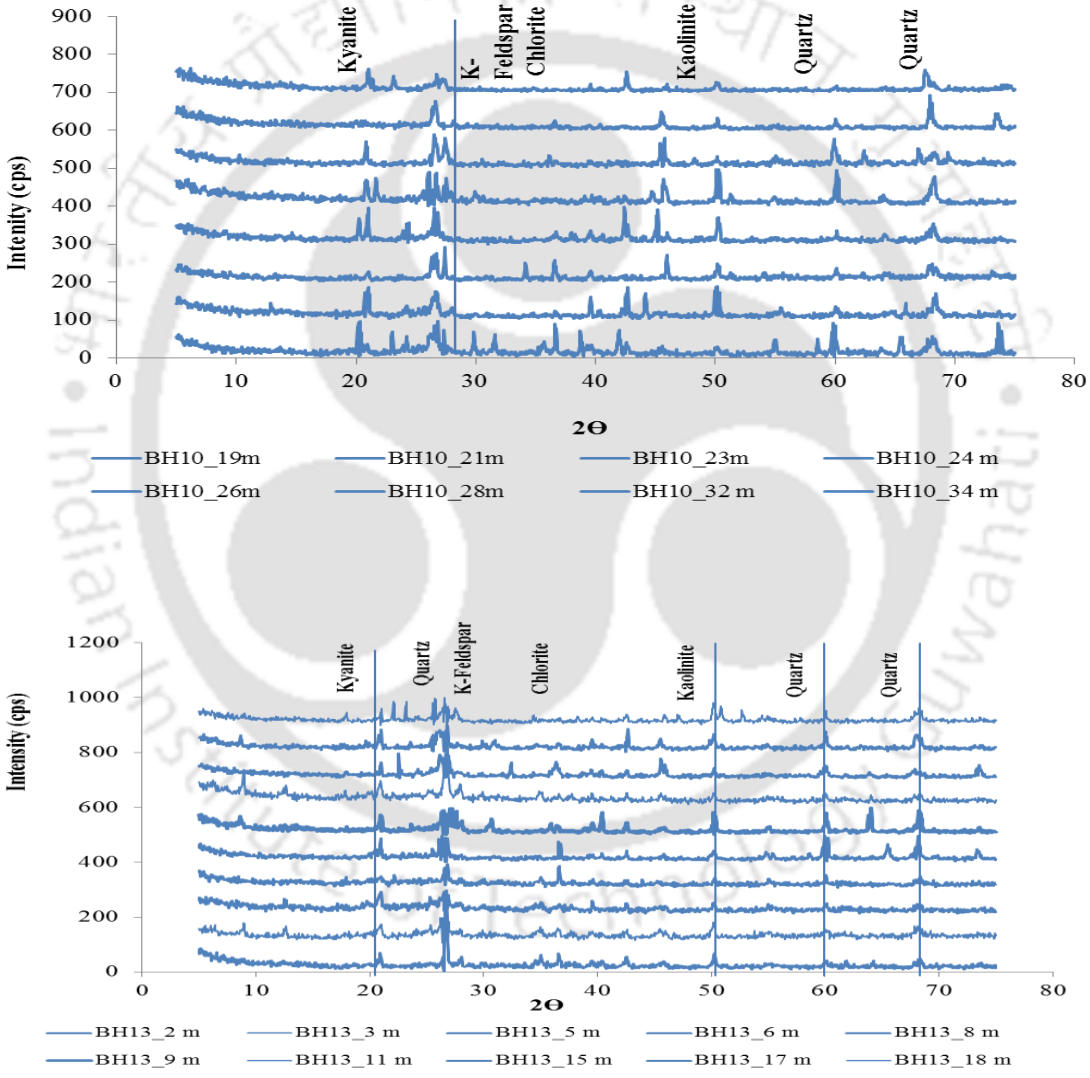

Figure 5.34(a) Comparative XRD patterns of sediment samples drilled from different depths of BH_10 and BH_13 along northern transect

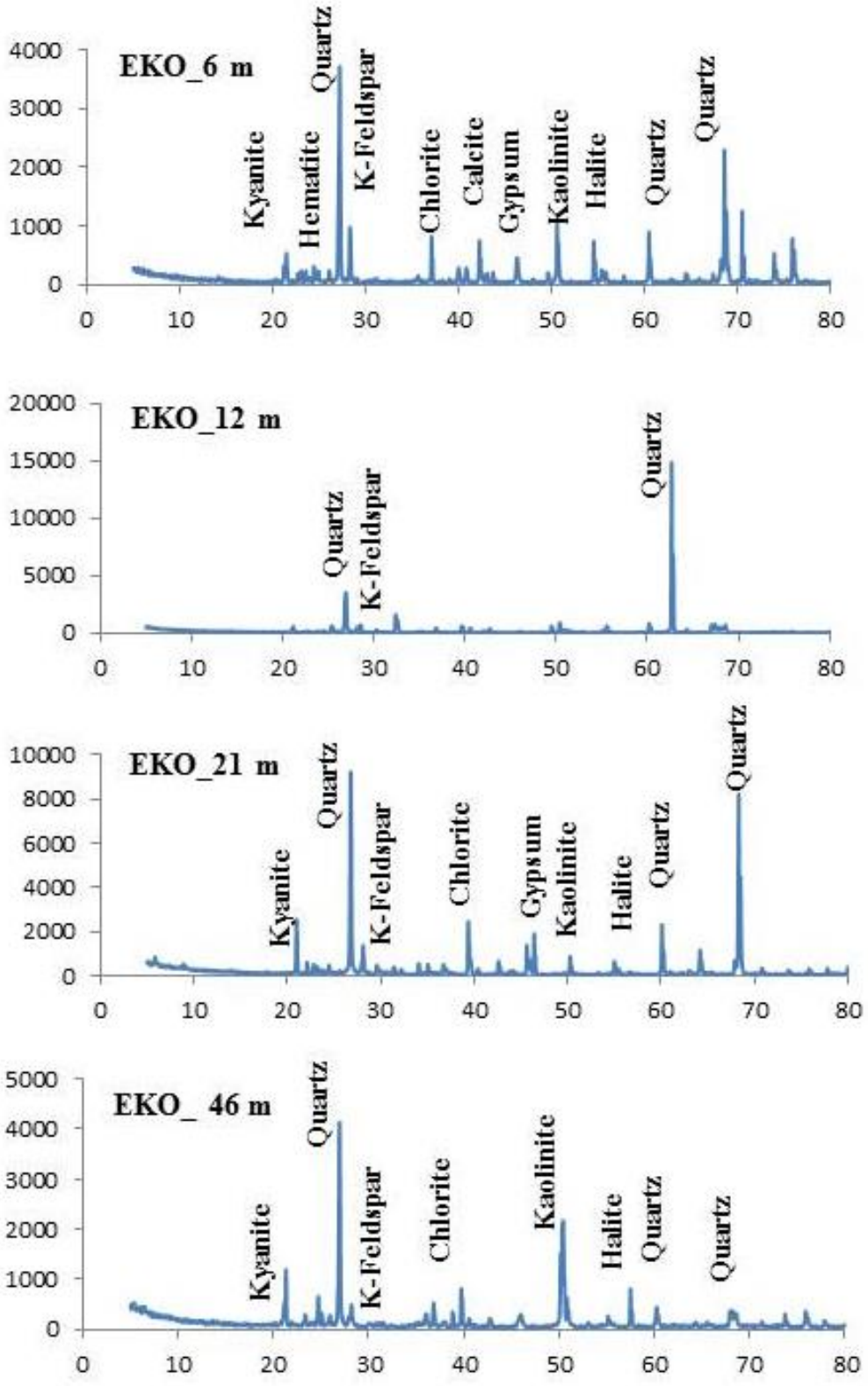

Figure 5.34(b) Comparative XRD pattern of sediment samples from different depths of borehole EKO along the southern transect

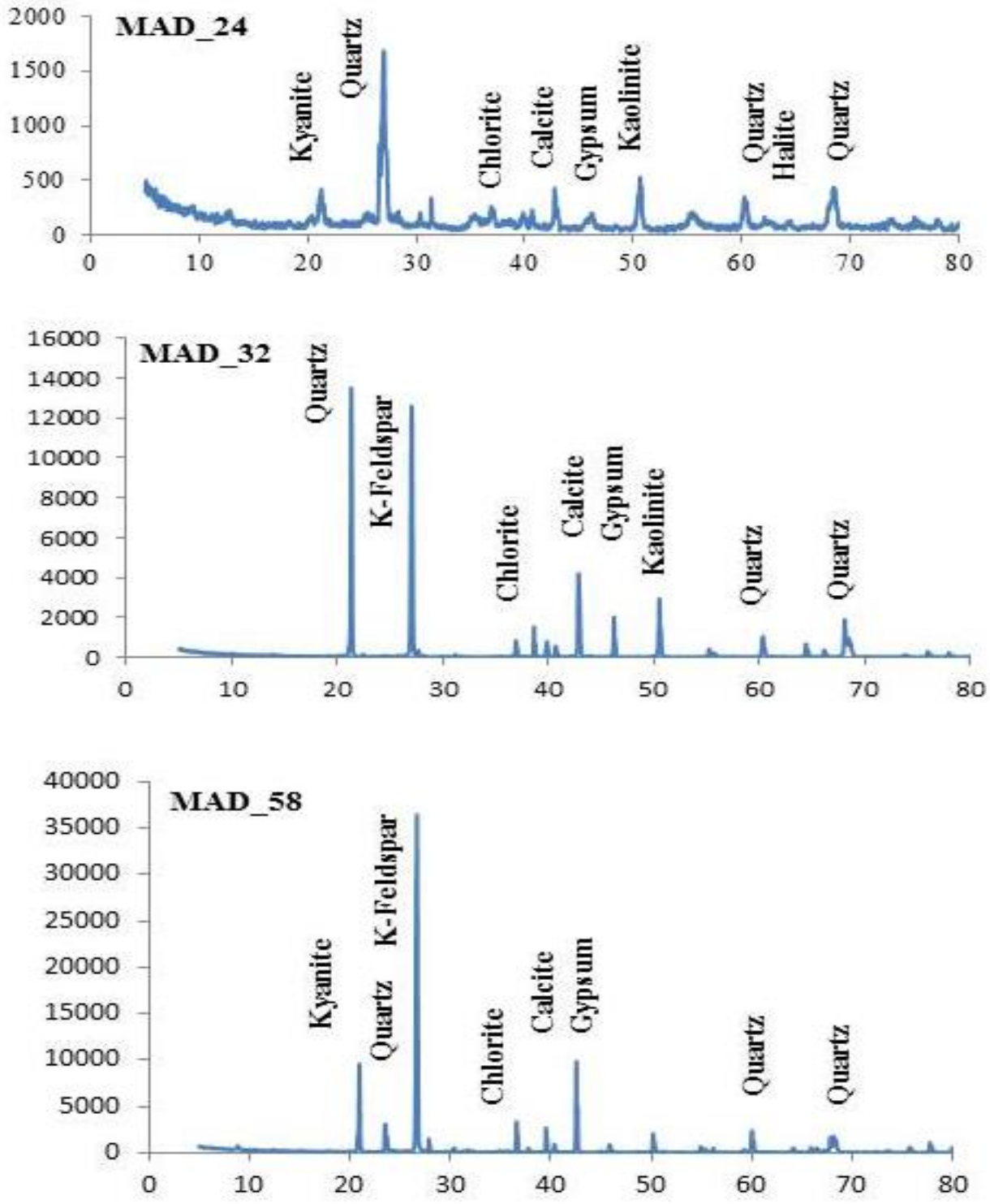

Figure 5.34(c) Comparative XRD pattern of sediment samples from different depths of borehole MAD along the southern transect

5.3.8 Bulk elemental compositions

Bulk solid phase As measured in 60 sediment samples from along the northern transect ranged from 1 to 15 mg/kg with an average value of 4 mg/kg, while bulk As measurement of 80 sediment samples from the southern bank range between 1 to 4 mg/kg. These values are comparable to the average value of modern unconsolidated sediments (Smedley and Kinniburgh, 2002) and those measured in other As-affected areas in Bangladesh (Ahmed et al., 1998, 2004; Nickson et al., 2000; BGS & DPHE, 2001), India (Bhattacharya et al., 1997; Acharyya et al., 2000), Vietnam (Berg et al., 2001), and USA (Smedley and Kinniburgh, 2002). Solid phase As enrichment were consistent along both the transects, indicating that high dissolved As concentrations in groundwater aquifer are not due to the elevated solid-phase As concentrations in the sediments of As-affected aquifers (Nickson et al., 2000; McArthur et al., 2001, 2004).

XRF measured total Fe revealed concentrations ranging between 6 to 63 g/kg in samples along the northern transect, and between 3 to 20 g/kg in samples along the southern transect (Figure 5.35). No obvious elemental difference was observed between the sampled regions that might account for the dissolved arsenic concentration variability. The size of the sediment particles did have a pronounced influence in controlling the distribution and mobility of As in the sediments. Primarily relevant is how high concentrations of As, Fe and Mn in sediments correspond to the aquifer along both the transects (Figure5.35a-5.35b). Fine grained fractions with their large surface area absorb higher portions of As on their surface and Fe, Mn and Al oxides and hydroxides being the major components of fine grained particles are thus thought to retain high As under specific pH conditions (Pierce and Moore, 1982).

Bulk measurements of Mn, ranging between 58 to 1041 mg/kg along the northern transect and 40 to 475 mg/kg along the southern transect demonstrated similar occurrence with higher concentrations being associated with the finer particles. The concentrations along both transects did not show any apparent difference in the concentrations. Bulk Ca measurements ranged between 49 to 14779 mg/kg along the northern transect and 66.5 to 14776 mg/kg along the southern transect, the concentrations being consistent for sediment samples from both the study transects (Appendix A.3.2). van Geen et al. (2013) found that bulk Ca concentrations of Holocene sediments were > 2000 mg/kg whereas the Pleistocene sediments usually had Ca concentrations < 500 mg/kg and often much lower. Patterns of Ca

concentration in sand cuttings provided an in-depth check on groundwater flow across the Pleistocene –Holocene boundary (Radloff et al., 2011). Gradually increasing trend of bulk Ca concentrations along the northern transect clearly demarked the Pleistocene –Holocene boundary, confirming that Pleistocene aquifers adjacent to the foothills have As concentrations below permissible limits. However, no such trends were observed along the southern transect, indicating the complex depositional and sedimentation history of aquifer sediments along the southern transect.

With the exception of Sr, XRF measured bulk composition of aquifer sands measured for other elements (K, Ca, Ti, Cr, Mn, Fe, Ni, Cu, Zn, Rb, Zr, Ba, Pb) demonstrated no marked differences in their concentrations along both transects. For boreholes along southern transect, concentrations of Sr in all but one sample of sand cuttings from the 6 sites closest to the Brahmaputra River along the southern transect ranged from 130 to 300 mg/kg (Appendix A.3.3). In contrast, the Sr content of 6 out of 10 sand samples from the closest and 3rd closet sites to the Naga Hills was ~50 mg/kg, ~90 for the 2 other samples and ~110 mg/kg for the 2 remainder samples. Sr content of clay samples from sites close to the River ranged from 60.3 to 116 mg/kg, while in samples in the intermediate zone middle portion and zone near close to the Naga Hills the Sr content range formed between 51 to 185 mg/kg and 46 to 166 mg/kg, respectively.

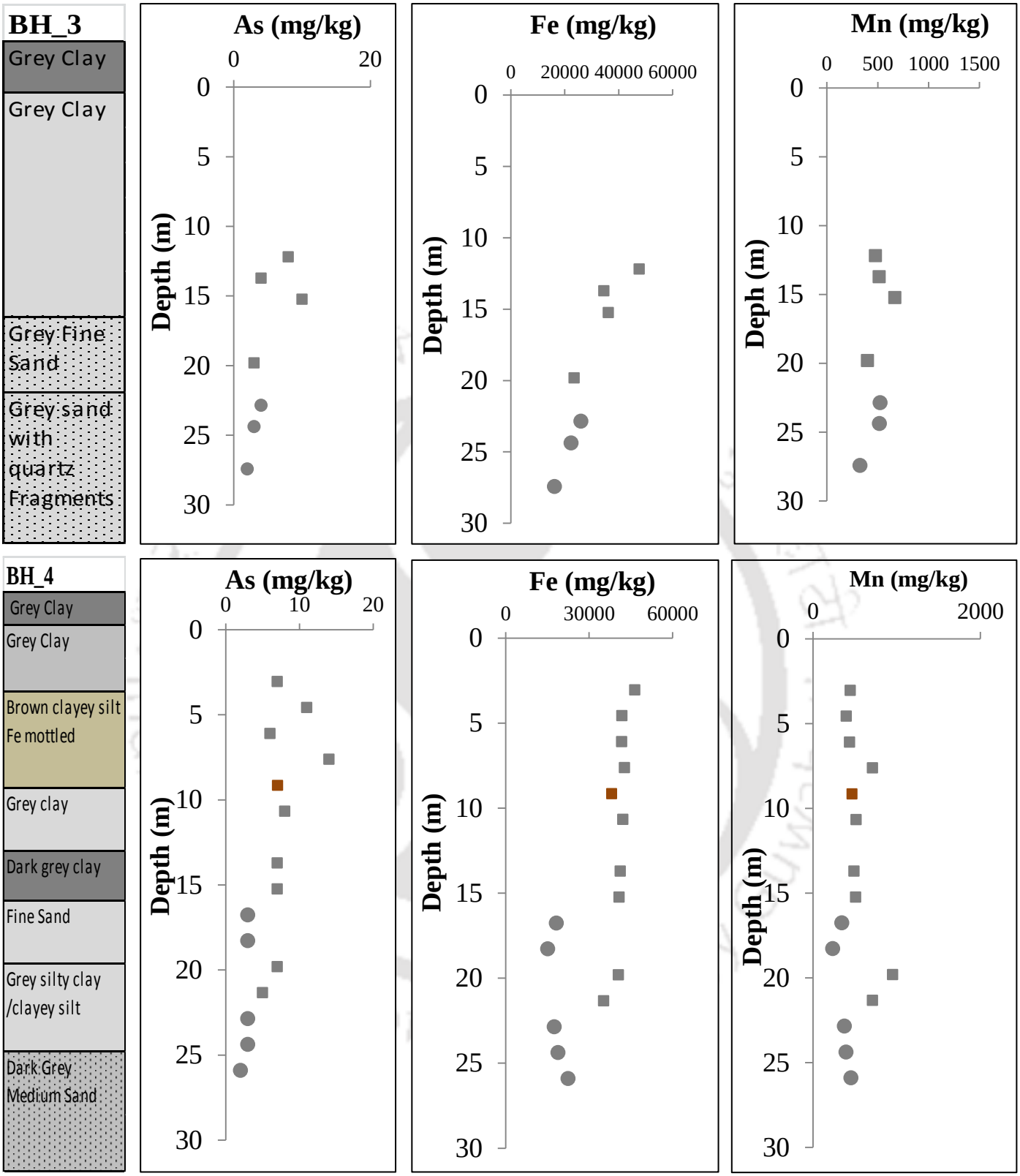

Figure 5.35a Bulk measurements of As, Fe, Mn for select boreholes along the northern transect. Squared symbols represent clays while round symbols indicate sands. The colours represent color of the sediments.

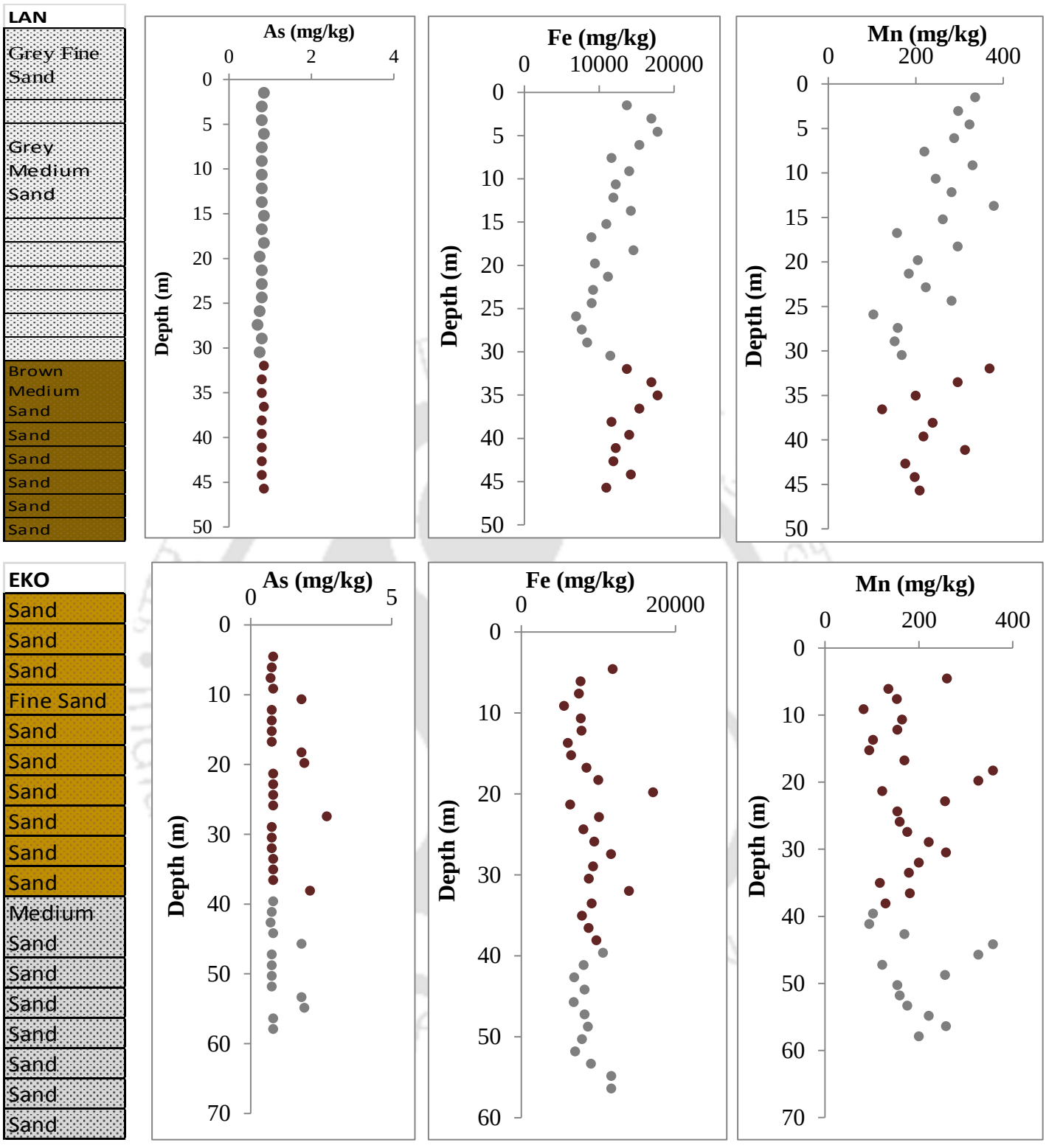

Figure 5.35b Bulk measurements of As, Fe, Mn for select boreholes along the southern transect. Squared symbols represent clays while round symbols indicate sands. The colors represents color of the sediments.

5.3.9 Major oxides in sediments

Metal oxides such as iron oxides, aluminium oxides and manganese oxides are the major minerals that bind As in sediments (Yadav et al., 2015). Average values of major oxides measured in selected sediment samples from both transect are presented in (Table 14; Figure 5.36-5.37). Concentrations of major oxides were found to be unevenly distributed. Sediment samples were dominated by SiO_2 (ranging from 62.95% to 82.55% with an average value of 75.17% for the northern transect; ranging between 60.23% to 65.97 % with an average value of 62.05 % for the southern transect), followed by Al_2O_3. CaO, K_2O and MgO showed similar concentrations in varying proportions based on nature of lithotypes. Values of Fe_2O_3 ranged between 0.99 to 4.49 % with an average of 2.26 % for the northern transect and 2.19 % to 5.08 % with and average value of 3.08% for the southern transect. With average % weight of Fe_2O_3 close to values (4.5 % by wt) found in upper continental crust, the possible role of iron oxide in reductive dissolution of Fe(III) oxyhydroxides can be re-emphasized (McArthur et. al., 2001; Nickson et al., 2000).

Table 14 Summary results of major and trace geochemical composition of borehole sediment from the study transects (unit for major composition is percentage)

		SiO_2	Al_2O_3	Fe_2O_3	MnO	MgO	CaO	Na_2O	K_2O	TiO_2	P_2O_5
Min	**Northern Transect**	62.95	11.68	0.99	0.01	0.15	0.01	2.19	1.14	0.14	0.02
Max		82.55	19.68	4.49	0.05	0.62	2.69	3.20	2.59	0.80	0.09
Average		75.17	13.40	2.56	0.03	0.28	0.41	2.37	1.73	0.33	0.04
Min	**Southern Transect**	60.23	13.80	2.19	0.04	0.61	2.27	2.61	2.16	0.35	0.22
Max		65.97	14.84	5.08	0.10	1.91	4.46	2.85	2.63	0.75	0.45
Average		62.05	14.22	3.08	0.06	1.01	3.34	2.75	2.35	0.46	0.30

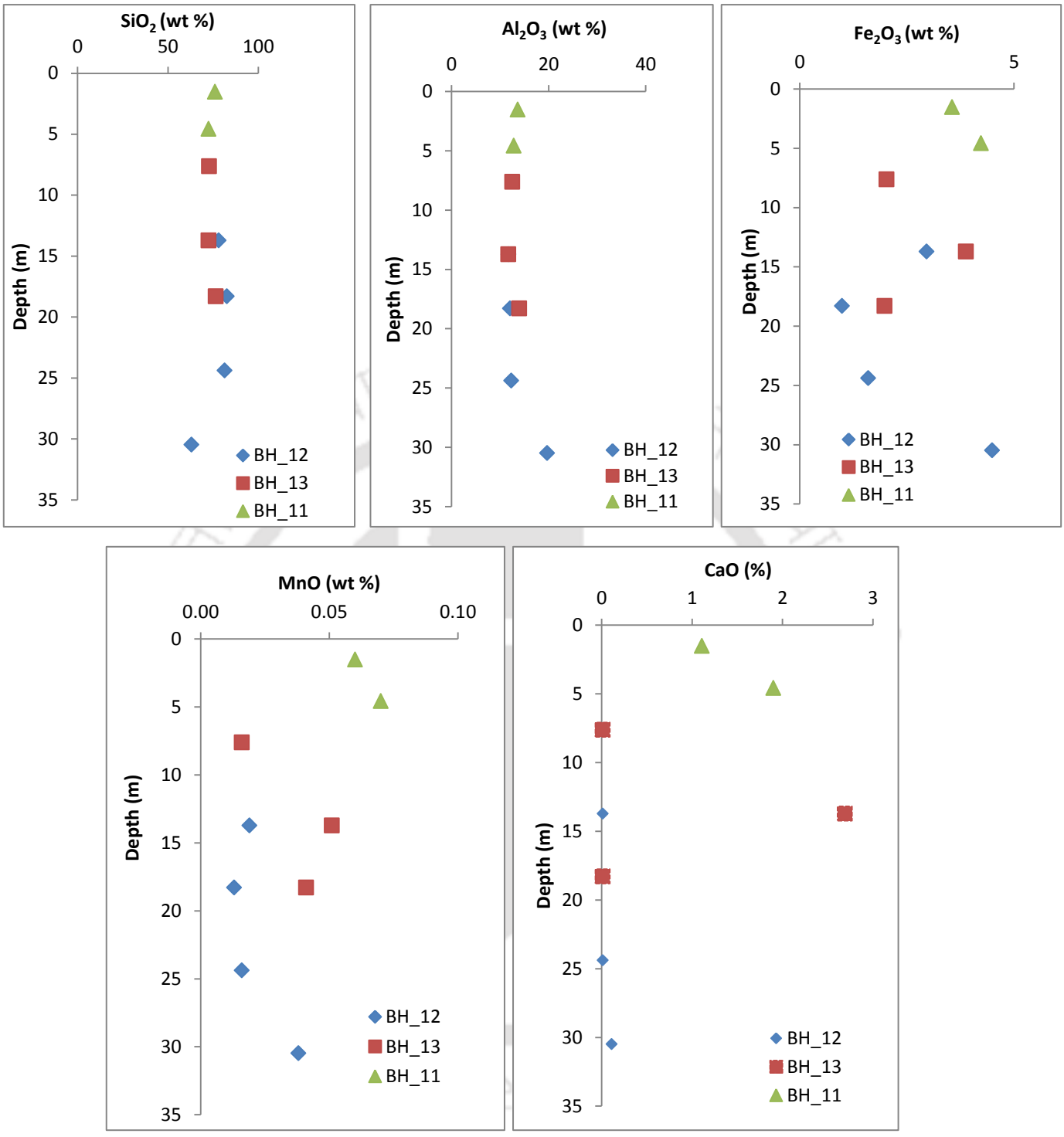

Figure 5.36(a) Depth wise variations of major oxides from selected sediment samples from northern transect

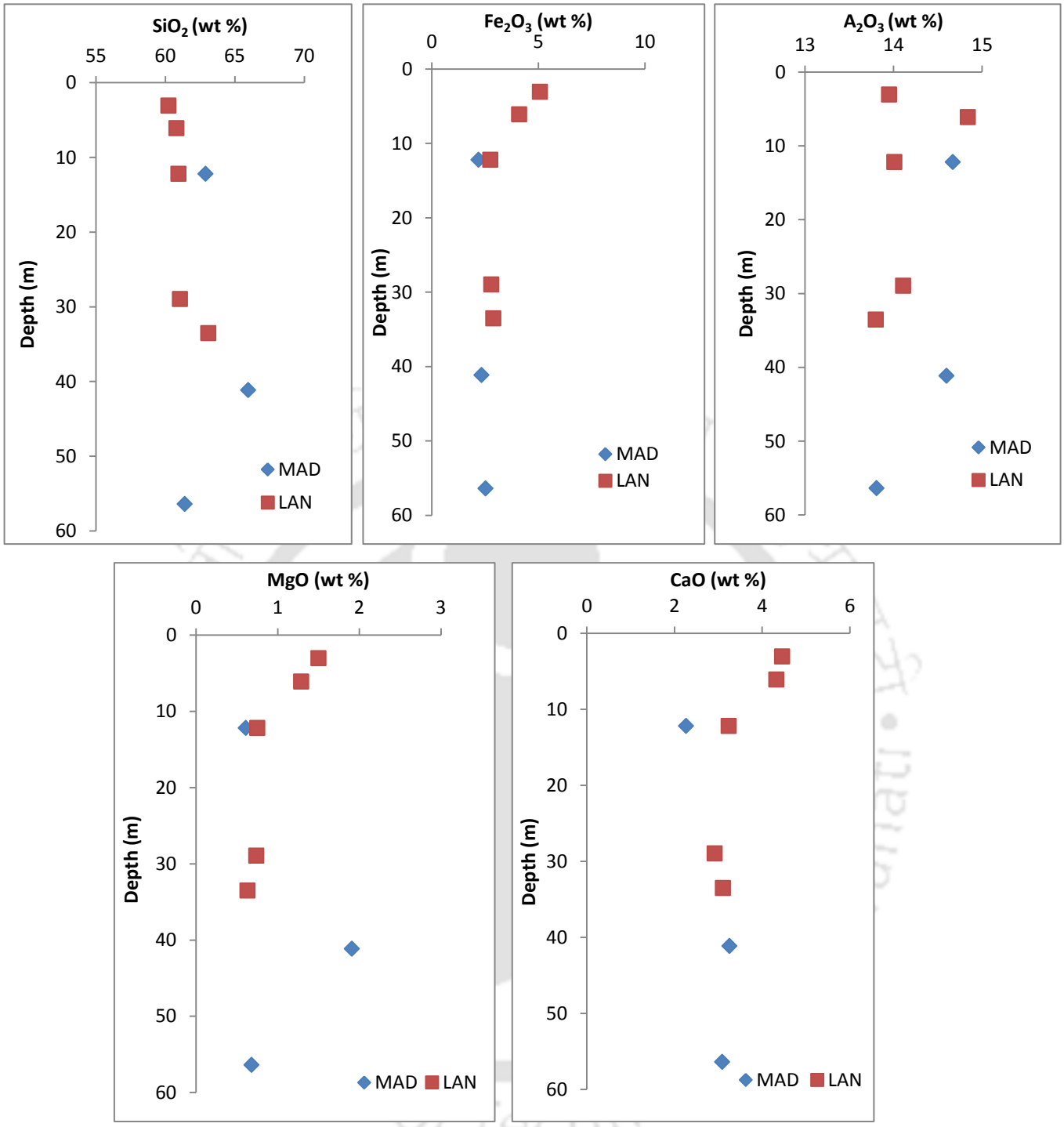

Figure 5.36(b) Depth wise variations of major oxides from selected sediment samples from southern transect

5.3.10 Diffuse Spectral Reflectance

To quantify aquifer redox conditions, depth wise measurements of reflectance from sand samples along the southern transect were conducted. The transformation, obtained by

subtracting the reflectance percentage for two adjacent 10 nm windows in wavelength, hereon referred to as ΔR are used to characterize the reflectance spectrum of the sediment. The reflectance data showed a wide range with values ranging between from 0 to 1.75 for samples close to the river; 0 to 1.13 and 0 to 1.85 for clay samples in the middle portion and near the Naga Foothills, respectively (Figure 5.37).

Aquifer redox conditions play significant role in arsenic mobilization (Horneman et al., 2004 Berg et al., 2008; Carraro et al., 2015). A significant linear relationship was observed between leachable Fe(II)/Fe and ΔR values measured at 520 nm (Horneman et al., 2004). The reflectance data indicate particularly reduced Fe oxides (ΔR <0.1%, Horneman et al., 2004) prevailed in the middle portion of the transect when compared to the less reduced sands above the layer of brown sand at the site closest to the river and also the thinner sand layer at two sites closer to the Naga Hills. Most clay samples along the 35 km southern transect was grey. Reflectance measurements of aquifer sediments showed that most reduced sands exist in the intermediate section of the transect instead of the region closest to the Naga Hills. It therefore does not appear that the redox state of aquifer sands can explain the pattern of groundwater As concentrations across the transect.

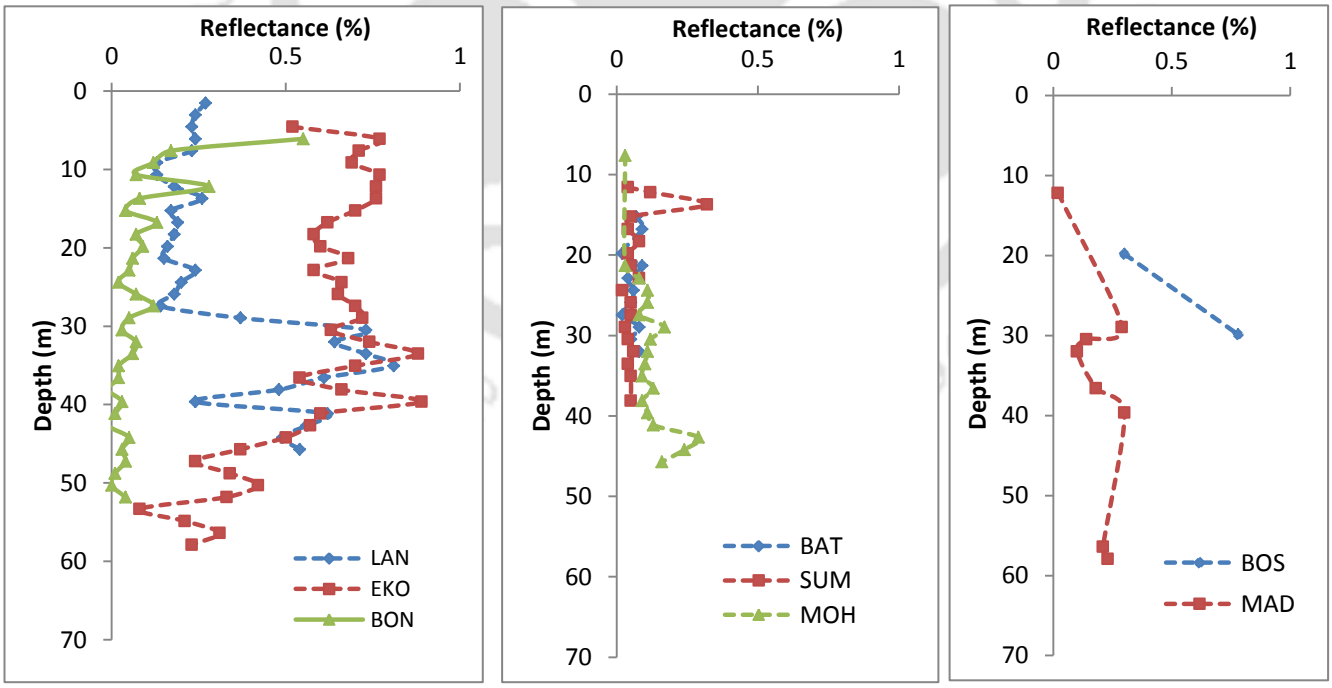

Figure 5.37 Reflectance measurements of sediment samples from boreholes in the low (LAN, EKO, BON), intermediate (BAT, SUM, MOH) and high (BOS, MAD) arsenic zones

5.3.11 Leachable Arsenic

Since one of the objectives of this study was to understand the underlying cause of spatial As distribution in the upper Brahmaputra River Basin, an attempt to study the amount of leachable As in the aquifer sands along the southern transect was made. The southern transect was studied in depth owing to the much discernable pattern of As variability along the transect. Leachable arsenic concentrations ranged between 0 to 50 µg/L (Figure 5.38). While the ranges of solid phase arsenic concentrations were almost similar in all the three zones, leachable arsenic fractions showed distinct variability. High leachable As fractions were observed in sand fractions of boreholes from the proximal zone, while relatively lower concentrations were observed in sand samples from boreholes close to the river. The low leachable As fraction in aquifer sands from the low As zone indicated that rapid flushing of aquifer sands has possibly led to flushing of leachable As fractions, thereby leading to low dissolved As concentrations in the aquifers.

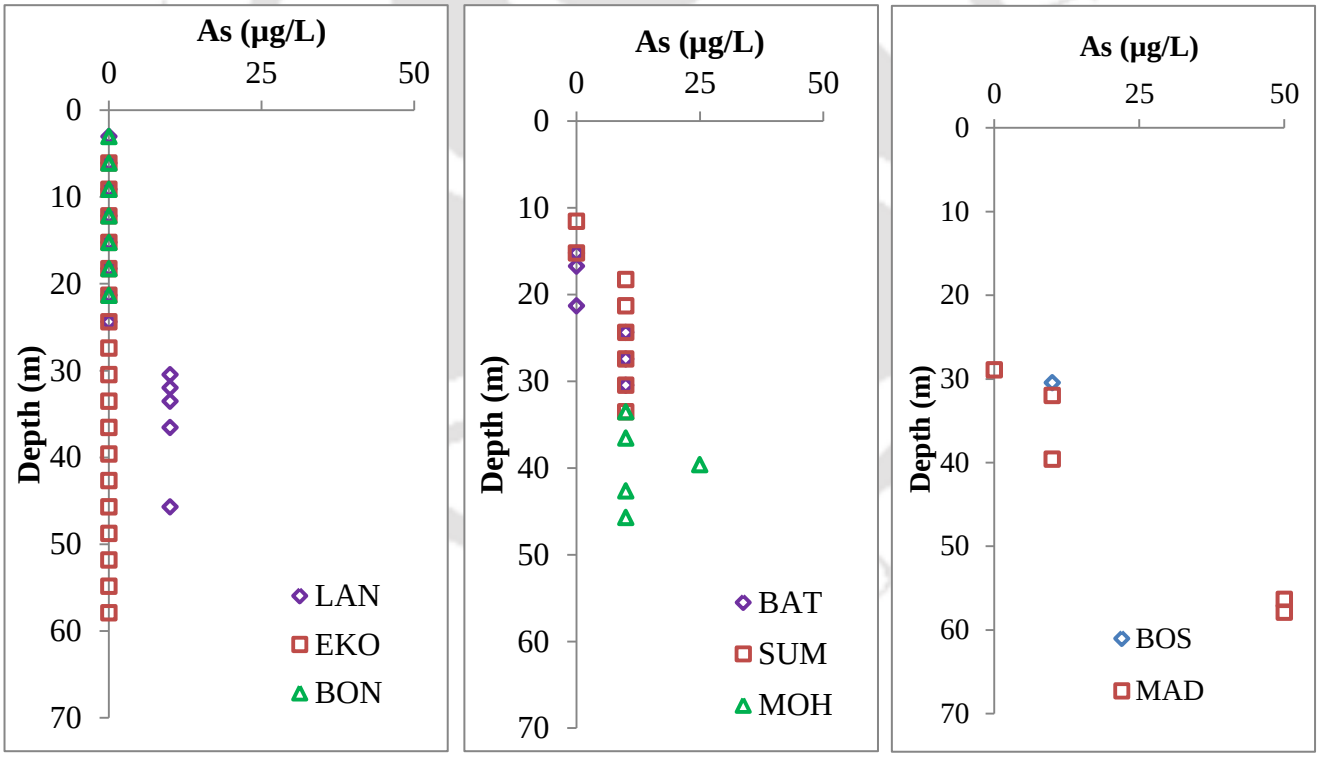

Figure 5.38 Depth wise concentrations of leachable arsenic in boreholes from sediment samples from borewells in the low (LAN, EKO, BON), intermediate (BAT, SUM, MOH) and high (BOS, MAD) arsenic zones.

5.3.12 Selective Sequential Extraction

5.3.12.1 Northern transect

Sequential extraction (semi quantitative estimates) gives an indication of how strongly As, Mn and Fe is bound to the sediments. Fraction 1, which represents the physisorbed (outer sphere surface complexed) fractions, that can readily move reversibly from the sediment phase to the groundwater and vice-versa (Wenzel, 2001), represents the lowest concentrations of the total extractable As for sediments samples from all the five borewells, indicating that this fraction does not contribute to groundwater As contamination in the study area. Concentrations of total extractable, physisorbed (outer sphere surface complexed) As in borehole BH_9 account for 0.54, 1.22, 0.11, 0.62, 0.40 and 0.15 %of the total As concentrations of the sediments (Figure 5.39), with values ranging between 0.1 to 0.3 % for sediment samples from BH_14, value ranging between 0.04 to 0.57 % for samples from BH_13 and BH_12 and values ranging between 0.5 to 8.1 % for sediment samples from BH_14 (Figure 5.40). Largely, the physisorbed portion of As in all five boreholes represents the lowest concentrations of the total extractable As.

Concentrations of P- extractable chemisorbed (inner sphere surface complexed) fractions which are the labile forms that can readily move reversibly from the sediment phase to the groundwater and vice-versa, were found to be slightly higher than the physisorbed fractions.Concentrations of P- extractable chemisorbed As, accounted for 1 to 2 % for BH_9, 2 % for BH_11, 6 to 20 % of total chemisorbed As for BH_12, 1 to 2 % and 10 to 25 % for BH_14. The non-labile As fractions associated with amorphous and/or poorly crystallized oxides of Fe (eg. Ferrihydrite; Fuller et al., 1993) and As bound to well crystallized oxide/oxyhydroxides of Fe (e.g., hematite, magnetite, lepidocrocite), Mn (e.g., birnessite, cryptomelane) and Al oxides (e.g., Gibbsite) (Haque et al., 2008), represent the significant fraction of the total extractable As for sediments from all five borewells, which are in conformity with studies conducted in West Bengal and Bangladesh using the same extraction procedures (Haque et al., 2008; Reza et al., 2010; Sankar et al., 2014).

Total extractable As in fraction five, which represents the residual phases i.e. the phases associated with residual minerals such as orpiment and those associated with aluminosilicates accounts for the highest percentage of As in sediments samples from all the three boreholes, with values ranging between 21 % to 69 % for the sediments samples collected from along the northern transect.

Fraction 1, which represents the physisorbed (outer sphere surface complexed) fractions, represents the lowest concentrations of the total extractable Mn with significant percentage of of Mn associated in the easily exchangeable phase (ie. the non-specifically sorbed, outer sphere surface complexes) at all depths for BH_12.Sankar et al., (2014 based on similar association of significant percentage of Mn bound to easily exchangeable phase in sediments samples from Murshidabad, West Bengal reported that the sediment bound Mn may react with the percolating groundwater and release Mn in groundwater. Higher occurrence of extractable Mn associated with the physiosorbed fraction may be indicative of the fact sediment bound Mn may react with percolating groundwater and release Mn into groundwater. Apart from non-specifically sorbed fraction, major percentage of extractable Mn, values ranging between 10 to 40 % are associated with amorphous and/or poorly crystallized oxides, crystalline phases and the residual phases. Sequential extraction results for Fe closely resembles that of Mn extractions, with major percentage of extractable Fe being associated with amorphous and/or poorly crystallized oxides, crystalline phases and the residual phases.

High concentrations of As, Mn and Fe in residual phases is possibly due to the release of organic matter bound As, Fe and Mn while digesting with H_2O_2, indicating that organic matter could also partly contribute to the As, Mn and Fe concentrations in residual phases (Sankar et al., 2014). Also, As, Mn and Fe in the residual phases are attributed to be, occurring in aluminosilicates (clay minerals), and chiefly in other chemically resistant minerals (e.g., quartz). These minerals are relatively stable compared to pH and redox sensitive Fe (Mn, Al) oxide/oxyhydroxides (Haque et al., 2008).

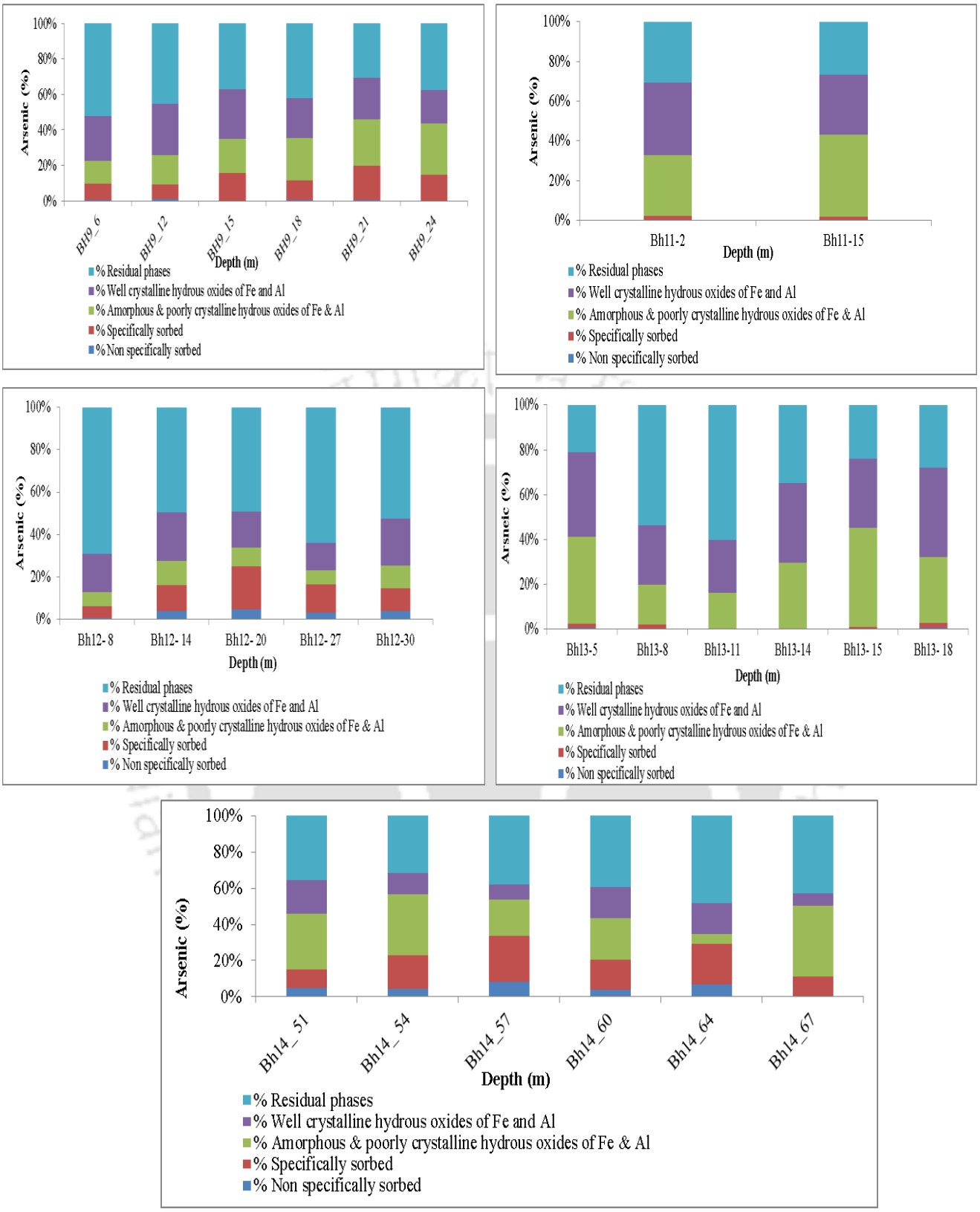

Figure 5.39 As extraction through SSE from sediment samples from northern transect (a) BH_09, (b) BH_11, (c) BH_12, (d) BH_13, (e) BH_14

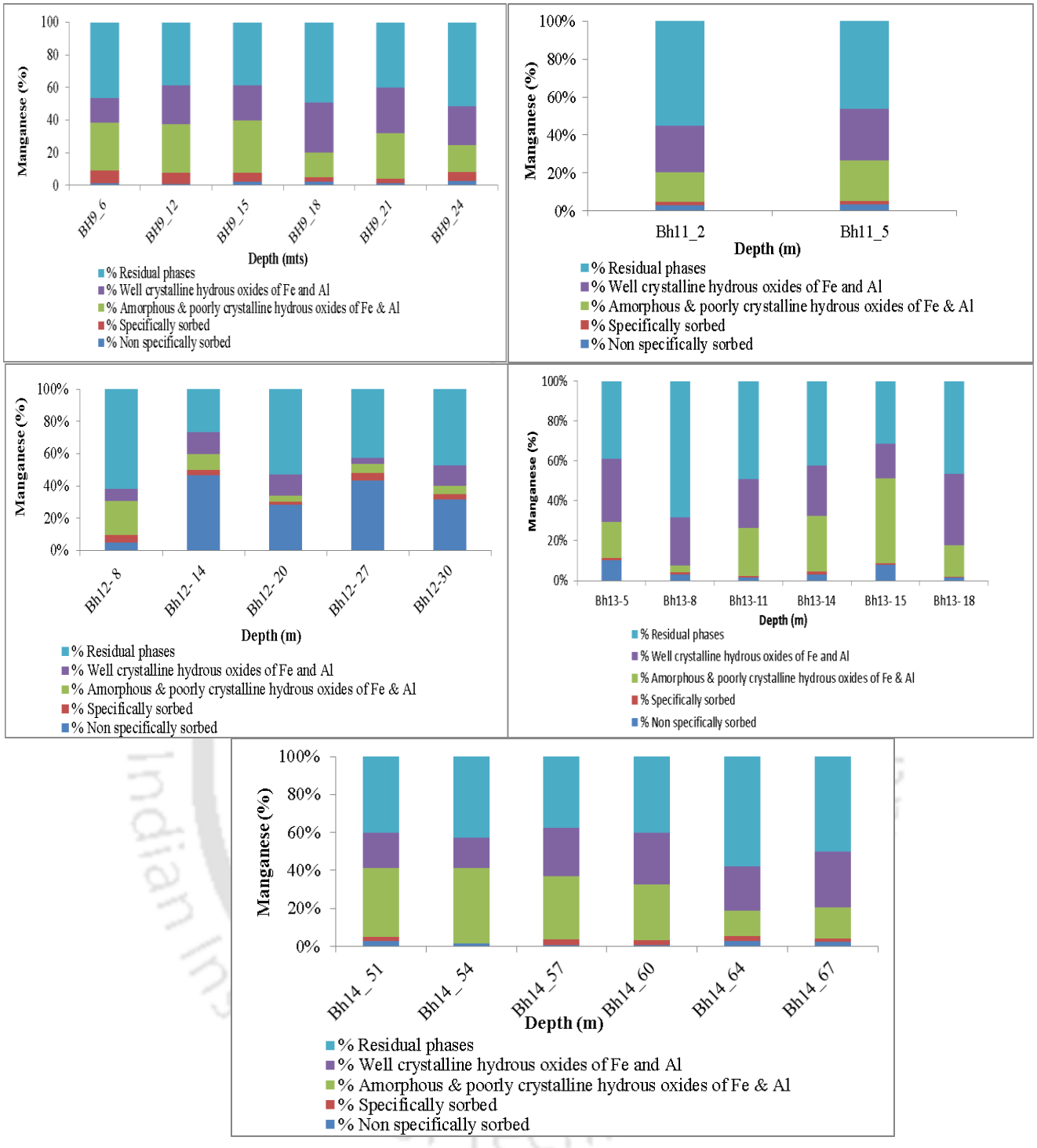

Figure 5.40 Mn extraction through SSE from sediment samples from northern transect (a) BH_09, (b) BH_11, (c) BH_12, (d) BH_13, (e) BH_14

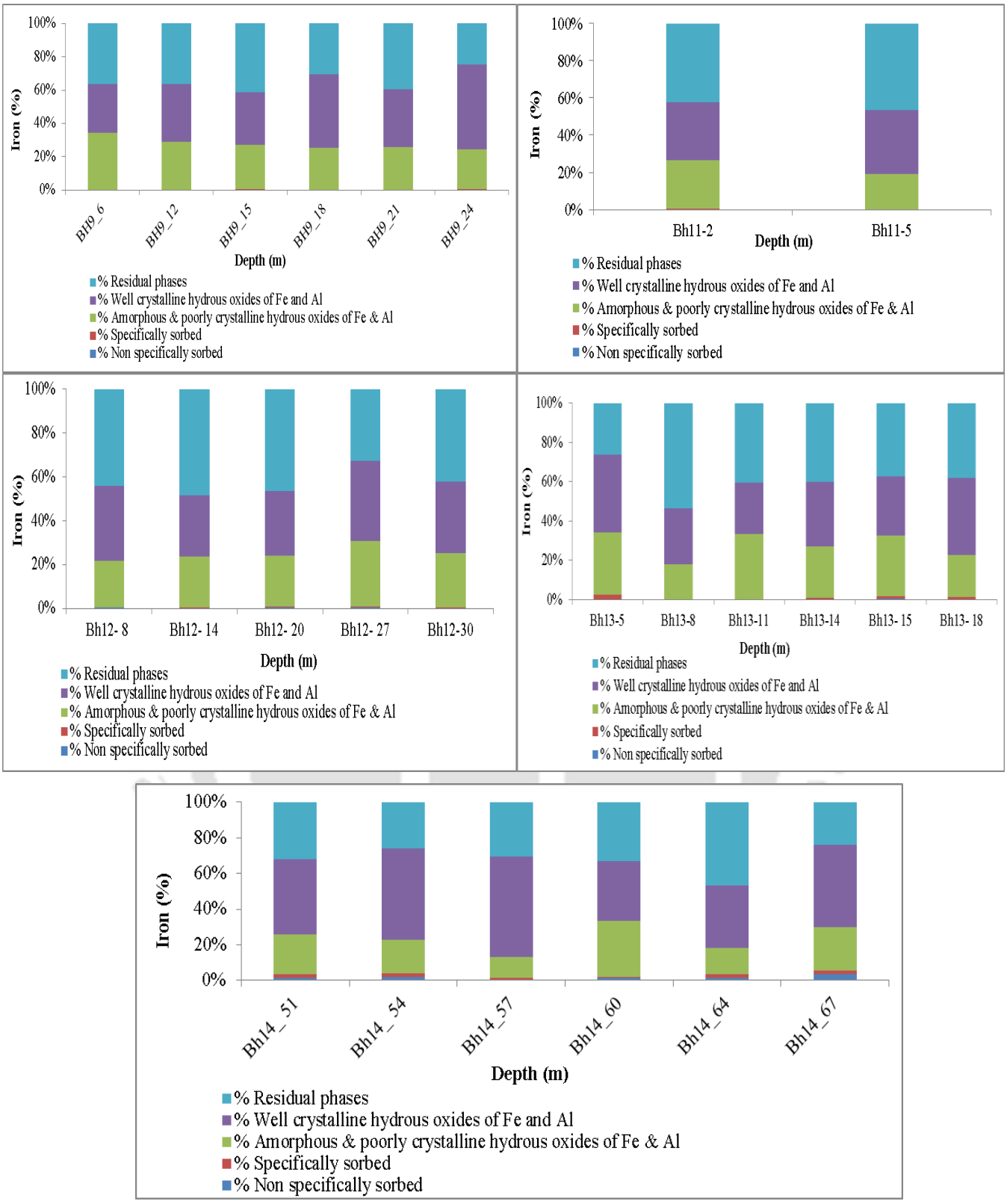

Figure 5.41 Fe extraction through SSE from sediment samples from northern transect (a) BH_09, (b) BH_11, (c) BH_12, (d) BH_13, (e) BH_14

5.3.12.2 Southern transect

Sequential extractions of aquifer sediments from three borewells viz. LAN, EKO and MAD, along southern transect indicate that, major fraction of the solid phases As is extracted with 0.05 M $NH_4H_2PO_4$ solution which represent the specifically adsorbed pool of As, and the amorphous and crystalline phases. Most of the sediment samples from the three boreholes, were characterized by the dominance of phosphate-extractable (strongly adsorbed) arsenic, which accounts for 8.64 to 21.62 % of the total extractable As (Figure.5.42). Apart from the physiosorbed fractions, As co-precipitated with iron oxyhydroxides and crystalline phases are the most abundant, accounting for up to 17 to 39 % and 18 to 30 % of the budgets. Overall, the non-labile As bound to crystallized Fe and Mn oxides represent the significant fraction of the total extractable As, which are in conformity with studies conducted in West Bengal using the same extraction previous studies from the study area (Sailo et al., 2015; Das et al., 2016; Choudhury et al., 2015), report similar findings with major pool of extractable arsenic being associated with the amorphous and crystalline phases.

The residual phase, is the most abundant fraction of extractable As for sediments from all three borewells, accounting for 26 to 49 % of the total extractable pool of As. As associated in the residual phase is bound to sulphides, silicates and detrital minerals in the sediments and cannot be remobilized under normal environmental conditions (Tessier et al., 1993, Wenzel et al., 2001, Wang and Mulligan, 2008).

Fractionation of Mn in aquifer sediments from the three boreholes along the transect represent similar occurrence of Mn in each of the different phases, with a large percentage of Mn (> 45 %) being extracted in the residual phase. At the three sites, the amount of Mn associated with crystalline phase was found to be comparatively higher than the amorphous phase (Figure 5.44). Fractionation of Fe represents a higher pool of Fe associated with amorphous, crystalline and the residual phases, with percentage varying between 29 to 45 %, 25 to 40 % and 24 to 43 % for each of the three different phases (Figure 4.43). Oxides of Fe and Mn act as sediment sinks for heavy metals as they have the capacity to retain substantial fractions of metals. They play a major role in controlling the fate and transport of heavy metals in the environment (Postma et al., 2007, 2010).

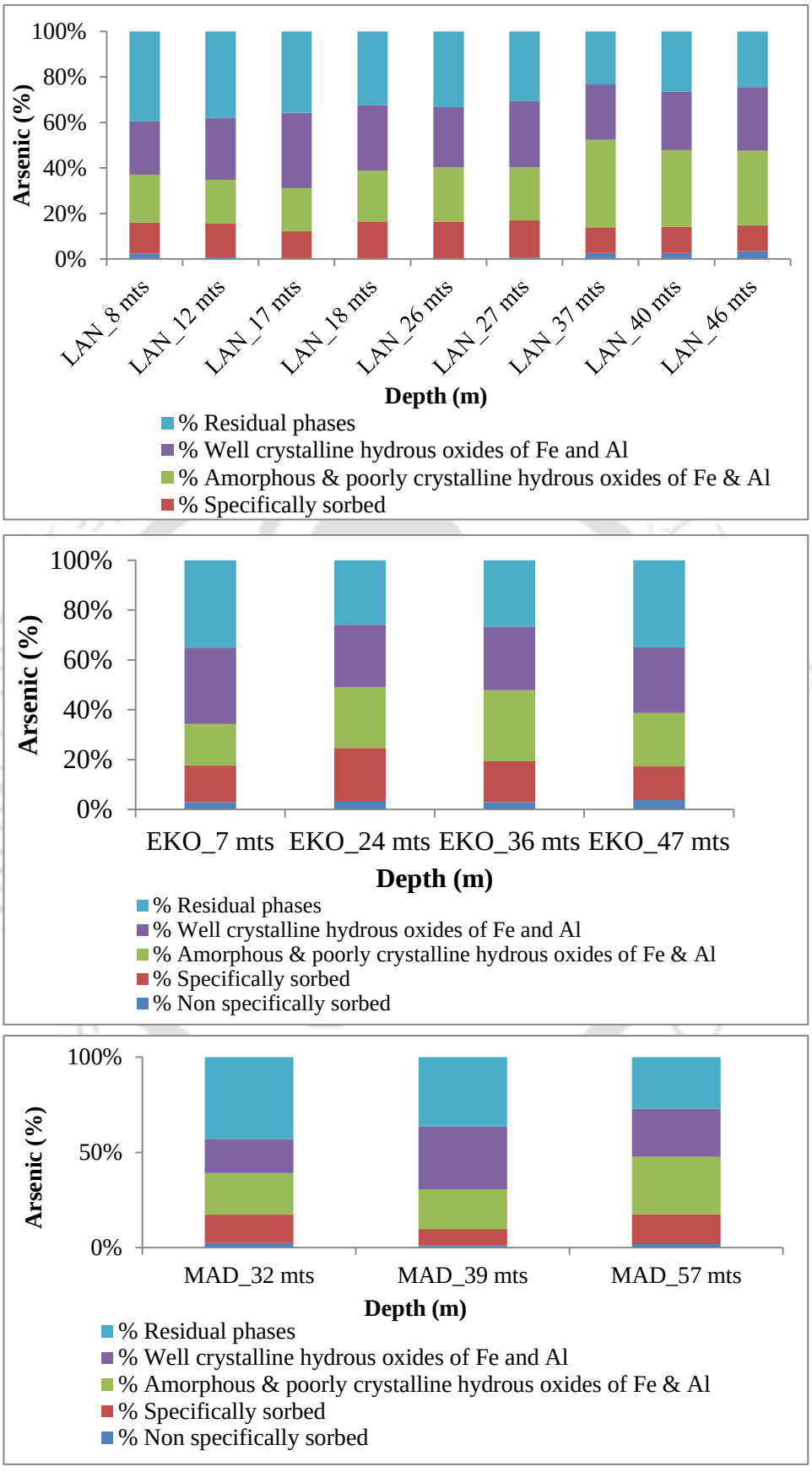

Figure 5.42 As extraction through SSE from sediment samples from southern transect (a) LAN (b) EKO, (c) MAD

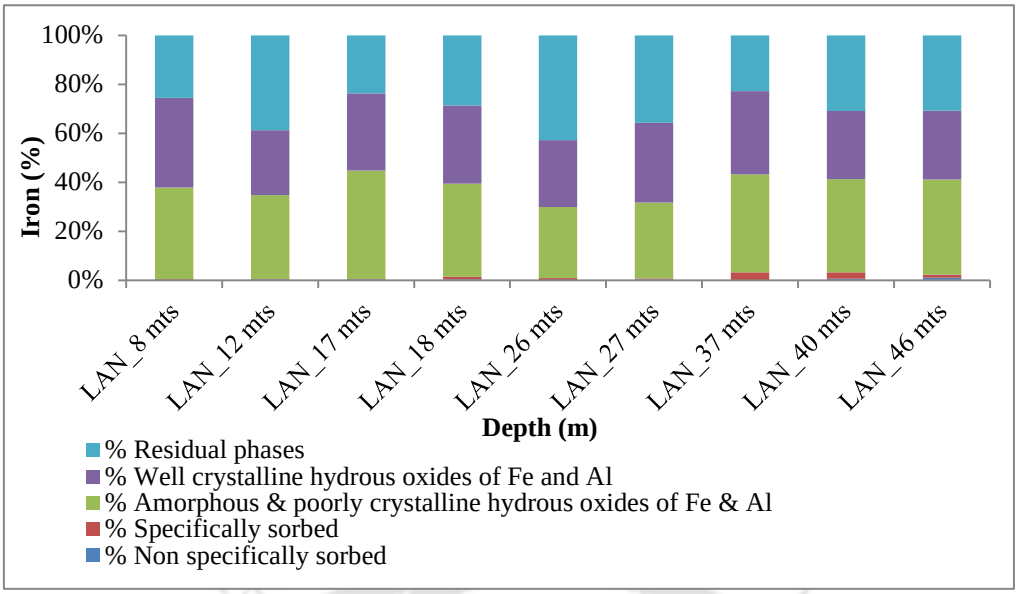

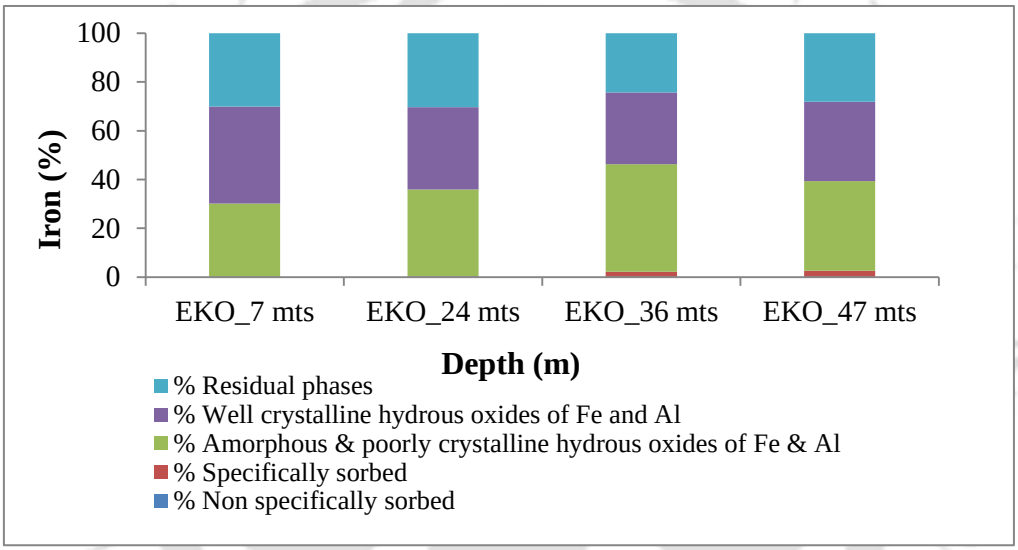

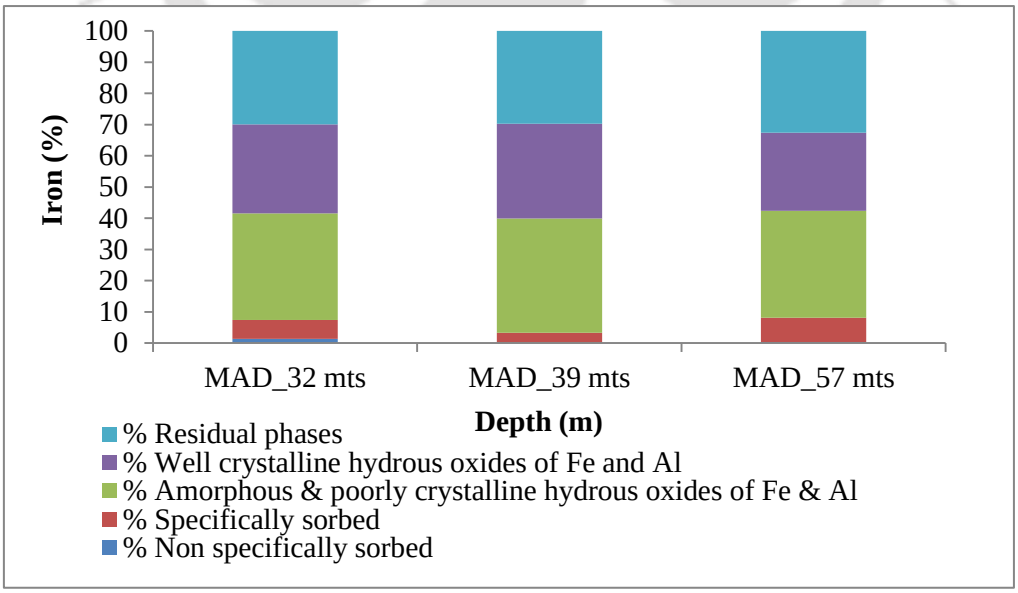

Figure 5.43 Fe extraction through SSE from sediment samples from southern transect (a) LAN (b) EKO, (c) MAD

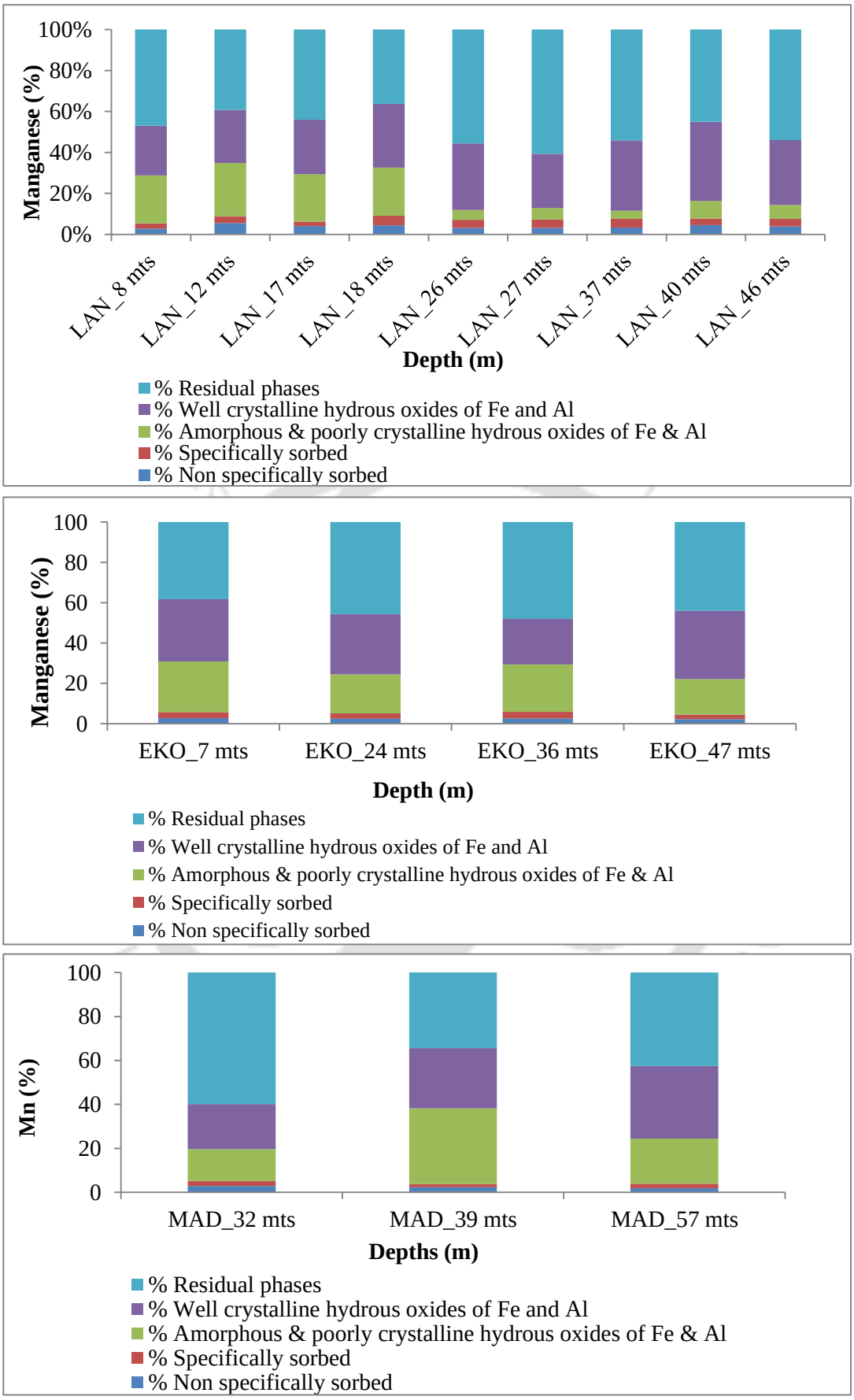

Figure 5.44 Mn extraction through SSE from sediment samples from southern transect (a) LAN (b) EKO, (c) MAD

5.4 Sedimentation geochemistry

Total arsenic in sediment samples from both transects, ranged from 7.77 mg/kg to 13.93 mg/kg with an average concentration of 10.08 mg/kg. Considering the world baseline concentrations of As in sediments in the range of 5-10 mg/kg (Smedley and Kinniburgh, 2002), the average levels of 10 mg/kg of As measured in the digested sediment samples are nearly within the natural range (Cullen and Reimer, 1989; Smedley and Kinniburgh, 2002). Concentration of total Mn and Fe range from 61.90 to 114 mg/kg and 1703 to 5129 mg/kg.

Sequential extractions demonstrated a relatively lower fraction of the total extractable As associated with the labile physisorbed fractions, with significant fractions being associated with the P- extractable specifically sorbed inner sphere complexes. It may thus be suggested that competitive ion exchange processes by which As in the specifically sorbed phases are replaced by PO_4^- present in groundwater may perhaps be a mechanism of As release in groundwater along both the transects (McArthur et al., 2001, Sankar et al., 2014).

Major portion of the extractable As are found to be primarily associated with amorphous and crystalline Fe (Mn, Al) oxide/oxyhydroxides, in non-labile forms. These results are consistent with studies conducted in Aquia aquifer, Maryland, USA and West Bengal adopting the same extraction procedures (Haque et al., 2009; Wang et al., 2010; Sankar et al., 2014; Yang et al., 2016). Amorphous iron oxyhydroxide mineral which form initially, has a surface area of more than 300 m^2/g, however in the process of crystallization and digenesis, the surface area gradually decreases to 15 m^2/g or less. Therefore, As associated mostly with Fe(III) oxide/oxyhydroxides in aquifer sediments either by process of co-precipitation or adsorption onto sediment surface sites (Tye et al., 2002, Fuller et al., 1993; Manning and Goldberg, 1996, 1997) may have the propensity to get released into groundwater as minerals crystalizes (Anwar et al., 2013). Microbially mediated redox induced reductive dissolution of minerals hosting As, such as Fe (III) oxide/oxyhydroxides are widely reported to release non-labile As into solution (Nickson et al. 1998, 2000; McArthur et al. 2004; Dixit and Hering 2003, Haque et al., 2008). Based on results of sequential extraction and mineralogical study, it can be suggested that reductive dissolution of Fe and Mn oxyhydroxides may trigger release of As in the study area along with competitive ion exchange processes as has been indicated by the presence of significant amount of As in the P- extractable specifically sorbed inner sphere complexes.

Relatively few extraction based studies conducted in the upper Brahmaputra Basin reported major As phases to be associated with the amorphous and crystalline phases (Sailo and Mahanta, 2015; Das et al., 2016). The association of As with Fe oxyhydroxide phases indicates that Fe-Mn-oxyhydroxides are the major As bearing phases in the aquifer sediments (Sankar et al., 2014).

High concentrations of As, Mn and Fe in residual phases is possibly due to the release of organic matter bound As, Fe and Mn while digesting with H_2O_2, indicating that organic matter could also partly contribute to the As, Mn and Fe concentrations in residual phases (Sankar et al., 2014). Also, As, Mn and Fe in the residual phases are attributed to be, occurring in aluminosilicates (clay minerals), and chiefly in other chemically resistant minerals (e.g., quartz). These minerals are relatively stable compared to pH and redox sensitive Fe (Mn, Al) oxide/oxyhydroxides (Haque et al., 2008).

5.5 Mechanism of As release in groundwater

Bearing close proximity to the Himalayas, which has been hypothesized to be the source of arsenic in the Ganges Brahmaputra Meghna (GBM) basin (McArthur et al., 2004; Polizzotto et al., 2006), the mechanism of arsenic release in the relatively lesser studied upper Brahmaputra Basin can be explained in terms of already prevailing mechanism of As release proposed for the Ganges Brahmaputra Meghna (GBM) basin. Much of our knowledge on the groundwater arsenic contamination issue are drawn from over three decades of research in the Bengal Delta Plains. On the process of arsenic release and mobilization, the reductive dissolution of Fe-oxyhydroxides and sulphide oxidation have been proposed to be the major mechanism of As release from the Bengal Delta Plain (BDP) sediments to groundwater (e.g., Bhattacharya et al., 1997, Nickson et al., 1998, Nickson et al., 2000, Acharyya et al., 1999, McArthur et al., 2001, Anawar et al., 2003, Nath et al., 2008).

Presence of As bearing pyrite in aquifer sediments (Das et al., 1996; Nickson et al., 2000) has led to the inference that As release in the Bengal Delta Plain (West Bengal, India and Bangladesh) occurs through pyrite oxidation (Das et al., 1996; Chowdhury et al., 1999; Chakraborty et al., 2001). However, the absence of pyrite/ arsenopyrite in aquifer sediments from both the study transects indicated that it is unlikely that oxidation of arsenic bearing sulphides (eg. Pyrite, Arsenopyrite) could release arsenic in groundwater. Further the weak correlation between As and SO_4^{2-} along the study transects suggests that SO_4^{2-} removal from

solution has occurred (or indeed that pyrite/sulphide oxidation has not occurred) (BGS and DPHE, 2001).

Groundwater chemistry along both the study transects revealed arsenic concentration above WHO guideline values. Elevated arsenic concentrations were coupled with high dissolved Fe, Mn and HCO_3- and low SO_4^{2-} and NO_3^- concentrations. Such association indicating dominance of reducing condition in aquifers is indicative of effects of microbially mediated Fe (III) reduction on As mobilization in the presence of natural organic matter (Bhattacharyya et al., 2000, McArthur et al., 2004). However, weak to poor correlations of As with other redox-sensitive components for groundwater samples along the northern transect(Fe, R^2 = 0.09; Mn, R^2 = 0.09; HCO_3,$^-$ R^2 = 0.14; SO_4^{2-}, R^2 = 0.06; NO_3^-, R^2 = 0.01) and for groundwater samples along the southern transect (Fe, R^2 = 0.01; Mn, R^2 = 0.01; HCO_3,$^-$ R^2 = 0.54; SO_4^{2-}, R^2 = 0.05; PO_4^-, R^2 = 0.3) indicated that As mobilization in groundwater was outcome of interplay of several mechanisms viz. pH dependent desorption, competing ions etc. and that the reductive dissolution of Fe(III) oxyhydroxides alone could not explain the complete As release and mobilization mechanism. Observed moderate correlation of As and PO_4^- indicated the likely competitive role of PO_4^- anion on As release.

Dissolved concentration and distribution of As, Fe and Mn in aquifers are controlled primarily by a series of different terminal electron accepting processes (TEAPs), coupled to oxidative degradation of organic matter (Appelo and Postma, 2005, Stumm and Morgan, 1981).The observed weak correlation of As with Fe and Mn, along both transects, can thus be explained in the light of Mn and Fe oxyhydroxides reduction. In the TEAPs sequence, Mn oxyhydroxides being the stronger terminal electron acceptor is reduced prior to Fe-oxyhydroxides releasing Mn in groundwater. Mn oxyhydroxides reduction can also release arsenic in groundwater, and this released arsenic is likely to be re-adsorbed into the Fe oxyhydroxides present in the aquifer sediments (Stuben et al., 2003). Subsequently, when the aquifer redox conditions reach the Fe oxyhydroxides reduction, As is mobilized and retained into groundwater along with Fe, until the stage of SO_4^{2-} reduction is reached (Bhattacharya et al., 2002; Biswas et al., 2011; McArthur et al., 2004; Nickson et al., 1998). In the transition period of redox state from Mn oxyhydroxides to Fe oxyhydroxides, Mn is often immobilized through precipitation of secondary mineral phases like $MnCO_3$, or by adsorption to to other carbonate phases like $FeCO_3$ and $CaCO_3$ (Ahamed et al., 2004; Saunders and Swann, 1992, Stollenwerk et al., 2007; von Brömssen et al, 2008). As enrichment in aquifers often couples

with enrichment of Fe and decouples with enrichment of Mn (Biswas et al., 2012; McArthur et al., 2011).

The limited studies on groundwater arsenic contamination in the upper Brahmaputra floodplains in Assam has mostly reported reductive dissolution of Fe-oxyhydroxides as the primary mechanism of As release into groundwater aquifers (Chetia et al., 2011; Choudhury et al., 2015, Baviskar et al., 2015, Verma et al., 2015, Das et al., 2016, Choudhury et al., 2017). However, some recent have reported possible roles of other mechanisms in asenic release. The mechanism of pH controlled desorption in arsenic enrichment in aquifers along the southern bank of the Brahmaputra River, where higher pH facilitated arsenic mobilization has been reported by Das et al., 2015. Verma et al., 2015 based on observed positive correlations of As with Fe, Mn and HCO_3^- in their study area on the northern bank of the Brahmaputra, reported reductive dissolution of (Fe-Mn)OOH and combined effect of pH dependent sorption and competitive ion-exchange as dominant mechanisms of arsenic mobilization.

5.6 Comparison with other As affected regions in South and South East Asia

Bearing a common Tibetan origin to the rivers, bringing in sediments and forming major floodplains and delta plains in SE Asia, a comparison of these groundwater arsenic scenario is warranted. Groundwater arsenic contamination in the Bengal Delta Plains, one of the worst affected areas around the globe, primarily occurs in the Holocene aquifers (Bhattacharya et al., 1997, 2000). The aquifers are mainly quaternary alluvial deposits in Bangladesh and West-Bengal, typically characterized by high concentration of Fe and HCO_3^-, and lower amounts of NO_3^- and SO_4^{2-}.Circum-neutral pH and reduced conditions dominate high arsenic groundwater aquifers, with arsenic distribution highly heterogeneous in nature, and As(III) being the most predominant form due to the reducing environment (Nickson et al., 1998, 2000; Bhattacharya et al., 2001; McArthur et al., 2001, 2004; Smedley and Kinniburgh, 2002; Harvey et al., 2002; Dowling et al., 2002; van Geen et al., 2004, 2006, 2008; Charlet et al., 2007; Nath et al., 2008; Halim et al., 2009, 2010).The groundwater type of GBM delta and major floodplain areas in Bangladesh is primarily of Ca-HCO_3 type (BGS and DPHE, 2001; Ahmed et al., 2004).

High arsenic groundwaters in China are reportedly concentrated in inland basins and river deltas (Guo et al., 2014). Among the inland basins, which are related to the presence of thick

Quaternary unconsolidated sediments, the Datong Basin, the Dzungaria Basin, the Hetao Basin, the Huhhot Basin, the Songnen Basin and the Yinchuan Basin are some of the worst arsenic affected areas in China (Guo et al., 2014). In Datong basin, high arsenic groundwater exists widely in weakly alkaline and reducing conditions, and contains low Fe (II) concentration (below 1mg/L) and very low dissolved oxygen content (b0.01 mg/L) (Xie et al., 2008).In shallow aquifers of the northern Yinchuan Basin, P.R. China, high As concentrations (up to 105 µg/L) are observed to be associated with reducing conditions and characterized by high concentrations of NH_4+, dissolved Mn, dissolved Fe and Fe(II), and low concentrations of NO_3^- and SO_4^{2-}. With the observed positive correlation between As and dissolved Fe, the reductive dissolution of Fe oxides is reported to be the key mechanism of As release into the shallow aquifers of the northern Yinchuan Basin (Guo et al., 2014).

In Mekong delta (Southern Vietnam and bordering Cambodia) groundwater arsenic contamination is attributed to be of geogenic origin and caused by natural anoxic conditions in the aquifers. In groundwater used as drinking water, arsenic concentrations ranged from 0.1–1340 µg/L, with 37% of the studied wells (n = 352) exceeding the WHO guidelines of 10 µg/L arsenic (Buschmann et al., 2008).

In Vietnam, high arsenic quantity in groundwaters are driven by high concentrations of Natural Organic Matter (NOM) present in the aquifer layers (Berg et al., 2001). Recent study by Merola et al., 2015; revealed that high arsenic are linked with depth (< 200m), low salinity and reducing conditions.

Elevated concentrations of As (50–630 µg/L) As in the lower Ayeyarwady basin in Myanmar are reported to be associated with high levels of Fe (up to 21 mg/L) and low SO_4^{2-} (<0.05 mg/L)concentrations. Concentrations of As <10 µg/L were measured in some shallow (<30 m) grey sands and in both shallow and deep orange sands (van Geen et al., 2013). These results indicated that the main mechanism of As release to groundwater in Myanmar is also the reductive dissolution of Fe oxyhydroxides, as in the neighbouring Bengal, Mekong, and Red River basins.

Groundwater in the Terai regions of Nepal are worst affected with As contamination, with an estimated thirty-one percent of the population (3.5 million) in the region exposed to arsenic levels between 10 and 50 µg/L (Pokhrel et al., 2009).The sources are reported to be leached

materials due to weathering of As-bearing minerals (Yadav et al., 2014). In Nawalparswi district in Terai, Nepal, high arsenic groundwater are associated with slightly alkaline and reducing groundwaters, with low concentrations of HCO_3^- and NO_3^-, indicating that here too reductive dissolution of Fe(III) hydroxides as the key mechanism of As release into groundwater of the region (Yadav et al., 2015).

In a recent study by Podgorski et al., (2017), high arsenic groundwater in the Indus Valley is attributed primarily to the pH-induced desorption, in contrast to the generally accepted reductive dissolution mechanism of arsenic release. High values of arsenic (>10 µg/L) are reported to correlate strongly with soil pH (R^2 = 0.98) and arsenic-contaminated groundwater for thresholds of 10 and 50µg/L are associated with oxidizing conditions. The major difference is the mechanism and processes of arsenic release India and the Brahmaputra Valley lies in the fact that the former has a semi arid to arid environment, while the latter is a monsoon dominated environment.

Although groundwater chemistry in the alluvial aquifer of the Upper Brahmaputra Basin in India bears some similarity to those in Bangladesh, the dissolved As concentrations in the study area (bdl ˷600µg/L) are generally relatively less than the values reported in Bangladesh (2.5–4700 µg/L; Rahman et al., 2009). Comparisons of dissolved As and Fe concentrations data from Bangladesh reveal a noticeable difference although dissolved Fe levels are higher, the concentration of aqueous As was not as higher, particularly for the groundwater samples along the northern transect. It can thus be inferred that all conditions remaining similar, the influence of local factors viz. geologic, hydrologic, geomorphic etc. controlling As release and mobilization play a much significant role in As mobilization into groundwater of the upper Brahmaputra Basin.

5.7 Role of Geology and Geomorphology in controlling As distribution

5.7.1 Role of Geology in As distribution

Considering the complexity of both the study transects lying in two different tectono-sedimentary regimes, the northern transect sandwiched between the eastern Himalayas and the Brahmaputra River and the southern transect between the Naga Patkai hill ranges and the Brahmaputra River, the influence of geology in distribution of arsenic was studied. Local geology and depositional history have been reported to play considerable role in controlling

arsenic distribution in the Bengal Basin (Stanger, 2005; Samsuddha et al., 2008; Mukherjee et al., 2013).

Sediment deposition along the 50 km northern transect were caused primarily by the northern tributaries of the Brahmaputra River, draining the Siwalik Himalayas. The Brahmaputra main channel contributes to sediment deposition primarily in the areas close to the main floodplains. The Siwalik's has been earlier reported to be the primary provenance of arsenic bearing minerals (Saunders et al., 2005a). Smaller rivers draining the Siwalik have higher arsenic load than larger rivers originating from the Higher Himalayas (Guilliot and Charlet, 2007). These Siwalik sediments consisting of Neogene foreland basin sediments (Burbank et al., 1996) are believed to be the sources of the arsenic load in aquifers of the northern transect, which under conditions conducive to arsenic release and mobilization, enriches the groundwater aquifers.

Arsenic distribution along the southern transect showed a trend with higher concentrations closer to the Naga Patkai hill ranges than the WHO guideline values. Depositional history was believed to be a probable control on the spatial distribution of arsenic along the southern transect. The study area in the southern bank of the Brahmaputra is a part of the Dhansiri Depression (Lahiri and Sinha, 2012). The depression has a significant lower average slope and has a distinctly different morphodynamics trend. Although a zone of degradation, in recent times this depression has seemingly started experiencing aggradation owing to the readjustment of the Brahmaputra valley to the 1950 earthquake (Lahiri and Sinha, 2012). Such depression provides accommodation spaces of the sediment accumulation and the continued sediment loading in these depressions caused further subsidence and reorganization of the hinterland–basin relationship. This trend can possibly be explained in the light of the sedimentation history along the southern transect.

Petrographic analysis of aquifer sediments revealed presence of quartz, plagioclase feldspars, hornblende, epidote and garnet. Presence of these mafic minerals viz. hornblende and epidote, indicated aquifer sediments possibly being derived directly from the Indo-Burma Ranges comprising of Cretaceous to Eocene pelagic sediments overlain by Eocene to Oligocene flysch, upper Miocene to Pleistocene molasses, and ophiolitic suites that were scraped off an oceanic part of the Indian plate (Curray et al., 1979; Sengupta et al., 1990; Kumar, 2004). Post depositional diagenesis and weathering of the sediments in turn became

active aquifer material hosting bulk arsenic, which under conducive biogeochemical condictions release arsenic into groundwater aquifers.

The provenance of arsenic contaminated groundwater aquifers in areas close to the eastern Himalayas viz. Nepal, and other areas of the sub-Himalayas, even as far west as the Indus provinces of Sindh and the south-west Punjab is attributed to the eroded materials from the Siwaliks (Mukherjee et al., 2013). Similarly, the Indus Tsangpo Suture Zone (ITSZ) enriched in ophiolite suites, referred to as Quamdo Simao (QS) volcanic and ophiolite province by Stranger (2005) is reported to be a likely reservoir of arsenic in the eastern part of Assam. Thus arsenic enrichment in the southern part of Assam, closer to the Naga Patkai hill ranges can be attributed to the ophiolite suite of rocks, particularly the areas where sediment deposition is carried out by tributaries draining the Naga Hills. Initially the sediments aggraded via sediment deposition from Naga Patkai hill ranges. Considerable post deposition digenesis occurred following burial on the floodplain and led to the formation of thick clay layers near the mountain front. Along the 35 kms southern transect, sediment deposition mostly occurs through the tributaries draining the Naga Patkai Hill ranges. The Naga Patkai Hill ranges with exposed sediments of the Tipam and Barail formations are the key sources of sediments in the study area (OIL Report, 2008). These sediments are mostly composed of siliciclastic materials with little or no carbonate minerals. The transect under study is between the North flowing Kakodonga River towards East and the Dhansiri River bounding West, having their catchment in the Naga Patkai Range of Hills exposing a thick pile of deformed Cenozoic clastics. The present floodplains of these rivers are narrow as indicated by their restricted meandering belts. Present sedimentation therefore is localized along these narrow floodplains besides the numerous erosional dissections where the older alluvium are recycled and deposited in these valley. It is common to find a younger alluvium abutting against and overlain/underlain by older alluvium. The older alluvium is likely to represent deposition by an earlier river regime periodically rejuvenated due to neo tectonics. It is also likely that the provenance for these sediments is both from the Pre Cambrian crystalline (Quartzo Feldspatic gneiss, quartzites, granites) and the Cenozoic sediments of the Naga Patkai Range. Contribution of sediments from the present Brahmaputra River itself is highly unlikely considering its very narrow active floodplain and absence of any geomorphic signatures suggesting its southward migration upto the study area.

While several authors have earlier described the role of geology in As release and enrichment in groundwater aquifers (Shah, 2013), Verma et al, (2016) based on their work on the Brahmaputra River basin have reported that As enrichment is a result of crustal evolution through which As is subsequently mobilized from aquifer matrix to solution in groundwater by water–rock reaction under favorable biogeochemical conditions. Based on observed mineralogy, potential provenance source, groundwater type and tributary morphodynamics, potential mechanim of arsenic release along the northern and southern study transect is given in Table 15.

Table 15 Potential Mechanism of As release along the northern and southern transects

Transect	Aquifer Lithology	Dominant Mineralogy	Source Area/ Provenance	Tributary Morphodynamics	Groundwater Type	Arsenic mobilization mechanism
Northern Transect	Dominated by sands with thin lenses of clays	Quartz, Feldspars, Chlorite, Kaolinite	Eastern Himalayas , Siwaliks	Steep gradients , Avulsion dominant	Ca-Na-HCO_3	Reductive dissolution of Fe-oxyhydroxides, Competitive ion exchange mechanism
Southern Transect	Thick surficial clays dominates areas adjacent to mountains, sands dominate aquifers close to the active floodplains	Quartz, Feldspars, Chlorite, Kaolinite	Naga Patkai Hill range , Ophiolites	Sluggish gradients, Meandering	Ca-Na-HCO3	Reductive dissolution of Fe-oxyhydroxides

5.8 Weathering and its role in spatial distribution of arsenic

Zone of high weathering intensity are reported to have arsenic enriched groundwaters (Xie et al., 2014). Chemical Index of Alteration (CIA) which measures the degree of chemical weathering of feldspars relative to unweathered parent rocks, is a chemical index widely used to determine the degree of source area chemical weathering (Nesbitt and Young, 1982, Xie et al., 2014).The chemical index of alteration (CIA) value is calculated using the equation that follows, in molecular proportions: CIA = (Al_2O_3/ (Al_2O_3 + CaO+ Na_2O + K_2O)) *100 (Nesbitt and Young, 1982), where CaO is the amount of CaO in the silicate minerals. Based on CIA values, earlier studies indicated systematic progression in the alteration of minerals

tracks incipient (CIA = 50–60) to intermediate (CIA = 60–80) to extreme (CIA > 80) chemical weathering (Fedo et al., 1995).

Degree of weathering during deposition is reported to control the variation of As content in sediments (Xie et al., 2014). Chemical weathering of primary silicate minerals release ferrous iron that is oxidized and precipitated as poorly crystalline iron oxide minerals such as ferrihydrite, and to more crystalline goethite and haematite during deposition (Wiederhold et al., 2007, Xie et al, 2014). Results of sequential extractions of sediments samples from both transect indicate that crystalline and poorly crystalline Fe oxide mineral phases are the dominant As sequesters in aquifer sediments (Figure 5.39- Figure 5.42). This can be attributed to the intense weathering rates indicated by the CIA values of sediment samples from the transects. For core samples from the northern transect, CIA values ranged between 60 to 75, while for the southern transect the values ranged between 60 to 80 indicating intermediate to extreme levels of chemical weathering undergone by the sediments. Provenance studies on the Brahmaputra river and its tributaries revealed that in contrast to northern tributaries, southern tributaries of the Brahmaputra with their distinct mineral dominance comprising of pitted and embayed quartz grains, low P/F ratio, abundant microcline, etched clinopyroxene, and laterite clasts along with their lower relief and higher sediment residence time support more intense weathering (Singh et al., 2005). The intermediate to intense chemical weathering rates observed along the southern transect is indicative of the intense chemical weathering of the lithounits in the Naga Patkai Ranges, which are the provenance of aquifer lithologies. The higher Na concentrations observed in groundwater along the southern transect provide further evidence of the intense chemical weathering in the southern and the subsequent release of high clays in the southern tributaries. The clay dominated southern tributaries (Singh et al., 2006), in turn deposits the same into their respective floodplains which eventually becomes aquifer materials. The high clay content observed in borewells located closer to the base of the Naga Patkai hill ranges are a manifestation of the clay dominated southern tributaries.

While, chemical weathering and subsequent formation of Fe-oxyhydroxides minerals are reported to control As accumulation and distribution in sediments, the role of redox environment in releasing these As into groundwater systems cannot be ruled out. Sediments from the northern transect has dissolved As concentration levels much lower than that of the southern transect. It is therefore possible that although intense weathering rates contributes to higher levels of Fe-oxyhydroxides in the northern transect, redox controls plays a greater role in releasing As into groundwater systems.

5.9 Sedimentation history and provenance

Weathering of bedrock around the basin including Naga Patkai Hill ranges and the Siwalik rocks are thought to be a major contributor of arsenic in the study transects. In order to understand the impact of sedimentary provenance on the accumulation of As in aquifer sediments, major oxide studies conducted on the aquifer sediments were used. Geochemical composition of siliciclastic sedimentary rocks has been used as a vital tool for determining the nature of the source rocks (Bhatia and Crook, 1986; Roser and Korsch, 1988). Major element discriminant functions are used to discriminate among four provenances, named mafic, intermediate, felsic and recycled quartzose (Roser and Korsch 1988). Discriminate diagram for core samples from both the study transect shows that almost all core sediment samples fall within the field of sedimentary provenance, indicating that most samples experienced the same sedimentary recycling (Figure 5.45).

Provenance studies of sediments from the Brahmaputra and its tributaries indicate that the tributaries in the northern transect mainly drain the Himalayan mountain ranges through rock types including Precambrian metamorphic (high-grade schists, gneisses, quartzite, and metamorphosed limestones), felsic igneous intrusive, and Paleozoic-Mesozoic sandstones and limestones (Heroy et al., 2003), while the southern tributaries drain the Indo-Burman ranges through Tertiary sandstones, shale and limestones and igneous intrusions, the provenance of the sediments were expected to show distinctive characteristics. However, the fact that it falls in the same provenance regime indicates that the aquifer materials are the remnant product of the weathered materials bought down by the rivers.

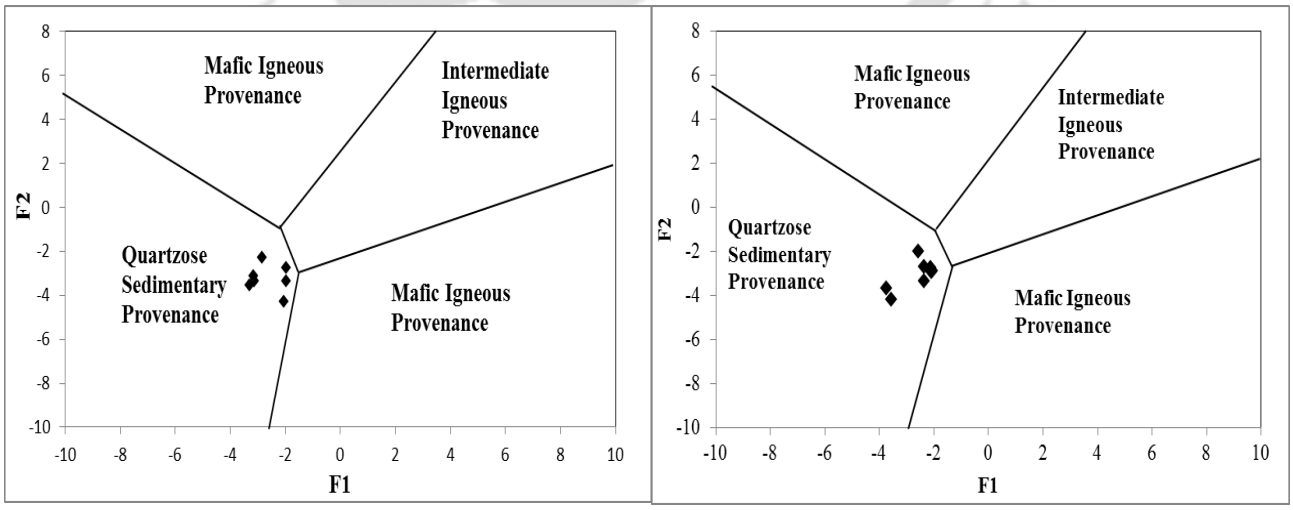

Figure 5.45 Discrimination diagram for determining sedimentary provenance of samples from (a) northern transect (b) southern transect

To understand the sedimentation history of the southern bank transect, 13 organic rich clay samples from drilled borewells along the southern transect were analyzed using AMS. Results of ^{14}C dating indicated very little sediments of Holocene age (Figure 5.46). Although, clay was not recovered during drilling next to main Brahmaputra river channel, however, the radiocarbon age of the recovered clay about 10 km away from the river also yielded an age greater than approximately 11,700 years before present, except one sample recovered at a depth 3 m below ground level showing younger age, indicating pre-Holocene deposits. Our current study indicated that groundwater in older alluvium were highly enriched with arsenic. Across basins, arsenic enriched groundwaters are mostly confined in the Holocene shallow subsurface (< 100 m) aquifers where reactivity of host minerals and organic matter needed to dissolve them are also high (Saha et al., 2009; Chatterjee et al., 2010; Erban et al., 2013). Recent study by Verma et al., (2015) in part of the study area along the northern transect reported similar dominance of high arsenic groundwater in older alluvium, attributing As accumulation in the older alluvium to the paleogeomorphology and hydrology , present day river channel morphology and sediment transportation rate.

Further, provenance classification based on bulk Sr measurements for sediment samples along the southern transect, demonstrate that although a common source of sediment provenance is attributed to be the Naga foothills, there could be a possibility where the sediments in the higher As zone are driven from the Sr depleted terrains of the Himalayas (<90 mg/kg), while in the zones of moderate and low As concentrations, the provenance of sediments are from comparatively Sr rich Tibet (>140 mg/kg). The difference in provenance could play an important role in controlling As distribution, although detailed study linking the paleo-geomorphological patterns of rivers to the depositional history of sediments and As accumulation along the study transect would be important to provide conclusive evidence. Pickering et al. (2013) and Goodbred et al. (2014) have shown that bulk Sr concentrations can be used to distinguish Brahmaputra River sediments in upper Bengal basin derived from comparatively Sr rich Tibet (>140 mg/kg) from Sr-depleted terranes of the Himalaya and Shillong Massif (<90 mg/kg). On this basis, a source other than Tibet can be assigned only to sands recovered from sites BOS and MAD closest to the Naga Hills. Whereas these sites span the region where the groundwater As are most consistently elevated, there are also wells that are elevated in As towards the middle of the transect. It therefore appears that although the broader provenance sources of aquifer materials possibly play roles in As enrichment, the

same cannot explain the pattern of groundwater As concentrations across the southern transect.

The Indo-Burma Hill Ranges, which contain Cretaceous to Eocene pelagic sediments overlain by Eocene to Oligocene flysch, upper Miocene to Pleistocene molasses, and ophiolitic suites that were scraped off an oceanic part of the Indian plate (Curray et al., 1979; Sengupta et al., 1990; Kumar, 2004), lie close to the southern study transect. Considering that sedimentation in the transect mostly occurred through rivers of Indo Burma ranges draining suits of deposits ranging from Cretaceous to Pleistocene along with the ophiolites, it can be argued that sediment provenance perhaps control arsenic distribution in the area.

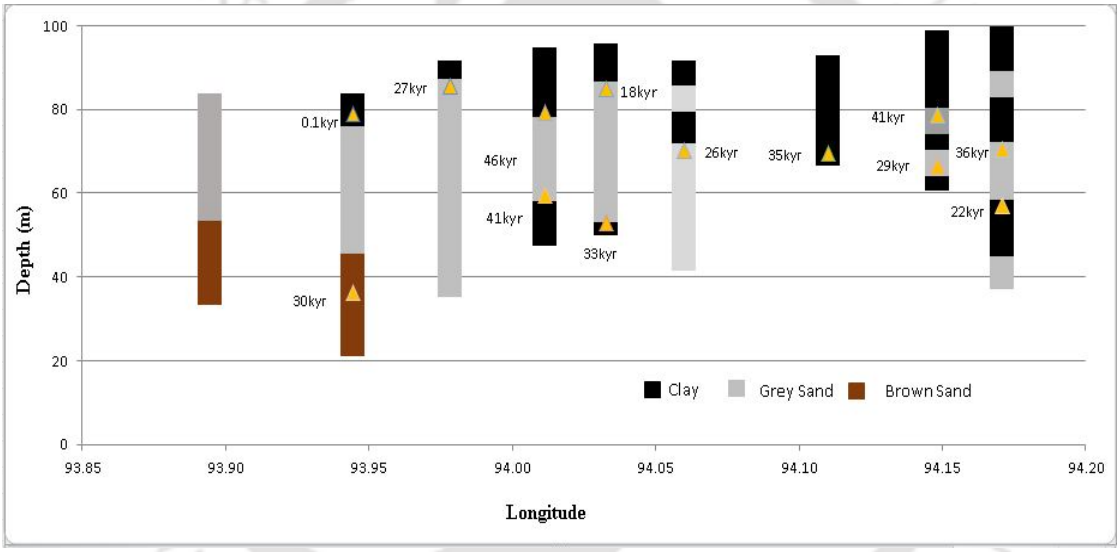

Figure 5.46 ^{14}C age dates of organic rich clay samples from borewells drilled along the transect

5.10 Geomorphic Controls on the spatial distribution of As

Geomorphic controls of arsenic distribution in the Bengal Basin and the Central Gangetic plains has been well established and reported (Weinman et al., 2008; McArthur et l., 2004; Sahu and Sukhla, 2013; Sahu and Saha, 2015). While the discernable controls of geochemistry on spatial variability of As has been established along the study transects, an attempt was made to understand the role of geomorphic controls on As distribution.

To investigate the influence of geomorphic features in aquifers of the Brahmaputra Basin, LISS 1V imagery of the southern transect was mapped. Most part of the study area are

marked by depositional geomorphic units of fluvial origin (viz. Active Floodplain, Alluvial Plains and Older Alluvium), while towards the Naga Patkai Range, hills of structural origin were observed (Figure 5.47). The study area forms a part of upper Brahmaputra River floodplain, a geomorphic unit denoting the alluvial plain between Brahmaputra River in its North and Naga Patkai Hill ranges in its south. The younger alluvium are sediments deposited as alluvial fan and floodplain sediments bought down by the Brahmaputra and its southern tributaries viz. Dhansiri and Bhogdoi that drain the Naga Patkai ranges (Evans, 1932; Mathur and Evans, 1964). The Quaternary sediments, overlying unconformably the Tertiary deposits, are described as Older Alluvium or High Level Terraces, consist of indurated yellowish or reddish clays with sand, shingle, gravel and boulder deposits. Natural levees occur as wedges all along the banks, breaching of some of which leads to development of crevasse splay deposits (Sharma, 2005). Most of the paleochannels that exists are manifestations of neotectonics (Sharma, 2005). These palaeochannels are the remnant geomorphic unit formed through the lateral shift of the rivers. Brahmaputra plain is covered by younger alluvial sediments at most of the places deposited from the sediment load carried by the river and its tributaries (Sarma and Phukan, 2004). The Brahmaputra River forms a large anabranching, multichannel and multipattern axial Tributary River in the Brahmaputra valley portion of the Himalayan foreland basin (Sharma 2005).

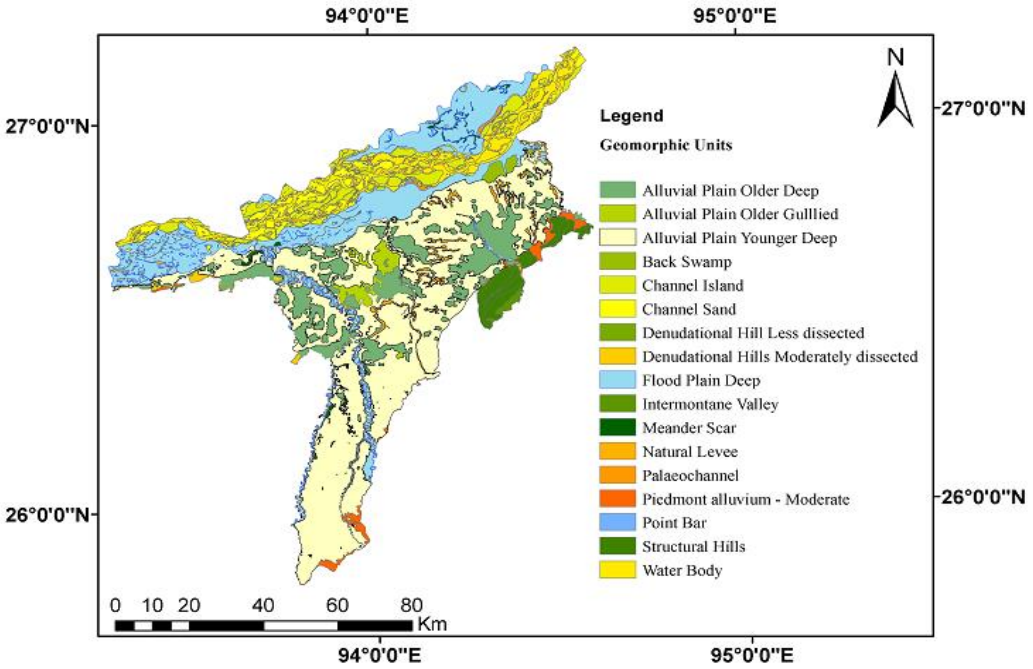

Figure 5.47 Geomorphology map of the area along the southern transect, showing different geomorphic units mapped out from LISS IV Imagery

Overlaying the 134 groundwater samples tested for As, on the geomorphic map revealed that, high arsenic concentrations were concentrated in geomorphic units comprising both Younger Alluvial Plains and the Older Alluviums. Observed high arsenic in zones of older alluvium are contrary to the widely reported observations which suggest that aquifers in older alluviums host low As aquifers (Ahmed et al., 2004; Nickson et al., 2000; Polya et al., 2005) (Figure 5.48). The older alluvium along the southern study transect are dominated by loamy sandy soils and are primarily used for tea plantations. Out of total 134 samples analyzed, 77 % located in Younger alluvium and 89 % located in older alluvium are found to be affected with As beyond permissible limit of 10 mg/L. Based on the median concentrations, As enrichment along the different geomorphic units followed the trend as Natural Levees> Younger Alluvium> Older Alluvium> Floodplain Deep (Figure 5.49, Table 16).

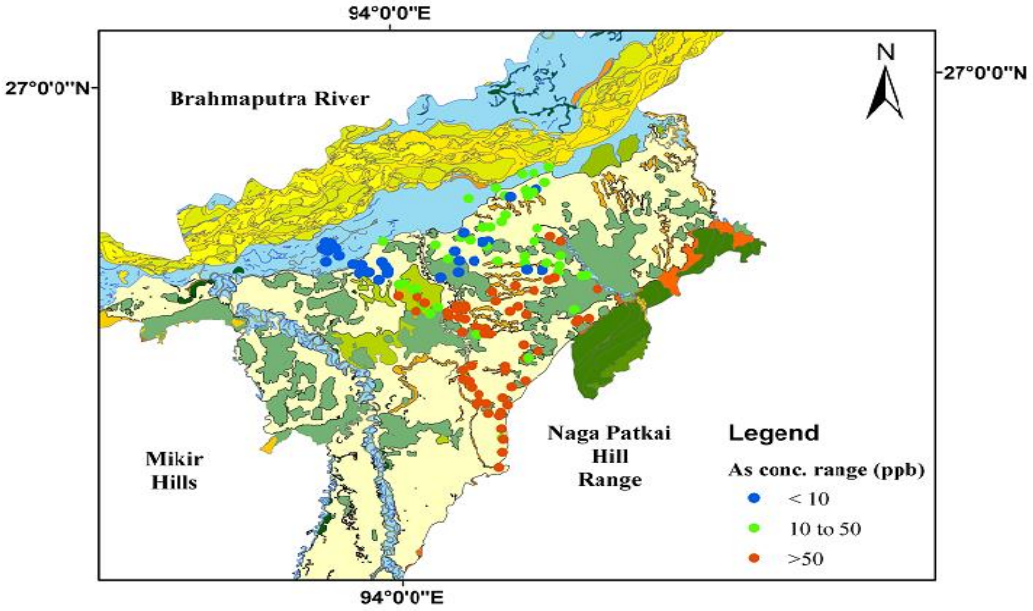

Figure 5.48 Overlayed map of groundwater As concentrations on the geomorphic map along the southern transect

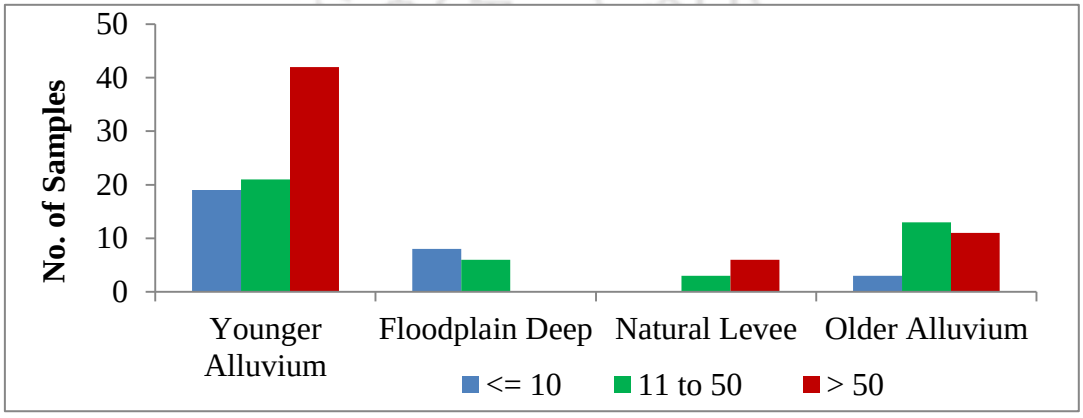

Figure 5.49 Arsenic contamination in groundwater samples in different geomorphic units

Table 16 Arsenic concentration in different geomorphic units along the southern transect

Geomorphological Units	No of Samples (n)	Min	Max	Average	Std. Dev	Median	% of samples > 10 µg/L
Younger	83	0.0	604.0	117.0	138.5	51	77
Floodplain Deep	14	0.0	35.5	9.3	11.7	3	43
Natural Levee	9	39.9	229.0	133.6	76.9	146	100
Older	27	0.5	299.0	72.4	87.1	38	89

In Bangladesh, older alluviums , which are the Pleistocene sands with their characteristics yellow to brown hue are reported to produce As safe aquifers, the understanding being that those aquifers have had considerable time to flush the arsenic from the aquifers (Ahmed et al., 2004; Nickson et al., 2000; Poyla et al., 2005). The high As concentration observed in the older alluvium in the study area can be attributed to the fact that the older alluvium units are depositional units with high potential for tea cultivation. Groundwater from deep borewells supply irrigation water in the plantations. The impact of deep irrigation in facilitating drawdown of As enriched Holocene water to Pleistocene aquifers have been well established in Bengal Basin and Vietnam (Berg et al., 2008). The observed contamination of older alluvium aquifers can thus be explained by the fact that deeper irrigation facilitates the As enriched water from Holocene aquifers to the Pleistocene aquifers.

While, paleochannels demonstrate good potential for groundwater (Hoque et al., 2011), these areas are ironically areas that host high As groundwater. Satellite mapping of LISS IV image of the southern study transect demonstrate no such paleochannels in the area close to the Naga Hills. These areas instead are part of the young alluvial deposits. Aquifers dominated by thick clay capping's, represent low energy environment. With little evidence of major south bank tributary system influencing the zone of high arsenic, it is hypothesized that weathered materials deposited from the Naga Patkai hills get accumulated in the topographic low in the frontal zone of the mountains. With limited scope of these materials to get flushed out, the high organic matter content of these materials facilitates the conducive environment for As release into groundwater.

In contrary to that observed in most As affected areas, areas of active floodplains in the study transect are observed to host low As groundwater, particularly along the studied transect.

Stahl et al., (2016) recently reported two different conditions under which riverine recharge could either contaminate or flush aquifers of As. Active depositional sites near rivers are sites hosting high As owing to those being reactive riverbed sediments. On the contrary, non-depositional areas are zones which host low As groundwater, as non-deposition will decreases the thickness of the reactive riverbed sediments. While these possibilities do exist in our study sites in the upper Brahmaputra Valley, considering that the active floodplain area near the Brahmaputra main channel is an area of active sediment deposition, we attribute that the low As aquifers in areas of active floodplains to the recurrent flooding events which flushes the aquifers of their As levels.

Natural levees in the study are observed to host high As groundwater, in conformity to that observed in the Bengal Basin. Weinman et al., (2008) associated high As groundwater with levees formed during relatively low-energy fluvial regime. The low energy regime facilitates accumulation of finer materials and formation of clay/mud capped aquifers. These clay capped aquifers host high As groundwater. The southern transect being an area where river meandering is a dominant characteristics of the tributaries, an analogy can be drawn.

5.11 Role of hydrogeological settings in controlling As distribution

Degree of spatial variability observed in groundwater As concentrations across areas still remains unanswered (e.g. Smedley and Kinniburgh, 2002; van Geen et al., 2003; Harvey et al., 2006). The spatial variability observed along both studied transect indicate that the spatial distribution is strongly affected by the hydraulic properties of the covering clay layer, through a control of the recharge rate, and the chemical composition of the water percolating through the confining clay layer.Controls of hydraulic gradient in promoting arsenic enrichment has been widely reported by previous researchers (Smedley et al., 2002; Nordstrom and Archer, 2003; Shamsudduha and Uddin, 2007;Fendorf et al., 2010) and more recently by Zhang et al., (2013); Guo et al., (2015) and Zhu et al., (2015). Low hydraulic gradient can slow down groundwater movement significantly and reduce aquifer flushing, while low topographic gradients are reported to favour accumulation of finer sediments and organic matter that can drive significant microbial activities (Fe-oxyhydroxide reduction) and cause release of high arsenic in groundwater mainly at shallow depths (Shamsudduha and Uddin, 2007).

Variations in surface topography and groundwater As levels for the northern transect are shown in Figure 5.50. STRM DEM was used to extract the topographic elevation for the

transect. The surface elevation for the transect range from 269 m to 59 m. Bivariate plots of topographic elevation and As showed a non–linear relationship, with areas of high topographic elevation demonstrating low As concentrations and lower topographic elevations demonstrating high As concentrations (Figure 5.51). These results are consistent with studies conducted in Bengal delta Plains using datasets from a national survey (Shamsuddha et al., 2008), where high As groundwaters are concentrated with lower floodplains. The spatial relationship between topographic slope and As distribution for the northern transect is shown in Fig.5.51. Similar non-linear relationship was observed between As and topographic slope. For most part of the alluvial plains the slope varies between 0 to 0.025, where sources with high As are concentrated in areas of low topographic slope. While a general pattern of high elevation and low arsenic is observed, which are consistent with studies reported in Bengal basin, some of the low elevated areas close to floodplain areas have low As levels. Two possible causes of these concentrations could be linked to the active flushing in aquifers adjacent to the Brahmaputra main channel, and the hydraulic conductivity of the aquifer sediments.

Characteristics of core sediments along the northern transect indicated grey and brown sands dominated aquifers close to the hills, while clays with interbeded gradual sand lenses dominated aquifers close to the river. The surface features point to the lack of a silt/clay layer capping the local aquifer in the areas closer to the floodplains indicating more recharge, thus facilitating low As groundwaters. Along the northern transect, aquifers in the proximal end close to the Eastern Himalayas are characterized by coarse grained sands and rock fragments. Active local recharge with relative high permeability and high hydraulic gradient facilitates low As groundwater aquifers. On the contrary, lithological profile shows thick clay capping in aquifers close to the base of the Naga Hills in the southern transect. These clay layers inhibit recharge to the aquifers below, allowing development of reducing conditions at the depth of the shallowest water-producing zones. The wells in elevated terrain, with aquifer lithologies dominated by coarse sands and rock fragments are closer to the infiltration point. During rainy season the general water flow increases and an assumption is that this reduces the contact time between water and sediment which would explain the trend of lower As levels in elevated terrain during this season. In the low-lying finer sediments water flow is slow year-round, and this may imply that more water only mobilises more As (Muñoz et al., 2013).

Nath et al., (2010) based on electrical resistivity investigation of arsenic affected alluvial aquifers in West Bengal, India, have reported that thick low resistive (<27 Ω m) surface layer (e.g., silt or clay) facilities necessary Fe-reduction condition for As release in groundwater, where the reduction is generally mediated through microbial metabolism of organic matter present in the aquifer sediment (e.g., McArthur et al. 2004; Islam et al. 2004).

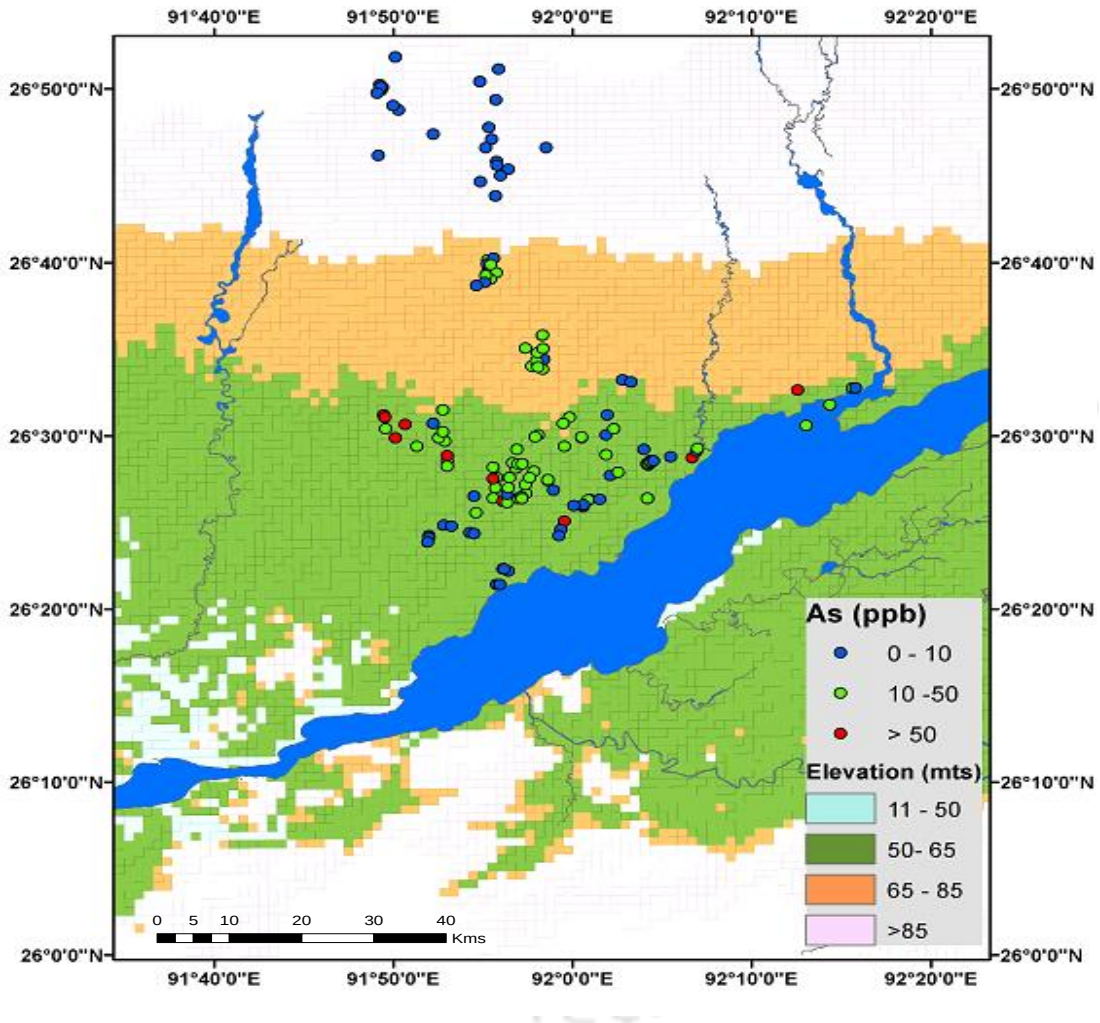

Figure 5.50 Maps showing relationship between As distribution and elevation for the northern bank transect

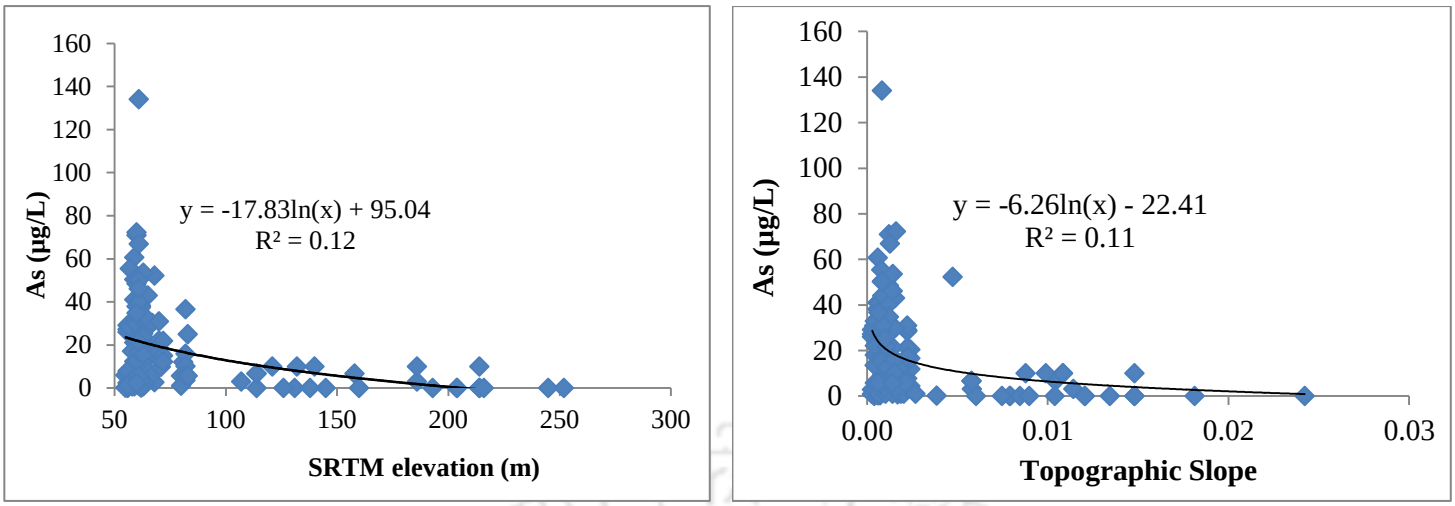

Figure 5.51 Bivariate scatter plots with best fit lines show relationship between groundwater As, SRTM elevation, slope and groundwater levels in shallow aquifers shows the weak non-linear relationship between groundwater As and surface elevation

5.11.1 Northern transect

To ascertain the role of hydrogeology in controlling As distribution, the northern transect was divided into three hydrogeomorphic zones. Based on hydrogeomorphological map obtained from Central Groundwater Board (CGWB) and our field investigations, the study area was divided into three distinct hydrogeological zones viz. Zone I comprising the piedmont, Zone II comprising the runoff areas and Zone III comprising the active floodplains and the discharge zones (Figure 5.52).

5.6.1.1 Arsenic and hydraulic gradient in the Piedmont (Zone I)

Located in the proximal fans, Zone I is characterized by active local recharge with relatively high permeability as observed by the dominance of coarse sands and rock fragments in borewells drilled adjacent to groundwater sampled wells (Figure 5.52). In the piedmont recharge areas groundwater is characterized by circum neutral pH. Arsenic concentrations lower than 10 µg/L are observed in groundwater samples collected from this zone. DO concentration in this zone range between 0.80 to 2.8 mg/L with a mean of 1.48 mg/L and median of 1.38 mg/L.

Controls of hydraulic gradient in promoting arsenic enrichment has been clearly shown by previous researchers (Nordstrom and Archer, 2003, Fendorf et al., 2010 and Smedley et al., 2002) and more recently by Zhang et al., (2013); Guo et al., (2016); Zhu et al., (2015).

Increasing trends of major ions and As along the selected flow line are in agreement with similar studies conducted in Hetao basin in China and Aquia aquifer, Maryland, USA (Jia et al., 2014; Hoque and Johannesson, 2008). These studies demonstrated that chemical composition of groundwater changes systematically with flow down gradient. Increase in groundwater parameters viz. As, Fe, Mn, along flow paths are reported to reflect increase in groundwater residence times (Johannesson et al 2008). Rapid recharge prevents release of As, possibly by supplying O_2^- and $NO_3^-$to oxidize organic matter rather than Fe-minerals (Neumann et al., 2010; van Geen et al., 2008). However, in areas of low relief, the aquifer sediment is usually fine and enriched in organic matter, which is beneficial to the accumulation of As with low flow rate (Fendorf et al., 2010; Aziz et al., 2008). Flushing history is reported to serve as a hydrogeological control on regional distribution of arsenic in shallow groundwater of Bengal basin (van Geen et al., 2008).

5.6.1.2 Arsenic and hydraulic gradient in the runoff (Zone II)

With a flatter gradient compared to Zone 1, in Zone II, the numerous tributaries viz. Bornadi, Nanoi, Noanadi, and Dhansiri draining the Bhutan Himalayas brings in sediment load and deposits the same within the floodplains of the respective tributaries. DO values for groundwater samples within this zone range between 0.13 to 1.94 mg/L, (mean 0.60 and median 0.50 mg/L), indicating highly reducing conditions of the groundwater aquifers. As concentration in this zone range between bdl to 134µg/L, with a median concentration of 17.3µg/L and mean of 24 µg/L. Under aquifer redox conditions conducive to As mobilization, As gets released into groundwater. Lithological information reveal that medium to fine sands with lenses of clays dominate the aquifer lithology in this zone (Figure 5.52). High As accumulation in this zone compared to Zone I and Zone III may possibly be attributed to the presence of numerous paleochannels that dot the study area and the frequent avulsions of the north bank tributaries (Lahiri and Sinha, 2012).

5.6.1.3 Arsenic and hydraulic gradient in the discharge zone (Zone III)

Located close to the Brahmaputra River (Figure 5.52), where groundwater is locally discharged, Zone III with a hydraulic gradient much lesser compared to the other two zones, is characterized by reducing conditions with DO values ranging from 0.21 to 2.72 mg/L with a mean of 0.79 mg/L and median of 0.70 mg/L. Arsenic concentrations in groundwater samples collected from this zone range between bdl to 60 µg/L with a median of 10 µg/L. The relatively low As concentrations compared to Zone II, is likely to be linked to the

presence of comparatively less reducing condition in this zone, possibly influenced by flooding events, when aquifers close to the active floodplains and discharge zone are exposed to repeated cycles of flushing.

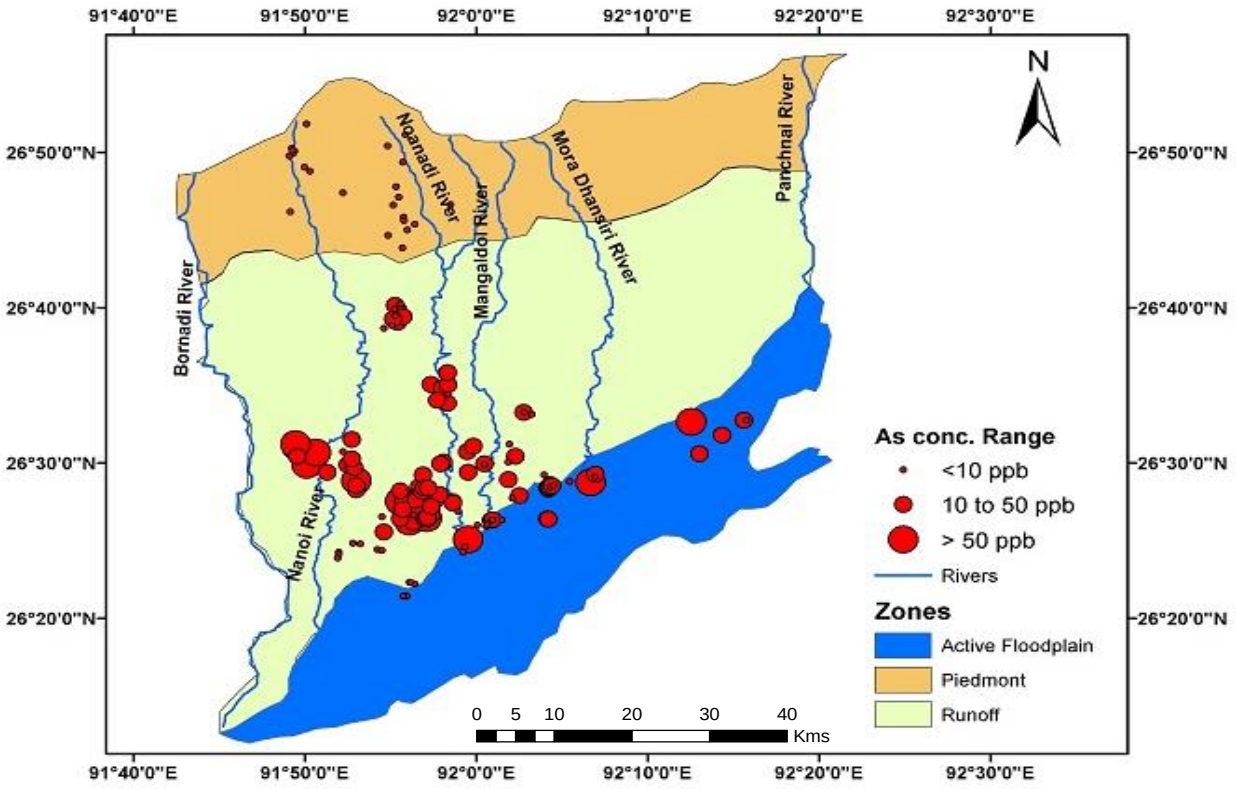

Figure 5.52 Map showing the As distribution along the three hydrogeomorphic zones in the northern transect

5.11.2 Southern transect

While the distinct role of hydrologic factors viz. hydraulic gradient, elevation and slope on the spatial distribution of As has been established for the northern transect, the more discernable spatial distribution pattern of As along the 35 km southern transect is attributed to differential flushing rates of aquifers along the transect, a mechanism that has been documented for shallower aquifers and generally younger groundwater further downstream the Brahmaputra River (van Geen et al., 2008). With higher groundwater flow rates, dissolved As can be readily flushed out of aquifers (Stute et al., 2007;Weinman et al., 2008), leading to a decrease in the concentrations of mobilizable As forms in aquifer sediments. In Bengal Delta Plains, low As groundwater was found in shallow aquifers underlying sandy soils with high hydraulic conductivity (Aziz et al., 2008; Nath et al., 2010). In contrast, both

dissolved and mobilizable As forms were readily enriched in groundwater systems with low hydraulic conductivities (Guo et al., 2003a; Yadav et al., 2015; Zhang et al.,2013).Clays have been reported to be a potential source of arsenic to groundwater in the Bengal basin and elsewhere regionally (Aziz et al., 2008; Erban et al., 2013; Lawson et al., 2016), therefore, areas with thick clay capped aquifers which contain a component of recharge from these low permeability sediments, can have high As groundwaters (Lawson et al., 2016).

^{14}Cis a widely used radiometric dating technique for groundwater because of the almost ubiquitous presence of dissolved inorganic carbon (DIC) (Hoque et al., 2012). This technique exploits the decay of ^{14}C from the onset of recharge to estimate groundwater age at locations along the flowpath (Hoque et al., 2012).However, reactions that occur during recharge and flow processes viz. congruent and incongruent reactions with carbonate minerals, mixing with older or recent water along with continuous exchange with atmosphere affect the ^{14}C activity associated with the total dissolved inorganic C in groundwater (Ma et al., 2013).

Measured DIC derived ^{14}C ages for groundwater samples collected along the southern transect reveal a distinct trend with older groundwater near the foothills and younger groundwater in aquifers close to the floodplains (Figure 5.53). Near foothills, confined groundwater had uncorrected age of 17kyr, while close to floodplains unconfined groundwater demonstrated uncorrected age of 0.2 kyr, indicating rapid recharge. Groundwater in the intermediate zone aquifers demonstrated an age of 4 kyr. Older groundwater age near the foothills, dominated by thick clay layers, support long residence time of groundwater and slow recharge, while relatively younger age in groundwater sample from areas close to the Brahmaputra main channel, indicates, intensive recharge into the sandy aquifers close to the rivers.

The role of differential flushing in controlling the distribution of As along the 35 km transect on a region of the floodplain of the upper Brahmaputra, can be emphasised from the data on ^{14}C groundwater age. Older groundwater at the base of the Naga Patkai hills confirm increased residence time of the groundwater as a result of the presence of 60 m of unusually thick clay layers in aquifers close to the hills. The gradually decreasing groundwater age along the transect indicates that the rapid flushing of sandy aquifers close to the Brahmaputra River have gradually flushed the aquifers of their exchangeable As over time. In addition, the presence of 20 and 40 m-thick intervals of orange sands in borewells close to the river

confirms the effect of flushing on the aquifer sands. Moderate levels of As concentrations along intermediate zone can be explained by the fact that the surface clay layer was sufficient to inhibit recharge.

Spatial As variability along the 35 km southern transect has been explained in terms of the differential flushing of aquifers. The same phenomenon can also be translated to explain the spatial variability along the northern transect. Comparison of dissolved As concentrations along both transect demonstrates that concerns along the southern transect are much more sever. A closer look at the tributary network along both the transects reveal that the northern transect, is dominated by more tributaries and distributaries compared to the southern transect. These tributaries and distributaries coupled with the sand dominated aquifer lithologies along the northern transect facilitates higher flushing of aquifers along the transect compared to those in the southern transect. This difference in the hydrogeological set up along both transect provides an explaining to the overall As distribution along both transect.

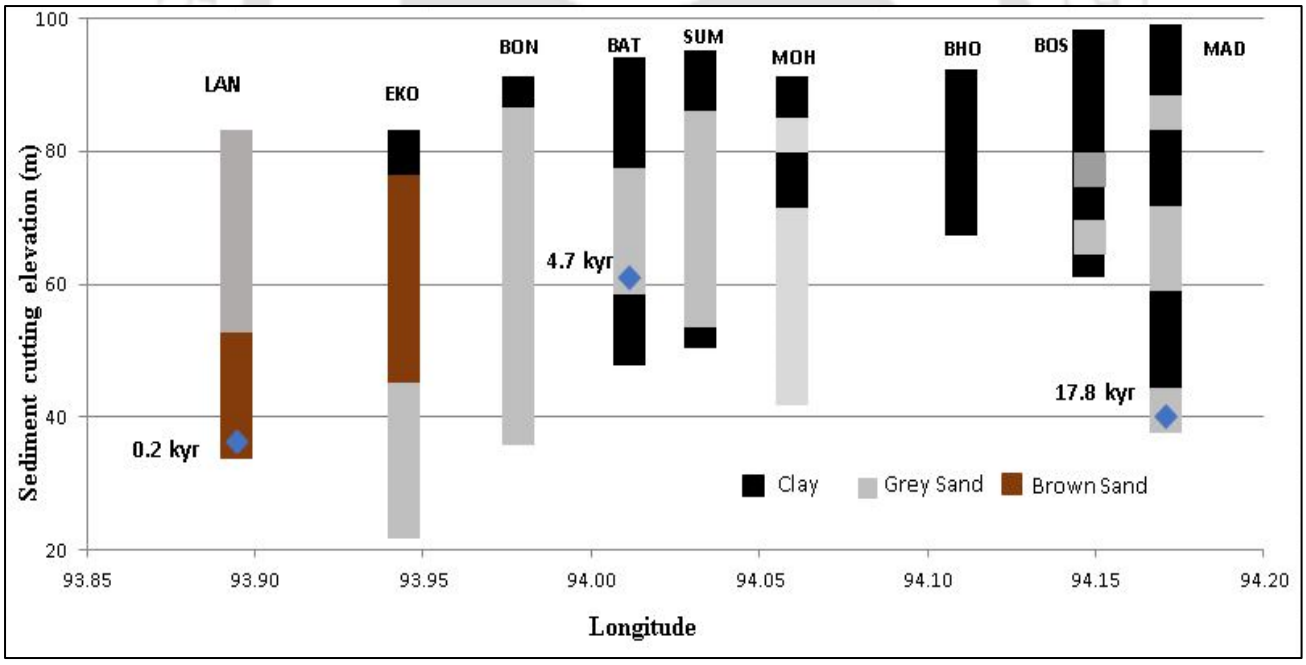

Figure 5.53 ^{14}C measurements for groundwater samples along the southern bank transect. The measurement of 14C in groundwater samples from three monitoring wells is shown (marked as diamonds). MAD, BAT and LAN are names of monitoring wells drilled along the southern transect

5.12 Attenuation Study

While much focus has been levied on surface water as major source of water supply yet with inherent issues of demand and supply gaps beset with O&M issues, communities continue to depend on groundwater sources. Hence it is almost mandatory that when groundwater As studies are carried out, to include potential remedial measures. A prerequisite to this is studies connected to natural attenuation behavior of aquifer sediments. Hence, as a conclusive part of this work, studies are conducted on aquifer sediments for grasping the adsorptive kinetics of sediments using few established batch and kinetic models.

As transport in groundwater is known to be considerably controlled by the adsorption behavior of aquifer sediments and changes in subsurface redox conditions (Stollenwerk et al., 2007, Robinson et al., 2011; Ma et al., 2015). Understanding the rates and controlling factors for adsorption of As on natural sediments aids in effective design and implementation of remediation schemes for contaminated soils and groundwaters (Hafeznezami et al, 2016). Three sediment samples viz. Brown Sand, Grey Sand and Greyish Brown Sand from boreholes drilled along the northern transect were chosen for the batch attenuation studies. Characteristics of the three sediments with their extraction (SSE) values used for the batch experiments are presented in Table (17).

Table 17. Characteristics of aquifer sediments used for the batch and kinetic experments

	Sample Id	**Color**	**Depth (mts)**	**Extracted Fe (mg/kg)**	**Extracted Mn (mg/kg)**	**Particle Size (SSA)**	**pH**
Sediment 1	BH 9_80	Brown	80	42408	620	0.025	6.4
Sediment 2	BH 9_60	Greyish	60	6769	94	0.020	6.57
Sediment 3	BH9_45	Greyish Brown	45	2766	112	0.015	6.2

5.12.1 Adsorption Kinetics

Study on adsorption kinetics describes the solute removal rate which controls the residence time of As at the solid–solution interface including the diffusion process (Naiya et al., 2009, Rajapaksha et al., 2011). Results of kinetic experimental data were fitted to pseudo-first order, pseudo-second order, and intra-particle diffusion models (Naiya et al., 2009; Srivastava et al., 2006). These models have been extensively used for fitting adsorption data

on different solid surfaces (Ho and Mckay, 1998; Zhang and Selim, 2005; Banerjee et al., 2008; Maji et al., 2008; Oke et al., 2008; Neupane et al., 2014, Hafeznezami et al, 2016). The three kinetic models used for fitting the experimental data are described below.

5.12.1.1 Pseudo-first order model

The pseudo-first order kinetic model or Lagergren's model given below is based on Lagergren's equation (Singh et al., 1988) considering the adsorbed concentration is written as;

$$\frac{dq_t}{dt} = K_1(q_e - q_t) \quad (4)$$

where q_e and q_t are the adsorbed concentration (µg g^{-1}) at time t and at equilibrium (ie. adsorption capacity). After integrating and applying boundary conditions the equation becomes,

$$\ln(q_e - q_t) = lnq_e - K_1 t \quad (5)$$

The pseudo-first order Lagrergren model was applied to the data using the equilibrium adsorption capacity at the final time point. However the coefficient of determination (r2) from the plots of each dataset revealed low correlation (r2 < 0.50).Comparison of experimental kinetic data and theoretical data indicated a poor simulation by the Lagrergren model revealing that the sorption process may be more complex than pseudo-first-order kinetics. Ho and Mckay, (1998) have earlier indicated that the pseudo-first order Lagrergren model in most cases does not fit the data well over the entire range of contact time. Further, the main disadvantage of this model is that it depends on adsorption capacity (q_e) to be known which in most cases is not effectively known and this subsequently introduces uncertainty to the model. In order to fit to data, one needs to either assume or determine the value of equilibrium sorption capacity (q_e) which could become problematic in some cases (Hafeznezami et al, 2016).

5.12.1.2 Pseudo-second order model

Disadvantage mentioned for the Lagergren equation are not present in pseudo-second order equation and can therefore be used to determine the parameters without prior knowledge of sorption capacity (Ho and Ofomaja, 2006). Pseudo-second order kinetic model was

developed on the basis that chemisorption is the operative reaction mechanism (Ho and McKay, 2000).

The pseudo second order model is expressed as,

$$\frac{dq_t}{dt} = K_2(q_e - q_t)^2 \qquad (6)$$

where K_2 is the rate constant of pseudo-second order adsorption (kg mg^{-1} h^{-1}). Applying boundary conditions t = 0 to t = t and q_t = 0 to q_t = q_e, the integrated and rearranged equation can be written as

$$\frac{t}{q_t} = \frac{1}{q_e}t + \frac{1}{K_2 q_e 2} \qquad (7)$$

Therefore, a linear plot of t/q_t versus time would indicate that data follow this kinetic model. Plots for the determination of parameters for pseudo-second-order kinetics has been shown (Figure 5.54) and the obtained parameters result have been tabulated (Table 18).

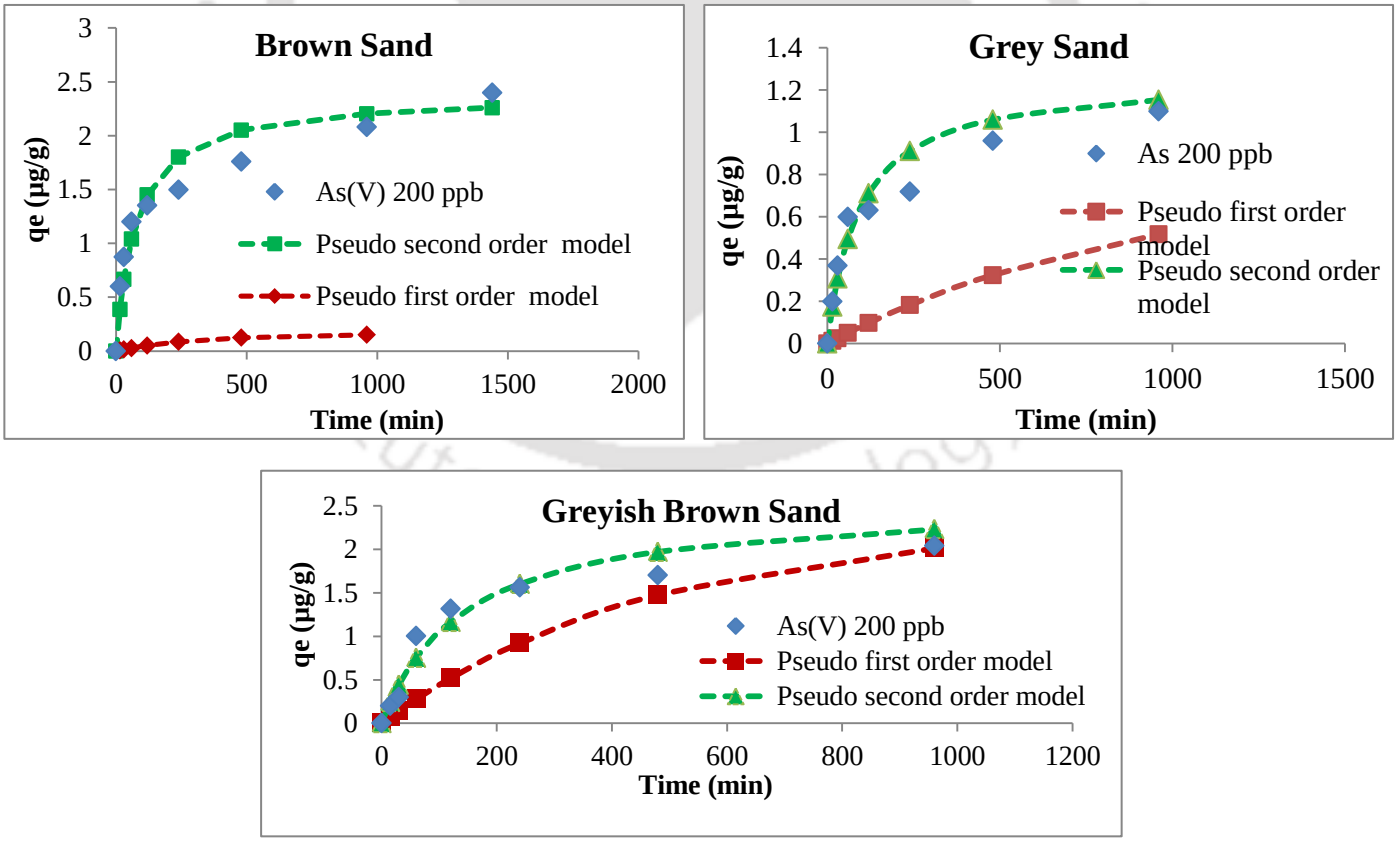

Figure 5.54 Plots of pseudo –first order and pseudo-second-order kinetics of As(V) adsorption for As (V) concentration of 200 ppb

Table 18 Correlation coefficients and kinetic parameters for pseudo-second order models and equilibrium adsorption capacity found in the experiments

	Initial As (V) (µg/L)	Second order kinetic model		
		k_2 (g/µg min)	R2	$\chi 2$
Brown Sand	100	0.05	0.99	0.22
Grey Sand	100	0.01	0.98	0.10
Greyish Brown	100	0.03	0.97	0.10
Brown Sand	200	0.08	0.99	0.16
Grey Sand	200	0.06	0.98	0.19
Greyish Brown	200	0.05	0.99	0.21

5.12.1.3 Intra Particle Diffusion Model

The Intra Particle Diffusion Model of Weber and Morris (1963) were fitted to the experimental data. A process is diffusion controlled if its rate is dependent upon the rate at which components diffuse towards one another. This phenomenon was explored by the intra-particle diffusion model (Eq.8) (Srivastava et al., 2006).

$$q_t = K_{id} t_{1/2} + C \quad (8)$$

Where, where q_t = mass adsorbed per g of adsorbent at time t (µg/g); K_{id} = intra-particle diffusion rate constant (µg/g $min^{1/2}$); C = constant (µg/g). Different kinetic parameters obtained for sediment samples are listed in Table 19.

Table 19 Correlation coefficients and kinetic parameters for Intra Particle Diffusion model and equilibrium adsorption capacity found in the experiments

As Species	Initial Conc.	Parameters	Brown Sand	Grey Sand	Greyish Brown Sand
As (V)	100 µg/L	K_{id} (µg g^{-1} $min^{-1/2}$)	0.03	0.02	0.03
		C (µg g^{-1})	0.22	0.21	0.18
		r2	0.87	0.82	0.84
As(V)	200 µg/L	Kid (µg g^{-1} $min^{-1/2}$)	0.03	0.01	0.02
		C (µg g^{-1})	0.21	0.19	0.23
		r2	0.88	0.80	0.85

The multi linearity of the plot showed that different adsorption mechanism takes place for the brown sediment (Figure 5.55). The initial step portion was attributed to surface adsorption occurring simultaneously or boundary layer diffusion of sorbate molecules, while gentle slope portion was attributed to the intra particle diffusion which is slow and possibly rate limiting (Gupta and Bhattacharyya, 2011; Sailo and Mahanta, 2015).

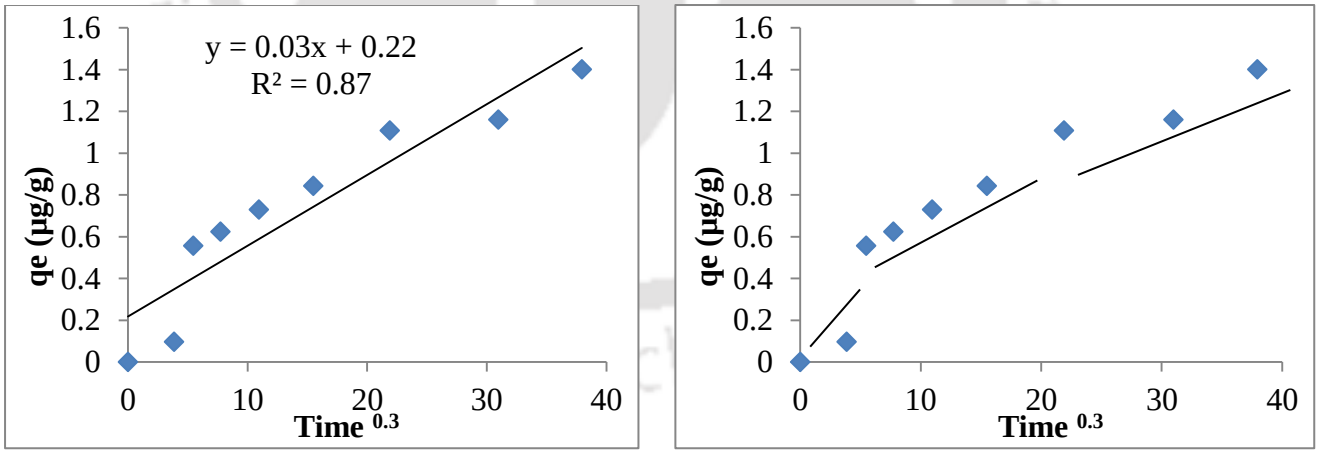

Figure 5.55 Intra-particle diffusion model for (a) Brown sediment with initial As(V) of 200 µg/L (b) two linear segment for Brown sediment.

Batch adsorption study demonstrated that sediment samples from groundwater aquifers adsorbed As(V) at circum neutral pH, which is the pH range of groundwater in the study area. Comparison of the three different sediment samples demonstrated that brown sediment with their high Fe and Mn concentrations had the highest adsorption potential. Adsorption kinetic

suggested that pseudo second order reaction model along with the rate limiting step controlled the adsorption of As(V) on the aquifer sediments.

5.12.2 Adsorption Isotherm

The adsorption isotherm data were plotted using Freundlich and Langmuir equations respectively. The isotherm models were used to provide quantitative information for describing the effect of As concentration on the surface loadings of As(V) on the sediment samples. Plots of the Langmuir and Freundlich isotherms are shown in Figure5.56, and the parameters that were obtained from those isotherms are shown in Table 18.

5.12.2.1 Langmuir isotherm

The Langmuir model assumes that monolayer adsorption occurs on a homogeneous adsorbent surface with a finite number of identical sites (Ma et al., 2015).

The nonlinear forms of the Langmuir are given as,

$$q_e = \frac{qmbCe}{1+bCe} \quad (9)$$

Where Ce is the residual As concentration in the solution (μg ml^{-1}), qe is the As equilibrium adsorption concentration in the solid adsorbent (μg g^{-1}), q_m is the monolayer maximum adsorption capacity (μg g^{-1}), b is a constant related to the energy of adsorption in the Langmuir model (ml μg^{-1}).

5.12.2.2 Freundlich isotherm

The Freundlich isotherm is empirical in nature and applies to solid surfaces with different affinities. Therefore model fitting with the Freundlich isotherm can be considered to have multilayer adsorption as well as surface heterogeneity (Ho et al., 2002). The Freundlich model which allows for multi-layer adsorption, includes an empirical parameter (n) that accounts for heterogeneity of surface sites with different adsorption energies (Hafeznezami et al, 2016).

The non-linear form of Freundlich models are given as Eqs. (10) and (11), respectively.

$$Q_e = K_f Ce^n \quad (10)$$

where K_f is a constant related to the adsorption capacity (μg g^{-1})(ml μg^{-1})n), n is a constant related to the energy of adsorption in the Freundlich model. Values of 1<n<10 show

favourable adsorption of As onto adsorbents (Namasivayam and Senthilkumar., 1998).The Freundlich equation is generally linearized in order to fit data as follows,

$$log\ Qe = nlogCe + \log Kf \quad (11)$$

The Freundlich isotherm model was applied to the experimental adsorption data and the adjusted parameters are presented in Table 18. The correlation coefficients were higher for the Freundlich model (R2=0.93–0.97) than for the Langmuir model, indicating that the Freundlich isotherm model fitted the data well. Therefore, Freundlich isotherm yielded better fit to the experimental data, denoting multi-layer adsorption of As onto sediments.The adsorption intensity 1/n was found to be below 1 in all the sediments, which confirmed normal adsorption for the arsenic species. Low 1/n demonstrates nonlinear behaviour of adsorption (Manning and Goldberg 1997; Zhang and Selim 2005; Yolcubal and Akyol 2008). Further, low 1/n values for all the three sediment samples indicate the extensive heterogeneity of adsorption sites in these soils (Zhang and Selim 2005).

Results of batch adsorption revealed that Sediment 1, which is the brown sediment demonstrated the highest adsorption capacity. This can be attributed to the high solid phase Fe and Mn content in the brown sediment relative to the grey sand and brownish grey sand. Stollenwerk et al., (2007) concluded studies on brown sands from As affected areas in the Bengal Basin and reported the higher adsorption rates of the brown sands compared to the grey sands. Studies by Zela and Mahanta (2015) on aquifer sands from higher As affected area in the upper Brahmaputra Basin reported similar adsorption behaviour with the adsorption trend of aquifer sands being Brown Sand> Greyish Brown Sand> Grey Sand.

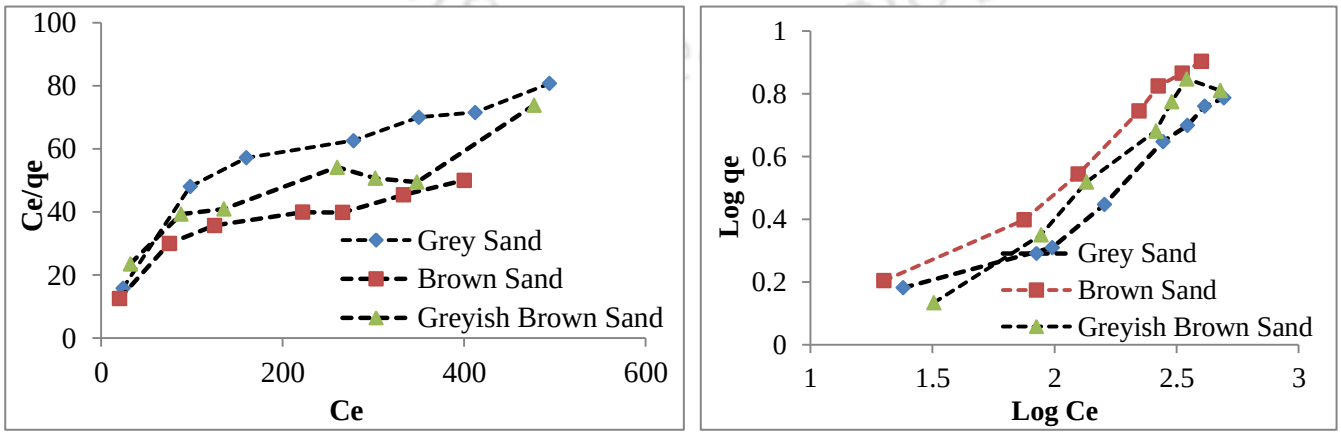

Figure 5.56 Plots of Langmuir and Freundlich isotherm model

Table 20 Correlation coefficients and isotherm parameters for the Langmuir and Freundlich isotherm models (dosage = 50 g/L, initial As concentration 100,200, 500, 600, 800 µg/L, contact time = 24 hr, pH 6.5)

Sediments from Northern transect	As Species	Isotherm	Parameters	Values
Brown Sand	As (V)	Langmuir	q_{max}	25
			K_L	0.002
			r2	0.84
		Freundlich	K_f	1.80
			1/n	0.57
			r2	0.97
Greyish Sand	As (V)	Langmuir	q_{max}	14
			KL	0.003
			r2	0.83
		Freundlich	Kf	1.76
			1/n	0.51
			r2	0.93
Grayish Brown Sand	As (V)	Langmuir	q_{max}	17
			KL	0.002
			r2	0.81
		Freundlich	Kf	2.40
			1/n	0.64
			r2	0.95

5.12.3 Role of competing ions

Batch experiments and geochemical modeling were performed to understand the effects of major factors controlling arsenic adsorption/desorption processes in the high arsenic groundwater system in Brahmaputra Basin. The role of competing ions in As adsorption was studied using three commonly existing ions in groundwater systems viz. HCO_3, Si and PO_4, which competes with arsenic for available adsorption sites and also alters the electrostatic surface charge of sorption (Choi et al., 2009, Kim et al., 2000; Roberts et al., 2004). The role of these ions on As adsorption on natural sediments has been extensively studied for sediment samples in West Bengal and Bangladesh (Dixit and Hering, 2003; Biswas et al., 2014; Stollenwerk et al., 2007; Stollenwerk et al., 2009; Robinson et al., 2011). Owing to similar charge, PO_4 is reported to play a significant role in As adsorption. Salio et al., 2015 studied the role of competing ions on As adsorption in sediments from the southern bank of the Brahmaputra river in Assam and reported that ion influence on As adsorption followed the

trend as PO_4>HCO_3> Si. The role of pH, and selected competing ions viz. HCO_3, Si and PO_4 on As(V) adsorption are presented below:

5.12.3.1 Effects of pH on As adsorption

The pH dependent adsorption of As(V) has been well established from experimental studies (Pierce and Moore, 1982; Anwar et al., 2004; Stollenwerk et al., 2007). Manning and Goldberg (1997) report that the As adsorption capacity by kaolinite reaches its maximum at pH 5.0, and it drops sharply when pH is over 6.5. Similarly, the adsorption capacity for illite and montmorillonite peaks at the range between 6-8 and 5-6 (Manning and Goldberg, 1997). Pierce and Moore (1982) studied the adsorption of arsenic acid and arsenious acid on hydroxides of iron and found that As adsorption peaked within the pH range of 4 -10. Similarly, Johnson and Sarkar, (2007) based on their experimental studies reported that As adsorption decreased when pH was over 8.5. These and other similar studies have reported the different pH ranges for maximum As adsorption. Thus, to study the effects of pH on As(V) adsorption on the three selected sediments, As adsorption study was conducted at pH 6.5, 7, 7.5, (Figure 5.57), the pH range corresponding to the natural groundwater conditions existing in the study area (pH range from 6 to 7.25). Plots of pH versus As (V) adsorbed demonstrates that As(V) adsorption decreased with increased pH, the optimal adsorption being at pH 6.5.

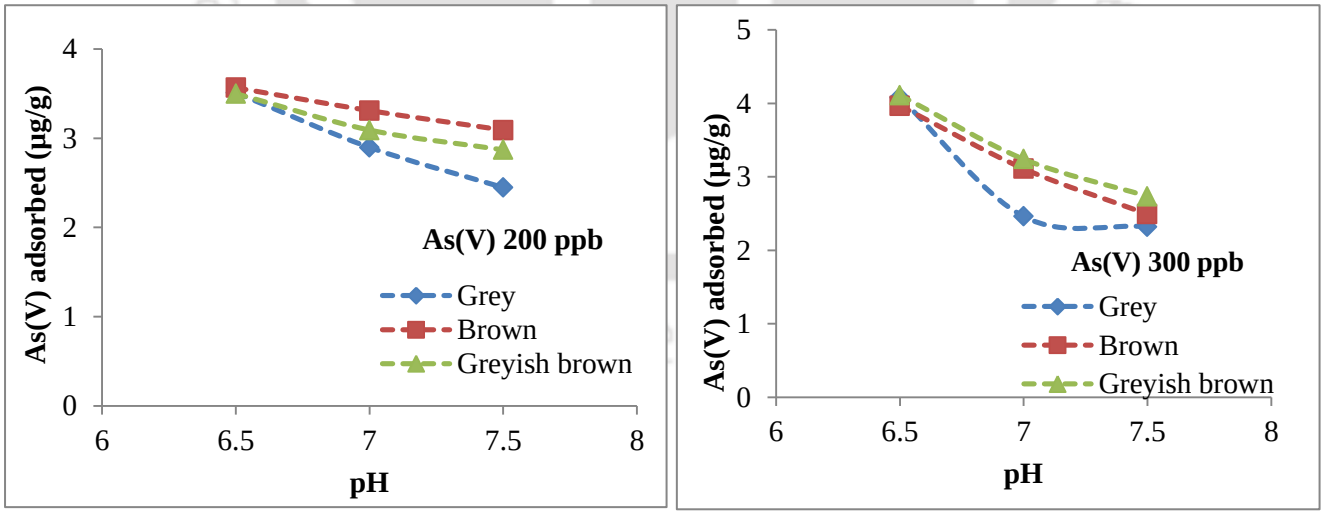

Figure 5.57 Effect of pH on adsorption of with initial concentration of 200 µg/l and 300 µg/l for sediment samples

5.12.3.2 Effects of HCO_3

Bicarbonate is the dominant anion in groundwater of the study area, with concentrations varying between 63 to 268 mg/L. Most HCO_3^- in groundwater is assumed to be due to the

oxidation of organic carbon. The effect of bicarbonate on arsenic adsorption onto aquifer sediments was studied by increasing the concentration of HCO_3^- from 200, 300 and 500 mg/L. Results of model simulations and laboratory experiments have earlier reported As adsorption is decreased at higher bicarbonate concentrations (Appelo et al., 2002; Gao et al., 2011). However, results of our batch study suggest no significant change in As adsorption with increase in HCO_3^- concentrations (Figure 5.58). This is in good agreement with Stollenwerk et al., (2007) and Gao et al. (2013), who report no competition between As(V) and HCO_3^- for aquifer sediments from and Bangladesh and Datong. Recent study by Mai et al., (2014) report similar finding that, HCO_3^- does not has the capability to displace neither As(III) nor As(V) from the surface complex to any significant extent.

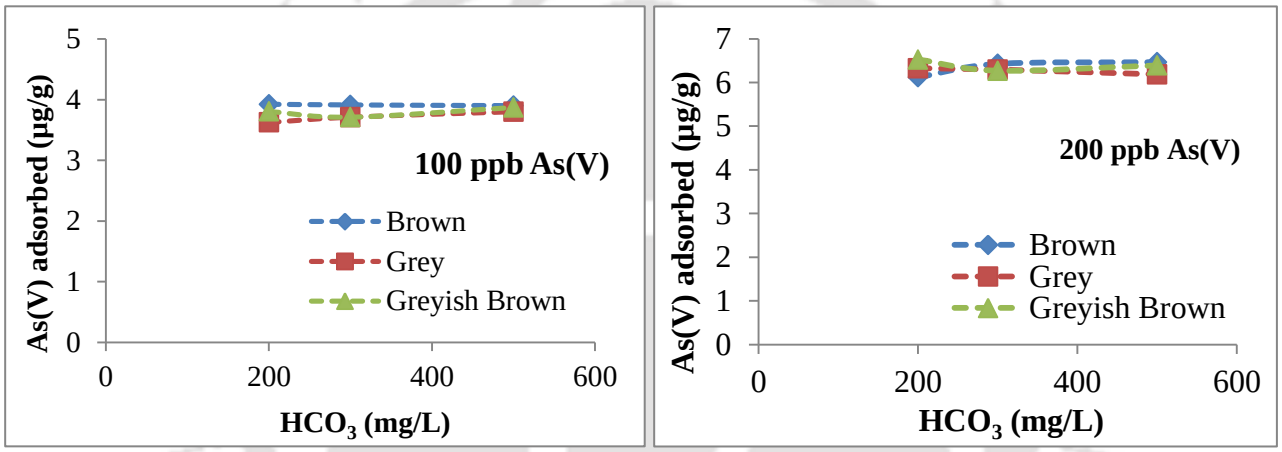

Figure 5.58 Effect of bicarbonate (HCO_3^-) on adsorption of As(V) with initial concentration of (a) 100 µg/l and (b) 200 µg/l for sediment samples.

5.12.3.3 Effects of Si

The effects of silica on the adsorption of As(V) was studied using balance solution with different initial silicate content (as Na_2SiO_3, at concentration viz. 10, 20, 30 mg/L). Experimental results suggest no distinct effects of SiO_2 on As adsorption for the three selected samples (Figure 5.59). Gao et al., 2011 report similar negligible impact of Si on arsenic mobility in the Datong sediment.

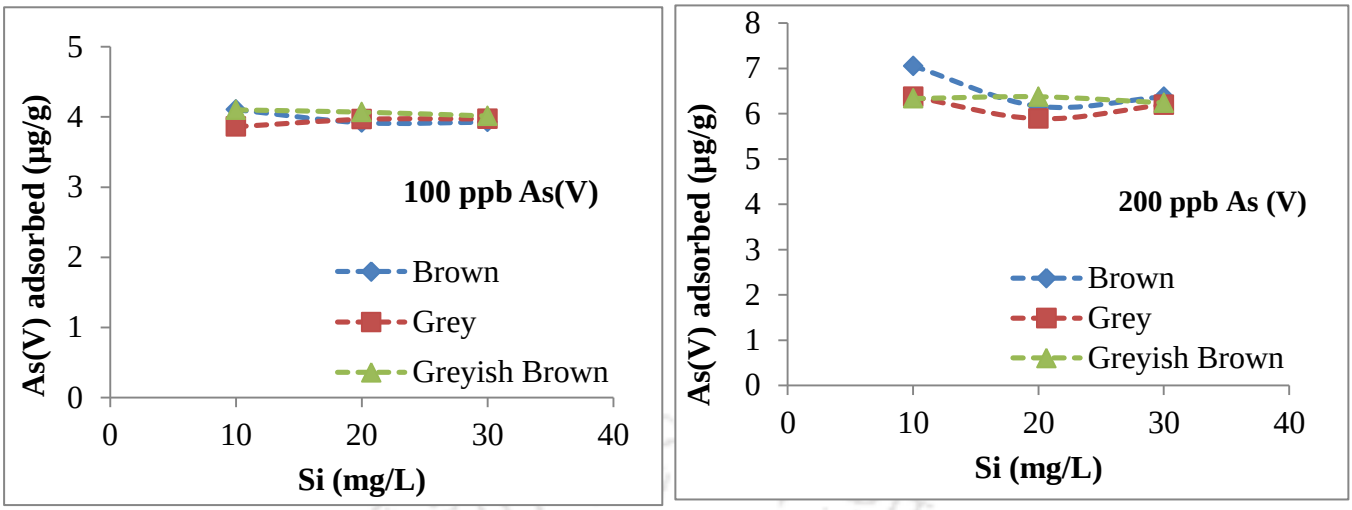

Figure 5.59 Effect of silica (SiO_2) on adsorption of As(V) with initial concentration of (a) 100 µg/L and (b) 200 µg/L for sediment samples.

5.12.3.4 Effects of PO_4

PO_4^{3-} ion is similar to that of arsenate in structure and deprotonation constants, and therefore, known to compete strongly with As for available binding sites on Fe(III) oxides (Acharyya et al., 2000; Manning and Goldberg, 1996; Williams et al. 2003). PO_4^{3-} forms a strong inner sphere surface complex with Fe hydroxides, which reduces the available adsorption sites and inhibits the adsorption of As (Jain and Leoppert, 2000; Su and Puls, 2001; Guan et al., 2009). Results of our experiments with aquifer sediment indicate that increase in PO_4 concentrations has significant effect on As(V) adsorption (Figure 5.60). This results are in conformity with those reported by Stollenwerk et al. (2007), Gao et al. (2013) based on their studies conducted on aquifer sediments from Bangladesh and Datong basin.

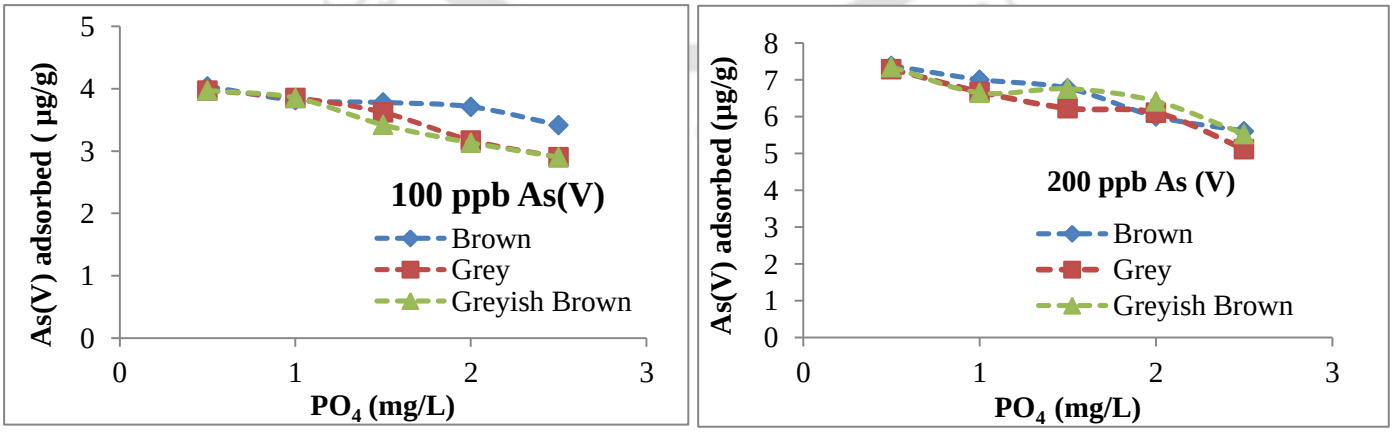

Figure 5.60 Effect of phosphate (PO_4) on adsorption of As(V) with initial concentration of (a) 100 µg/l and (b) 200 µg/l for sediment samples.

5.12.3.5 Combined anions effect

The competitive nature of anions present in the groundwater was investigated using a solution that could closely simulate the actual groundwater conditions in the northern transect. The concentration of major anions viz. HCO_3^- = 250 mg/l, SiO_2 = 15 mg/l were included. The concentration of PO_4^{3-}, which has highest effect on the adsorption capacity, was varied from 0.5 mg/l to 3 mg/l. Results demonstrate the decrease in the adsorption capacities observed for initial As(V) concentrations (Figure 5.61). Studies on role of competing ion on adsorption capacity of As has been extensively reported.

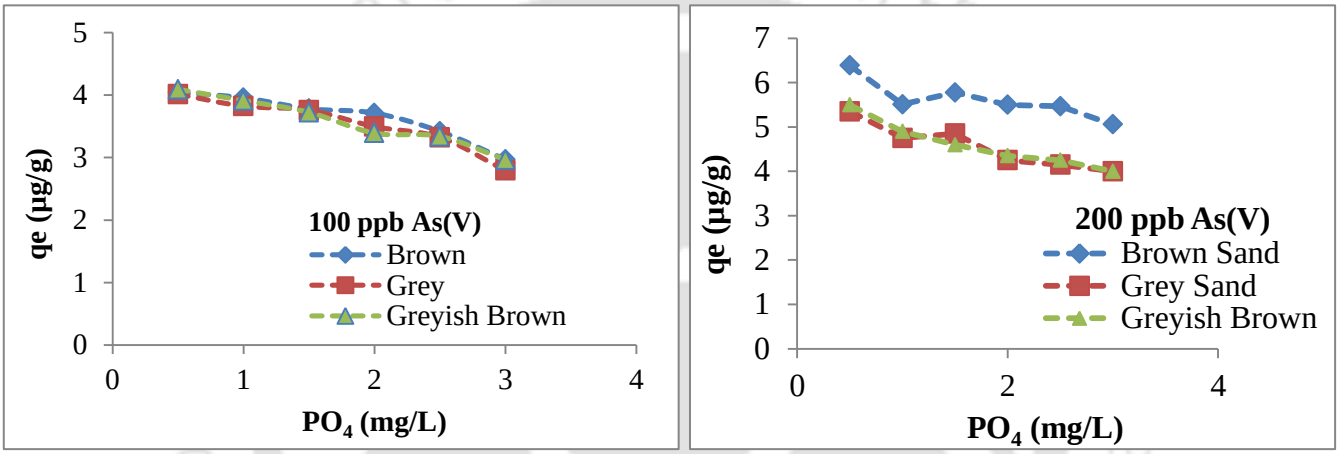

Figure 5.61 Combined effects of ions on adsorption of As(V) with initial concentration of (a) 100 µg/l and (b) 200 µg/l for sediment samples.

5.13 Surface Complexation Model

As adsorption on aquifer sediments was simulated as surface complexation reactions on oxides of iron using Diffuse Layer Model (DLM) of Dzombak and Morel (1990).The equilibrium surface complexation model (SCM) of PHREEQC (Parkhurst and Appelo, 1999) was used to predict the differences between As sorbed on Hfo (Hydrous ferric oxides) phases as well as goethite (more crystalline phase), which were derived from the selective sequential extraction (SSE) data and the modeled simulations. The SCM was run using As data extracted during Fraction 3 and Fraction 4 of the sequential extractions, which targets arsenic associated with amorphous and crystalline Fe- oxides and hydroxides. The Diffuse Double Layer (DDL) option of PHREEQC was used for the model simulation, assuming that the system was in chemical equilibrium. The concentrations of iron in the sediments targeting the amorphous (Ferrihydrite) and crystalline phase (Goethite) were used to back calculate the

amount of Hfo present on the surface of the sediment grains (Table 21 - 22). The extraction and subsequent calculations estimate the potential number of sorption site forming metal atoms, rather than truly defining the surface area of the available mineral phases. The best fit models were those that provide results that are internally consistent with the ratios of arsenic and Hfo forming elements found in the extractions.

Table 21 Thermodynamic data of surface complexation constants for arsenite, arsenate, phosphate, sulphates and carbonate for PHREEQC surface complexation model with strong (Hfo_s) and weak (Hfo_w) adsorption sites (Allison et al., 1990; van Geen et al., 2004)

Adsorption reaction	**Log K**
Arsenite	
Hfo_ sOH + H3AsO3=Hfo_sH2AsO3 + H2O	5.41
Hfo_ wOH + H3AsO3=Hfo_wH2AsO3 + H2O	5.41
Arsenate	
Hfo_ sOH + H3AsO4=Hfo_sH2AsO4 + H2O	8.61
Hfo_ wOH + H3AsO4=Hfo_wH2AsO4 + H2O	8.61
Hfo_ sOH + H3AsO4=Hfo_sHAsO−4 + H2O + H+	2.81
Hfo_ wOH + H3AsO4=Hfo_wHAsO−4 + H2O + H+	2.81
Hfo_ sOH + H3AsO4=Hfo_sOHAsO3−4 + 3H+	−10.12
Hfo_ wOH + H3AsO4=Hfo_wOHAsO3−4 + 3H+	−10.12
Phosphate	
Hfo_ sOH + PO3−4 + 3H+=Hfo_sH2PO4 + H2O	31.29
Hfo_ wOH + PO3−4 + 3H+=Hfo_wH2PO4 + H2O	31.29
Hfo_ sOH + PO3−4 + 2H+=Hfo_sHPO−4 + H2O	25.39
Hfo_ wOH + PO3− 4 + 2H+=Hfo_wHPO− 4 + H2O	25.39
Hfo_ sOH + PO3−4 + H+=Hfo_PO2−4 + H2O	17.72
Hfo_ wOH + PO3−4 + H+=Hfo_wPO2−4 + H2O	17.72
Sulphates	
Hfo_ wOH + SO2−4 + H+=Hfo_wSO−4 + H2O	7.78
Hfo_ wOH + SO2−4 = Hfo _ wOHSO2−	0.79
Carbonate	
Hfo_ wOH + CO2− 3 + H+=Hfo_wCO− 3 + H2O	12.56
Hfo_ wOH + CO2−3 + 2H+=Hfo_wHCO3 + H2O	20.62

Table 22 Thermodynamic data of surface complexation constants for arsenite, arsenate, phosphate, carbonate, fluoride, sulphate, ferrous, calcium and magnesium for PHREEQC surface complexation model with Goethite as adsorption sites (Allison et al., 1990; van Geen et al., 2004)

Surface reaction	Log K	Reference
Goethite		
Goe_OH + H+ = Goe_OH2+	7.52	Dixit and Hering (2003)
Goe_OH = Goe_O + H+	-10.6	
Phosphate		
Goe_OH + H3PO4 = Goe_H2PO4 + H2O	8.05	Sigg (1979)
Goe_OH + H3PO4 = Goe_HPO4- + H2O + H+	3.4	
Goe_OH + H3PO4 = Goe_PO42- + H2O + 2H+	-2.2	
Arsenate		
Goe_OH + AsO4-3 + 3H+ = Goe_H2AsO4 + H2O	30.94	Dixit and Hering (2003)
Goe_OH + AsO4-3 + 2H+ = Goe_HAsO4- + H2O	26.75	
Goe_OH + AsO4-3 + H+ = Goe_H2AsO42- + H2O	20.16	
Arsenite		
Goe_OH + AsO3-3 + 3H+= Goe_H2AsO3 + H2O	39.87	
Goe_OH + AsO3-3 + 2H+= Goe_HAsO3- + H2O	32.34	
Silicate		
Goe_OH + H4SiO4 = Goe_H3SiO4 + H2O	4.35	Sigg (1979)
Goe_OH + H4SiO4 = Goe_H2SiO4- + H2O + H+	-3.04	
Carbonates		
Goe_OH + 2H++ CO32- = Goe_HCO3 + H2O	20.78	van Geen et al. (1994)
Goe_OH + H++ CO32- = Goe_CO3- + H2O	12.71	
Goe_OH + CO32- = Goe_OHCO32-	3.56	Appelo et al. (2002)
Flouride		
Goe_OH + F- = Geo_F + OH-	-4.54	Sigg (1979)
Sulfate		
Goe_OH + SO42- + 2H+ = Geo_ HSO4 + H2O	13.61	Ali and Dzombak (1996)
Goe_OH + SO42- + H+ = Geo_ SO4- + H2O	8.19	
Goe_OH + SO42- = Geo_ OSO43- + H+	-6.26	
Goe_OH + SO42-+ Cu2+ = Geo_ OHCuSO4 + H+	9.46	
Ferrous		
Goe_OH + Fe2+ + H2O = Goe_OFeOH+ + 2H+	-10.95	Dixit and Hering (2006)
Goe_OH + Fe2+ = Goe_OFe+ + H+	-0.6	
Calcium		
Goe_OH + Ca2+ = Goe_OCa+ + H+	-7.18	Ali and Dzombak (1996)
Magnesium		
Goe_OH + Mg2+ = Goe_OMg+ + H+	-5.94	Sigg (1979)

Table 23 Input parameters for PHREEQC surface complexation model in amorphous Fe-oxides for surface site densities (mol sites/mol Fe)

Sample Name	Depth (m)	Amorphous Fe (mg/kg)	Ferrihydrite (g/kg)	Hfo_wOH	Hfo_sOH	Goe
Bh12- 8	8	902.06	6.05	1.364E-02	3.409E-04	1.012E-02
Bh12- 14	14	251.49	1.69	3.801E-03	9.504E-05	2.821E-03
Bh12- 20	20	975.97	6.55	1.475E-02	3.688E-04	1.095E-02
Bh12- 27	27	365.18	2.45	5.520E-03	1.380E-04	4.096E-03
Bh12-30	30	1059.47	7.11	1.601E-02	4.004E-04	1.188E-02
Bh11-2	2	1968.5	13.21	2.976E-02	7.439E-04	2.208E-02
Bh11-5	5	1427.02	9.58	2.157E-02	5.393E-04	1.601E-02
Bh13-5	5	1300.83	8.73	1.966E-02	4.916E-04	1.459E-02
Bh13-8	8	1283.57	8.61	1.940E-02	4.851E-04	1.440E-02
Bh13-11	11	1667.28	11.19	2.520E-02	6.301E-04	1.870E-02
Bh13-14	14	1487.87	9.99	2.249E-02	5.623E-04	1.669E-02
Bh13- 15	15	1862.93	12.50	2.816E-02	7.040E-04	2.090E-02
Bh13- 18	18	1326.27	8.90	2.005E-02	5.012E-04	1.488E-02
Bh14_ 51	51	1633.02	10.96	2.468E-02	6.171E-04	1.832E-02
Bh14_ 54	54	2220.86	14.91	3.357E-02	8.393E-04	2.491E-02
Bh14_57	57	2340	15.70	3.537E-02	8.843E-04	2.625E-02
Bh14_60	60	2002.98	13.44	3.028E-02	7.569E-04	2.247E-02
Bh14_64	64	1981.53	13.30	2.995E-02	7.488E-04	2.223E-02
Bh14_67	67	2411.01	16.18	3.644E-02	9.111E-04	2.704E-02

Table 24 Input parameters for PHREEQC surface complexation model in amorphous Fe-oxides for surface site densities (mol sites/mol Fe)

Depth	Depth (m)	Crystalline Fe (mg/kg)	Ferrihydrite (g/kg)	Hfo_wOH	Hfo_sOH	Goe
Bh12- 8	8	2084.36	13.99	3.151E-02	7.877E-04	2.338E-02
Bh12- 14	14	511.23	3.43	7.728E-03	1.932E-04	5.723E-03
Bh12- 20	20	745.87	5.01	1.127E-02	2.819E-04	8.367E-03
Bh12- 27	27	263.93	1.77	3.990E-03	9.974E-05	2.961E-03
Bh12-30	30	1523.64	10.23	2.303E-02	5.758E-04	1.709E-02
Bh11-2	2	2392.58	16.06	3.617E-02	9.041E-04	2.684E-02
Bh11-5	5	2550.25	17.12	3.855E-02	9.637E-04	2.861E-02
Bh13-5	5	1625.1	10.91	2.456E-02	6.141E-04	1.823E-02
Bh13-8	8	2060.21	13.83	3.114E-02	7.785E-04	2.306E-02
Bh13-11	11	1323.22	8.88	2.000E-02	5.000E-04	1.481E-02
Bh13-14	14	1883.34	12.64	2.847E-02	7.117E-04	2.108E-02
Bh13- 15	15	1809.62	12.15	2.735E-02	6.838E-04	2.030E-02
Bh13- 18	18	2422.19	16.26	3.661E-02	9.153E-04	2.717E-02
Bh14_ 51	51	2561.05	17.19	3.871E-02	9.678E-04	2.873E-02
Bh14_ 54	54	2543.58	17.07	3.845E-02	9.612E-04	2.853E-02
Bh14_57	57	2948.04	19.79	4.456E-02	1.114E-03	3.307E-02
Bh14_60	60	2002.33	13.44	3.027E-02	7.567E-04	2.246E-02
Bh14_64	64	2455.95	16.48	3.712E-02	9.281E-04	2.755E-02
Bh14_67	67	2198.21	14.75	3.323E-02	8.307E-04	1.118E+00

The SCM results demonstrated contrasting variation between modeled results and the extracted As in the sediments. Previous studies conducted to predict As adsorption on natural sediments using SCM, have reported that SCM model outputs are very sensitive to sediment type and the extraction method used, which controls the surface-site density and sorption intensity along with groundwater composition, competitive sorption of As with other ions (e.g. HCO_3^- , PO_4^{3-}, $H_4SiO_4^0$ and Fe^{2+}) on reactive surface sites of sorbents (Sharif et al., 2008; Robinson et al., 2011). For a few samples the modeled results of As adsorption onto HFO demonstrated good agreement with the extraction results, indicating that, the modeling

can be used to predict As distribution in sediments with a moderate to high level of uncertainty. Under predictability observed between the experimental and simulated results may occur due to a number of factors viz. (i) Selection of the proper HFO phases is one of the most important factors influencing the model fit, as each phase has a different specific surface area and sorption capacity (ii) Small variation in the surface-site densities of sorbents may produce a difference of several orders of magnitude in the modeled concentrations of As in sediments (iii) Model output is very sensitive to the concentration of As and other competitive ions in groundwater (Sharif et al., 2008). The role of adsorption in the control of dissolved As was supported by geochemical modeling. The retention of As seems to be governed by HFO adsorption, indicating that Fe oxyhydroxides dissolution is responsible for As release. SCMs using internally consistent laboratory-derived sorption constants, calculated surface-site densities from chemical extraction data and published sorbent-site densities, measured water–rock ratios, and detailed chemical analyses of groundwater can thus be used to predict the distribution of As in sediments with a moderate to high level of uncertainty.

Results of hydrogeochemical and sedimentological study coupled with local geologic, hydrologic and geomorphic factors helped unravel some interesting answers regarding the groundwater arsenic contamination issue in the unique terrain. The role of local hydrology in controlling As distribution and accumulation have been well demonstrated along both transects. Many recent studies are focused on accessing the role of physical processes in contoroling arsenic release and attenuation (Ziegler et al., 2017), some of which indicate a strong alignment with the present research work. The present study thus indicates that while multiple factors control arsenic distribution, yet physical factors like hydrology seems to play more discernable roles.

Chapter 6

Summary and Conclusions

6.1 Summary and Conclusion

Distinct areas of spatial variability of dissolved arsenic emerged during the study. Scrutiny of the hot spot areas motivated selection of two transects on each side of the dynamic Brahmaputra River, sandwiched between the foreland basins of two major tectonic regimes viz. the Eastern Himalaya and the Indo Burma Hill ranges. As enrichment along these tectono-sedimentary regimes was evaluated using a suite of groundwater and sediment analysis. In view of established tectonic influence on topographic, geologic and hydrologic framework, the controls of geologic and hydrologic factors on the high spatial As distribution were assessed. Attenuation study on the role of sediments in trapping As was conducted on aquifer sediments collected from the northern transect. Surface complexation processes were simulated to predict As adsorption on aquifer sediments.

Hydrogeochemical analysis of 288 groundwater samples collected from the selected transects demonstrated that groundwater occurred under reducing conditions with low Eh , NO_3^- and SO_4^{2-} concentrations and with HCO_3^- as the dominant anion. The maximum concentration of aqueous As along the northern transect was 134 µg/L while concentrations as high as 600 µg/L occurred along the southern transect. Observed difference in groundwater chemistry can be attributed to subsurface redox conditions. Measured stable isotopes (δ^2H and $\delta^{18}O$) values showed that groundwater along both transects fall sub-parallel to the Global Meteoric Water Line (GMWL) (GMWL: $\delta^2H = 8\ \delta^{18}O + 10$) of Craig (1961), suggesting influence of evaporation and recharging along both the transects, the trend of samples being $\delta^2H = 7.15\ \delta 1^8O + 4.27$ for the northern transect and $\delta 2H = 6.8\ \delta^{18}O + 2.7$ for the southern transect respectively.

Contrary to widely reported positive correlation of As with redox sensitive elements (viz. Fe, Mn etc.), this could not be established as conclusively between As and redox elements for groundwater from both transects, indicating that along with the widely accepted mechanism of As release, the reductive dissolution of Fe(III) oxyhydroxides, coupled mechanism of As release viz. subsequent adsorption to available hydroxide sites, competitive adsorption/ desorption also influence As release and distribution in the studied transects. Positive correlation of As with PO_4 and HCO_3 along the southern transect indicated the competitive

ion mechanism, where groundwater anions compete for adsorption sites with As, thereby releasing As into groundwater.

Bivariate plots of major anions and cations revealed that groundwater in the northern transect primarily exhibited silicate and carbonate weathering indicating their concurrent influence on the groundwater evolution along the northern transect. Along the southern transect, groundwater samples exhibited silicate weathering dominance. Within transects, sediment samples representing zones of high, moderate and low dissolved arsenic concentrations showed similar bulk solid As concentration and mineralogical abundances, indicating that dissolved As need not be related to solid phase concentrations alone. Similar to bulk concentrations, mineralogy and petrographic characterization revealed no apparent difference in sediment compositions from the two different transects. Within each transect, sediment samples representing zones of high, moderate and low arsenic notwithstanding difference in texture and color, demonstrated similar suites of minerals, with quartz, feldspars, chlorites and micas being predominant.

Selective sequential Extractions (SSE) used to estimate how strongly As is bound to the sediments revealed higher percentage of extracted As associated with crystalline (30% to 55 %) and amorphous (35%to 57 %) phases. The residual phase of As accumulation accounted for 70 % of the total extractable phases. Dominance of crystalline and amorphous As phases suggested Fe-oxyhydroxides minerals in aquifer sediments to be the key sources of As.

^{14}C dating of sediment samples indicated pre- Holocene sediments. Although drilled cores didn't reveal clay in proximity to main Brahmaputra river channel, radiocarbon age of the recovered clay at10 km distance from the river yielded an age greater than 11,700 years, except one sample at a 3 m depth showing younger age, representing pre-Holocene deposits. Irrespective of sediment age, batch and kinetic studies representing subsurface attenuation processes demonstrated the dominant role of brown sands in adsorbing As, with presence of anions viz. PO_4^- diminishing the As adsorption capacity of brown sands. The competition of adsorption sites for anions generally followed the order $PO_4^{3-} > HCO_3^- = SiO_2$.

Major conclusions drawn from this study are:

Objective 1: Examining the underlying causes of spatial and temporal variability of dissolved arsenic distribution in alluvial aquifers of the Brahmaputra River Valley

- Arsenic (As) distribution along two tectono-sedimentary regimes, straddled between the Eastern Himalayas and Brahmaputra River and the Naga Patkai Hills and the Brahmaputra River, , demonstrated difference in As accumulation; with the northern transect being moderately enriched (max. dissolved As conc. 134µg/L) while the southern transect hosting As enrichment levels (max. dissolved As conc. 600 µg/L) much beyond the WHO guideline of 10 µg/L. Close scrutiny of spatial distribution pattern demonstrated a unique pattern of As distribution, particularly along the 35 km southern transect where As enrichment levels were higher farther from the Brahmaputra River, in contrast to the previously documented scenario further downstream in Bangladesh where groundwater arsenic (As) concentrations decreases with distance away from the river.

- The reductive dissolution of Fe(III)(oxyhydroxides), did explain As mobilization mechanism, yet alternative mechanism explored along the southern transect, suggested two possibilities - first, the unusually thick clay capping inhibiting recharge and secondly, the presence of groundwater of different age indicating differential flushing. This was evident by the presence of 20 and 40 m-thick layers of orange sands in borewells which consolidated the flushing mechanism involving aquifer sands.

- Reductive dissolution of Fe oxyhydroxides coupled with degradation of organic matter released As in the shallow groundwater of the study area. Strong positive correlation of dissolved As and PO_4, indicated competitive As adsorption into aquifer sediment might play an additional role in As mobilization into dissolved phase, particularly along the southern transect.

Objective 2: Evaulating arsenic geochemistry in aquifers of the study transect

- Clay, silt, sand and rock fragments/gravels dominated the aquifer lithology along both transects. While lithology along the northern transect was dominated by brown sands, the southern transect was dominated by 60 m thick clay accumulation. XRF analysis demonstrated that bulk As concentrations were within the comparable range of global average, with higher concentrations being associated with finer deposits. Bulk solid phase As measured in 60 sediment samples from along the northern transect ranged from 1 to 15 mg/kg with an average value of 4 mg/kg, while bulk As measurement of

80 sediment samples from the southern bank ranged between 1 to 4 mg/kg. Absence of concentration difference in bulk As measurements between sampled regions indicated that solid phase As concentrations need not in this case be the controlling factor for high As enrichment in groundwater. Geochemical processes like reductive dissolution and desorption of As from Fe oxyhydroxides surfaces and effects of competing ions, notwithstanding aquifer sediments with relatively low bulk As contents are seemingly more important factors controlling dissolved As release.

- Sequential leaching indicated that major pool of extractable As are associated with the amorphous and crystalline Fe oxides phases, indicating that Fe-Mn oxyhydroxides are the major sources of solid phase As in the aquifers.

Objective 3: Examining arsenic levels and other lithological properties of sediments in the study transect

- Aquifer sands along both transects were petrographically similar, primarily composed of quartz (mono- and polycrystalline), feldspar (mostly potassium and plagioclase), mica (biotite and muscovite), and lithic fragments. Discriminate diagrams revealed that sediments from both transects were derived from quartzose sedimentary provenance, but on the contrary, Chemical Index of Alteration (CIA) calculations indicated higher chemical weathering intensity along the southern transect. The latter enhances Fe- chemical weathering and subsequent formation of Fe-oxyhydroxides minerals which in turn control As accumulation and distribution in sediments.

- Reflectance measurements of aquifer sediments measured along southern transect indicates that more reduced Fe oxides ($\Delta R < 0.1\%$) prevailed in the middle portion of the transect when compared to the less reduced sands above the layer of brown sand at the site closest to the river and also the thinner sand layer at two sites closer to the Naga Hills. This indicates that notwithstanding the established generic geochemical controls on spatial As variability, hydrologic controls are more discernable in controlling As distribution pattern along the 35 km southern transect.

Objective 4: Determine hydrogeochemical characteristics of groundwater and sediments to develop a conceptual model of arsenic release

- Topographic elevation, slope and gradients were major drivers controlling arsenic enrichment along the northern transect, while the role of aquifer flushing in controlling spatial distribution of As was distinct along the southern transect. Differential recharge/ flushing and variable extent of water sediment interaction can explain the high and relatively low As concentrations in groundwater along the transects. ^{14}C measurements of DIC in groundwater samples from the southern transect confirmed older groundwater in clay capped impermeable aquifers (age ~ 17.4 kyr) near the Naga Hills and relatively younger groundwater (age ~ 0.2 kyr) in sand dominated aquifers close to the floodplains. At places where hydrologic gradients were steep, water containing electron acceptors (O_2^-, NO_3^-) was apparently transported into the aquifer through fractures, or sandy outcrops, and influenced the redox conditions in the underlying aquifer, thereby precluding accumulation of As. This phenomenon was more distinct in the recharge zones of the northern transect, where areas in topographic highs, near the Bhutan foothills host low As groundwater. Contrarily, aquifers along sluggish gradients, host high As groundwater due to high residence time of groundwater vis-A-vis greater water rock interaction. The spatial variation in the As content of the groundwater accordingly, turned into a function of hydrogeological setting.

- Among geomorphic features that host high As groundwater, simultaneously with the organic carbon rich younger alluvial deposits, older alluvium units along the southern study transect were too observed to host high As groundwater. ^{14}C measurement of organic rich clay layers further suggested As enrichment in older alluvium, in contrast to those observed in the Bengal Plains and elsewhere where pre-Holocene deposits host As safe groundwater, the understanding being that older alluvium had considerable time to flush out arsenic from the aquifers. Observed high As in older alluvium deposits along the southern transect is attributed to the fact that the older alluvium units are sites for tea cultivation, where groundwater abstraction is used to supply irrigation water to the plantations. It can be presumed that, similar to the established phenomenon in the Bengal Delta and the Red River Delta; intensive

pumping of groundwater from deep aquifers might possibly have facilitated transport of As enriched Holocene water to aquifers located in the older alluvium.

Objective 5: Assessment of arsenic kinetics towards developing a arsenic-remediation model

Batch study carried out using three different aquifer materials viz. Brown Sand, Grayish sand and Grayish Brown sand indicated that brown sands possessing high total solid phase Fe had the highest adsorption capacity for As(V). Isotherm studies demonstrated that As adsorption on the selected samples followed Freundlich model, indicating multilayer adsorption playing a role in As adsorption. Kinetic study demonstrated that 2^{nd} order kinetic model better described As(V) adsorption on aquifer materials along with the rate limiting intra particle diffusion model describing the adsorption behavior. Simulations using Surface Complexation model demonstrated that significant difference existed between experimental and simulated As concentrations for most samples, while few other samples demonstrated good predictability between experimental and adsorbed values.

- The findings of this study can lead to development of a rational management and mitigation strategy for future use of groundwater resources in the upper Brahmaputra River basin. Most initiatives for As mitigation in the upper Brahmaputra basin is currently centered around supply of treated deep groundwater and surface water using piped water networks. Early initiative to reduce risk in the As affected hotspot areas near the base of the Naga Patkai foothills, has focused on setting up of a major piped water supply scheme, drawing water from two major tributaries of the Brahmaputra River viz. the Doyang and the Dhansiri Rivers. While communities adjacent to the schemes have greatly benefitted from piped water supply, a large section of the rural community still are at an increased risk of drinking arsenic contaminated groundwater, the only treated option adopted being the household sand filters. Under the National Water Quality Sub Mission, a program within the National Rural Drinking Water Supply programme of India; there is a major intervention on supply of treated surface water through piped water supply schemes. This is a direct solution to the groundwater arsenic issue. However, governance issues detrimentally affecting such schemes have time and again drastically compromised consistent water supply.

A large proportion of the communities depend on private tube wells which generally tap shallow aquifers, and consequently tap As laced groundwater. The benefit accrued by piped water supply may be jeopardized by the intermittent use of shallow contaminated groundwater by the communities. The findings of the current research, if integrated during the planning and implementation stage of the proposed supply of treated surface water; can enhance the sustainability of the water supply initiatives. Prior information on the regional patterns of As distribution and in-depth information of aquifer lithologies coupled with information on aquifer hydraulic properties can help prioritize mitigation initiatives. Groundwater development vis a vis As safe aquifers are to be pursued primarily for domestic supply while strongly discouraging installation for irrigation- or production wells. Monitoring for sustaining low arsenic aquifers is to be prioritized based on vulnerabilities to arsenic intrusion, along with complete elimination of groundwater from thick clay capped aquifers.

Scope of Future Studies

The present research could develop an understanding of the groundwater arsenic enrichment issue in the upper Brahmaputra Basin in Assam. Yet, critical questions remain which need to be addressed to gain further insights that will aid in providing mitigation solutions thereby ensuring attainment of the sustainable development goal of providing safe drinking water. Some of the scopes of future research on arsenic in the upper Brahmaputra River Basin are,

- The upper Brahmaputra basin in Assam, comprising the Assam shelf and the Assam Arakan Basin lies in a complex tectonic regime. Hence, there is need for an in-depth study on the role of depositional history and neo-tectonics in controlling dissolved As distribution in the region.
- The southern bank of upper Brahmaputra basin in Assam is one of the hotspots of groundwater As contamination. The probable role of petroleum accumulation contributing to As enrichment needs to be ascertained or eliminated
- Results of batch and adsorption kinetic studies can be additionally used in reactive transport models to simulate column experiments for better assessing in-situ remediation strategies.
- In terms of health implications, reported cases of arsenicosis in the region is yet to be verified, indicating the need for a health based mapping relating clinical symptoms to arsenic consumption through drinking water or other modes.

References

ASTAC, 2014. Assam Science and Technology Application Center, www.astac.nic.in

Ahmed, M.F., Ahuja, S., Alauddin, M., Hug, S.J., Lloyd, J.R., Pfaff, A., et al., 2006. Ensuring safe drinking water in Bangladesh. *Science* 314: 1687-1688.

Ahmed, K.M., Bhattacharya, P., Hasan, M.A., Akhter, S.H.,Alam, S.M.M., Bhuyian, M.A.H., 2004. Arsenic contamination in groundwater of alluvial aquifers in Bangladesh: an overview. *Applied Geochemistry* 19, 181-200.

Aggarwal, P.K., Basu, A.R., Poreda, R.J., Kulkarni, K.M., Froehlich, K., Tarafdar, S.A., Ali, M., Ahmed, N., Hussain, A., Rahman, M., Ahmed, S.R., 2000. A report on isotope hydrology of groundwater in Bangladesh: implications for characterization and mitigation of arsenic in groundwater. International Atomic Energy Agency-TC Project BGD/8/016, 64p.

Allison, J.D., Brown, D.S., Novo-Gradac, K.J., 1990.MINTEQA2/ PRODEFA2-A Geochemical Assessment Model for Environmental Systems. US Environmental Protection Agency, Athens, Georgia

Anwar, H., Komaki, K., Takada, J., Ishizuka, T., Takahashi, T, Yoshioka, T. and Kato, K., 2002. Diagenetic Control on Arsenic Partitioning in Sediments of the Meghna River Delta, Bangladesh. *Environmental Geology* 41, 816-825.

Anawar, H.M., Akai, J., Komaki, K., Terao, H., Yoshika, T., Ishizuka, T., Safiullah,S., Kato,K., 2003. Geochemical occurrences of arsenic in groundwater of Bangladesh: sources and mobilization processes. *Journal of Geochemical Exploration* 77, 109-131.

Appelo,C.A.J., van-der-Weiden, M.J.J., Tournassat, C.,Charlet, L., 2002. Surface complexation of ferrous iron and carbonates on ferrihydrite and the mobilization of arsenic. *Environmental Science and Technology* 36, 3096-3103.

Appelo, C.A.J and Postma, D., 2005. Geochemistry, Groundwater and Pollution, second ed. A.A. Balkema, Rotterdam.

Apodaca, L.E., Jeffrey, B.B., Michelle, C.S., 2002. Water quality in shallow alluvial aquifers, Upper Colorado River Basin, Colorado, 1997. *Journal of the American Water Resources Association* 38, 133–143.

Arai,Y., Sparks, D., Davis, J.A., 2005. Arsenate adsorption mechanism at the allopane –water interface. *Environmental Science and Technology* 39,2537-2544

Armienta, M.A., Segovia, N., 2008. Arsenic and fluoride in the groundwater of Mexico. *Environmental Geochemistry and Health* 30, 345-353.

Artinger, R, Buckau G, Geyer S, Fritz P, Wolf M., Kim J.I., 2000. Characterization of groundwater humic substances: influence of sedimentary organic carbon. *Applied Geochemistry* 15, 97–116.

Banerjee, K., Amy, G.L., Prevost, M., Nour, S., Jekel, M., Gallagher, P.M. and Blumenschein, C.D. 2008. Kinetic and thermodynamic aspects of adsorption of arsenic onto granular ferric hydroxide (GFH). *Water Research* 42(13),3371-3378.

Berg, M., Luiz, S., Trang, P.T.K., Viet, P.H., Giger, W., Stuben, D. 2006. Arsenic Removal from Groundwater by Household Sand Filters: Comparative Field Study, Model Calculations, and Health Benefits. *Environmental Science and Technology* 2006, 40, 5567-5573

Belkhiri, L., Boudoukha, A., Mouni, L. and Baouz, T., 2010. Application of multivariate statistical methods and inverse geochemical modeling for characterization of groundwater—a case study: Ain Azel plain (Algeria). *Geoderma* 159(3), 390-398.

BGS, DPHE, 2001. Arsenic contamination of groundwater in, Bangladesh. British Geological Survey Report WC/00/19. BGS Technical Report WC/00/19. British Geological Survey, Keyworth, U.K.. Keyworth, UK.

Bhattacharya, P., Chatterjee, D., Jacks, G., 1997. Occurrences of arsenic contaminated groundwater in alluvial aquifer from delta plains eastern India: option for safe drinking water supply. *Journal of Water Resource Development* 13, 79- 92.

Bhattacharya, P., Jacks, G., Ahmed, K.M., Routh, J., Khan, A.A., 2002. Arsenic in groundwater of the Bengal delta plain aquifers in Bangladesh. *Bulletin of Environmental Contaminant Toxicology* 69, 538–45.

Bhaviskar,S., Choudhury,R., Mahanta, C., 2015. Dissolved and solid-phase arsenic fate in an arsenic-enriched aquifer in the river Brahmaputra alluvial plain. *Environmental Monitoring and Assessment* 187, 93.

Berg, M., Tran, H.C., Nguyen, T.C., Pham, H.V., Schertenleib, R., Giger, W., 2001. Arsenic contamination of groundwater and drinking water in Vietnam: a human health threat. *Environmental Science and Technology* 35, 2621–2626.

Berg, M, Trang, P.T.K., Stengel, C., Buschmann, J., Viet, P.H., Dan, N.V., Giger, W., Stuben, D., 2008. Hydrological and sedimentary controls leading to arsenic contamination of groundwater in the Hanoi area, Vietnam: The impact of iron arsenic

ratios, peat, river bank deposits, and excessive groundwater abstraction. *Chemical Geology* 249, 91- 112.

Bhattacharya, P., Mukherjee, A., Mukherjee, A.B. 2011. Arsenic contaminated groundwater of India. In Nriagu, J. (ed.): Encyclopedia of Environmental Health. Elsevier B.V. (Netherlands). 150-164.

Biswas, A., Nath, B, Bhattacharya, P., Halder. D., Kundu, A., Mandal, U., Mukherjee, A., Chatterjee, D., Morth, C.M., Grunar, J, 2012. Hydrogeochemical contrast between brown and grey aquifers in shallow depth of Bengal basin: Consequences for sustainable drinking water supply. *Science of the Total Environment* 431, 402-412.

Biswas, A., Bhattacharya, P., Mukherjee, A., Nath, B Alexanderson, H., Kundu, A.K., Chatterjee, D., Jacks, G., 2014. Shallow hydrostratigraphy in an arsenic affected region of Bengal Basin: Implication for targeting safe aquifers for drinking water supply. *Science of the Total Environment* 485–486, 12–22.

Bose, P. and Sharma, A., 2002. Role of iron in controlling speciation and mobilization of arsenic in subsurface environment. *Water Research* 36. 4916–4926

Brikowski, T.H., Neku, A., Shrestha, S.D., Smith, L.S. 2014. Hydrologic control of temporal variability in groundwater arsenic on the Ganges floodplain of Nepal. *Journal of Hydrology* 518, 342–353.

Bristow, C. S. 1987. Brahmaputra River: Channel migration and deposition. In: Ethridge, F. G., Flores, R. M. & Harvey, M. D. (eds) Recent Developments in Fluvial Sedimentology. *Society of Economic Paleontologists and Mineralogists Special Publications* 39, 63-74

Bundschuh, J., Litter, M.I., Parvez, F., Roman-Ross, G., Nicolli, H.B., Jean, J.S., Liu, C.W., Lopez, D., Armienta, M.A., Guilherme, L.R.G., Gomez Cuevas,A., Cornejo, L., Cumbal, L., Toujaguez, R., 2012. One century of arsenic exposure in Latin America: A review of history and occurrence from 14 countries. *Science of the Total Environment* 429, 2-35.

Bundschuh, J., Litter, M., Bhattacharya, P., 2010. Targeting arsenic-safe aquifers for drinking water supplies. *Environmental Geochemistry and Health* 32, 307-315.

Buschmann, J., Berg, M., Stengel, C., Sampson, M., 2007. Arsenic and manganese contamination of drinking water resources in Cambodia: Coincidences of risk areas with low relief topography. *Environmental Science and Technology* 41, 2146-2152.

Burbank, D.W., Leland, J., Fielding, E., Anderson, R.S., Brozovic, N., Reid, M.R., Duncan, C., 1996. Bedrock incision, rock uplift and threshold hillslopes in the northwestern Himalayas. *Nature* 379, 505–510

Bauer, M., Fulda, B. & Blodau, C. Groundwater derived arsenic in high carbonate wetland soils: Sources, sinks, and mobility. *Science of the Total Environment* 401, 109–120.

Carraro, A., Fabbri, P., Giaretta,A., Peruzzo, L., Tateo, F., Tellini, F. 2015. Effects of redox conditions on the control of arsenic mobility in shallow alluvial aquifers on the Venetian Plain (Italy). *Science of the Total Environment* 532, 581–594

Central Ground Water Board Report (1995) Hydro geological and Groundwater resources of Nalbari District, Govt of India, Ministry of Water Resource.

Central Ground Water Board Report (2012) Hydro geological and Groundwater resources of Jorhat District, Govt of India, Ministry of Water Resource

Charlet, L., Chakraborty, S., Appelo, C.A.J., Roman –Ross. G., Nath, B., Ansari, A.A., Musso,M., Chatterjee, D., Mallick, S.B., 2007. Chemodynamics of an arsenic "hotspot" in a West Bengal aquifer: a field and reactive transport modeling study. *Applied Geochemistry* 22, 392-401.

Chetia, M., Chatterjee, S., Banerjee, S, Nath M.J., Singh L., Srivastava R.B., Sarma H.P., 2011 Groundwater arsenic contamination in the Brahmaputra river basin: a water quality assessment in the Golaghat (Assam), India *Environmental Monitoring and Assessment* 173: 371–385.

Cheng, Z,. van Geen, A., Seddique, A..A., Ahmed, K.M., 2005. Limited temporal variability of arsenic concentrations in 20 wells monitored for 3 years in Araihazar, Bangladesh. *Environmental Science and Technollogy* 39, 4759–66. http://dx.doi.org/10.1021/es048065f.

Choi, S.Y., O'Day, P.A., Hering, J.G., 2009. Natural attenuation of arsenic by sediment sorption and oxidation. *Environmental Science and Technology* 43, 4253–4259.

Chakraborty, D., Mukherjee, S.C., Pati, S., Sengupta, M.K., Rahman, M.M., Chowdhury, U.K., Lodh, D., Chanda, C.R., Chakraborti, A.K., Basu, G.K., 2003. Arsenic groundwater contamination in Middle Ganga Plain, Bihar, India: a future danger? *Environmental Health Perspective*, 111, 1194–1201.

Chakraborty, A., Sengupta, A., Bhadu, M.K., Pandey, A.., Mondal, A.., 2014. Efficient removal of arsenic (V) from water using steel-making slag. *Water Environment Research* 86, 524-531.

Chowdhury, T.R., Basu, G.K., Mandal, B.K., Biswas, B.K., Samanta, G., Chowdhury, U.K., Chanda, C.R., Lodh, D., Roy, S.L., Saha, K.C. and Roy, S., 1999. Arsenic poisoning in the Ganges delta. *Nature* 401,545-546.

Choudhury,R., Sharma,P., Mahanta,C., Sarma,H.P., 2015. Evaluation of the processes controlling arsenic contamination in parts of the Brahmaputra floodplains in Assam, India. *Environmental Earth Science*. DOI 10.1007/s12665-014-3735-2.

Choudhury, R., Mahanta, C., Verma, S., Abhijit, M. 2017. Arsenic distribution along different hydrogeomorphic zones in parts of the Brahmaputra River Valley, Assam (India) *Hydrogeology Journal*, 25, 1153–1163

Ciardelli, M.C., Xu, H., Sahai, N., 2008. Role of Fe(II), phosphate, silicate, sulfate and carbonate in arsenic uptake by coprecipitation in synthetic and natural groundwater. *Water Resources* 42, 615–624

Coleman, J. M., 1969. Brahmaputra River channel processes and sedimentation. *Sedimentary Geology* 3, 129-239.

Craig, H., 1961. Isotopic variations in meteoric waters. *Science*, 133, 1702-1703.

Cullen, W.R., Reimer, K.J., 1989. Arsenic speciation in the environment. *Chemical Reviews* 89, 713–764.

Cummings, D.E., Caccavo, Jr.F., Fendorf ,S., and Rosenzweig,R.F. 1999. Arsenic Mobilization by the Dissimilatory Fe(III)-Reducing Bacterium Shewanella algae BrY. *Environment Science and Technology* 33 (5), 723–729

Das, D., Samanta, G., Mandal, B.K., Roy Chowdhury, T., Chanda, C.R., Chowdhury, P.P., Basu, G.K. and Chakraborti, D., 1996. Arsenic in groundwater in six districts of West Bengal, India. *Environmental Geochemistry and Health 18*, 5-15.

Das, N., Deka, J. P., Shim, J., Patel, A. K., Kumar, A., Sarma, K. P., & Kumar, M. , 2016b. Effect of river proximity on the arsenic and fluoride distribution in the aquifers of the Brahmaputra floodplains, Assam, northeast India. *Groundwater for Sustainable Development* 2, 130-142.

Datta, S., 2015. Hydrological Aspects of Arsenic Contamination of Groundwater in Eastern India. Advances in Agronomy, Volume 132, ISSN 0065-2113, http://dx.doi.org/10.1016/bs.agron.2015.02.001

Davis, J.A., Coston, J.A., Kent, D.B. and Fuller, C.C., 1998. Application of the surface complexation concept to complex mineral assemblages. *Environmental Science & Technology 32*, 2820-2828

Dean, W.E., Jr. 1974. Determination of carbonate and organic matter in calcareous sediments and sedimentary rocks by loss on ignition: Comparison with other methods. *Journal of Sedimentary Petrology* 44, 242-248.

Dixit, S., Hering, J.G., 2003. Comparison of arsenic (V) and arsenic (III) , sorption onto iron oxide minerals : Implications for arsenic mobility. *Environmental Science and Technology* 37, 4182-4189.

Dowling, C.B., Poreda, R.J., Basu, A.R., Peters, S.L., Aggarwal, P.K. 2002. Geochemical study of arsenic release mechanisms in the Bengal Basin groundwater. *Water Resources Research*, vol. 38, No. 9, 1173, doi:10.1029/2001WR000968, 2002.

Dowling ,C.B., Poreda, R,J,, Basu, A,R .2003. The groundwater geochemistry of the Bengal basin: weathering, chemsorption, and trace metal flux to the oceans. *Geochimica et Cosmochim Acta* 67, 2117–2136

Dousova, B., Buzek, F., Rothwell, J., Krejcova, S. and Lhotka, M., 2012. Adsorption behavior of arsenic relating to different natural solids: soils, stream sediments and peats. *Science of the Total Environment* 433, 456-461

Dhar, R.K., Zheng, Y., Stute, M., van Geen A., Cheng, Z., Shanewaz, M., Shamsudduha, M., Hoque, M.A., Rahman, M.A., Ahmed, K.M., 2008. Temporal variability of groundwater chemistry in shallow and deep aquifers of Araihazar, Bangladesh. *Journal of Contaminant Hydrology* 99, 97-111.

Drahota P., Filippi M., 2009. Secondary arsenic minerals in the environment: A review. *Environment International* 35, 1243-1255.

Dzombak, D.A. and Morel, F.M.M., 1990. Surface complex modeling. Hydrous ferric oxide.John Wiley & Sons.

Donselaar, M.E., Bhatt, A.G., Ghosh, A.K. 2017. On the relation between fluvio-deltaic flood basin geomorphology and the wide-spread occurrence of arsenic pollution in shallow aquifers. *Science of the Total Environment* 574, 901-913

Elder K.L., Mcnichol, A.P., Gagnon, A.R., 1998. Reproducibility of Seawater, Inorganic and Organic Carbon 14C Results at NOSAMS *Radiocarbon* 40, 223-230.

Erban, L.E., Gorelick, S.M., Zebker,H.A. and Fendorf. S., 2013. Release of arsenic to deep groundwater in the Mekong Delta, Vietnam, linked to pumping-induced land subsidence. Proceedings of the National Academy of Sciences U S A. 110, 13751–13756.

Etmannski, T.R., and Darton, R.C., 2014. A methodology for the sustainability assessment of arsenic mitigation technology for drinking water. *Science of the Total Environment* 488–489, 505–511

Evans, P. 1964: The tectonic framework of Assam, *Journal of Geological Society of India* 5, 80-96.

Farmer, J. G., and Lovell, M. A., 1986. Natural enrichment of arsenic in Loch Lomond sediments. *Geochimica et Cosmochimica Acta* 50(9), 2059-2067.

Faure, G., 1998. Principles and Applications of Geochemistry: A Comprehensive Textbook for Geology Students. Prentice Hall.

Fedo, C. M., Nesbitt, H. W., & Young, G. M., 1995. Unraveling the effects of potassium metasomatism in sedimentary rocks and paleosols, with implications for paleoweathering conditions and provenance. *Geology* 23, 921-924. http://dx.doi.org/10.1130/0091-7613

Ferreccio, C., Smith, A.H., Duran, V., Barlaro, T., Benitez, H., Valdes, R., Aguirre, J.J., Moore, L.E., Acevedo, J., Vasquez, M.I., Perez, L., Yuan, Y., Liaw, J., Cantor, K.P., Steinmaus, C., 2013. Case–control study of arsenic in drinking water and kidney cancer in uniquely exposed Northern Chile. *American Journal of Epidemiology* 178 (5), 813–818.

Fendorf S.E., Eick,M., Grossl,P., Sparks,D.L., 1997. Arsenate and chromate retention mechanisms on goethite. 1. Surface structure. *Environmental Science and Technology* 31, 315-319.

Foster, Andrea L. 2003. Spectroscopic investigations of arsenic species in solid phases. In Arsenic in Ground Water, 27-65. Springer US, 2003.

Frau, F., Biddau, R. and Fanfani, L., 2008. Effect of major anions on arsenate desorption from ferrihydrite-bearing natural samples. *Applied Geochemistry* 23, 1451-1466

Gaillardet, J., Dupré, B., Louvat, P. and Allegre, C.J., 1999. Global silicate weathering and CO 2 consumption rates deduced from the chemistry of large rivers. *Chemical Geology 159*, 3-30.

Galy, A., France-Lanord, C., 2001. Higher erosion rates in the Himalaya: geochemical constraints on riverine fluxes. *Geology* 29, 23–26.

Galy, V., France-Lanord, C., Peucker-Ehrenbrink, B., Huyghe, P., 2010. Sr–Nd–Os evidence for a stable erosion regime in the Himalaya during the past 12 Myr. *Earth and Planetary Science Letters* 290, 474–480.

Guillot, S, and Laurent C., 2007. Bengal arsenic, an archive of Himalaya orogeny and paleohydrology. *Journal of Environmental Science and Health Part A* 42, 12,1785-1794.

Grafe, M., M.J. Eick, and P.R. Grossl., 2001. Adsorption of arsenate(V) and arsenite(III) on goethite in the presence and absence of dissolved organic carbon. *Soil Science Society of America Journal* 65:1680-1687.

George C.M., Zheng Y., Graziano J.H., Bin Rasul S., Hossain Z., Mey J.L., van Geen A. 2012. Evaluation of an arsenic test kit for rapid well screening in Bangladesh. *Environment Science and Technology* 46:11213–11219. doi: 10.1021/es300253p

Gao, X.B., Wang, Y.X., Hu, Q.H., Su, C.L., 2011. Effects of anion competitive adsorption on arsenic enrichment in groundwater. *Journal of Environmental Science and Health*, Part A 46, 1-9

Giménez, J., Martínez, M., de Pablo, J., Rovira, M., & Duro, L., 2007. Arsenic sorption onto natural hematite, magnetite, and goethite. *Journal of Hazardous Materials 141*, 575-580.

Goldberg,S., Glaubig, R.A., 1988. Anion adsorption on a calcareous, montmorillonite site-Arsenic. *Soil, Science, Society American Journal* 66, 413-421.

Goswami, R., Rahman, M.M., Murrill, M., Sarma, K.P., Thakur, R., Chakraborti, D., 2013. Arsenic in the groundwater of Majuli – The largest river island of the Brahmaputra: Magnitude of occurrence and human exposure. *Journal of Hydrology* 518, 354-362.

Gorny, J., Billon, G., Lesven, L., Noiriel., C., 2016. Arsenic behavior in river sediments under redox gradient: A review. *Science of the Total Environment* 505, 423-434.

Gray, J.R., Khalil, A., Prior, J.C., 1989. Acute arsenic toxicity: an opaque poison. *Canadian Association of Radiologists Journal* 40, 226–227.

Grosz, A. E., J. N. Grossman, R. Garrett, P. Friske, D. B. Smith, A. G. Darnley, and E. Vowinkel , 2004. A preliminary geochemical map for arsenic in surficial materials of Canada and the United States. *Applied Geochemistry* 19, 257–260.

Guo, H., Wang, Y., Shpeizer, G.M., Yan, S., 2003. Natural occurrence of arsenic in shallow groundwater, Shanyin, Datong Basin, China. *Journal of Environmental Science and Health. Part A, Toxic/hazardous Substances & Environmental Engineering* 38, 2565-2580

Guo, H., Zhang, Y., Jia, Y., Zhao, K., Li, Y., Tang, X., 2013. Dynamic behaviors of water levels and arsenic concentration in shallow groundwater from the Hetao Basin, Inner Mongolia. *Journal of Geochemical Exploration 135*, 130-140.

Guo, H., Wen, D., Liu, Z., Jia, Y., Guo, Q., 2014. A review of high arsenic groundwater in Mainland and Taiwan, China: Distribution, characteristics and geochemical processes. *Applied Geochemistry* 41, 196–217.

Guo, H., Jia, Y., Wanty, R.B., Jiang, Y., Zhao, W., Xiu, W., Shen, J., Li, Y., Cao, Y., Wu, Y. and Zhang, D., 2016. Contrasting distributions of groundwater arsenic and uranium in the western Hetao basin, Inner Mongolia: Implication for origins and fate controls. *Science of the Total Environment* 541,1172-1190.

Guan, X., Dong, H., Ma, J. and Jiang, L., 2009. Removal of arsenic from water: effects of competing anions on As (III) removal in $KMnO_4$–Fe (II) process. *Water Research* 43, 3891-3899.

Halim, M. A., Majumder, R. K., Nessa,S.A., Hiroshiro, Y., Uddin, M.J., Shimada, J., Jinno, K., 2009. Hydrogeochemistry and arsenic contamination of groundwater in the Ganges Delta Plain, Bangladesh. *Journal of Hazardous Material* 164, 1335–1345.

Halim, M.A,. Majumder, R.K., Nessa, S.A, Hiroshiro, Y., Sasaki, K., Saha, B.B., Saepuloh, A., Jinno, K., 2010. Evaluation of processes controlling the geochemical constituents in deep groundwater in Bangladesh: spatial variability on arsenic and boron enrichment. *Journal of Hazardous Material* 180, 50-62.

Hafeznezami, S., Faust, A.G.Z, Dunne, A., Tran, T., Yang, C., Lam, J.R., Reynolds, M.D., Davis, J.A., Jay, J.A., 2016. Adsorption and desorption of arsenate on sandy sediments from contaminated and uncontaminated saturated zones: Kinetic and equilibrium modeling. *Environmental Pollution* 215, 290-301

Handique, G.K., A.K.Sethi., S.C.Sarma., 1989. Review of Tertiary Stratigraphy of parts of Upper Assam Valley, Geological Survey of India, Special Publication, 23,23-36

Harvey, C.F., Swartz, C.H., Badruzzaman, A.B.M., Keon-Blute, N., Yu, W., Ali, M.A., Jay, J.,Beckie, R., Niedan, V., Brabander, D., Oates, P.M., Ashfaque, K.N., Islam, S., Hemond, H.F.,Ahmed, M.F., 2002. Arsenic Mobility and Groundwater Extraction in Bangladesh. *Science* 298, 1602-1606.

Harvey, C.F., Ashfaque, K.N., Yu,W., C.H., Badruzzaman, Ashraf, A.M., Oates, P.M., Michael, H.A., Neumann, R.B., Beckie, R., Islam, S., Ahmed, M.F., 2006. Groundwater dynamics and arsenic contamination in Bangladesh. *Chemical Geology* 228, 112-136.

Haque, S., Ji, Junfeng, Johannesson, K.H., 2008. Evaluating mobilization and transport of arsenic in sediments and groundwaters of Aquia aquifer, Maryland, USA. *Journal of Contaminant Hydrology* 99 , 68–84.

Hendricks, D.W., 2006. Water Treatment Unit Processes: Physical and Chemical. CRC Press.

He, Y.T., Fitzmaurice, A.G., Bilgin, A., Choi, S., O'Day, P., Horst, J., Harrington, J., Reisinger, H.J., Burris, D.R. and Hering, J.G., 2010. Geochemical processes controlling arsenic mobility in groundwater: A case study of arsenic mobilization and natural attenuation. *Applied Geochemistry* 25, 69–80.

Helgeson, H.C., 1968. Evaluation of irreversible reactions in geochemical processes involving minerals and aqueous solutions—I. Thermodynamic relations. *Geochimica et Cosmochimica Acta* 32, 853-877.

Hemond, H.F., 1995. Movement and Distribution of Arsenic in the Aberjona Watershed. *Environmental Health Perspectives* 103.

Ho, Y. S., and Gordon McKay., 1998. A comparison of chemisorption kinetic models applied to pollutant removal on various sorbents. *Process Safety and Environmental Protection* 76, 332-340.

Hopenhayn-Rich, C., Biggs, M.L., Smith, A.H., 1998. Lung and kidney cancer mortality associated with arsenic in drinking water in Cordoba, Argentina. *International Journal of Epidemiology* 27, 561–569.

Hoque, M.A., Burgess, W.G. 2012. 14C dating of deep groundwater in the Bengal Aquifer System, Bangladesh: Implications for aquifer anisotropy recharge sources and sustainability. *Journal of Hydrology* 444–445, 209–220.

Horneman,A. van Geen,A., Kent,D.V., Mathe,P.E., Zheng,Y Dhar,R., O'Connell, S., Hoque,M.A., Aziz, Z., Shamsudduha, M., Seddique, A.A., Ahmed, K.M., 2004. Decoupling of As and Fe release to Bangladesh groundwater under reducing conditions. Part I: Evidence from sediment profiles. *Geochimica et Cosmochimica Acta* 68, 3459–3473.

Hossain, M. Bhattacharya, P., Jacks, G., von Brömssen, M., Ahmed,K.M., Hasan, M.A. and Frape, S.K. 2017 in Prosun Bhattacharya, David A. Polya and Dragana Jovanovic (Eds.) Best Practice Guide on the Control of Arsenic in Drinking Water,. IWA Publishing, DOI:10.2166/9781780404929_099

Hsueh, Y.M., Chung, C.J., Shiue, H.S., Chen, J.B., Chiang, S.S., Yang, M.H., Tai, C.W., Su, C.T., 2009. Urinary arsenic species and CKD in a Taiwanese population: a case–control study. *American Journal of Kidney Diseases* 54, 859–870.

Huang, C.Y., Chu, J.S., Pu, Y.S., Yang, H.Y., Wu, C.C., Chung, C.J., Hsueh, Y.M., 2011. Effect of urinary total arsenic level and estimated glomerular filtration rate on the risk of renal cell carcinoma in a low arsenic exposure area. *The Journal of Urology* 185, 2040–2044.

Itai, T., Takahashi, Y., Seddique, A.A., Maruoka, T. and Mitamura, M., 2010. Variations in the redox state of As and Fe measured by X-ray absorption spectroscopy in aquifers of Bangladesh and their effect on As adsorption. *Applied Geochemistry 25*, 34-47.

Islam, F.S.., Gault, A.G., Boothman, C., Poyla, D.A., Charnock, J.M., Chatterjee,D., Lloyd,J. 2004. Role of metal reducing bacteria in arsenic release in Bengal Delta sediments. *Nature* 430, 69-71.

Islam, F.S., Pedrick, R.L., Gault, A.G., Adams, L.K., Poyla, D.A., Charnok, J.M., Lloyd, J.R., 2005. Interaction between Fe(III)–reducing bacterium Geobacter sulfurreducens and arsenate , and capture of the metalloid by biogenic Fe(II). *Applied and Environmental Microbiology* 71, 8642-8648.

Jain A, Loeppert RH. 2000. Effect of competing anions on the adsorption of arsenate and arsenite by ferrihydrite. *Journal of Environmental Quality* 29:1422–1430.

Jessen, S., Postma, D., Larsen, F., Nhan, P.Q., Trang, P.T.K., Long, T.V., Viet, P.H. and Jakobsen, R., 2012. Surface complexation modeling of groundwater arsenic mobility: Results of a forced gradient experiment in a Red River flood plain aquifer, Vietnam. *Geochimica et Cosmochimica Acta 98*,186-201.

Johannesson, K.H. and Tang, J., 2009. Conservative behavior of arsenic and other oxyanion-forming trace elements in an oxic groundwater flow system. *Journal of Hydrology 378*, 13-28.

Johannesson, K.H., and Zhou X., 1999. Origin of middle rare earth element enrichments in acid water of a Canadian High Arctic lake. *Geochim.Cosmochim.Acta* 63,153-165.

Johnston, R.B., Hanchett, S., Hoque, Khan, M. 2010. The socio economics of arsenic removal. *Nature Geoscience* 243-246.

Jakariya, M., von Bromssen, M., Jacks, G., Chowdhury, A.M.R., Ahmed, K.M., Bhattacharya, P., 2007. Searching for sustainable mitigation strategy in Bangladesh: experiences from two Upazilas. *International Journal of Environmental Pollution* 31, 415-430.

Kapaj, S., Peterson, H., Liber, K., Bhattacharya, P., 2006. Human health effects from chronic arsenic poisoning: a review. *Journal of Environmental Health and Toxicological Hazardous Substances in the Environment* 41, 3299-2428.

Katsoyiannis, I.A. and Zouboulis, A.I., 2002. Removal of arsenic from contaminated water sources by sorption onto iron-oxide-coated polymeric materials. *Water Research, 36,* 5141-5155.

Kent,D.B., Fox, P.M., 2004.The influence of groundwater chemistry on arsenic concentrations and speciation in a quartz sand and gravel aquifer. *Geochemical Transactions* 5, 1-5.

Khanikar, L., Gogoi, R.R., Das, N., Deka, J.P., Das, A., Kumar, M. and Sarma, K.P., 2017. Groundwater appraisal of Dhekiajuli, Assam, India: an insight of agricultural suitability and arsenic enrichment. *Environmental Earth Sciences* 76(15), 530.

Kim, M.J., Nriagu, J., Haack, S., 2000. Carbonate ions and arsenic dissolution by groundwater. *Environmental Science and Technology* 34, 3094–3100.

Koretsky, C., 2000. The significance of surface complexation reactions in hydrologic systems: a geochemist's perspectives. *Journal of Hydrology*.230, 127-171.

Kurttio, P., Pukkala, E., Kahelin, H., Auvinen, A., Pekkanen, J., 1999. Arsenic concentrations in well water and risk of bladder and kidney cancer in Finland. *Environmental Health Perspective* 107, 705–710.

Klump, S., Kipfer, R., Olaf, A.C., Harvey, C.F., Brennwald, M.S., Khandkar, N.A., Badruzzaman, A.B.M., Hug, S., Imboden, D.M., 2006. Groundwater dynamics and arsenic mobilization in Bangladesh assessed using noble gases and tritium. *Environmental Science and Technology* 40, 243–250.

Kumar, K., Das, A., Das, N., Goswami, R., Singh, U.K., 2016. Co-occurrence perspective of arsenic and fluoride in the groundwater of Diphu, Assam, Northeastern India. *Chemosphere* 150, 227-238

Kumar, G. Geology of the Arunachal Pradesh, Geol. Soc. India, Bangalore, 1997, 217 pp.

Lahiri, S and Sinha, R. 2012. Tectonic controls on the morphodynamics of the Brahmaputra River system in the upper Assam valley, India. *Geomorphology* 169-170, 74–85.

Langmuir, D., 1997. Aqueous Environmental Geochemistry. Prentice-Hall, Upper Saddle River, NJ

Lawson, M., Polya, D.A., Boyce, A.J., Bryant, C. and Ballentine, C.J., 2016. Tracing organic matter composition and distribution and its role on arsenic release in shallow Cambodian groundwaters. Geochimica et Cosmochimica Acta 178,160-177.

Lin, Z., Puls, R.W., 2000. Adsorption, desorption and oxidation of arsenic affected by clay minerals and ageing process. *Environmental Geology* 32, 753-759.

Luiz, S., Berg M., Pham, T.KT., Pham, H.V., and Schertenleib, R., 2004. Household sand filters for Arsenic removal- Technical Report. Swiss Federal Institute for environmental Science and Technology (EAWAG). Ueberlandstr.133, CH-8600 Duebendorf, Switzerland.

Leupin, O.X., Hug, S.J., 2005. Oxidation and removal of arsenic (III) from aerated groundwater by filtration through sand and zero valent iron, *Water Research* 39, 1729–1740.

Mai, N.T.H., Postma, D., Trang, P.T.K., Jessen, S., Viet, P.H., Larsen, F., 2014. Adsorption and desorption of arsenic to aquifer sediment on the Red River floodplain at Nam Du, Vietnam. *Geochimica et Cosmochimica Acta* 141, 587-600.

Maji, Sanjoy Kumar, Anjali Pal, and Tarasankar Pal. 2008. Arsenic removal from real-life groundwater by adsorption on laterite soil. *Journal of Hazardous Materials* 151(2), 811-820.

Mallick, S., Rajgopal, N.R., 1996. Groundwater development in the arsenic affected alluvial belt of West Bengal-some questions. *Current Science* 70, 956- 958.

Mandal, B.K., Suzuki, K.T., 2002. Arsenic around the world: a review. *Talanta* 580, 201-235.

Ma, J., Guo, H., Lei, M., Zhou, X., Li, F., Yu, T., Wei, R., Zhang, H., Zhang, X., Wu, Y., 2015. Arsenic Adsorption and its Fractions on Aquifer Sediment: Effect of pH, Arsenic Species, and Iron/Manganese Minerals. *Water Air Soil Pollution* 226, 260 DOI 10.1007/s11270-015-2524-1

Maji, S.K., Pal, A. and Pal, T. 2008. Arsenic removal from real-life groundwater by adsorption on laterite soil. *Journal of Hazardous Materials*, 151(2), 811-820.

Manning, B.A., Goldberg, S., 1996. Modeling competitive adsorption of arsenate with phosphate and molybdate on oxide minerals. *Soil Science Society American Journal*. 60, 121-131.

Manning, B.A., Goldberg, S., 1997. Arsenic (III) and Arsenic (V) adsorbtion on Three California Soils. Soil Science, V. 162(12) p.886-895

Manning, B.A., Fenrof, S.E., Bostick, B., Suarez, D.L., 2002. Arsenic(III) oxidation and arsenic (V) adsorption reactions on synthetic birnessite. *Environmental Science and Technology* 36, 976-981.

Marshall, G., Ferreccio, C., Yuan, Y., Bates, M.N., Steinmaus, C., Selvin, S., Liaw, J., Smith, A.H., 2007. Fifty-year study of lung and bladder cancer mortality in Chile related to arsenic in drinking water. *Journal of the National Cancer Institute* 99, 920–928.

Mahanta, C., Subramanian, V. 2004. Water Quality, Mineral Transport ans Sediment Biogeochemistry. In V.P.Singh, N.Sharma, C.Shekhar, P. Ojha (Ed) The Brahmaputra Basin Water Resources, Springer Publications.

Mahanta, C., Enmark,G., Nordborg, D., Sracek, O., Nath, B., Nickson, R.T., Herber, R., Jacks, G., Mukherjee, A., Ramanathan, A. L., Choudhury, R., Bhattacharya, P. 2015. Hydrogeochemical controls on mobilization of arsenic in groundwater of a part of Brahmaputra river floodplain, India. *Journal of Hydrology: Regional Studies* 4, 154–171

Mathur, L.P. and Evans, P.[Ed.] (1964): Oil in India: International Geological Congress, 22nd session, India, 1964, New Delhi, 85p.

McClintock, R.T., Chena Yu, Parvez, F., Makarov, D.V., Ge, W., Islam, T., Ahmed, A.., Zamanh, M. R., Hasanh,R., Sarwar,G., Slavkovich,V., Bjurlin, M.A., Graziano, J.H., Ahsan , H., 2014. Association between arsenic exposure from drinking water and hematuria: Results from the Health Effects of Arsenic Longitudinal Study. *Toxicology and Applied Pharmacology* 276, 21–27.

McArthur, J.M.; Banerjee, D.M.; Sengupta, S.; Ravenscroft, P.; Klump, S.; Sarkar, A.; Disch, B.; Kipfer, R., 2010. Migration of As, and 3H/3He ages, in groundwater from West Bengal: implications for monitoring. *Water Research* 44, 4171–4185.

McArthur, J.M., Ravenscroft, P., Safiulla, S., Thirlwall, M.F., 2001. Arsenic in groundwater: testing pollution mechanisms for sedimentary aquifers in Bangladesh. *Water Resource Research* 37, 109–117.

McArthur, J.M., Banerjee, D.M., Hudson-Edwards, K.A., Mishra, R., Purohit, R., Ravenscroft, P., Cronin, A., Howarth, R.J., Chatterjee, A., Talukder, T. and Lowry, D., 2004. Natural organic matter in sedimentary basins and its relation to arsenic in anoxic ground water: the example of West Bengal and its worldwide implications. *Applied Geochemistry 19*, 1255-1293.

Meng , X.G., Bang,S., Korfiatis,G.P., 2000. Effects of silicate, sulfate and carbonate on arsenic removal by ferric chloride. *Water Research* 34, 1255-1261.

Merola, R.B., Hien T.T.., Quyen, D.T.T., Vengosh, A.., 2015. Arsenic exposure to drinking water in Mekong Delta. *Science of the Total Environment* 511, 544–552.

Michael, H.A., Voss, C.I., 2008. Evaluation of the sustainability of deep groundwater as an arsenic-safe resource in the Bengal Basin. *Proceedings of the National Academy of Sciences USA* 105, 8531-8536.

Michael, H.A., 2013. An arsenic forecast for China, *Science*, 341, 852-853, doi: 10.1126/science.1242212.

Michael, H.A., and, Khan, M.R., 2016. Impacts of physical and chemical aquifer heterogeneity on basin-scale solute transport: vulnerability of deep groundwater to arsenic contamination in Bangladesh. *Advances in Water Resources*, 98, 147-158.

Miller,G.P., 2001. Surface Complexation modeling of arsenic in natural water and sediment systems. Doctoral Dissertation, New Mexico Institute of Mining and Technology, Socorro, NM, USA

Moore J. N., Ficklin W. F., Johns C., 1988. Partitioning of arsenic and metals in reducing sulfidic sediments. *Environmental Science and Technology* 22,432–437.

Munoz, Mauricio Ormachea, Hannes Wern, Fredrick Johnsson, Prosun Bhattacharya, Ondra Sracek, Roger Thunvik, Jorge Quintanilla, and Jochen Bundschuh. 2013. Geogenic arsenic and other trace elements in the shallow hydrogeologic system of Southern Poopó Basin, Bolivian Altiplano. *Journal of hazardous materials* 262, 924-940.

Mukherjee, A.B. and Bhattacharya, P., 2001. Arsenic in groundwater in the Bengal Delta Plain: Slow Poisoning in Bangladesh. *Environmental Reviews* 9, 189-220.

Mukherjee, A., Fryar, A.E., Rowe, H.D., 2007. Regional-scale stable isotopic signatures of recharge and deep groundwater in the arsenic affected areas of West Bengal, India. *Journal of Hydrology* 334, 151– 161.

Mukherjee, A., Fryar, A.E., 2008. Deeper groundwater chemistry and geochemical modeling of the arsenic affected western Bengal Basin, West Bengal, India. *Applied Geochemistry*. 23, 863–894.

Mukherjee, A., von Brömssen, M., Scanlon, B.R., Bhattacharya, P., Fryar, A.E., Aziz Hasan, M., Ahmed, K.M., Chatterjee, D., Jacks, G., Sracek, O., 2008. Hydrogeochemical comparison and effects of overlapping redox zones on groundwater arsenic near the Western (Bhagirathi sub-basin, India) and Eastern (Meghna sub-basin, Bangladesh) margins of the Bengal Basin. *Journal of Contaminant Hydrology* 99, 31– 48.

Mukherjee, A., Scanlon, B.R., Fryar, A.E., Saha,D., Ghosh, A., Chowdhuri, S., Mishra, R. 2012. Solute chemistry and arsenic fate in aquifres between the Himalayan foothills and Indian craton (including Central Gangetic Plain): Influence of geology and geomorphology. *Goechimica et Cosmochimica Acta*. 90, 283-302.

Mukherjee, A., Verma, S., Gupta, S, Henke, R.K., Bhattacharya, P., 2014. Influence of tectonics, sedimentation and aqueous flow cycles on the origin of global groundwater arsenic: Paradigms from three continents. *Journal of Hydrology* 284–299.

Namasivayam, C. and Senthilkumar, S., 1998. Removal of arsenic (V) from aqueous solution using industrial solid waste: adsorption rates and equilibrium studies. *Industrial & Engineering Chemistry Research* 37, 4816 - 4822.

Nandy, D.R. 2000. General Consideration in Geodynamics of Northeastern India and adjoining region. abc publication, pp. 1-8.

Naiya, T.K., Bhattacharya, A.K., Das, S.K., 2009. Adsorption of Cd(II) and Pb(II) from aqueous solutions on activated alumina. *Journal of Colloid and Interface Science* 333, 14–26.

Nath, B., Berner, Z., Chatterjee, D., Mallik,S. B., Stu¨ben, D., 2008. Mobility of arsenic in West Bengal aquifers conducting low and high groundwater arsenic. Part II: Comparative geochemical profile and leaching study. *Applied Geochemistry* 23, 996–1011.

Nath, B., Chakraborty, S., Burnol, A., Stüben, D., Chatterjee, D. and Charlet, L., 2009. Mobility of arsenic in the sub-surface environment: An integrated hydrogeochemical study and sorption model of the sandy aquifer materials. *Journal of Hydrology 364*, 236-248.

Nath, B., Mallik, S.B., Stuben, D., Chatterjee, D., Charlet, L., 2010. Electrical Resistivity investigation of the arsenic affected alluvial aquifers in West Bengal, India: usefulness in identifying the areas of low and high groundwater arsenic. *Environmental Earth Science* 60, 873–884.

Nakano, A., Kurosawa, K., Shamim, U.M. and Tani, M., 2014. Geochemical assessment of arsenic contamination in well water and sediments from several communities in the Nawalparasi District of Nepal. *Environmental Earth Sciences 72*, 3269-3280.

Neidhardt, H., Berner, B. Z., Freikowski, D., Biswas, A., Majumder, S., Winter, J., Gallert, C., Chatterjee, D., Norra, S., 2014. Organic carbon induced mobilization of iron and manganese in a West Bengal aquifer and the muted response of groundwater arsenic concentrations. *Chemical Geology* 37, 51-62.

Nesbitt, H. W., G. W. Canning, and G. M. Bancroft, 1998. XPS study of reductive dissolution of 7Å-birnessite by H_3SiO_3, with constraints on reaction mechanism. *Geochimica et Cosmochimica Acta* 62, 2097-2110.

Nesbitt, H. W., & Young, G. M., 1982. Early Proterozoic climates and plate motions inferred from major element chemistry of lutites. *Nature* 299, 715–717. http://dx.doi.org/10.1038/299715a0

Neupane , G., Donahoe, R.J., Arai, Y., 2014. Kinetics of competitive adsorption/desorption of arsenate and phosphate at the ferrihydrite–water interface, *Chemical Geology* 368, 31–38

Nickson, R.T., McArthur, J.M., Burgess, W., Ahmed, K.M., Ravenscroft, P., Rahmanñ, M., 1998. Arsenic poisoning of Bangladesh groundwater. *Nature* 395, 338.

Nickson, R., McArthur, J., Ravenscroft, P., Burgess, W.G., Ahmed, K.M., 2000. Mechanism of arsenic release to groundwater, Bangladesh and West Bengal. *Applied Geochemistry* 15, 403–413.

Nordstrom, D. K, Archer, D.G., Arsenic thermodynamic data and environmental geochemistry. In *Arsenic in ground water*, 1-25. Springer US, 2003.

Nriagu, J.O., Bhattacharya, P., Mukherjee, A.B., Bundschuh, J., Zevenhoven, R. and Loeppert, R.H., 2007. Arsenic in soil and groundwater: an overview. *Trace Metals and other Contaminants in the Environment* 9, 3-60.

O'Day PA, Vlassopoulos D, Root R, Rivera N., 2004. The influence of sulfur and iron on dissolved arsenic concentrations in the shallow subsurface under changing redox conditions. *Proceedings of the National Academy of Sciences* 101: 13703-13708

Oke, I.A., Olarinoye, N.O. and Adewusi, S.R.A., 2008. Adsorption kinetics for arsenic removal from aqueous solutions by untreated powdered eggshell. *Adsorption* 14, 73-83.

Oscarson, D. W., P. M. Huang, and W. K. Liaw., 1980. The oxidation of arsenite by aquatic sediments. *Journal of Environmental Quality* 9, 700-703.

Ouvrard, S., Ph De Donato, M. O. Simonnot, S. Begin, J. Ghanbaja, M. Alnot, Y. B. Duval, F. Lhote, O. Barres, and M. Sardin., 2005 Natural manganese oxide: combined analytical approach for solid characterization and arsenic retention. *Geochimica et Cosmochimica Acta* 69, 2715-2724.

Oremland, Ronald S., and Stolz.,J.F. 2003. The ecology of arsenic. *Science* 300, 939-944.

Papacstas, N.C., Bostick, B.C., Quicksall, A.N., Landis, J.D., Sampson, M. 2008. Geomorphic controls on groundwater arsenic distribution in the Mekong River Delta, Cambodia. *Geology* 36, 891-894.

Parkhurst, D.L., Appelo, C.A.J., 1999. Users Guide to PHREEQC (Version 2) – A Computer Program for Speciation, Batch Reaction, One-dimensional Transport and Inverse Geochemical Calculations. U.S. Geol. Surv. *Water-Resources Investigations Reports* 95-4259.

Pederick, R. L., A. G. Gault, J. M. Charnock, D. A. Polya, and J. R. Lloyd., 2007. Probing the biogeochemistry of arsenic: response of two contrasting aquifer sediments from Cambodia to stimulation by arsenate and ferric iron. *Journal of Environmental Science and Health Part A* 42, 1763-1774.

Peikam, E.N. and Jalali, M., 2016. Application of Inverse Geochemical Modeling for Predicting Surface Water Chemistry in Ekbatan Watershed, Hamedan, Western Iran. *Hydrological Sciences Journal*, *61*, 1124-1134.

Pickering, J.L., Goodbred , S.L.,. Reitz, M.D., Hartzog , T.R., Mondal , D.R., Hossain, M.H., 2013. Late Quaternary sedimentary record and Holocene channel avulsions of the Jamuna and Old Brahmaputra River valleys in the upper Bengal delta plain. *Geomorphology*, 1-14.

Postma, D., Larsen, F., Minh Hue, N.T., Thanh Duc, M., Viet, P.H., Nhan, P.Q., Jessen, S., 2007. Arsenic in groundwater of the Red River floodplain, Vietnam: Controlling geochemical processes and reactive transport modeling. *Geochimica et Cosmochimica Acta* 71, 5054– 5071.

Postma, D., Jessen, S., Nguyen, T.M.H., Mai, T.D., Koch, C.B., Pham, H.V., Pham, Q.N., Larsen, F., 2010. Mobilization of arsenic and iron from Red River floodplain sediments, Vietnam. *Geochimica Cosmochimica Acta* 74, 3367–338.

Polizzotto, M.L., Kocar, B.D., Benner, S.G., Sampson, M., Fendrof, S., 2008. Near surface wetland sediments as a source of arsenic release to groundwater in Asia. *Nature*, 454, 505- 508.

Podgorski, J. E., Eqani, S. A. M. A. S., Khanam, T., Ullah, R., Shen, H., Berg, M., 2017. Extensive arsenic contamination in high-pH unconfined aquifers in the Indus Valley. *Science Advances* 3, 1-10

Plummer, L.N., 1992. Geochemical modeling of water-rock interaction: past, present, future. In: Kharaka, Y.K., Maest, A.S. (Eds), Water–Rock Interaction. Proc 7th Int. Conf. Balkema, Rotterdam, 23–33.

Pierce, M.L., and Moore, C.B., 1982. Adsorption of arsenite and arsenate on amorphous iron hydroxide. *Water Research* 16, 1247–1253.

Ravenscroft, P., Brammer, H., Richards, K.S., 2009. Arsenic pollution: a global synthesis. Wiley Blackwell, U.K.

Rajapaksha, A.U., Vithanage, M., Jayarathna, L. and Kumara, C.K., 2011. Natural Red Earth as a low cost material for arsenic removal: Kinetics and the effect of competing ions. *Applied Geochemistry* 26, 648-654.

Raju, N.J., Patel, P., Gurung, D., Ram, P., Gossel, W., Wycisk, P., 2015. Geochemical assessment of groundwater quality in the Dun valley of central Nepal using chemometric method and geochemical modeling. *Groundwater for Sustainable Development* 1, 135-145.

Raven KP, Jain A, Loeppert R.H., 1998. Arsenite and arsenate adsorption on ferrihydrite: kinetics, equilibrium, and adsorption envelopes. *Environmental Science and Technology* 32, 344–349.

Ray, D., Ghosh, Basu, D.R., S., Mohanty., Mandal. S.K. and Sardar, G.D., 1983. Subsurface Stratigraphy of an area northwest of Nazira syncline, Upper Assam Valley, *Journal of Geological Mineralogical Meterological Society of India*, 46.

Radloff, K.A., Zheng, Y., Michael, H.A., Stute, M., Bostick, B.C., Mihajlov, I., Bounds, M., Huq, M.R., Choudhury, I., Rahman, M.W. and Schlosser, P., 2011. Arsenic migration to deep groundwater in Bangladesh influenced by adsorption and water demand. *Nature Geoscience* 4, 793-798.

Radloff , K.A., Zheng, Y., stute, M., Weinman, B., Bostick, B., Mihajlov, I., Bouns, M., Rahman, M.M., Huq, M.R., Ahmed, K.M., Schlosser, Geen, A.V., 2017. Reversible adsorption and flushing of arsenic in a shallow, Holocene aquifer of Bangladesh. *Applied Geochemistry* 77, 142-157.

Randall, S.R., Sherman, D.M. and Ragnarsdottir, K.V., 2001. Sorption of As (V) on green rust ($Fe_4(II)Fe_2(III)(OH)_{12}SO_4 \cdot 3H_2O$) and lepidocrocite (γ-FeOOH): Surface complexes from EXAFS spectroscopy. *Geochimica et Cosmochimica Acta* 65, 1015-1023.

Redman, AD., Macalady, D.L. and Ahmann, D. 2002. Natural organic matter affects arsenic speciation and sorption onto hematite. *Environmental Science and Technology* 36, 2889-2896.

Reza, A.S., Jean, J.S., Yang, H.J., Lee, M.K., Woodall, B., Liu, C.C., Lee, J.F. and Luo, S.D., 2010. Occurrence of arsenic in core sediments and groundwater in the Chapai-Nawabganj District, northwestern Bangladesh. *Water Research 44*, 2021-2037.

Reza, A.H.M.S., Jean, J.S., Lee, M.K., Liu, C.C., Bundschuh, J., Yang, H.J., Lee, J.F., Lee, Y.C., 2010. Implications of organic matter on arsenic mobilization into groundwater: Evidence from northwestern (Chapai-Nawabganj), central (Manikganj) and southeastern (Chandpur) Bangladesh. *Water Research* 44, 5556-5574.

Rowland, H.A.L., Polya, D.A., Lloyd, J.R., Pancost, R.D., 2006. Characterisation of organic matter in a shallow, reducing, arsenic-rich aquifer, West Bengal. *Organic Geochemistry* 37, 1101-1114.

Robinson, C., von Bromssen, M., Bhattacharyya, P., Haller, S., Biven, A., Hossain, M., Jacks, G., Ahmed, K.M., Hasan, M.A., Thunvik, R., 2011. Dynamics of arsenic adsorption in the targeted As safe aquifers in Matlab, south eastern Bangladesh: Insights from experimental studies. *Applied Geochemistry* 26, 624-635

Rochette EA, Bostick BC, Li G, Fendorf S., 2000.Kinetics of arsenate reduction by dissolved sulfide. *Environmental Science and Technology* 34:4714–20

Roberts, L.C., Hug, S.J., Thomas, R., Morsaline Billaii, M.D., Khan, A.W., Mohammad, T.R., 2004. Arsenic removal with Iron(II) and Iron(III) in waters with high silicate and phosphate concentrations. *Environmental Science and Technology* 38, 307-315.

Rodriguez, R., Ramos, J.A., and Armienta, M.A. 2000. Groundwater arsenic variations: The role of local geology and rainfall. In Arsenic in groundwater of sedimentary aquifers. Edited by P. Bhattacharya and A.H. Welch. Pre-Congress Workshop Abstract Volume, 31st International Geological Congress, Rio de Janeiro, Brazil. pp. 75–77.

Saha, K.C., 2003. Review of arsenicosis in West Bengal, India: a clinical perspective. *Critical Reviews in Environmental Science and Technology* 30, 127–163.

Sahoo, M, Gogoi, K.D., 2011. Structural Styles and Its Implication on Petroleum Systems of North Assam Shelf, Upper Assam Basin, India. Search and Discovery Article #40750; Adapted from extended abstract presented at GEO-India, Greater Noida, New Delhi, India

Sahu, S., Saha, D., 2015. Role of shallow alluvial stratigraphy and Holocene geomorphology on groundwater arsenic contamination in the Middle Ganga Plain, India. *Environmental Earth Sciences* 73(7), 3523–3536

Saha, D., Shukla, R.R., 2013. Genesis of arsenic rich groundwater and the search for alternative safe aquifers in the Gangetic Plain India. *Water Environment Research* 85(12), 2254–2264

Sailo, L., Mahanta, C., 2016. Natural attenuation processes of arsenic in the groundwater of the Brahmaputra floodplain of Assam, India *Environmental Science.: Processes Impacts* 18, 115-125

Sankar, M. S., Vega, M. A., Defoe, P. P., Kibria, M. G., Ford, S., Telfeyan, K., et al. 2014. Elevated arsenic and manganese in groundwaters of Murshidabad, West Bengal, India. *Science of the Total Environment* 488–489, 570–579.

Saunders, J.A., Lee, M. K., Uddin, A., Mohammad, S., Wilkin, R.T., Fayek, M., Korte, N.E. 2005a. Natural arsenic contamination of Holocene alluvial aquifers by linked tectonic, weathering and microbial processes. *Geochemisty Geophysics Geosystems*, 6(4).

Savage, K.S., Bird, D.K., O'Day, P.A., 2005. Arsenic speciation in synthetic jarosite. *Chemical Geology* 215, 473-498.

Sengupta, S., Mukherjee, P. K., Pal, T., Shome, S., 2004. Nature and origin of arsenic carriers in shallow aquifer sediments of Bengal Delta, India. *Environmental Geology* 45, 1071–1081.

Sengupta, S., McArthur, J.M., Sarkar, A., Leng, M.J., Ravenscroft, P., Howarth, R.J. and Banerjee, D.M., 2008. Do ponds cause arsenic-pollution of groundwater in the Bengal Basin? An answer from West Bengal. Environmental Science & Technology 42, 5156-5164.

Sharif, M.S.U., Davis, R.K., Steele, K.F., Kim, B., Hays, P.D., Kresse, T.M. and Fazio, J.A., 2011. Surface complexation modeling for predicting solid phase arsenic concentrations in the sediments of the Mississippi River Valley alluvial aquifer, Arkansas, USA. *Applied Geochemistry* 26,496-504.

Shivanna, K., Sharma, S., Sinha, U.K., Nair, A.R., Navada, S.V., Ray, A., Talukdar, T., Mehta, B.C., Ghosh, A.K., 1999. Arsenic pollution in ground water of West Bengal. In: Proceedings of Workshop on Groundwater Pollution and Its Protection with Special Reference to Arsenic Contamination. Central Ground Water Board, Calcutta.

Sherman, D.M. and Randall, S.R., 2003. Surface complexation of arsenic (V) to iron (III)(hydr) oxides: structural mechanism from ab initio molecular geometries and EXAFS spectroscopy. *Geochimica et Cosmochimica Acta* 67, 4223-4230.

Smedley, P.L., Kinniburgh, D.G., 2002. A review of the source, behavior and distribution of arsenic in natural waters. *Applied Geochemistry* 17, 517–568.

Smedley, P.L., Zhang, M., Zhang, G., Luo, Z. 2003. Mobilization of arsenic and other trace elements in fluvio lacustrine aquifers of the Huhhot Basin, Inner Mongolia. *Applied Geochemistry* 18, 1453–1477

Smedley, P L., 2008. Sources and distribution of arsenic in groundwater and aquifers. In: Arsenic in Groundwater: a World Problem. Appelo, C A J (editor). Proceedings of an IAH Seminar, Utrecht, November 2006, pp 4–32.

Smith, S.L., Jaffe, P.R., 1998. Modeling the Transport and Reactions of Trace Metal in Water Saturated Soils and Sediments. *Water Resources Research*, 34(11), 3135-3147.

Smith, A.H., Lingas, E.O. and Rahman, M., 2000. Contamination of drinking-water by arsenic in Bangladesh: a public health emergency. B*ulletin of the World Health Organization* 78(9), 1093-1103.

Singh, D.B., Prasad, G., Rupainwar, D.C. and Singh, V.N., 1988. As (III) removal from aqueous solution by adsorption. *Water, Air, & Soil Pollution* 42(3), 373-386.

Singh, A.K. Arsenic contamination in groundwater of North Eastern India. In Proceedings of 11th National Symposium on Hydrology with Focal Theme on Water Quality, National Institute of Hydrology, Roorkee, 2004, 255–262.

Singh, S.K., Kumar, A. and France-Lanord, C., 2006. Sr and $^{87}Sr/^{86}Sr$ in waters and sediments of the Brahmaputra river system: Silicate weathering, CO 2 consumption and Sr flux. *Chemical Geology* 234, 308-320.

Sikdar P. K., Sahu, P. 2009. Understanding wetland sub-surface hydrology using geologic and isotopic signatures. *Hydrology and Earth System Sciences Journal* 13, 1313–1323.

Sparks, D.L., 1999. Soil physical chemistry. CRC press, Taylor and Francis group.

Sposito,G., 1989.The Chemistry of Soils. Oxford University Press, New York.

Stollenwerk, K.G., 2005. Arsenic Attenuation by Oxidized Aquifer Sediments, Bangladesh, Behavior of Arsenic in Aquifers, Soils and Plants: Implications for Management. International Maize and Wheat Improvement center (CYMMYT),Cornell University, Texas A&M University, United States Geological Survey, Geological Survey of Bangladesh, Dhaka, Bangladesh.

Stollenwerk, K.G., Breit, G.N., Welch, A.H., Yount, J.C., Whitney, J.W., Foster, A.L., Uddin, M.N., Majumder, R.K., Ahmed, N., 2007. Arsenic attenuation by oxidized sediments in Bangladesh. *Science of the Total Environment* 379, 133–150.

Stumm , W., Morgan, J.J., 1996. Aquatic Chemistry. 3rd Edition, Wiley and Sons, New York.

Stute, M., Zheng, Y., Schlosser, P., Horneman, A., Dhar, R.K., Datta, S., Hoque, M.A., Seddique, A.A., Shamsudduha, M., Ahmed, K.M., van Geen, A., 2007. Hydrological control of As concentrations in Bangladesh Groundwater. *Water Resources Research* 43, W09417.

Steinmaus, C.M., Ferreccio, C., Acevedo Romo, J., Yuan, Y., Cortes, S., Marshall, G., Moore, L.E., Balmes, J.R., Liaw, J., Golden, T., Smith, A.H., 2013. Drinking water arsenic in northern Chile: high cancer risks 40 years after exposure cessation. *Cancer Epidemiology Biomarkers Prevention* 22,623–630.

Stachowicz, M., Hiemstra, T., van Riemsdijk, W.H., 2008. Multi competitive interactions of As(III) and As(V) oxyanions with Ca^{2+}, Mg^{2+}, PO_4^{3-} and CO_3^{2-} ions on goethite. *Journal of Colloid and Interface Science* 320, 400-414

Stüben, D., Berner, Z., Chandrasekharam, D. and Karmakar, J., 2003. Arsenic enrichment in groundwater of West Bengal, India: geochemical evidence for mobilization of As under reducing conditions. *Applied Geochemistry* 18, 1417-1434.

Smedley,P.L., Kinniburgh, D.G. A review of the source, behavior and distribution of arsenic in natural waters. 2002. *Applied Geochemistry* 17, 517–568.

Sracek, O., Bhttacharyya, P., Jack,G., Gustafsson, Bromssen, M.V., 2004. Behaviour of arsenic and geochemical modeling of arsenic enrichment in aqueous environments. *Applied Geochemistry* 19, 169-180.

Su, C. and Puls, R.W., 2001. Arsenate and arsenite removal by zerovalent iron: kinetics, redox transformation, and implications for in situ groundwater remediation. *Environmental Science & Technology*, *35*:1487-1492.

Stollenwerk, K.G., Breit, G.N., Welch, A.H., Yount, J.C., Whitney, J.W., Forster , A.L., Uddin, M.N., Majumdar , R.K., Ahmed, N., 2007. Arsenic attenuation by oxidized sediments in Banglaesh. *Science of the Total Environment* 379, 133-150.

Swedlund, P.J, Webster, J. G. 1999. Adsorption and polymerization of silicic acid on ferrihydrite and its effect on arsenic adsorption. *Water Research* 33, 3413–22.

Swartz, C.H., Blute, N.K., Badruzzman, B., Ali, A., Brabander, D., Jay, J., Besancon, J., Islam, S., Hemond, H.F, Harvey, C., 2004. Mobility of arsenic in Bangladesh aquifer: inferences from geochemical profiles, leaching data and mineralogical characterization. *Geochimica et Cosmochimica Acta* 68, 539-557.

Stahl, M. O., C. F. Harvey, A. van Geen, J. Sun, P. Thi Kim Trang, V. Mai Lan, T. Mai Phuong, P. Hung Viet, and Bostick. B. C., 2016. River bank geomorphology controls groundwater arsenic concentrations in aquifers adjacent to the Red River, Hanoi Vietnam, *Water Resources Res*earch 52, 6321– 6334, doi: 10.1002/2016WR018891.

Tardy, Y., 1971. Characterization of the principal weathering types by the geochemistry of waters from some European and African crystalline massifs. *Chemical Geology* 7, 253-271.

Thronton, I., 1996. Sources and pathways of arsenic in the geochemical environment: health implications. In: Appleton, J.D., Fuge, R., McCall, G.J.H. (Eds.), *Environmental Geochemistry and Health*, 113, 153-161.

Tucker, M.E., 1991. Sedimentary Petrology. Blackwell Science, UK.

Umitsu, Masatomo, 1993.Late Quaternary sedimentary environments and landforms in the Ganges Delta. *Sedimentary Geology* 83, 177-186.

van Geen, A., Zheng, Y., Versteeg, R., Stute, M., Horneman, A., Dhar, R.K., Steckler, R., Gelman, M., Small, C., Ahsan, H., Graziano, J.H., Hussein, I., Ahmed, K.M., 2003. Spatial variability of arsenic in 6000 tubewells in a 25 km2 area of Bangladesh. *Water Resource Research*, 39, 1140.

van Geen, A.., Rose, J., Thoral, S., Garnier, J.M., Zheng, Y., Bottero, J.Y., 2004. Decoupling of As and Fe release to Bangladesh groundwater under reducing conditions. Part II: evidences from sediment incubations. *Geochemica et Cosmochimica Acta* 68, 3475-3486.

van Geen, A.., 2011. International Drilling to Recover Aquifer Sands (IDRAs) and Arsenic Contaminated Groundwater in Asia, *Scientific Drilling* 12, 49-52, https://doi.org/10.2204/iodp.sd.12.06.2011, 2011.

van Geen, A., Bostick, B.C., Trang, P.T.K., Lan, V.M., Mai, N.N., Manh, P.D., Viet, P.H., Radloff, K., Aziz, Z., Mey, J.L. and Stahl, M.O., 2013. Retardation of arsenic transport through a Pleistocene aquifer. *Nature* 501, 204-207.

Verma. S., Mukherjee, A., Choudhury, R., Mahanta, C., 2014. Brahmaputra river basin groundwater: Solute distribution, chemical evolution and arsenic occurrences in different geomorphic settings. *Journal of Hydrology: Regional Studies* 1-23

von Brömssen, M., Jakariya, M., Bhattacharya, P., Ahmed, K.M., Hasan, M.A., Sracek, O., Jonsson, L., Lundell, L., Jacks, G., 2007. Targeting low-arsenic aquifers in Matlab Upazila, southeastern Bangladesh. *Science of the Total Environment* 379, 121–132.

Voegelin, Andreas, and Stephan J. Hug., 2003. Catalyzed oxidation of arsenic (III) by hydrogen peroxide on the surface of ferrihydrite: an in situ ATR-FTIR study. *Environmental Science & Technology* 37, 972-978.

Waltham, C., Eick, M., 2002. Kinetics of arsenic adsorption on goethite in the presence of sorbed silicic acid. *Soil Science Society of America Journal* 66, 818–825. doi:10.2136/sssaj2002.8180

Welch A.H., Lico M.S., Hughes J.L., 1988. Arsenic in ground water of the western United States. *GroundWater* 26, 333–347.

Welch, A.H., Westjohn, D.B., Helsel, D.R., Wanty, R.B., 2000. Arsenic in groundwater of the United States : occurrences and geochemistry. *Ground Water* 38, 589-604.

Weber, W.J. Jr., Morris, J.C. 1963. Kinetics of adsorption on carbon from solution. *Journal of the Sanitation Engineering Division* 89, 31–59

Wenzel, W.W., Kirchbaumer, N., Prohaska, T., Stingeder, G., Lombi, E., Adriano, D.C., 2001. Arsenic fractionation in soils using an improved sequential extraction procedure. *Analytica Chimica Acta* 436, 309–323.

Weidemann, D., Kuo, C.C., Acien , A.N., , Abrahama, A.G., Weaver , V., Fadrowski, J., 2015. Association of arsenic with kidney function in adolescents and young adults: Results from the National Health and Nutrition Examination Survey 2009–2012. *Environmental Research* 140 , 317–324

Wilkie, J.A., and Hering, J.G., 1996. Adsorption of arsenic onto hydrous ferric oxide: Effects of adsorbate-adsorbent ratios and co-occurring solutes. *Colloids Surfaces A*, 107, 97-110.

Winkel, L., Berg, M., Amini, M., Hug, S.J., & Johnson, Annette, C., 2008. Predicting groundwater arsenic contamination in Southeast Asia from surface parameters. *Nature Geoscience* 1, 536 – 542.

Weinman, B., Goodbred, S.L., Zheng, Y., Aziz, Z., Steckler, M., van Geen, A., Singhvi, A.K. and Nagar, Y.C. (2008). Contributions of floodplain stratigraphy and evolution to the spatial patterns of groundwater arsenic in Araihazar, Bangladesh. *Geological Society of America Bulletin* 120(11-12): 1567-1580.

Williams, L.E., Barnett, M.O., Kramer, T.A. and Melville, J.G., 2003. Adsorption and transport of arsenic (V) in experimental subsurface systems. *Journal of Environmental Quality* 32, 841-850.

Xie, X., Wang, Y, Ellis, A., Liu, C., Duan, M., Li, J. 2014. Impact of sedimentary provenance and weathering on arsenic distribution in aquifers of the Datong basin, China: Constraints from elemental geochemistry. *Journal of Hydrology*. 519, 3541–3549

Yadav, I.C., Devi, N.L., Singh, S., 2015. Spatial and temporal variation in arsenic in the groundwater of upstream of Ganges River Basin. Nepal. *Environmental Earth Science* 73(3), 1265-1279.

Yang, N., Winkel, L. H.E., and Johannesson, K.H., 2014. Predicting Geogenic Arsenic Contamination in Shallow Groundwater of South Louisiana, United States. *Environment Science and Technology* 48, 5660−5666

Yang, H.J.,Lee, C.U., Chiang, Y.J., Jean,J.S., Shauc, Y.., Takazawa,E., Jiang.W.T., 2016. Distribution and hosts of arsenic in a sediment core from the Chianan Plain in SW Taiwan: Implications on arsenic primary source and release mechanisms. *Science of The Total Environment* 569, 212–222.

Yuan, Y., Marshall, G., Ferreccio, C., Steinmaus, C., Liaw, J., Bates, M., Smith, A.H., 2010.Kidney cancer mortality: fifty-year latency patterns related to arsenic exposure. *Epidemiology* 21, 103–108.

Zela, S and Mahanta, C. 2015. Natural attenuation processes of Arsenic in the groundwater of Brahmaputra floodplain of Assam, India. *Environmental Science: Processes and Impact* 18(1), 115-125.

Zhang, Hua, and H. M. Selim. 2005. Kinetics of arsenate adsorption− desorption in soils. *Environmental Science & Technology* 39, 6101-6108.

Zhang, Y., Cao, W., Wang, W. and Dong, Q., 2013. Distribution of groundwater arsenic and hydraulic gradient along the shallow groundwater flow-path in Hetao Plain, Northern China. *Journal of Geochemical Exploration* 135, 31-39.

Zheng, Y., Stute, M., van Geen, A., Gavrieli, I., Dhar, R., Simpson, H.J., Schlosser, P., Ahmed, K.M., 2004. Redox control of arsenic mobilization in Bangladesh groundwater. *Applied Geochemistry*19, 201–14.

Zhou, Y., Zeng, Y., Zhou, J, Guo, H., Li,Q., Jia, R., Chen, Y., Zhao, J., 2016. Distribution of groundwater arsenic in Xinjiang, P.R. China. *Applied Geochemistry* 77,116-125.

Zhu, Y., Zhao, X., Chen, M., Luo, Y. and Zhou, X., 2015. Characteristics of high arsenic groundwater in Hetao Basin, Inner Mongolia, northern China. S*cience of Cold and Arid Regions* 7, 104-110.

Ziegler,B.A., Schreiber,M.E., Cozzarelli, I.M., 2017. The role of alluvial aquifer sediments in attenuating a dissolved arsenic plume. *Journal of Contaminant Hydrology* doi: 10.1016/j.jconhyd.2017.04.009.

Appendix A1

Groundwater Quality from the study transects

A.1.1 Groundwater Quality from along Northern Transect

Sample ID	Latitude	Longitude	Type of Source	pH	EC	TDS	As (ppb)	Fe	Mn	Na	K	Ca	Mg	HCO_3	SO_4	NO_3	Cl	PO_4	Depth (m)
N1	26.4409	91.9515	Private	6.6	326.0	208.6	60.7	23.3	1.1	8.0	3.2	8.3	5.2	118.0	5.4	0.1	7.0	1.1	19.8
N2	26.4406	91.9508	Private	7.0	104.0	66.6	27.2	24.0	0.4	10.4	1.4	12.4	1.2	111.0	4.4	2.2	10.0	1.0	19.8
N3	26.4403	91.9503	Private	6.7	301.0	192.6	41.0	30.5	1.2	16.1	1.0	12.9	6.7	104.0	10.4	2.8	9.0	0.4	16.8
N4	26.4405	91.9506	Private	6.7	184.0	117.8	26.8	33.0	0.8	11.5	2.2	8.7	13.2	120.0	10.0	1.2	12.0	1.2	19.8
N5	26.4447	91.9564	Private	6.8	146.4	93.7	21.1	18.6	0.7	11.5	2.5	7.4	12.2	118.0	8.8	0.6	9.5	0.6	37.8
N6	26.4398	92.0698	Private	6.9	269.0	172.2	26.0	18.8	1.4	8.7	2.5	10.0	18.2	85.0	10.0	1.2	9.0	1.1	19.8
N7	26.4398	92.0693	Private	6.7	160.0	102.4	27.1	10.9	1.1	7.6	2.0	11.3	10.7	95.0	12.0	0.3	11.5	1.3	24.0
N8	26.4400	92.0693	Private	6.7	168.0	107.5	29.0	10.8	1.3	7.6	2.0	1.1	24.6	105.0	8.7	1.1	10.5	1.2	13.8
N9	26.4399	91.9495	Private	6.7	190.5	121.9	32.0	27.1	0.6	14.7	1.7	8.1	10.6	108.0	15.1	0.2	9.2	1.4	19.8
N10	26.4413	91.9524	Private	6.7	177.0	113.3	21.1	26.0	0.8	9.5	1.8	8.0	4.2	80.0	3.3	0.0	9.4	1.2	30.0
N11	26.4413	91.9516	Private	7.0	169.0	108.2	26.8	25.4	0.4	13.3	1.8	7.5	13.4	95.0	6.3	0.5	7.1	1.1	25.8
N12	26.4397	91.9525	Private	6.7	150.1	96.1	28.1	17.1	0.5	10.8	2.0	11.4	4.7	114.0	8.0	2.0	15.2	1.0	22.8
N13	26.4740	92.0725	Private	6.8	174.0	111.4	28.8	23.2	1.1	9.4	3.1	8.7	10.7	123.0	7.1	1.3	6.0	1.2	25.5
N14	26.4735	92.0690	Private	6.9	153.0	97.9	28.4	13.9	1.0	8.0	2.1	9.1	6.1	120.0	2.5	1.3	11.5	0.9	22.5
N15	26.4733	92.0690	Private	6.7	164.0	105.0	28.9	17.1	1.2	7.8	2.3	8.2	12.5	105.0	6.2	1.0	11.0	1.2	24.0
N16	26.4754	92.0734	Private	6.9	136.0	87.0	11.7	15.5	0.6	7.2	2.7	3.6	8.5	95.0	10.4	1.8	9.5	1.1	25.8
N17	26.4765	92.0720	Private	6.7	151.5	97.0	20.4	18.9	0.6	7.7	3.0	8.5	12.3	126.0	6.5	0.9	4.0	1.1	19.8
N18	26.4741	92.0714	Private	6.7	194.6	124.5	15.2	24.5	1.5	8.8	2.3	8.1	14.5	114.0	3.9	2.8	9.0	1.0	27.0
N19	26.4390	92.0157	Private	6.8	139.5	89.3	6.9	16.3	0.5	8.3	3.6	8.7	3.5	119.0	6.7	0.0	10.0	1.2	18.0
N20	26.4390	92.0157	Private	6.7	149.7	95.8	10.8	19.1	0.7	7.6	2.0	8.6	4.5	120.0	8.9	0.3	12.1	1.1	18.0
N21	26.4381	92.0146	Private	6.7	152.7	97.7	8.7	14.2	0.5	7.3	2.8	8.7	10.3	112.0	10.0	0.5	8.0	1.4	13.8
N22	26.4385	92.0144	Private	6.7	172.0	110.1	12.4	23.1	1.0	8.2	2.7	10.4	23.8	104.0	4.2	0.0	11.0	1.4	13.5
N23	26.4319	92.0094	Private	6.7	775.0	496.0	1.6	1.8	1.3	27.4	7.9	13.0	6.1	164.0	2.1	0.6	12.1	1.0	10.5

N24	26.4340	92.0099	Private	6.9	162.5	104.0	0.7	10.1	0.8	8.7	7.0	8.2	12.5	110.0	8.9	0.4	12.0	1.4	25.8
N25	26.4800	92.0910	Public	6.9	183.0	117.1	0.1	2.7	0.2	10.6	5.4	15.6	8.8	172.1	13.0	1.7	12.7	1.1	39.6
N26	26.4790	92.1110	Public	7.4	195.0	124.8	55.4	0.7	1.4	9.1	3.3	30.9	8.5	135.4	16.6	1.2	6.1	1.1	24.4
N27	26.4850	92.1150	Public	7.5	93.0	59.5	2.9	2.9	0.6	6.3	3.1	12.9	7.4	128.1	4.4	3.2	2.8	1.4	39.6
N28	26.4880	92.1160	Public	7.3	163.0	104.3	28.2	6.4	0.9	6.2	9.5	23.1	9.6	120.8	4.0	2.5	3.2	1.0	23.2
N29	26.3570	91.9290	Public	7.5	189.0	121.0	0.0	1.8	0.6	23.3	1.9	18.0	9.4	172.1	4.9	1.1	2.6	1.2	20.1
N30	26.3570	91.9320	Public	7.7	231.0	147.8	2.4	1.8	0.8	19.6	1.8	27.3	15.0	201.4	2.3	1.7	3.6	1.2	39.6
N31	26.5460	92.2600	Public	6.8	172.0	110.1	20.4	19.4	0.9	7.6	5.1	19.1	6.8	128.1	0.9	1.4	2.1	1.0	39.6
N32	26.5460	92.2630	Public	6.8	228.0	145.9	3.7	5.6	0.4	11.7	4.4	16.8	2.6	113.7	0.7	1.3	4.6	1.1	39.6
N33	26.5300	92.2390	Public	7.1	134.0	85.8	21.9	9.2	1.3	13.3	2.4	13.3	5.8	113.7	1.5	1.2	2.2	1.1	23.2
N34	26.5100	92.2170	Public	6.8	117.0	74.9	18.7	6.3	2.2	12.9	3.9	24.1	8.6	135.6	1.2	1.2	2.2	1.2	39.6
N35	26.4180	91.9920	Public	6.5	316.0	202.2	50.4	14.9	4.8	11.2	3.5	28.3	17.0	226.9	2.6	2.0	5.2	0.6	36.6
N36	26.4100	91.9890	Public	6.5	188.0	120.3	4.3	20.7	1.6	9.1	5.9	12.0	7.4	107.7	2.8	5.1	5.9	1.4	20.1
N37	26.4040	91.9870	Public	6.6	142.0	90.9	1.0	10.1	1.1	14.1	3.7	8.3	4.7	108.5	3.0	4.8	2.0	1.2	39.6
N38	26.4480	91.9820	Public	6.2	101.0	64.6	1.1	9.8	1.4	6.6	2.4	6.7	6.0	95.3	4.5	4.1	2.1	1.3	39.6
N39	26.4570	91.9770	Public	6.5	205.0	131.2	38.2	25.9	1.2	11.9	3.6	9.1	7.0	106.9	2.8	1.3	2.9	0.8	19.8
N40	26.4580	91.9770	Public	6.6	195.0	124.8	40.9	23.6	1.2	11.7	2.4	10.8	7.3	174.8	2.5	6.5	2.1	0.9	20.1
N41	26.4530	91.9560	Public	6.5	198.0	126.7	16.2	8.5	1.2	17.0	1.5	13.9	5.4	131.9	14.2	1.4	2.8	1.2	20.1
N42	26.4720	92.0700	Public	7.3	180.0	115.2	30.9	27.4	1.5	9.3	3.3	14.9	11.4	110.0	2.6	31.0	2.6	1.2	20.1
N43	26.4730	92.0700	Public	6.9	164.0	105.0	21.2	24.6	0.9	13.0	3.2	15.1	9.0	110.1	2.7	1.2	3.0	0.9	14.7
N44	26.4740	92.0720	Public	6.8	209.0	133.8	7.7	25.5	1.6	11.2	3.1	15.4	9.3	241.8	4.1	1.3	7.2	2.0	32.0
N45	26.4750	92.0730	Public	6.9	172.0	110.1	16.6	18.1	1.2	11.6	3.3	15.4	7.9	154.0	2.7	1.2	2.0	1.7	30.3
N46	26.4760	92.0750	Public	6.7	114.0	73.0	4.3	18.1	0.6	8.8	2.3	12.7	4.8	121.1	2.9	1.2	1.7	1.2	32.0
N47	26.4870	92.0660	Public	7.0	122.0	78.1	9.3	1.6	1.3	14.5	2.9	10.6	5.8	150.0	5.4	1.5	3.5	1.7	39.6
N48	26.4420	91.9080	Public	7.6	152.0	97.3	5.9	3.0	0.4	23.5	2.2	5.7	3.8	113.5	5.4	1.5	3.4	1.2	36.6
N49	26.4260	91.9100	Public	7.2	205.0	131.2	14.5	7.7	0.8	9.1	1.1	14.2	7.8	106.2	3.4	1.3	2.9	1.0	36.6
N50	26.4070	91.9040	Public	7.1	140.0	89.6	2.8	5.2	0.4	11.4	1.0	19.6	5.6	114.8	2.9	1.3	5.4	1.2	38.1
N51	26.4060	91.9080	Public	7.5	129.0	82.6	0.8	3.9	0.4	11.7	2.3	15.8	6.3	113.6	5.4	1.4	7.6	1.0	42.7
N52	26.4040	91.8660	Public	7.4	171.0	109.4	0.5	1.1	0.2	10.7	1.3	17.4	6.6	157.5	7.6	2.2	8.9	1.0	32.6
N53	26.4020	91.8660	Public	7.3	172.0	110.1	0.2	1.3	0.2	15.0	1.3	18.0	7.5	150.0	8.9	1.2	4.8	2.7	59.2
N54	26.3980	91.8650	Public	7.5	184.0	117.8	0.2	1.2	0.2	5.1	2.3	10.6	1.5	164.7	4.8	1.2	5.0	2.1	44.2

N55	26.4140	91.8800	Public	7.4	157.0	100.5	1.1	11.3	0.6	13.2	1.2	15.3	5.4	128.1	5.0	1.3	1.3	1.5	38.1
N56	26.4130	91.8870	Public	7.2	148.0	94.7	5.8	7.5	0.6	11.7	2.0	16.8	5.0	150.2	1.3	1.6	2.1	1.8	25.5
N57	26.3700	91.9400	Public	7.6	165.0	105.6	7.9	3.2	0.5	15.9	2.1	19.4	9.9	142.7	0.9	1.8	1.9	1.8	39.6
N58	26.3720	91.9350	Public	7.6	144.0	92.2	1.0	2.1	0.3	12.8	1.6	15.2	8.0	150.1	2.1	1.3	2.0	1.2	36.6
N59	26.3720	91.9360	Public	7.5	201.0	128.6	1.0	2.9	0.3	18.9	1.8	22.1	11.2	172.1	1.6	1.7	3.2	1.1	36.6
N60	26.4330	92.0010	Public	6.2	165.0	105.6	6.0	28.8	1.4	8.0	4.0	11.9	9.1	113.5	3.5	9.1	3.8	1.0	6.4
N61	26.4390	92.0250	Public	6.8	215.0	137.6	3.2	20.1	1.0	12.3	4.3	16.0	8.4	142.9	0.9	1.4	4.4	1.1	39.6
N62	26.5440	92.2090	Public	7.0	324.0	207.4	52.2	4.8	3.5	6.7	3.9	60.5	17.8	98.9	4.1	1.2	1.6	1.1	46.2
N63	26.5540	92.0460	Public	6.5	159.2	101.9	17.5	14.8	0.7	9.1	5.9	9.7	5.6	69.8	1.6	1.4	5.6	1.2	39.6
N64	26.5540	92.0460	Public	6.4	58.0	37.1	2.6	16.6	0.9	8.0	2.8	7.2	2.8	62.7	5.6	1.6	1.0	1.2	14.3
N65	26.5520	92.0540	Public	6.1	164.0	105.0	5.4	22.6	1.4	9.3	3.1	8.1	4.9	70.0	4.3	3.3	4.6	2.0	32.0
N66	26.5200	92.0320	Public	6.4	124.0	79.4	2.0	2.6	1.4	9.5	3.6	14.2	5.5	106.3	1.2	1.4	2.2	1.6	17.3
N67	26.5010	92.0310	Public	6.3	120.0	76.8	0.8	2.3	5.9	8.7	1.7	12.7	7.5	99.6	2.3	1.4	3.1	2.7	39.6
N68	26.5070	92.0380	Public	6.3	201.0	128.6	10.3	20.2	1.7	10.3	5.3	15.4	8.1	107.4	1.3	1.4	5.2	1.2	39.6
N69	26.4820	92.0310	Public	6.4	204.0	130.6	31.5	17.1	2.2	10.8	1.6	15.1	10.2	142.9	2.6	1.6	2.9	1.2	39.6
N70	26.4620	92.0350	Public	6.5	230.0	147.2	0.9	22.1	1.1	12.2	3.2	15.8	13.4	128.3	4.4	1.2	8.4	1.9	36.6
N71	26.4650	92.0420	Public	6.4	219.0	140.2	17.6	17.9	2.2	10.9	3.6	20.2	11.2	113.7	10.6	2.8	10.0	1.6	36.6
N72	26.4500	91.9280	Public	6.1	225.0	144.0	14.7	15.4	0.7	25.1	1.4	11.4	6.4	171.1	2.7	6.5	4.9	1.3	39.6
N73	26.4600	91.9290	Public	6.3	319.0	204.2	48.5	18.2	1.7	17.8	5.9	23.3	16.2	227.4	2.9	6.5	5.8	0.6	36.6
N74	26.4400	91.9260	Public	6.2	258.0	165.1	17.1	4.1	0.9	46.6	1.4	13.1	10.3	215.0	2.8	5.2	4.4	0.2	39.6
N75	26.4690	91.9470	Public	6.3	192.0	122.9	18.0	16.5	1.1	18.4	1.6	11.2	7.6	193.9	3.1	1.9	2.1	0.1	26.2
N76	26.4740	91.9440	Public	6.8	199.0	127.4	30.7	28.3	0.9	11.0	1.6	11.0	7.1	127.7	11.1	1.7	2.3	1.5	39.6
N77	26.4730	91.9490	Public	6.3	171.0	109.4	13.5	15.2	0.9	15.7	1.9	12.4	5.9	137.8	7.0	3.9	2.3	1.4	39.6
N78	26.4730	91.9530	Public	6.2	197.0	126.1	12.4	23.8	1.4	12.1	3.7	11.6	6.8	133.5	6.0	4.2	4.0	1.5	39.6
N79	26.4660	91.9640	Public	6.6	217.0	138.9	16.5	24.6	2.1	11.0	6.9	11.0	8.7	98.8	3.1	1.8	7.9	1.4	36.6
N80	26.4600	91.9600	Public	6.6	230.0	147.2	37.9	27.2	1.1	15.0	1.7	12.9	8.4	150.9	2.9	2.0	3.3	1.6	36.6
N81	26.4700	91.9260	Public	6.7	214.0	137.0	25.7	14.9	1.1	28.2	2.3	16.1	8.3	168.4	3.0	1.6	2.3	0.8	19.8
N82	26.4590	91.9260	Public	6.9	195.0	124.8	70.9	11.5	1.6	15.8	1.4	16.2	6.3	170.7	3.1	1.5	2.7	1.5	20.5
N83	26.4760	91.8830	Public	6.6	174.0	111.4	29.5	11.7	0.7	22.8	1.0	10.9	5.6	139.1	5.1	2.8	3.2	1.1	39.6
N84	26.4710	91.8830	Public	6.6	202.0	129.3	37.9	15.4	0.9	24.0	1.5	11.5	6.3	154.0	3.6	1.4	2.0	1.1	36.6
N85	26.4810	91.8830	Public	6.6	199.0	127.4	50.4	14.2	0.9	25.1	1.1	12.6	7.0	124.5	3.4	1.4	2.3	1.2	18.3

N86	26.4950	91.8810	Public	6.7	220.0	140.8	40.9	17.2	0.7	25.5	1.2	13.5	7.4	153.8	4.0	2.3	2.6	1.0	19.8
N87	26.4980	91.8750	Public	6.6	180.0	115.2	43.9	13.5	0.5	23.3	1.1	10.6	5.8	153.9	2.7	1.9	1.9	1.4	39.6
N88	26.5040	91.8790	Public	6.5	204.0	130.6	37.4	16.8	0.9	23.4	1.2	12.2	6.4	164.8	2.6	1.6	2.4	1.2	39.6
N89	26.5110	91.8440	Public	6.8	153.0	97.9	53.5	14.0	0.5	21.4	1.1	8.2	5.0	139.2	3.9	5.5	2.5	1.0	36.6
N90	26.5200	91.8240	Public	7.4	158.0	101.1	50.1	11.4	0.5	21.2	1.4	12.5	6.1	124.5	2.8	1.3	1.7	1.0	39.6
N91	26.5180	91.8250	Public	7.1	209.0	133.8	134.0	12.7	0.9	26.6	1.3	14.4	8.4	268.5	2.7	1.2	1.7	0.6	26.2
N92	26.4980	91.8350	Public	7.2	215.0	137.6	72.2	16.2	0.7	25.4	1.1	14.1	7.5	198.5	0.1	1.2	2.1	1.1	38.1
N93	26.5070	91.8260	Public	7.2	170.0	108.8	33.5	11.3	0.4	20.9	1.3	11.2	6.2	139.9	3.7	2.7	2.0	0.7	21.0
N94	26.5120	91.8700	Public	6.9	264.0	169.0	3.3	41.0	1.8	14.0	11.0	14.9	10.4	98.4	3.3	5.6	2.6	2.0	38.1
N95	26.5250	91.8790	Public	7.6	189.0	121.0	43.0	17.7	0.6	22.5	1.5	12.6	6.5	139.4	2.9	1.3	2.1	0.9	38.1
N96	26.4900	91.9920	Public	6.9	178.0	113.9	40.0	15.8	2.1	11.2	3.1	14.2	9.4	128.3	2.1	1.3	0.9	1.9	38.1
N97	26.5180	91.9970	Public	6.5	149.0	95.4	29.7	22.2	1.5	8.5	2.1	10.4	4.7	70.0	0.9	1.4	2.7	1.4	39.6
N98	26.5120	91.9910	Public	6.4	202.0	129.3	30.1	20.5	2.4	12.4	5.3	16.1	12.1	142.9	2.7	3.1	1.0	1.7	38.1
N99	26.4980	92.0080	Public	6.3	111.0	71.0	5.6	1.2	1.7	9.9	1.7	12.9	11.0	113.6	1.0	2.2	3.1	2.1	21.0
N100	26.4990	92.0080	Public	6.5	111.0	71.0	15.8	6.2	1.3	14.4	1.6	16.2	7.1	91.7	3.1	3.1	4.1	1.1	39.6
N101	26.5010	91.9680	Public	6.8	203.0	129.9	33.0	23.6	1.0	11.4	3.8	9.9	8.0	106.2	0.7	1.1	2.7	0.8	38.1
N102	26.4990	91.9650	Public	6.6	199.0	127.4	25.3	23.1	1.3	10.1	3.2	11.1	8.6	113.7	1.5	2.3	2.2	1.8	21.0
N103	26.4900	91.8550	Public	6.5	211.0	135.0	32.8	20.1	1.5	15.0	2.9	12.0	8.7	135.7	1.2	1.6	2.5	2.1	21.0
N104	26.4870	91.9480	Public	6.6	217.0	138.9	23.6	26.8	2.4	16.2	2.2	11.4	7.8	106.5	2.9	1.4	3.0	1.5	39.6
N105	26.4370	91.9350	Public	7.4	385.0	246.4	66.9	23.1	2.1	23.0	2.3	12.7	5.7	245.2	2.0	1.9	17.4	1.1	38.1
N106	26.4360	91.9390	Public	7.0	246.0	157.4	46.0	36.9	1.8	16.0	2.9	10.4	7.0	189.7	5.3	1.9	10.0	1.3	38.1
N107	26.4440	91.9390	Public	6.4	220.0	140.8	2.3	1.1	0.7	21.4	1.1	11.5	6.0	99.7	1.3	1.5	2.3	1.0	38.1
N108	26.4500	91.9400	Public	6.7	246.0	157.4	34.7	22.1	1.5	17.2	1.6	12.1	7.2	129.3	1.2	1.7	2.9	1.2	38.1
N109	26.4600	91.9410	Public	6.4	184.0	117.8	21.4	19.4	1.1	19.7	1.7	10.8	5.5	113.5	1.1	3.1	3.3	1.3	38.1
N110	26.5736	91.9729	Private	6.5	176.0	112.6	9.8	30.4	1.7	10.0	2.7	6.3	2.7	92.0	11.5	0.7	16.7	1.1	26.2
N111	26.5671	91.9618	Private	7.2	190.0	121.6	13.5	25.6	0.8	10.8	13.2	6.6	3.9	71.2	11.3	0.8	14.6	1.9	8.2
N112	26.5719	91.9659	Private	7.1	117.0	74.9	17.5	30.0	0.9	12.2	1.5	4.4	2.3	78.0	2.2	0.6	7.6	1.9	19.7
N113	26.5801	91.9670	Private	6.9	135.0	86.4	15.1	10.5	0.5	13.7	5.3	6.7	2.7	102.0	4.1	0.3	11.8	1.4	21.6
N114	26.5841	91.9558	Private	7.1	194.0	124.2	31.0	25.0	0.7	19.6	1.2	7.9	4.4	145.6	0.9	1.0	2.5	1.1	26.2
N115	26.5641	91.9720	Private	7.8	132.0	84.5	16.7	9.2	0.7	14.0	2.4	5.3	3.2	92.1	0.9	0.5	3.3	1.4	15.1
N116	26.5661	91.9674	Private	7.5	189.0	121.0	22.0	35.2	1.6	14.1	2.1	5.1	3.0	98.2	1.2	0.3	8.8	1.1	15.1

N117	26.5839	91.9723	Private	7.4	164.0	105.0	15.0	10.9	0.5	20.9	1.2	8.2	3.4	114.3	0.6	0.7	1.7	1.7	21.6
N118	26.5966	91.9715	Private	7.4	205.0	131.2	21.8	31.5	1.1	15.3	6.6	5.9	5.2	120.4	1.7	0.7	11.0	1.8	26.2
N119	26.5969	91.9719	Private	7.5	163.0	104.3	12.2	17.0	0.7	19.4	1.3	7.7	3.4	94.5	0.9	0.8	8.1	1.7	23.0
N120	26.6580	91.9210	Private	7.4	160.0	102.4	3.5	28.3	0.9	6.9	9.4	4.2	4.1	105.8	0.7	0.6	3.3	2.3	6.6
N121	26.6568	91.9287	Private	7.0	182.0	116.5	12.0	30.0	0.5	4.9	19.8	5.8	4.0	111.0	4.2	2.3	14.0	1.2	6.6
N122	26.6508	91.9234	Private	7.3	200.0	128.0	15.9	10.4	1.1	9.7	3.0	4.2	4.2	96.4	1.0	1.0	6.1	1.6	4.9
N123	26.6541	91.9189	Private	7.2	180.0	115.2	10.1	11.4	0.8	11.0	3.4	4.1	3.4	105.5	0.6	0.3	5.8	1.4	6.6
N124	26.6474	91.9180	Private	6.9	252.0	161.3	5.7	15.1	0.6	35.9	13.3	16.1	3.6	119.2	2.1	0.6	30.8	1.8	6.6
N125	26.6445	91.9101	Private	7.6	135.0	86.4	1.0	12.3	0.3	16.9	1.3	5.9	2.9	105.2	2.5	0.4	2.2	1.2	6.6
N128	26.6692	91.9209	Private	7.4	93.0	59.5	6.6	2.5	0.1	5.5	2.1	3.2	4.0	94.5	18.7	3.5	1.8	1.6	3.3
N129	26.6651	91.9204	Private	7.5	165.0	105.6	3.0	2.6	0.6	8.7	3.0	4.5	4.2	146.1	20.1	7.6	7.4	1.1	3.3
N130	26.6706	91.9263	Private	7.6	231.0	147.8	24.9	11.0	0.8	10.7	6.3	4.4	6.4	148.6	1.6	1.4	6.6	1.7	3.3
N131	26.6646	91.9236	Private	7.4	151.0	96.6	5.8	21.4	0.4	7.6	5.7	3.7	4.8	117.3	0.9	0.6	7.4	1.2	6.6
N132	26.7896	91.8701	Private	7.2	78.0	49.9	5.7	32.5	0.8	9.7	5.9	4.2	3.7	90.2	1.1	0.5	5.9	1.1	8.2
N133	26.8130	91.8379	Private	7.7	241.0	154.2	36.6	36.9	1.2	13.5	4.9	6.0	5.7	150.8	0.9	0.8	10.4	1.9	3.3
N134	26.8637	91.8350	Private	6.7	113.0	72.3	6.6	1.9	0.0	0.9	0.7	7.6	0.3	112.0	14.0	1.3	4.5	2.6	
N135	26.8319	91.8215	Private	6.4	135.0	86.4	3.0	1.4	0.0	1.4	0.1	21.9	0.7	104.0	9.0	0.6	6.3	2.5	
N136	26.8346	91.8229	Private	6.3	98.0	62.7	0.0	0.0	0.0	1.0	0.1	2.4	0.3	97.0	12.0	0.0	3.6	1.9	
N137	26.8374	91.8204	Private	6.0	90.0	57.6	0.0	1.0	0.0	1.4	0.4	12.1	0.6	123.0	9.4	0.5	2.1	1.7	
N138	26.8352	91.8212	Private	6.2	123.0	78.7	10.0	0.4	0.1	1.7	1.3	11.7	0.5	145.0	11.6	0.2	6.6	3.5	
N139	26.8291	91.8179	Private	6.9	111.0	71.0	0.0	0.2	0.0	1.9	11.6	9.6	0.5	103.0	15.0	2.0	4.3	1.8	
N140	26.8173	91.8327	Private	6.3	109.0	69.8	0.0	0.3	0.1	4.1	16.1	22.7	0.5	119.0	12.5	3.0	4.2	2.9	
N141	26.7695	91.8190	Private	6.5	142.0	90.9	0.0	0.1	0.1	7.1	7.6	29.6	0.7	90.0	16.4	0.6	3.5	2.1	
N142	26.7770	91.9750	Private	6.5	134.0	85.8	10.0	0.2	0.0	5.4	1.1	10.1	0.6	154.0	10.0	0.0	2.8	2.8	
N143	26.7560	91.9400	Private	6.0	189.0	121.0	10.0	2.8	0.3	1.4	0.0	4.6	0.5	125.0	8.9	1.3	4.9	1.3	
N144	26.7499	91.9327	Private	6.5	176.0	112.6	10.0	1.1	0.2	1.2	1.2	5.7	0.4	109.0	13.0	1.5	4.4	1.3	
N145	26.7636	91.9292	Private	6.6	155.0	99.2	10.0	1.2	0.8	1.4	2.1	4.4	0.3	149.0	8.6	2.1	3.9	1.9	
N146	26.7600	91.9295	Private	6.8	176.0	112.6	0.0	0.1	0.0	1.7	2.8	2.9	0.3	108.0	7.9	0.4	6.2	2.8	
N147	26.8226	91.9284	Private	6.9	187.0	119.7	0.0	0.7	0.2	2.1	3.2	3.0	0.4	132.0	9.3	2.9	5.3	1.8	
N148	26.8403	91.9137	Private	6.0	211.0	135.0	0.0	0.1	0.0	1.2	0.4	5.1	0.3	141.0	13.0	0.2	3.2	2.4	
N149	26.8521	91.9310	Private	6.2	189.0	121.0	0.0	2.4	0.0	1.5	0.6	4.7	0.3	119.0	17.0	8.2	4.4	2.1	

N150	26.7963	91.9220	Private	6.4	173.0	110.7	0.0	1.0	0.0	0.8	0.8	4.8	0.2	120.0	12.8	6.2	7.1	2.2
N151	26.7849	91.9245	Private	6.7	201.0	128.6	0.0	0.2	0.0	1.2	0.7	1.5	0.5	198.0	14.7	0.2	4.3	2.2
N152	26.7768	91.9191	Private	6.9	139.0	89.0	0.0	0.1	0.0	1.0	0.1	9.7	0.5	119.0	14.0	7.0	4.1	2.2
N153	26.7442	91.9139	Private	6.0	176.0	112.6	0.0	0.1	0.0	0.9	0.0	6.8	0.4	146.0	12.8	6.4	3.9	2.3
N154	26.7307	91.9280	Private	6.2	187.0	119.7	0.0	0.3	0.0	0.9	0.3	9.8	0.5	176.0	14.0	0.2	1.9	2.2

A.1.2 Groundwater Quality from along Southern Transect

Sample ID	Latitude	Longitude	Type of Source	As (ppb)	Fe	Mn	Na	K	Ca	Mg	HCO_3	SO_4	NO_3	Cl	PO_4
S1	26.610214	94.082887	Private	499.0	1.43	0.34	42.2	2.4	9.1	22.9	382.0	7.13	2.50	10.0	2.20
S2	26.616291	94.098424	Private	301.0	9.42	0.24	197.8	5.6	157.1	22.2	209.0	14.13	2.04	1.0	2.25
S3	26.617462	94.106997	Private	297.0	6.34	0.24	80.3	1.8	76.8	23.7	185.0	7.45	1.34	0.0	2.22
S4	26.617996	94.111763	Private	283.0	5.78	0.28	84.1	0.5	17.3	16.3	198.0	4.60	5.40	1.0	2.00
S5	26.622230	94.110584	Private	299.0	6.24	0.25	72.4	2.1	42.8	16.9	221.0	10.05	5.87	0.0	2.40
S6	26.622115	94.097078	Private	231.0	5.68	0.26	174.8	0.0	64.9	18.9	234.0	23.81	7.19	4.0	1.45
S7	26.604646	94.085278	Private	55.0	19.64	0.30	34.8	1.7	24.6	22.5	148.0	6.58	3.67	4.0	0.87
S8	26.602206	94.101421	Private	65.0	19.48	0.22	170.2	0.0	97.7	20.1	175.0	5.61	2.05	1.0	1.05
S9	26.599529	94.110591	Private	129.0	11.47	0.20	175.4	0.0	37.6	19.7	164.0	8.23	7.45	3.0	1.01
S10	26.586065	94.127587	Private	189.0	8.69	0.18	85.2	8.8	27.1	22.1	210.0	11.44	4.55	2.0	1.66
S11	26.583472	94.134177	Private	62.0	19.50	0.24	87.9	2.9	18.6	18.6	170.0	20.57	2.03	1.0	0.98
S12	26.582610	94.144593	Private	146.0	13.94	0.29	76.2	2.4	46.0	12.4	184.0	3.37	10.50	1.0	1.07
S13	26.553810	94.205049	Private	569.0	4.19	0.35	25.5	0.2	15.6	7.9	396.0	7.97	6.80	3.0	2.55
S14	26.531612	94.207026	Private	153.0	12.08	0.26	22.8	0.5	13.8	7.0	215.0	4.02	4.30	5.0	1.65
S15	26.483252	94.183742	Private	257.0	9.01	0.39	60.2	2.1	32.2	10.9	194.0	12.99	2.45	2.0	1.40
S16	26.435023	94.162964	Private	256.0	8.64	0.44	67.1	2.0	59.2	15.6	192.0	9.69	1.10	3.0	1.05
S17	26.412532	94.166124	Private	137.0	5.04	0.50	31.4	0.0	20.2	12.5	160.0	5.06	1.11	4.0	1.14
S18	26.396658	94.166767	Private	16.0	7.09	0.51	64.9	0.6	45.4	9.4	86.0	7.58	5.50	3.0	0.76
S19	26.394777	94.168432	Private	276.0	5.71	0.64	56.0	1.3	37.0	16.9	235.0	6.97	3.45	2.0	1.50
S20	26.373118	94.166440	Private	159.0	8.28	0.62	78.1	2.0	52.9	11.0	157.0	7.58	2.07	0.0	1.15
S21	26.347607	94.160452	Private	194.0	12.22	0.63	68.7	1.4	65.8	16.6	184.0	4.22	4.98	1.0	1.46
S22	26.440290	94.165913	Private	157.0	7.96	0.28	91.5	4.6	61.6	8.4	176.0	7.42	10.05	4.0	1.02
S23	26.464888	94.169111	Private	176.0	7.30	0.58	40.6	0.0	29.6	12.0	210.0	6.87	8.45	0.0	1.19
S24	26.452896	94.176738	Private	74.0	15.68	0.49	28.5	3.3	15.8	15.0	156.0	3.92	6.35	4.0	1.05
S25	26.511469	94.174549	Private	226.0	8.21	0.32	38.5	0.0	22.0	10.2	170.0	6.06	7.90	2.0	1.14

S26	26.645798	94.327026	Private	213.0	19.66	0.70	93.0	2.2	3.4	3.5	146.0	18.50	5.90	17.0	0.87
S27	26.471528	94.130583	Private	248.0	10.54	0.32	62.6	1.7	35.2	20.7	210.0	10.82	4.00	0.0	1.05
S28	26.483617	94.118803	Private	264.0	6.85	0.29	72.6	1.8	46.0	12.4	214.0	6.26	6.65	2.0	1.45
S29	26.494233	94.114764	Private	289.0	6.28	0.22	91.9	2.6	40.4	24.4	258.0	8.10	4.00	2.0	0.89
S30	26.513028	94.105697	Private	124.0	12.36	0.26	86.3	7.0	63.0	22.5	168.0	6.13	8.50	0.0	0.97
S31	26.520388	94.119304	Private	229.0	5.23	0.23	201.4	0.7	115.1	20.5	160.0	6.58	10.50	2.0	1.76
S32	26.496976	94.105150	Private	51.0	26.78	0.31	197.8	0.7	54.8	21.8	205.0	4.90	5.50	3.0	1.34
S33	26.459155	94.129977	Private	604.0	0.35	0.34	53.5	0.0	38.6	14.4	438.0	13.61	2.78	1.0	1.08
S34	26.439164	94.145741	Private	95.0	4.44	0.29	49.0	2.8	24.4	9.5	200.0	3.83	5.50	1.0	0.62
S35	26.454275	94.126495	Private	164.0	3.16	0.19	75.1	4.4	47.8	17.0	178.0	6.22	8.15	6.0	2.00
S36	26.455681	94.142985	Private	105.0	3.17	0.32	45.2	7.8	23.6	15.4	204.0	6.97	10.00	2.0	1.15
S37	26.492555	94.206151	Private	285.0	12.38	0.53	32.0	5.8	14.6	11.4	260.0	3.47	12.50	2.0	1.04
S38	26.531487	94.211462	Private	30.0	7.12	0.63	12.6	2.0	0.0	8.3	152.0	10.34	6.70	11.0	0.98
S39	26.542819	94.228190	Private	51.0	8.96	0.31	14.4	2.7	26.6	7.3	218.0	11.44	1.14	16.0	0.97
S40	26.572257	94.132753	Private	42.0	15.29	0.13	200.0	2.0	133.2	20.9	168.0	10.69	0.67	4.0	1.43
S41	26.577245	94.105608	Private	94.0	8.79	0.29	78.5	0.0	53.4	23.2	210.0	7.58	1.54	0.0	1.02
S42	26.573058	94.128038	Private	14.0	2.47	0.30	54.4	0.9	0.0	20.0	156.0	8.20	1.22	1.0	1.21
S43	26.574148	94.143525	Private	64.0	3.21	0.32	61.6	2.8	13.3	14.8	178.0	5.80	1.04	2.0	0.99
S44	26.572873	94.151780	Private	103.0	1.50	0.15	64.4	0.7	8.7	15.5	170.0	2.40	0.69	1.0	0.89
S45	26.703818	94.209840	Private	34.7	9.79	0.35	9.9	0.9	7.2	7.9	73.3	2.60	1.08	6.0	1.03
S46	26.692239	94.209428	Private	26.1	26.22	0.37	21.5	1.5	13.1	11.1	140.0	16.43	2.15	4.0	0.19
S47	26.679754	94.238483	Private	4.5	0.00	0.19	16.0	1.3	10.0	5.8	105.0	20.36	12.35	8.0	1.05
S48	26.680816	94.212775	Private	0.0	0.00	0.41	9.9	0.9	6.7	5.7	80.0	30.04	10.01	7.0	0.50
S49	26.691612	94.246482	Private	41.6	20.37	0.18	8.8	0.7	6.4	6.7	65.0	0.00	7.70	6.0	1.05
S50	26.686457	94.266258	Private	39.8	21.53	0.25	15.6	1.0	9.2	6.9	87.5	7.07	15.00	6.0	1.08
S51	26.703443	94.268623	Private	26.8	25.60	0.35	9.7	0.8	6.7	5.5	67.5	0.00	11.00	2.0	1.40
S52	26.727743	94.269601	Private	277.3	1.68	0.28	17.8	1.9	11.5	7.2	120.0	2.63	9.50	9.0	2.80
S53	26.736450	94.252980	Private	65.2	13.60	0.34	13.4	1.0	8.6	7.1	102.5	6.15	12.00	2.0	0.89
S54	26.750220	94.230942	Private	48.1	0.70	0.43	11.8	1.0	7.7	6.9	97.5	0.00	17.70	3.0	1.03
S55	26.611875	94.288194	Private	46.0	22.29	0.38	12.5	1.0	9.1	6.9	85.0	3.37	7.50	3.0	1.45
S56	26.594788	94.294282	Private	93.1	18.72	0.83	6.2	1.1	4.3	4.1	40.0	4.49	9.00	6.0	1.55

S57	26.590540	94.291036	Private	237.0	4.82	0.25	19.9	1.0	12.2	9.2	115.0	8.48	5.30	10.0	1.45
S58	26.596510	94.311167	Private	258.2	16.41	0.24	17.3	1.0	11.6	9.8	140.0	0.00	4.50	3.0	1.56
S59	26.669629	94.308864	Private	39.7	25.68	0.36	8.8	1.1	6.4	7.1	72.5	9.57	16.20	7.0	1.08
S60	26.668939	94.302487	Private	15.2	21.84	0.83	3.6	0.6	2.4	4.3	37.5	4.90	11.50	21.0	0.95
S61	26.675134	94.264190	Private	29.9	18.96	1.06	5.2	0.8	4.1	5.3	30.0	0.00	14.30	2.0	0.88
S62	26.666249	94.257979	Private	59.9	22.91	0.73	7.1	0.8	4.6	4.3	120.0	0.52	9.00	7.0	1.23
S63	26.806650	94.181099	Private	18.9	7.23	0.34	24.5	1.2	14.6	7.4	142.5	0.01	10.50	6.0	0.78
S64	26.819798	94.167094	Private	13.0	3.75	0.44	13.7	1.1	9.1	2.1	97.5	10.11	8.50	6.0	0.76
S65	26.805469	94.217213	Private	39.9	0.14	0.33	8.4	1.4	6.4	8.5	102.5	19.02	4.50	8.0	0.87
S66	26.802845	94.120743	Private	11.4	0.00	0.14	28.9	1.8	17.9	9.9	177.5	14.13	10.00	1.0	0.56
S67	26.730027	94.152640	Private	0.0	26.41	0.39	9.2	1.1	6.3	7.3	55.0	9.31	7.50	0.0	1.67
S68	26.722169	94.149379	Private	14.4	7.88	0.79	8.4	1.5	6.3	5.0	22.5	5.83	6.00	17.0	1.45
S69	26.696079	94.166333	Private	17.2	0.00	0.28	20.8	1.6	13.5	10.1	87.5	2.79	13.50	0.0	1.09
S70	26.696848	94.128255	Private	2.9	1.67	0.50	8.4	0.7	6.4	14.8	130.0	13.30	6.50	3.0	0.75
S71	26.729056	94.142804	Private	4.7	4.97	1.11	8.2	0.9	5.6	11.3	92.5	0.00	9.00	1.0	0.87
S72	26.713984	94.097106	Private	6.0	3.34	0.35	7.1	2.2	5.7	10.4	105.0	17.49	3.50	5.0	0.72
S73	26.697916	94.104049	Private	6.8	2.04	0.27	39.5	2.0	23.7	14.2	132.5	7.68	4.60	14.0	0.68
S74	26.670358	94.073216	Private	0.5	12.96	0.60	7.8	2.0	5.9	8.4	40.0	15.28	3.30	4.0	1.18
S75	26.678522	94.102336	Private	6.3	26.15	0.76	7.8	1.0	5.3	8.0	95.0	35.70	10.00	0.0	0.87
S76	26.701535	94.086150	Private	10.1	4.38	0.38	7.4	1.7	5.2	16.5	127.5	23.94	9.00	18.0	0.76
S77	26.804247	94.189800	Private	4.7	9.44	0.56	25.3	1.5	15.5	10.7	102.5	1.67	7.50	2.0	1.34
S78	26.815281	94.214435	Private	17.8	2.68	0.36	28.3	1.5	17.1	11.1	190.0	2.66	8.80	1.0	1.16
S79	26.842835	94.209383	Private	35.5	0.55	0.31	9.4	0.5	6.4	11.5	75.0	21.19	3.60	2.0	0.87
S80	26.843381	94.228280	Private	17.7	1.86	0.51	16.5	1.9	11.1	13.4	177.5	7.49	9.00	0.0	0.78
S81	26.853238	94.253342	Private	30.3	0.09	0.83	10.0	0.7	7.2	16.3	95.0	7.14	5.70	0.0	0.77
S82	26.827470	94.246457	Private	17.3	1.13	0.40	23.7	2.0	14.6	16.2	190.0	20.62	8.00	2.0	0.95
S83	26.816520	94.231441	Private	9.8	14.52	0.46	11.3	1.1	7.8	9.5	70.0	10.72	6.50	1.0	1.20
S84	26.811464	94.227471	Private	42.8	24.76	1.25	3.9	1.6	3.1	5.3	25.0	6.79	2.20	1.0	0.54
S85	26.728621	94.226725	Private	19.8	5.98	0.49	9.8	0.8	6.6	6.7	55.0	9.12	4.00	28.0	1.05
S86	26.774009	94.180898	Private	38.9	11.72	0.33	14.9	1.8	10.7	6.0	65.0	9.60	6.00	2.0	0.32
S87	26.762605	94.174557	Private	41.7	9.72	0.42	10.3	2.8	7.6	7.6	65.0	16.08	7.70	9.0	0.89

S88	26.753738	94.156307	Private	32.8	4.41	0.29	8.0	1.8	6.0	11.0	112.5	14.84	3.10	2.0	0.49
S89	26.753657	94.144029	Private	29.0	5.16	0.37	11.2	0.9	7.5	7.7	100.0	15.22	6.80	3.0	0.95
S90	26.732457	94.122375	Private	34.4	12.62	0.44	9.2	0.9	6.6	4.7	75.0	3.02	7.00	0.0	1.02
S91	26.737341	94.107178	Private	23.5	9.46	0.30	8.8	1.6	6.2	10.2	32.5	17.62	4.00	2.0	0.87
S92	26.725178	94.066490	Private	20.7	5.13	0.54	8.2	1.3	6.4	10.8	110.0	4.93	2.20	3.0	0.43
S93	26.663000	94.249000	Private	300.0	17.80	0.76	12.7	1.6	21.0	7.9	215.0	5.80	1.20	10.6	1.12
S94	26.619000	94.197000	Private	204.0	20.60	0.88	18.9	0.9	18.0	10.0	205.0	4.50	0.50	8.7	0.90
S95	26.605000	94.210000	Private	222.0	22.00	1.02	20.6	2.5	19.0	11.0	199.0	7.80	3.20	9.1	1.06
S96	26.629000	94.162000	Private	287.0	15.00	0.81	11.9	2.0	26.0	8.7	156.0	5.50	2.10	11.7	1.41
S97	26.654000	94.194000	Private	210.0	18.00	0.55	8.0	1.8	25.0	9.0	190.0	8.60	5.00	10.9	1.04
S98	26.622000	94.042000	Private	17.0	7.80	0.67	15.9	2.0	10.0	10.0	111.0	12.50	7.00	7.7	0.78
S99	26.700100	93.888000	Private	0.0	11.00	0.49	15.0	1.1	15.0	8.7	105.0	11.60	5.00	3.6	0.77
S100	26.722000	93.884000	Private	2.5	8.50	0.82	17.4	0.7	13.0	8.0	111.0	18.50	4.40	9.1	1.06
S101	26.710000	93.909000	Private	0.0	9.00	0.87	12.7	3.6	18.0	7.6	105.0	13.50	2.20	4.5	0.89
S102	26.695000	93.931000	Private	3.3	5.60	0.77	17.9	3.1	16.0	10.6	134.0	12.40	1.50	3.6	1.04
S103	26.668000	93.973000	Private	0.0	7.00	0.56	13.7	1.8	11.0	11.0	85.0	18.60	3.10	5.6	0.78
S104	26.679000	93.987000	Private	0.0	11.00	0.78	10.7	2.1	16.0	14.0	108.0	16.30	2.40	7.5	0.87
S105	26.652000	94.034000	Private	25.8	9.00	0.43	21.7	4.8	18.0	13.0	135.0	12.80	6.00	3.6	1.05
S106	26.628000	94.047000	Private	52.5	4.50	0.78	19.7	2.5	15.0	12.0	127.0	11.65	3.00	3.9	1.32
S107	26.638000	94.034000	Private	61.5	7.00	0.69	6.9	1.6	18.0	7.0	176.0	9.06	3.50	6.0	1.63
S108	26.518000	94.174000	Private	50.5	12.00	0.88	9.8	1.7	17.0	7.0	150.0	11.43	4.00	4.7	0.67
S109	26.640000	94.004000	Private	55.0	10.70	0.87	7.0	2.1	23.0	6.9	145.0	12.06	2.00	4.8	1.87
S110	26.661000	94.013000	Private	17.4	17.00	0.46	10.0	1.8	21.0	16.0	130.0	15.20	4.00	3.5	0.67
S111	26.684000	93.988000	Private	5.0	15.70	0.54	9.0	1.4	10.0	10.0	78.0	9.10	2.20	5.6	1.04
S112	26.680000	93.941000	Private	5.0	12.00	0.38	11.6	2.1	7.0	14.0	115.0	13.10	3.00	3.8	0.78
S113	26.698000	93.979000	Private	3.5	11.00	0.56	12.5	1.80.7	10.0	4.0	125.0	21.00	1.50	6.0	1.04
S114	926.682000	93.949000	Private	6.5	18.00	0.69	11.0	0.6	12.0	8.0	95.0	18.00	6.00	5.0	1.06
S115	26.694000	93.946000	Private	4.6	21.00	0.55	15.7	1.2	11.0	5.0	115.0	20.60	12.00	3.6	1.21
S116	26.693000	93.943000	Private	6.1	14.00	0.87	14.3	2.5	17.0	12.4	105.0	22.00	6.00	3.0	0.78
S117	26.609000	94.055000	Private	37.6	18.00	0.87	19.1	1.7	18.5	8.7	145.0	7.00	11.50	6.0	0.66
S118	26.620000	94.068000	Private	24.0	11.00	1.02	4.7	1.5	16.0	10.0	137.0	9.50	3.50	4.0	1.04

S119	26.651000	94.028000	Private	27.0	16.00	0.98	14.5	2.6	12.0	6.0	215.0	11.20	5.00	6.0	1.07
S120	26.718000	93.891000	Private	3.3	6.00	0.67	19.0	2.8	21.0	8.0	117.0	27.00	6.00	2.0	1.32
S121	26.723000	93.903000	Private	0.0	11.00	0.77	12.5	1.8	23.6	5.7	110.0	22.00	7.70	4.0	0.77
S122	26.645000	94.224000	Private	360.0	17.00	1.21	11.8	1.6	17.0	7.5	233.0	7.90	8.50	7.0	1.12
S123	26.614000	94.032000	Private	60.1	14.00	1.20	16.0	2.9	18.0	5.0	135.0	11.40	10.60	4.0	1.43
S124	26.660000	94.005000	Private	25.7	11.00	0.78	21.5	1.3	13.0	1.0	150.0	8.02	11.50	2.0	0.76
S125	26.681000	93.958000	Private	6.8	9.00	0.53	18.8	1.0	13.7	8.0	125.0	7.50	7.70	5.0	1.56
S126	26.683010	93.952210	Private	5.2	8.70	0.44	12.9	0.5	17.0	11.0	115.0	8.05	11.30	2.0	0.56
S127	26.733100	93.981200	Private	13.7	4.60	0.65	11.9	1.1	16.0	8.9	95.0	15.00	8.00	4.0	1.32
S128	26.731200	93.896200	Private	0.0	6.70	0.89	10.0	3.6	15.8	11.8	120.0	12.90	20.50	1.5	1.04
S129	26.733100	93.888200	Private	0.0	7.10	0.14	14.0	2.8	14.8	10.8	106.0	14.00	12.50	3.0	1.32
S130	26.690110	93.984420	Private	8.5	11.00	0.54	13.6	4.1	16.0	7.0	145.0	7.90	7.50	10.0	1.04
S131	26.611020	94.184330	Private	375.6	22.00	0.91	11.0	2.7	22.0	6.0	56.0	7.90	5.40	11.0	1.15
S132	26.644700	94.156700	Private	215.0	17.00	0.89	14.3	17.0	26.0	5.9	155.0	8.50	6.50	8.0	1.43
S133	26.745000	94.112000	Private	2.8	7.80	0.65	11.0	1.2	12.0	11.0	115.0	26.90	7.00	5.0	1.07

Appendix A2

A.2 XRD Results of sediment samples

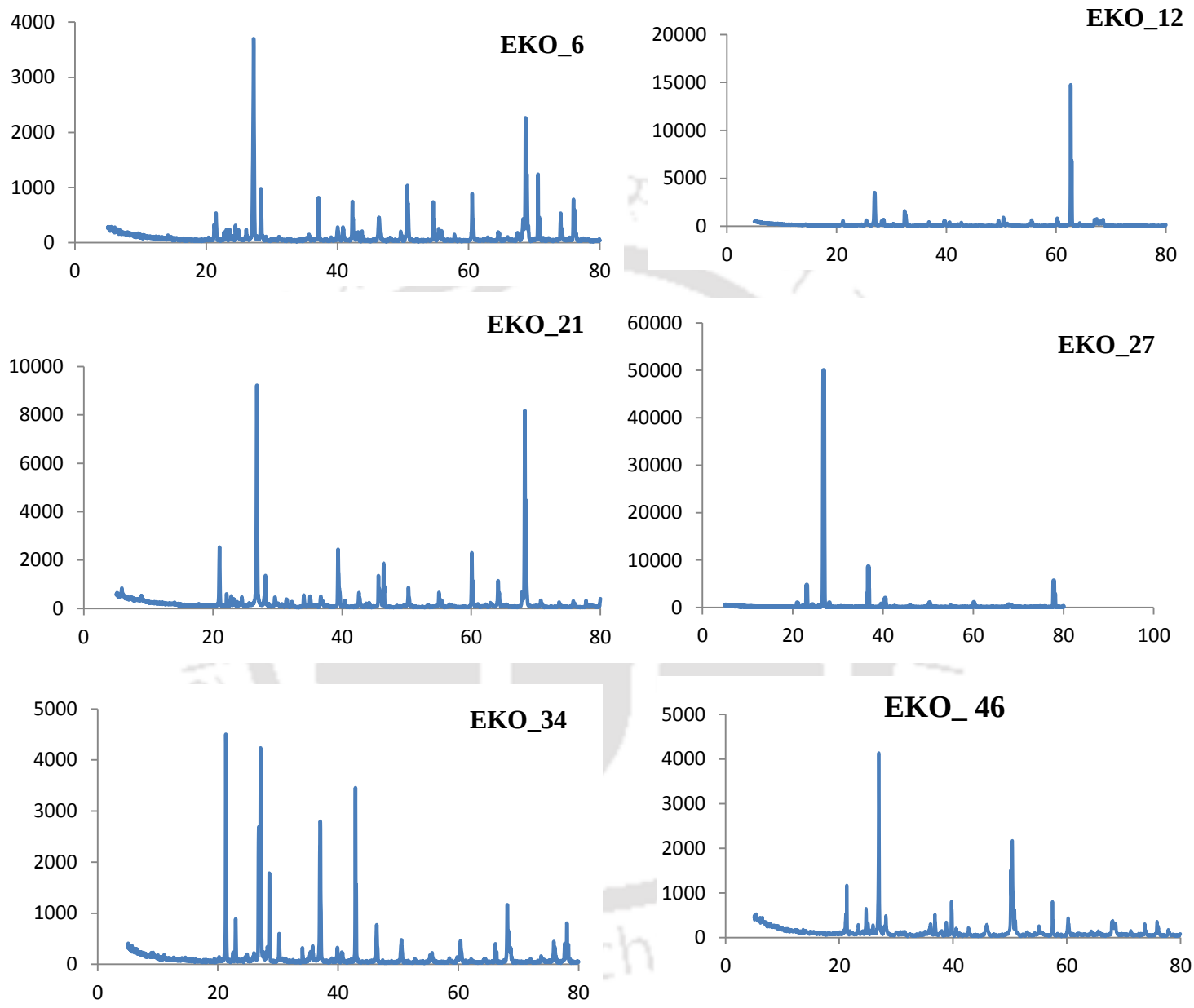

Figure A.2 a. XRD results of depthwise sediment samples from BH_ EKO along the southern transect

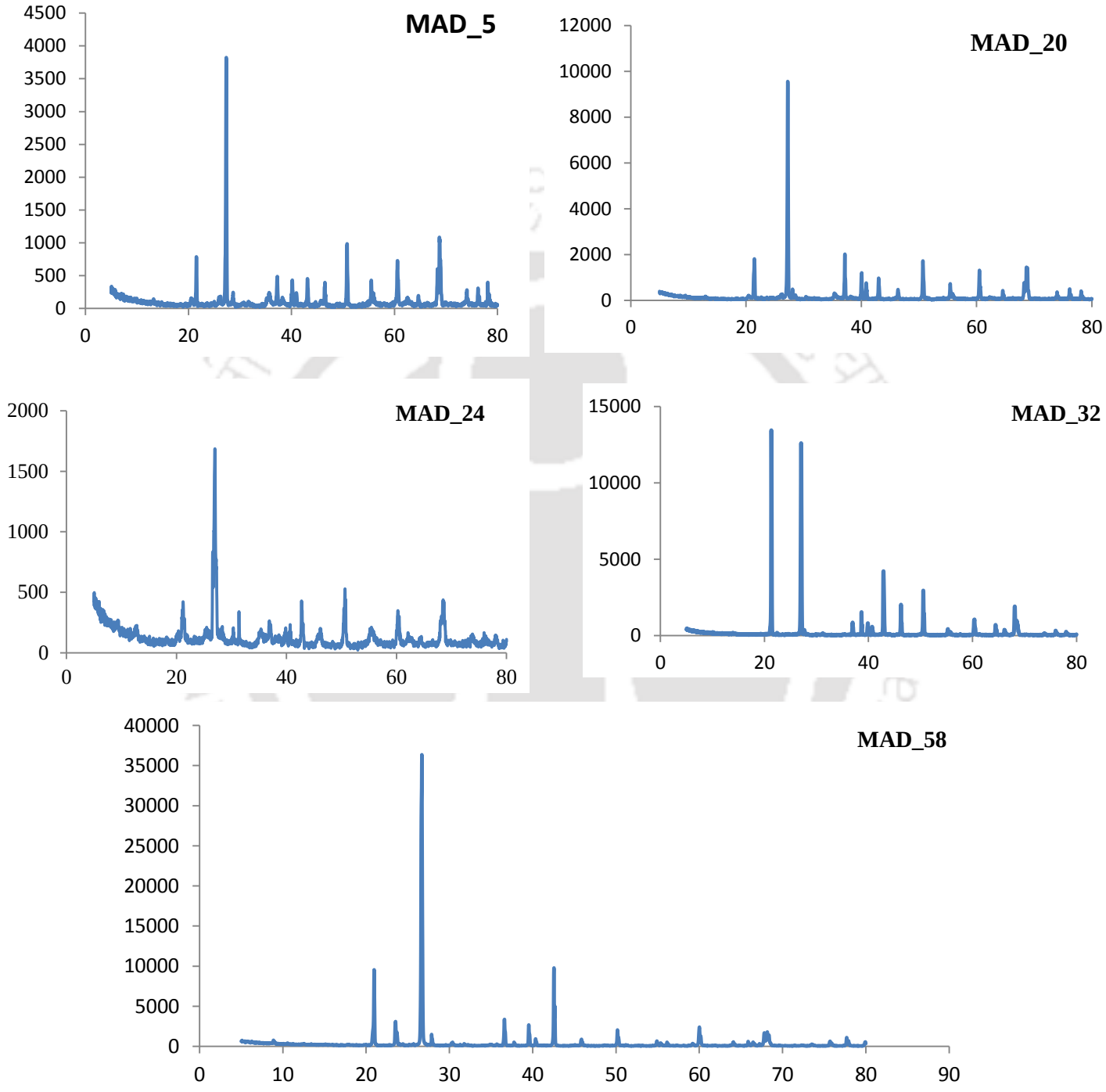

Figure A.2.b. XRD results of depthwise sediment samples from BH_ MAD along the southern transect

Appendix A3

A.3.1 XRF measurements of As, Fe and Mn in mg/kg for sediment samples from borewells drilled along northern transect

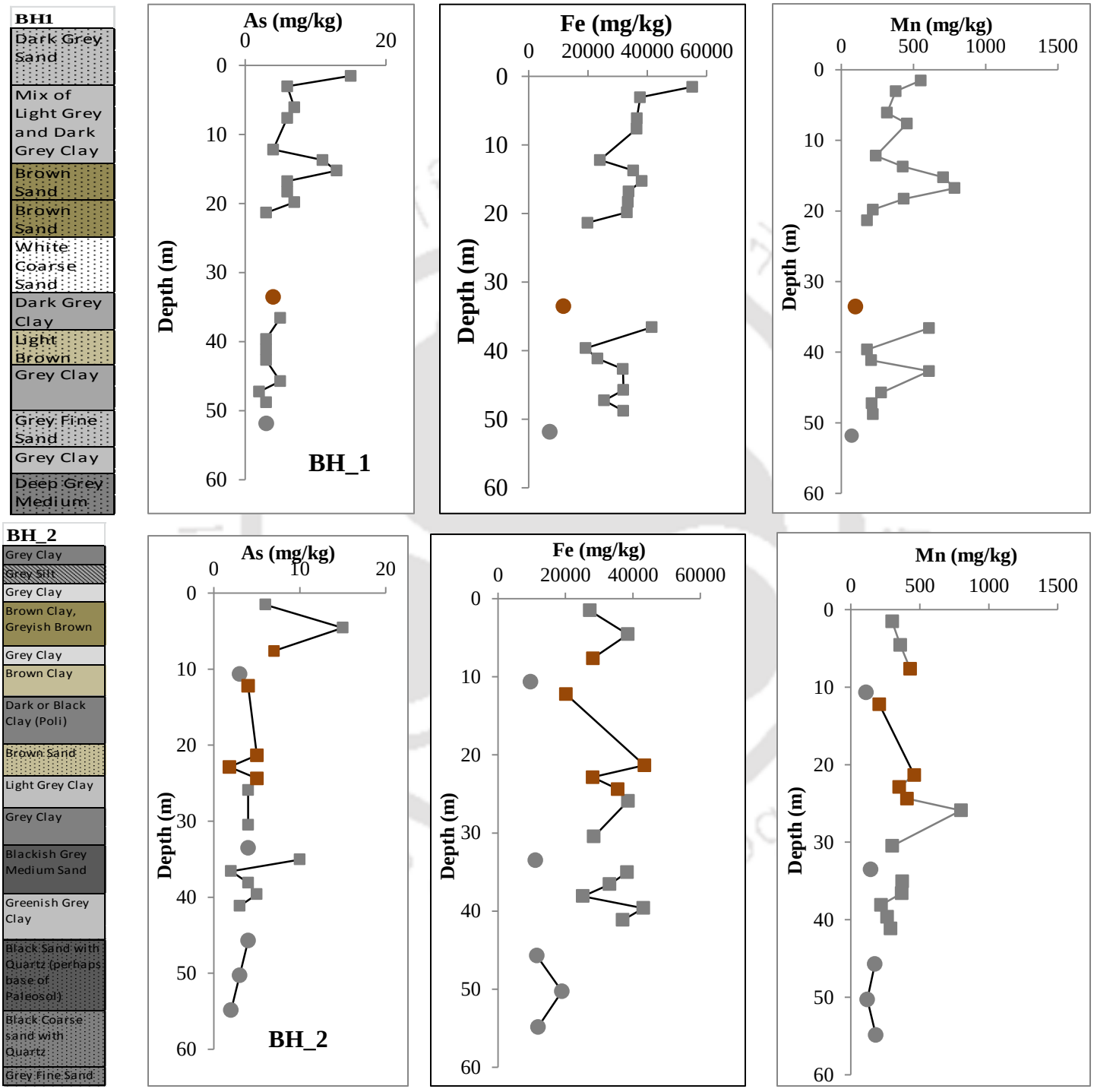

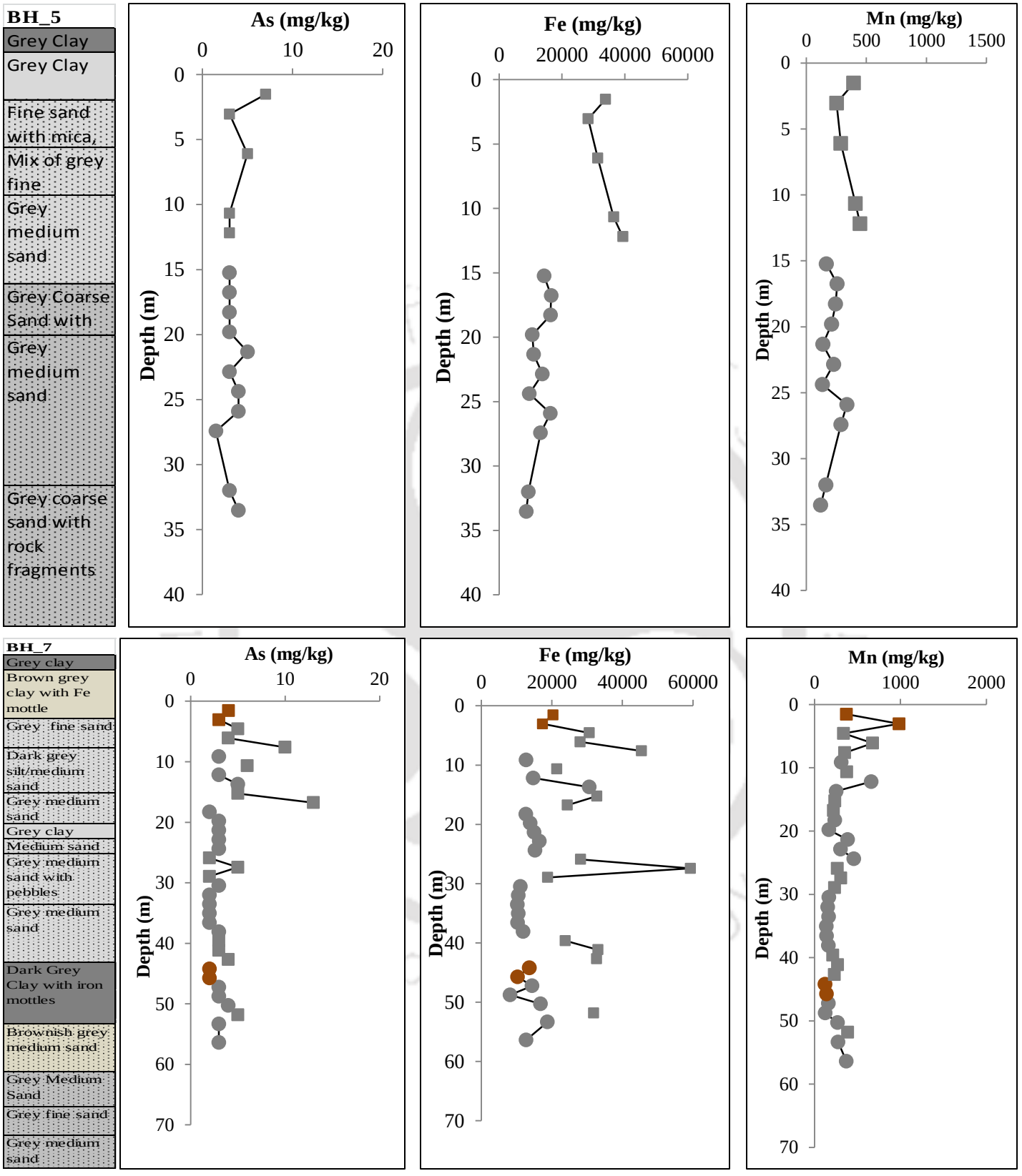

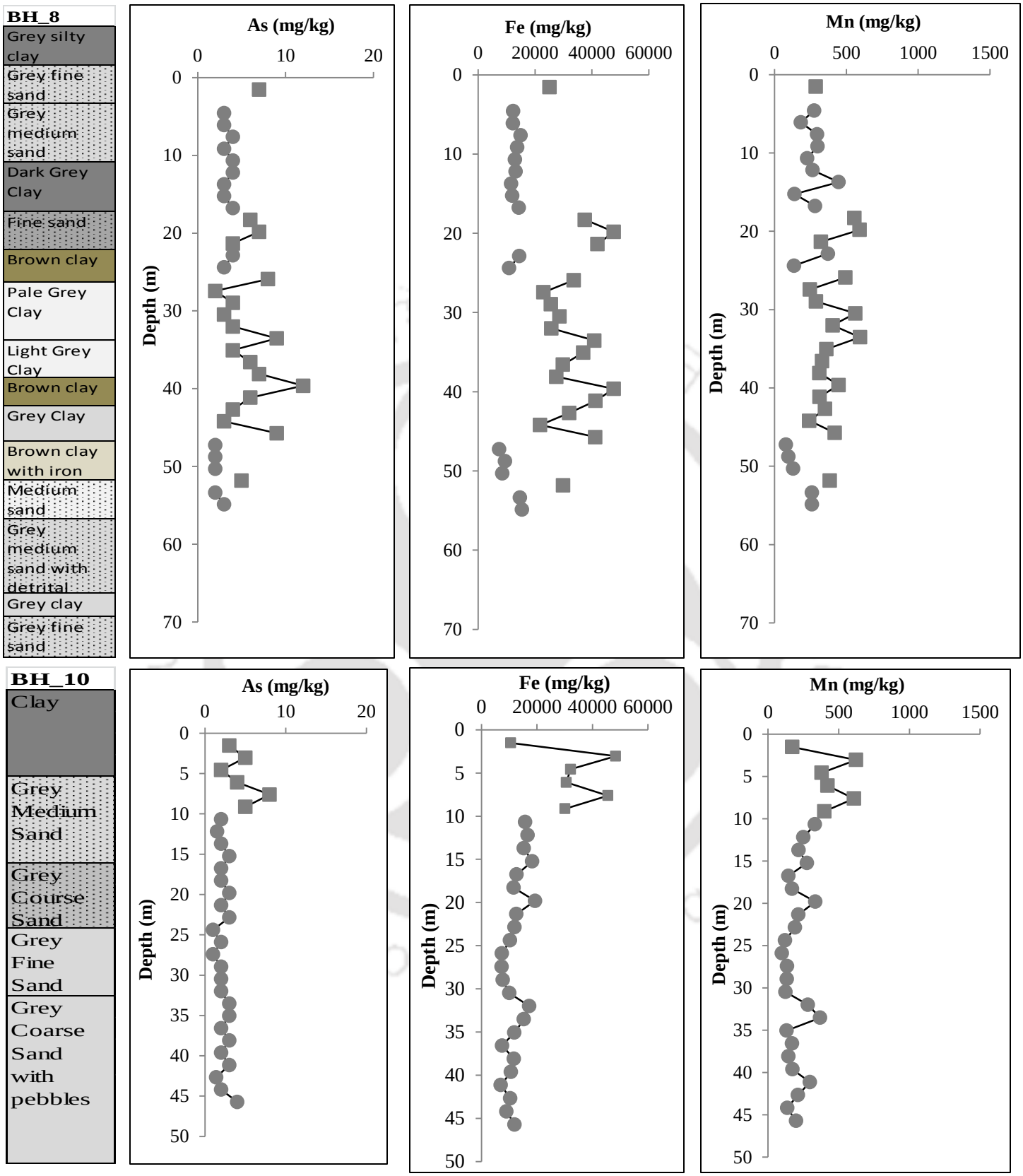

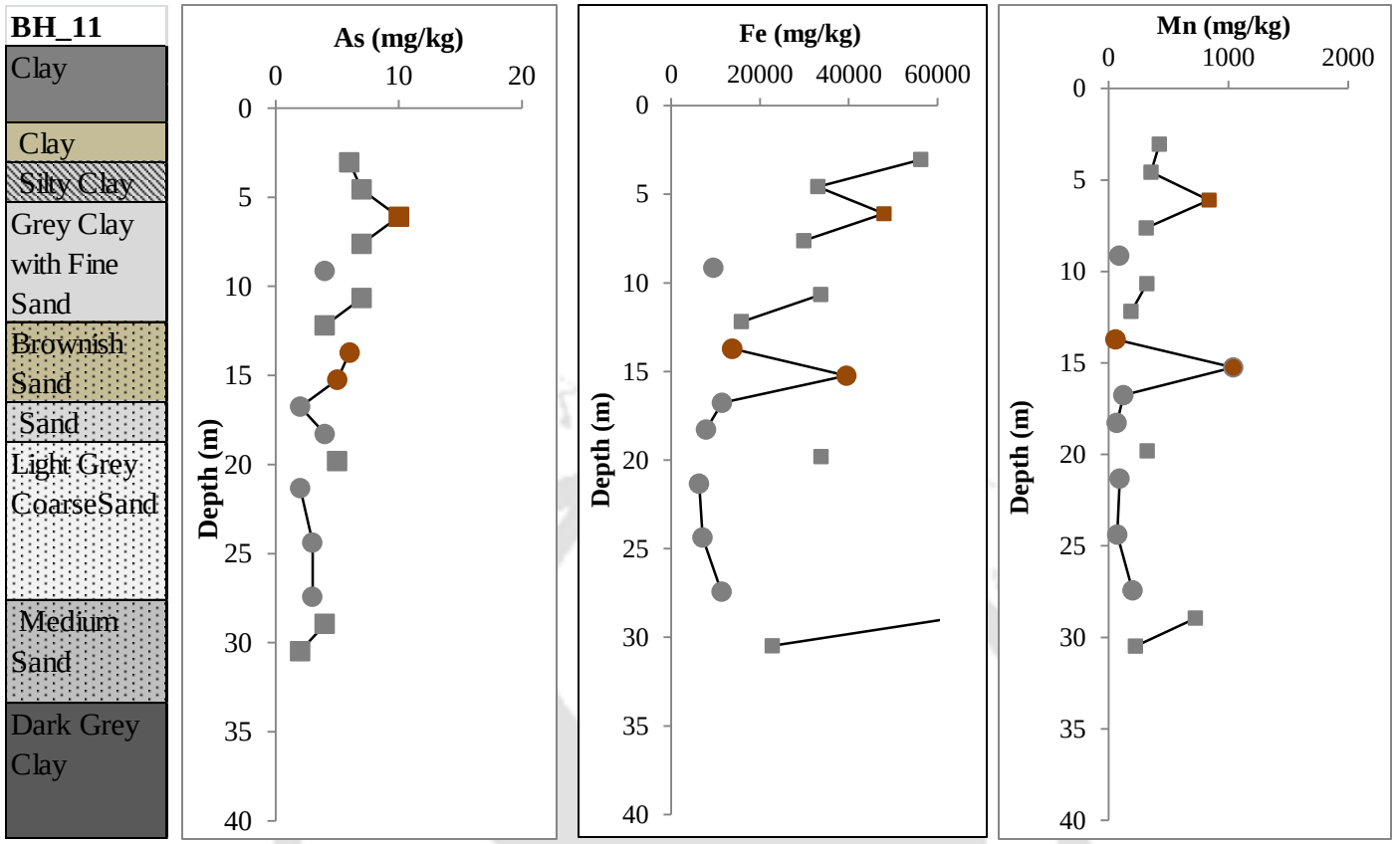

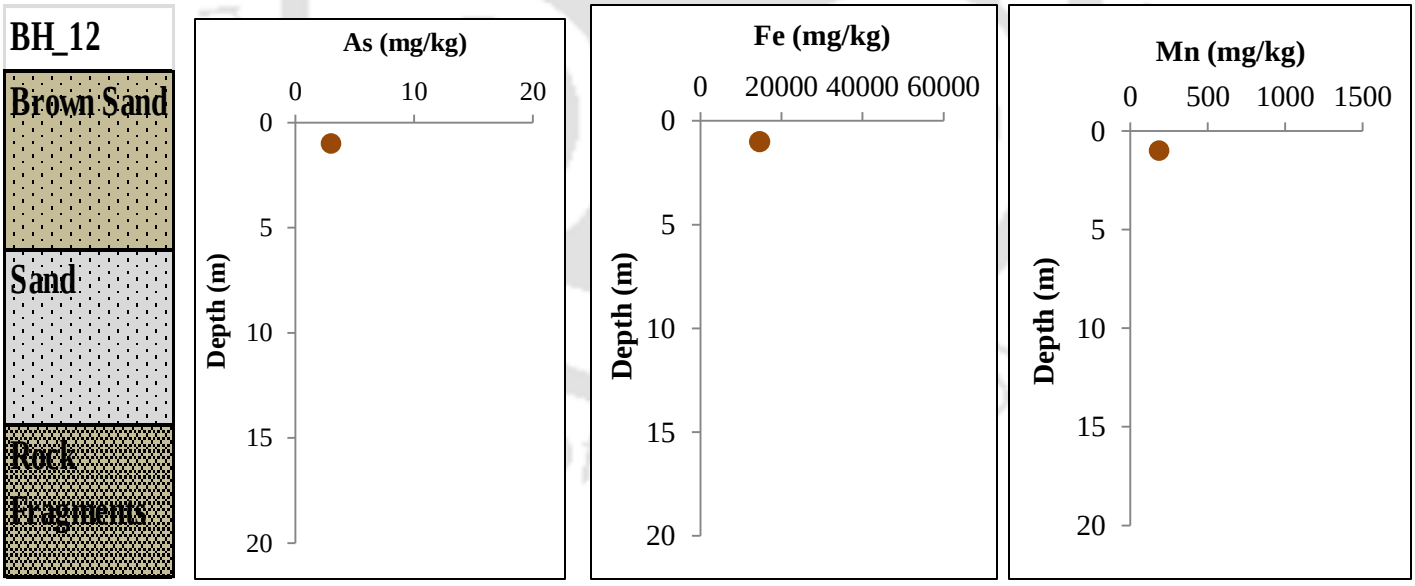

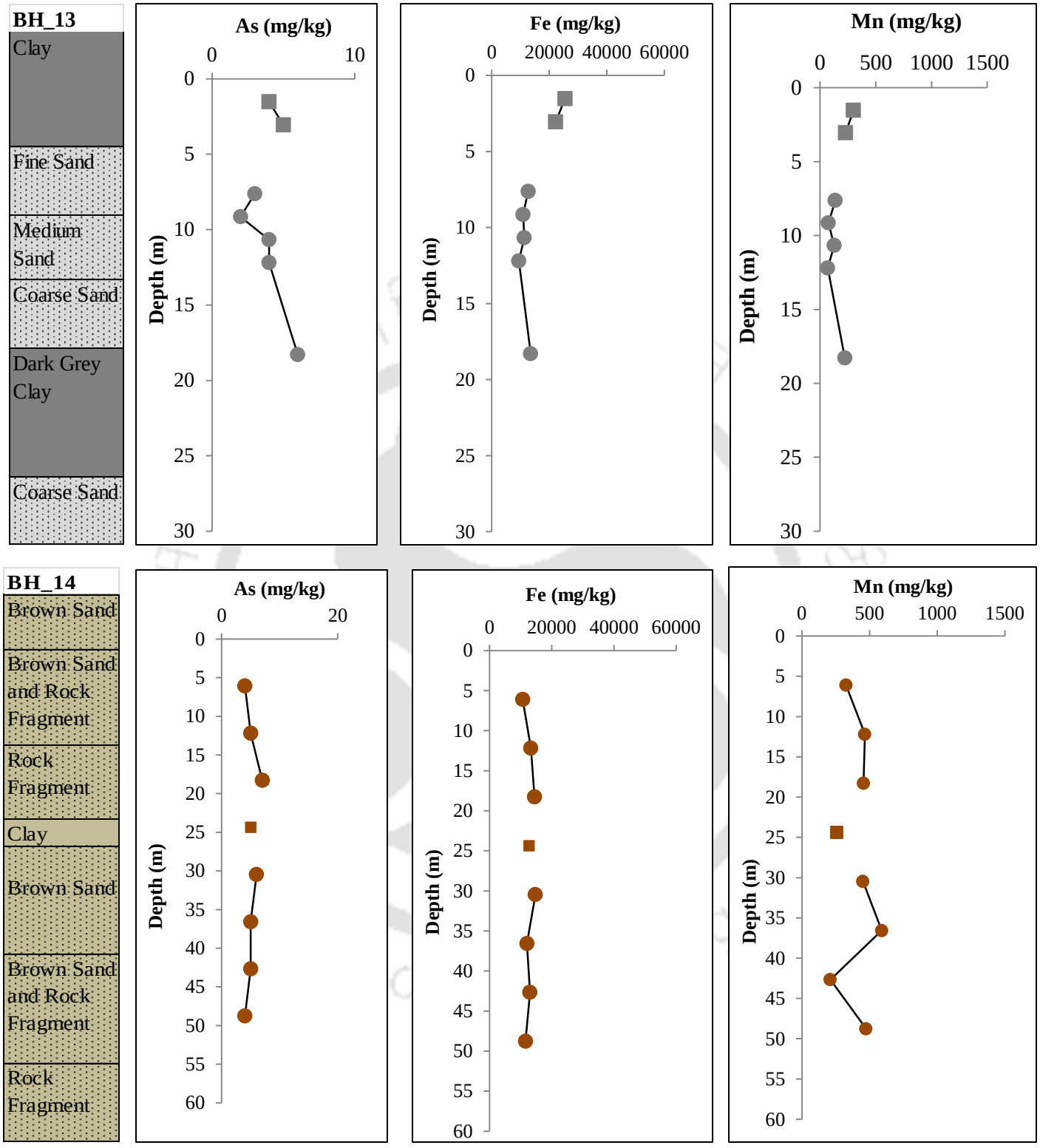

Figure A.3.1a Total As, Fe and Mn (mg/kg) concentration in sediment samples along depth profile of boreholes along northern transect

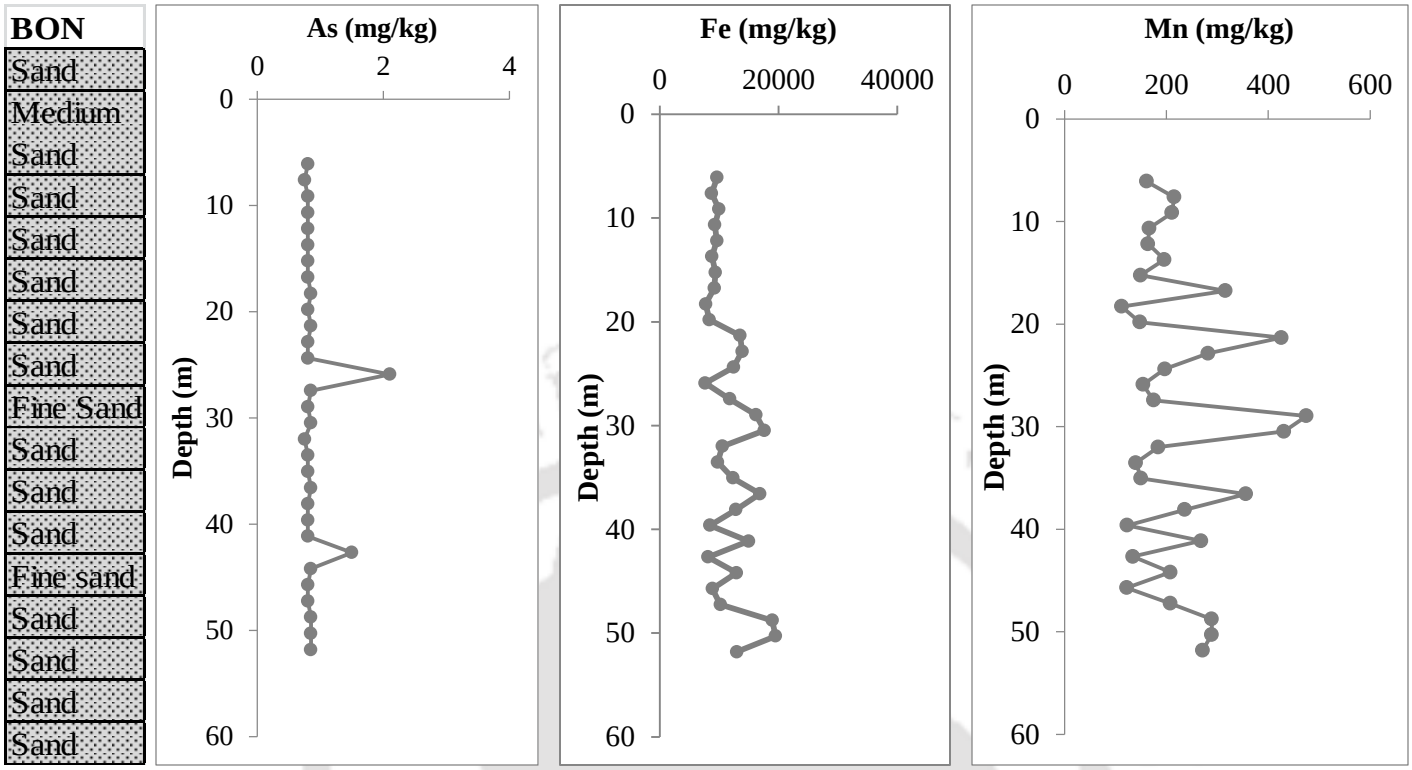

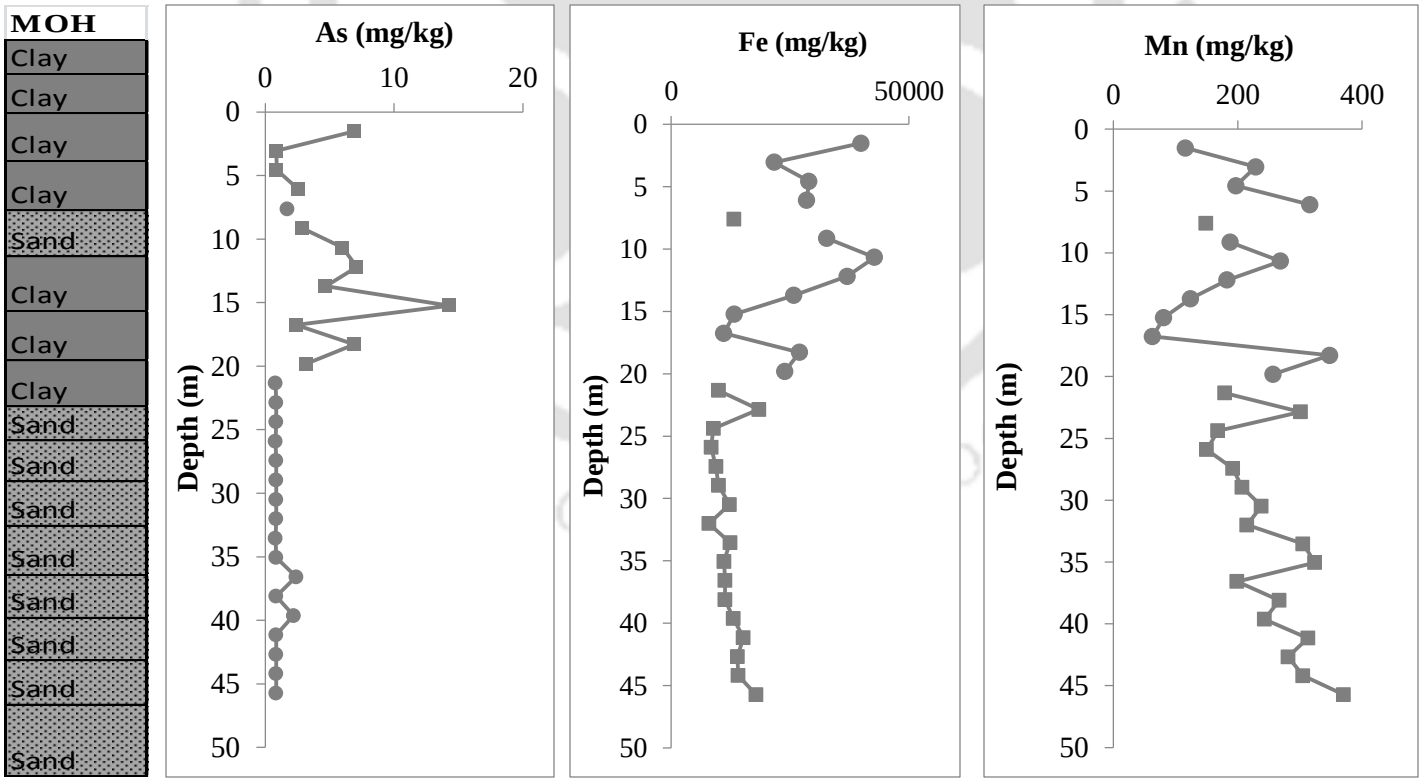

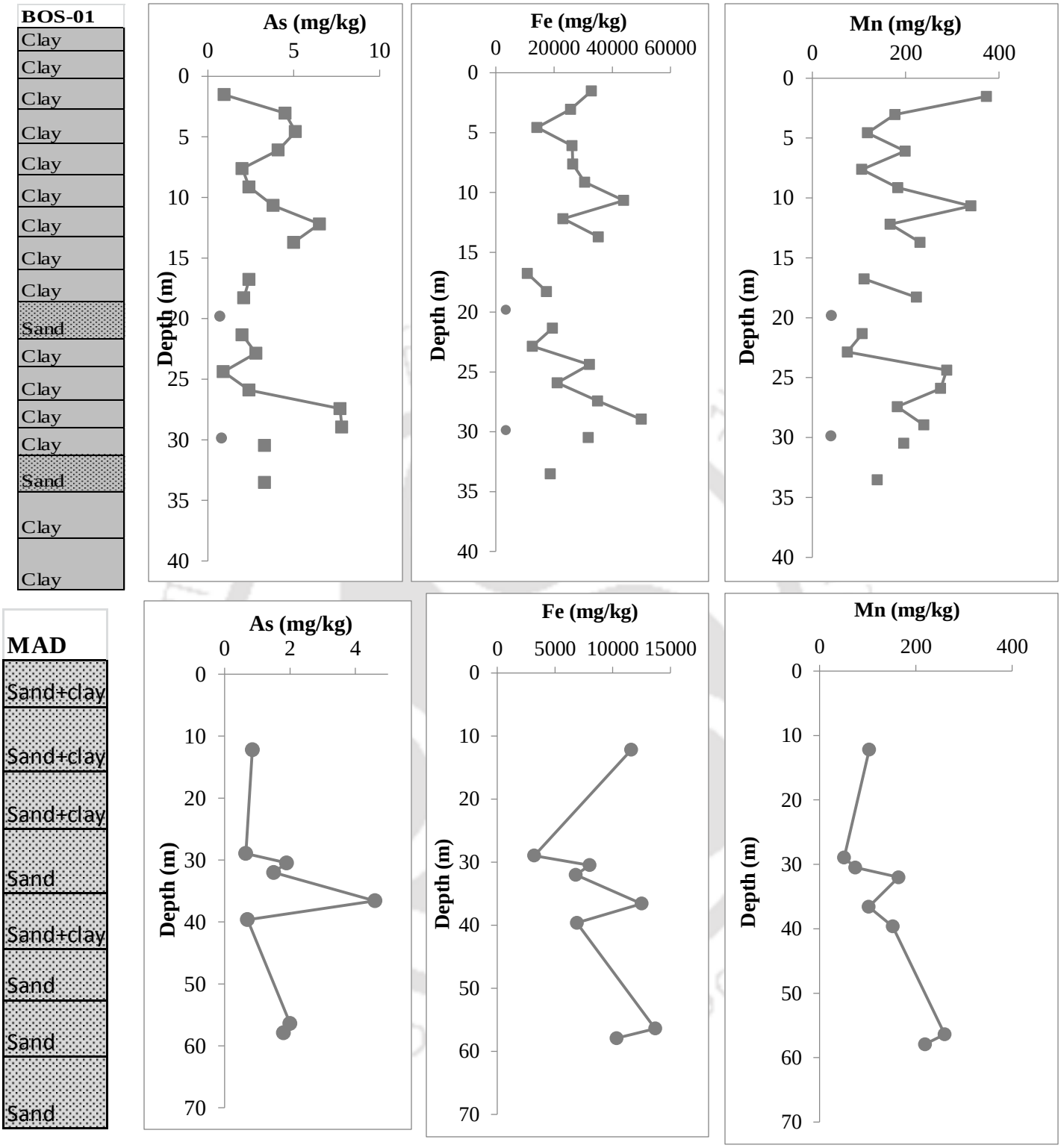

Figure A.3.1b Total As, Fe and Mn (mg/kg) concentration in sediment samples along depth profile of boreholes along southern transect

A.3.2 XRF measurements of Ca in mg/kg for sediment samples from borewells drilled along northern and southern transect

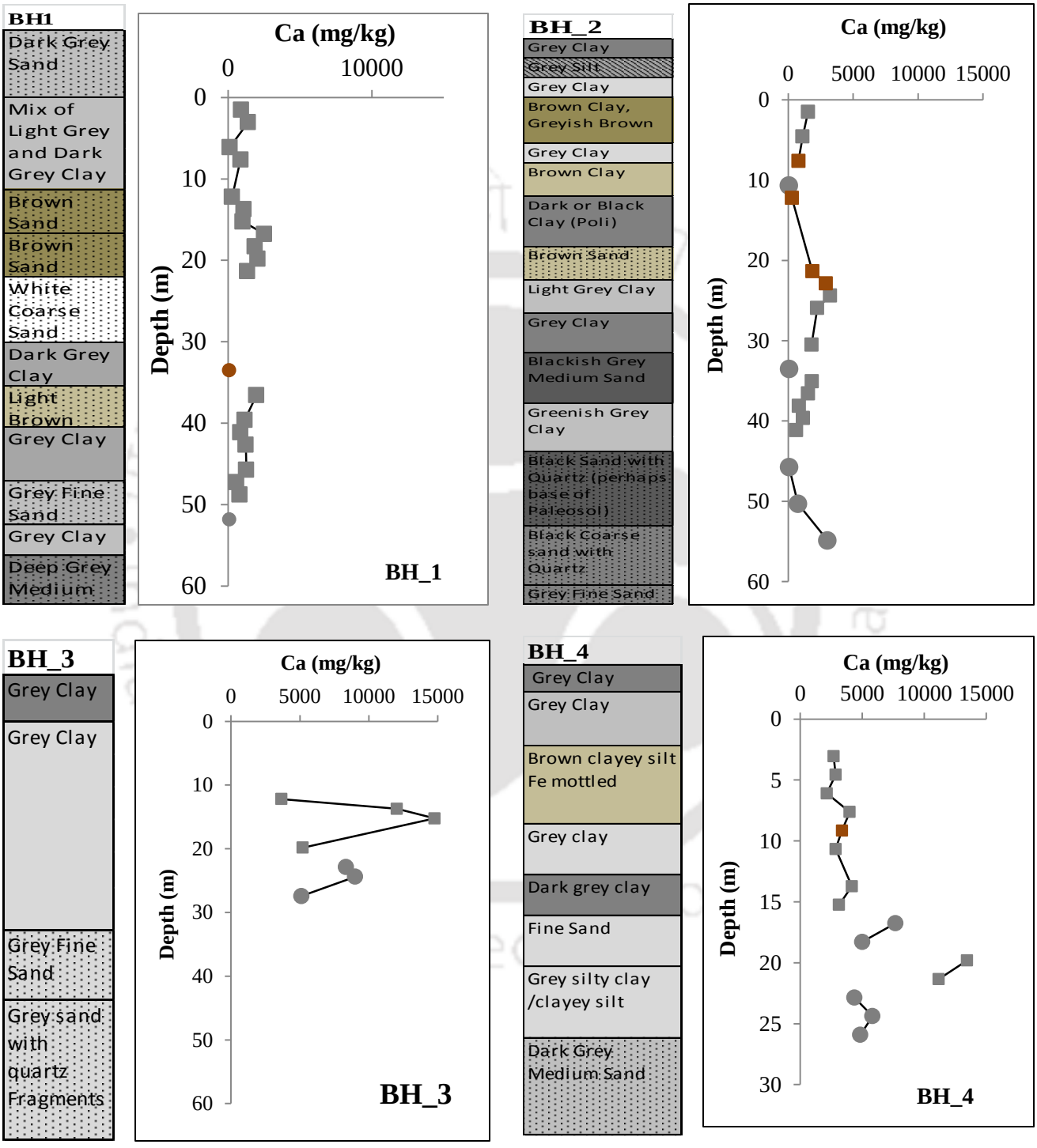

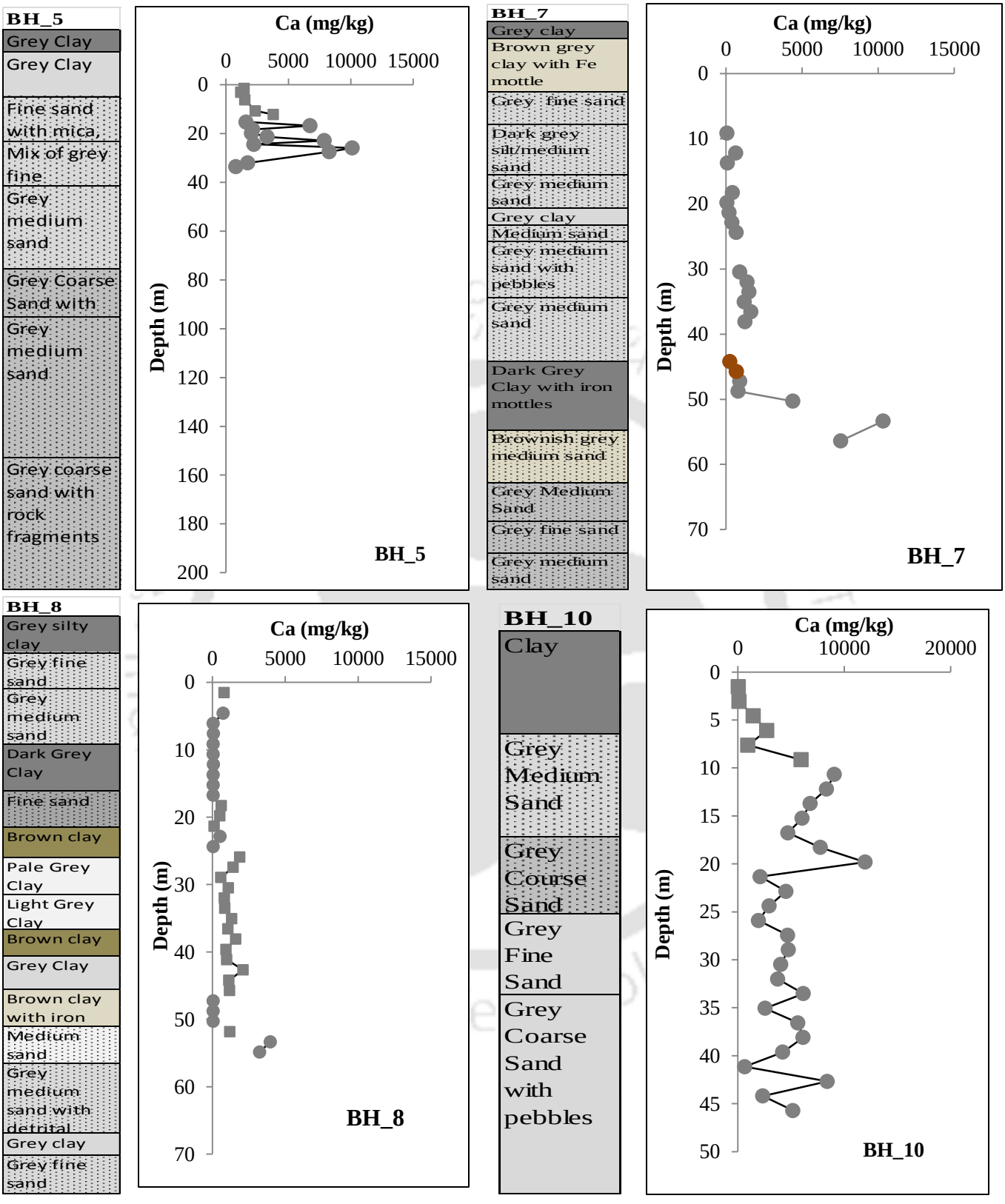

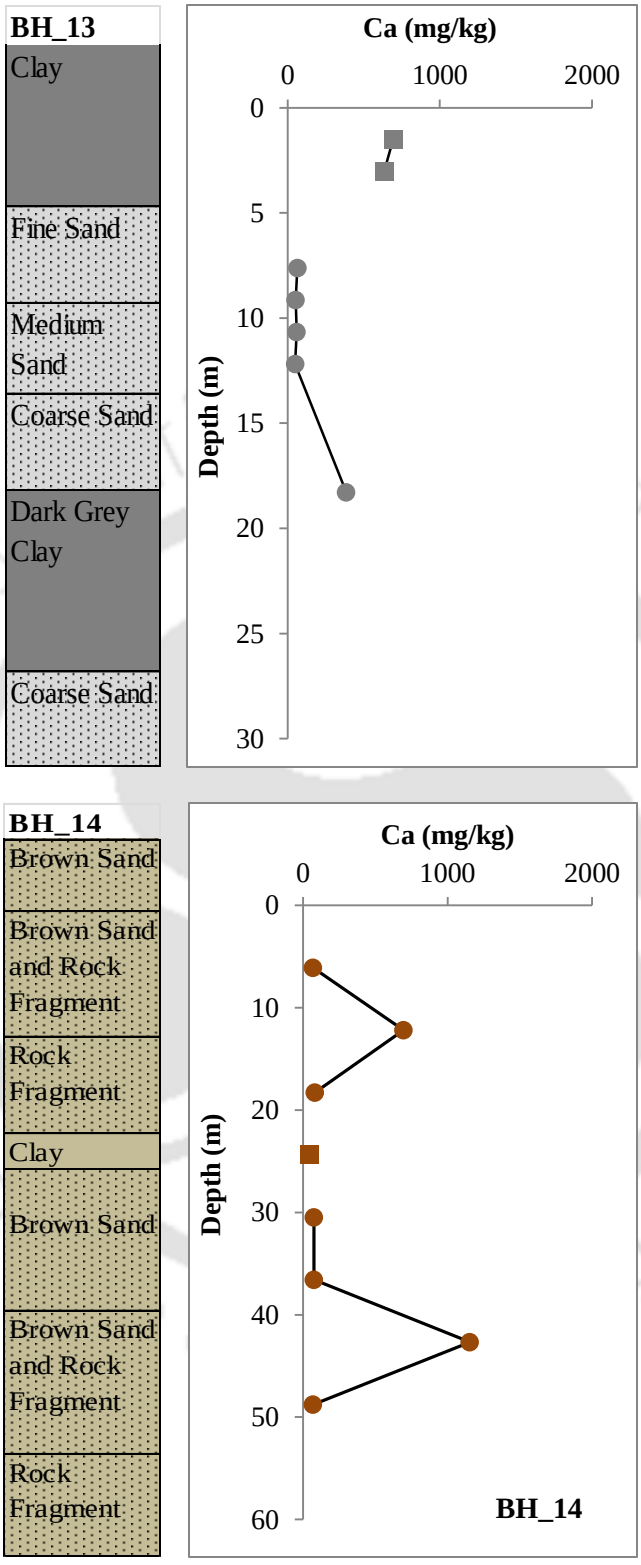

Figure A.3.2a Total Ca (mg/kg) concentration in sediment samples along depth profile of boreholes along northern transect

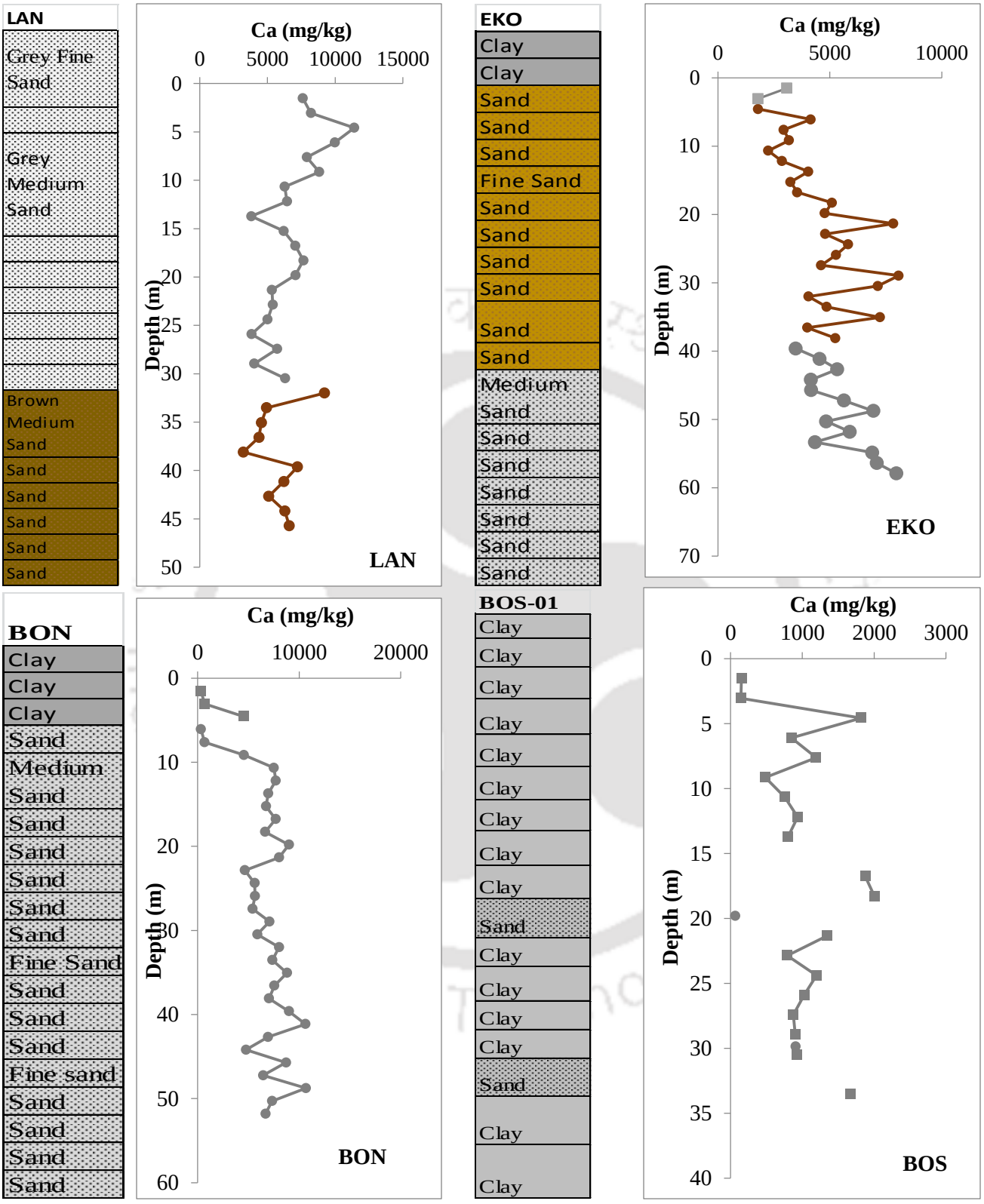

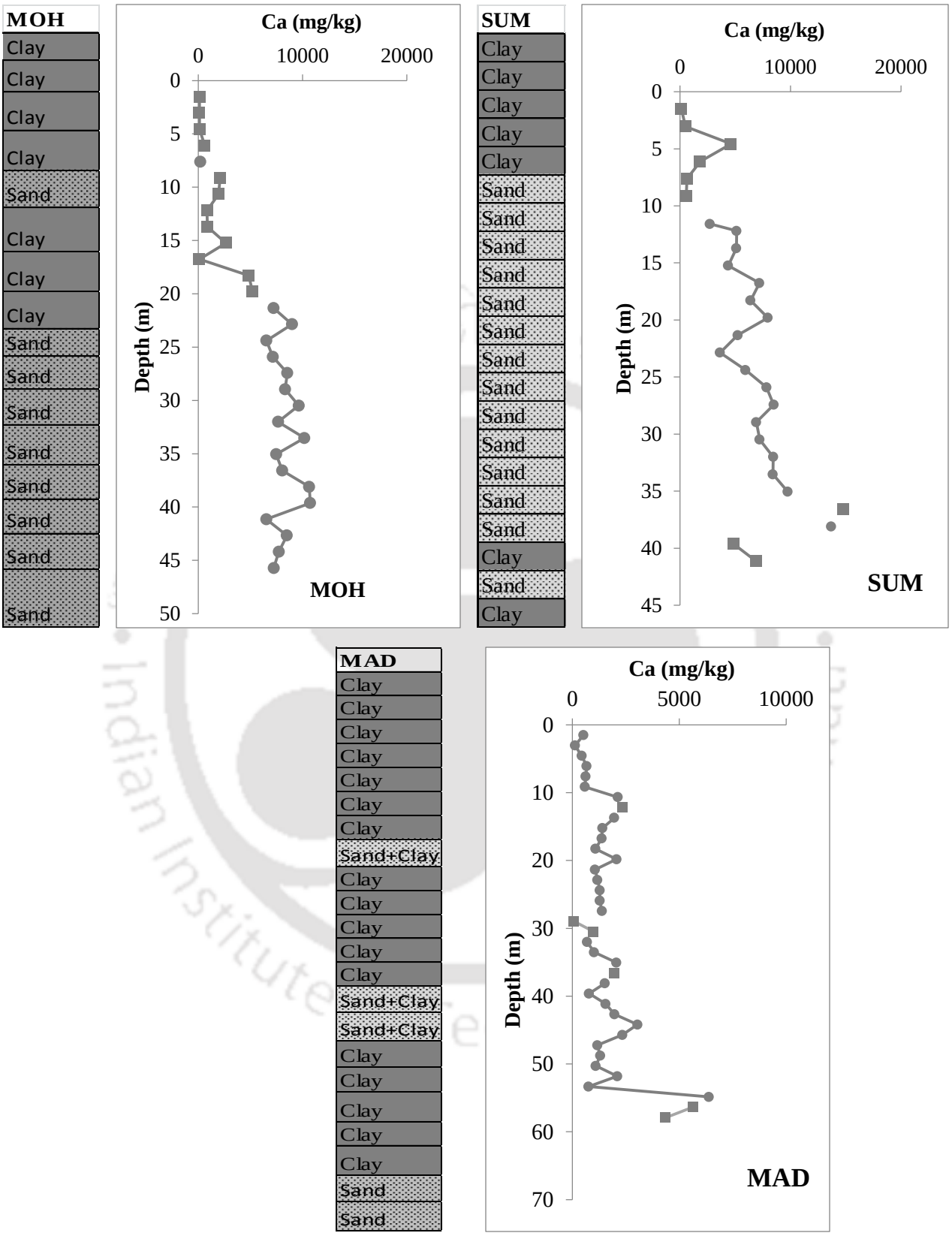

FigureA.3.2b Total Ca (mg/kg) concentration in sediment samples along depth profile of boreholes along southern transect

A.3.3 XRF measurements of Sr in mg/kg for sediment samples from borewells drilled along southern transect

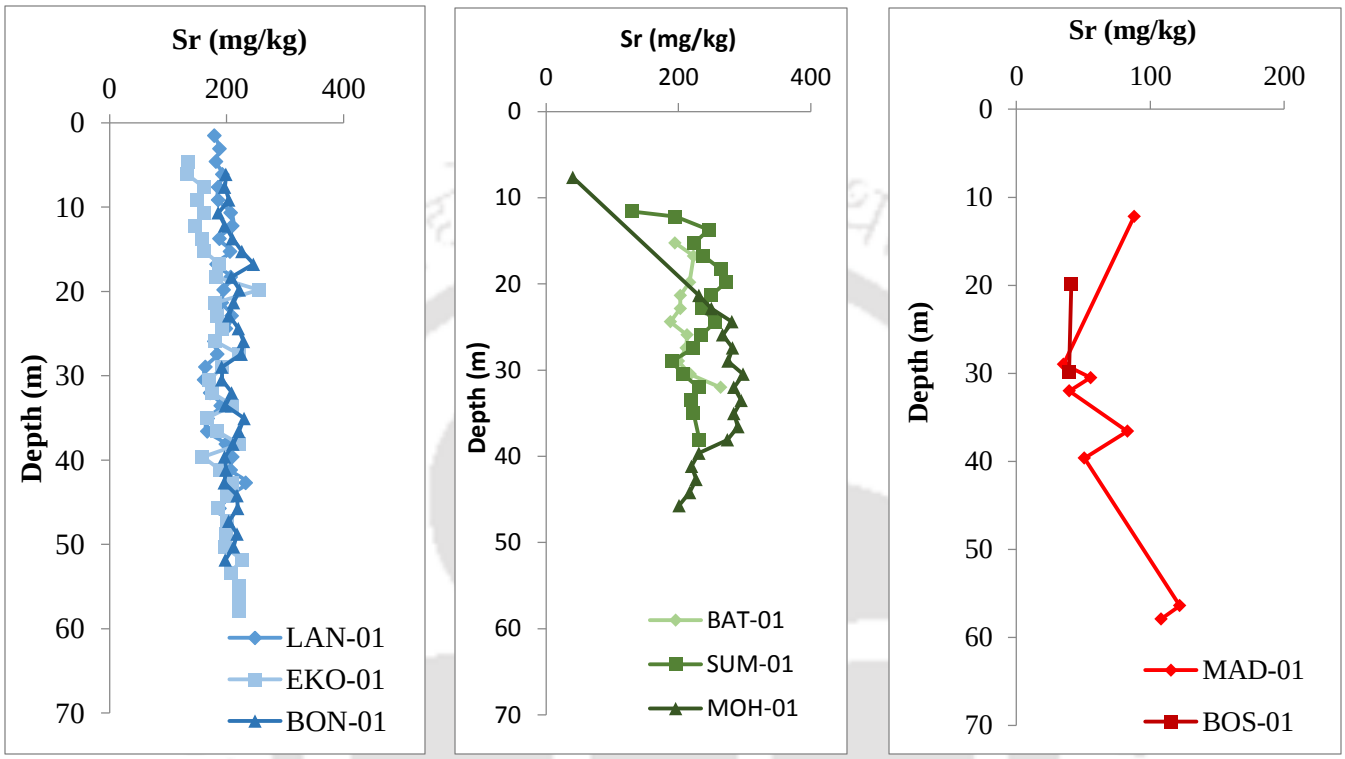

Figure A.3.3 Depth profile of bulk Sr (mg/kg) in boreholes along southern transect. The colour graphs indicate boreholes drilled in different zones viz. boreholes with blue graphs are located in Zones where groundwater As conc. <10µg/L, green indicates boreholes in zones where groundwater As concentration range between 10 to < 50 µg/L and red graphs are for boreholes in zones where As concentrations are > 50 µg/L

Appendix A4

A.4.1 Results of Selective Sequential Extraction (SSE) (As) in mg/kg for sediment samples from northern transect

Borewell Name	Depth (m)	F1	F2	F3	F4	F5	Total
BH_12	Bh12- 8	0.1	0.6	0.7	1.9	7.3	10.6
	Bh12- 14	0.3	0.9	0.9	1.8	3.9	7.8
	Bh12- 20	0.5	2.0	0.9	1.6	4.7	9.6
	Bh12- 27	0.4	1.9	0.9	1.8	8.9	13.9
	Bh12-30	0.3	0.9	0.9	1.9	4.5	8.5
BH_11	Bh11-2	0.0	0.0	0.6	0.7	0.6	1.9
	Bh11-15	0.0	0.0	0.9	0.7	0.6	2.3
BH_13	Bh13-15	0.0	0.1	1.4	1.3	0.8	3.6
	Bh13-25	0.0	0.1	0.8	1.1	2.3	4.3
	Bh13-35	0.0	0.0	0.6	0.9	2.3	3.8
	Bh13-45	0.0	0.0	1.3	1.6	1.5	4.5
	Bh13- 50	0.0	0.0	1.9	1.3	1.0	4.3
	Bh13- 60	0.0	0.1	1.0	1.3	0.9	3.2
BH_14	Bh14_ 51	0.1	0.2	0.7	0.4	0.7	2.1
	Bh14_ 54	0.1	0.6	1.0	0.3	0.9	2.9
	Bh14_57	0.3	1.0	0.8	0.3	1.5	3.9
	Bh14_60	0.1	0.4	0.6	0.4	1.0	2.6
	Bh14_64	0.1	0.5	0.1	0.4	1.0	2.1
	Bh14_67	0.0	0.4	1.6	0.3	1.7	3.9

A.4.2 Results of Selective Sequential Extraction (SSE) (As) in mg/kg for sediment samples from southern transect

Depth (m)	F1	F2	F3	F4	F5	Total
MAD_32	0.10	0.60	0.89	0.72	1.75	4.07
MAD_39	0.04	0.28	0.68	1.08	1.19	3.27
MAD_57	0.08	0.72	1.38	1.16	1.24	4.59

Depth (m)	F1	F2	F3	F4	F5	Total
EKO_7	0.12	0.61	0.70	1.28	1.46	4.17
EKO_24	0.13	0.92	1.04	1.06	1.10	4.23
EKO_36	0.12	0.68	1.19	1.05	1.11	4.15
EKO_47	0.11	0.41	0.65	0.80	1.06	3.03

Depth (m)	F1	F2	F3	F4	F5	Total
LAN_8	0.03	0.19	0.29	0.33	0.55	1.39
LAN_12	0.01	0.33	0.43	0.61	0.85	2.24
LAN_17	0.01	0.29	0.45	0.80	0.86	2.41
LAN_18	0.01	0.38	0.53	0.67	0.76	2.34
LAN_26	0.00	0.39	0.58	0.63	0.80	2.40
LAN_27	0.01	0.40	0.57	0.71	0.74	2.43
LAN_37	0.07	0.30	1.01	0.64	0.61	2.64
LAN_40	0.08	0.32	0.95	0.72	0.75	2.83
LAN_46	0.08	0.28	0.82	0.69	0.61	2.48

Appendix A5

A.5.1 Radiocarbon dating of sediment samples from southern transect, upper Brahmaputra Basin

Receipt NOSAMS#	Date Reported	Submitter Identification	Type	Process	Accession #	F Modern	Fm Err	d13C Corr	Age	Age Err	d13C	d13C Source
136163	01-05-16	7, EKO-01 10ft	Sediment Organic carbon	(OC) Organic Carbon	OS-125433	0.9832	0.0022	*	135	20	-23.59	Measured
136164	25-04-16	8, EKO-01 150ft	Sediment Organic carbon	(OC) Organic Carbon	OS-125315	0.0242	0.0015	*	29,900	510	-19.16	Measured
136168	25-04-16	12, SUM-01 30ft	Sediment Organic carbon	(OC) Organic Carbon	OS-125317	0.1061	0.0015	*	18,050	110	-23.12	Measured
136169	03-05-16	13, SUM-01 135ft	Sediment Organic carbon	(OC) Organic Carbon	OS-125435	0.0174	0.001	*	32600	470	-22.5	Measured
136167	05-05-16	11, MOH-01 65ft	Sediment Organic carbon	(OC) Organic Carbon	OS-125488	0.037	0.0011	*	26500	250	-21.52	Measured
136157	26-04-16	1, BAT-01 45ft	Sediment Organic carbon	(OC) Organic Carbon	OS-125344	0.0032	0.0006	*	46200	1600	-25.14	Measured
136158	27-04-16	2, BAT-01 110ft	Sediment Organic carbon	(OC) Organic Carbon	OS-125345	0.0063	0.0006	*	40700	780	-26.6	Measured
136160	04-05-16	4, BON-01 15ft	Sediment Organic carbon	(OC) Organic Carbon	OS-125487	0.0355	0.0011	*	26800	250	-22.96	Measured
136159	28-04-16	3, BHO-01 70ft	Sediment Organic carbon	(OC) Organic Carbon	OS-125346	0.0122	0.0006	*	35400	430	-16.38	Measured
136161	29-04-16	5, BOS-01 60ft	Sediment Organic carbon	(OC) Organic Carbon	OS-125347	0.0064	0.0006	*	40600	800	-14.85	Measured
136162	30-04-16	6, BOS-01 100ft	Sediment Organic carbon	(OC) Organic Carbon	OS-125432	0.0275	0.001	*	28900	300	-20.93	Measured
136165	25-04-16	9, MAD-01 90ft	Sediment Organic carbon	(OC) Organic Carbon	OS-125316	0.0109	0.0015	*	36,300	1,100	-26.17	Measured
136166	02-05-16	10, MAD-01 135ft	Sediment Organic carbon	(OC) Organic Carbon	OS-125434	0.0647	0.0012	*	22000	140	-17.03	Measured

* The asterisks indicate that the radiocarbon result was corrected for isotopic fractionation using unreported d13C values measured on the accelerator.
[c] NOSAMS# is the tracking number at the National Ocean Science Accelarator Mass-Spectrometer facility

Appendix A6

A.6.1 Radiocarbon dating of groundwater samples from southern transect, upper Brahmaputra Basin

Submitter Identification	Process	Accession #	F Modern	Fm Err	d13C Corr	Age	Age Err	d13C	d13C Source	DIC Conc (mmol/kg)
Dergaon, 20160205	(WS) Water Strip	OS-125507	0.5580	0.0013	*	4,690	20	-15.5	Measured	5
BAT Gologhat, 20160205	(WS) Water Strip	OS-125508	0.9724	0.0022	*	225	20	-10.15	Measured	4.13
Mad2, 20160206	(WS) Water Strip	OS-125509	0.1083	0.0006	*	17,850	40	-2.9	Measured	4.33

Appendix A7

A.7.1 Reflectance measurements of sand samples from bore wells along the southern transect

Borehole Name	Lithology	Depth (m)	Reflectance
BON_01	sand	15.2	-0.07
BON_01	sand	41.1	-0.01
BON_01	sand	45.7	0.00
BON_01	sand	47.2	0.00
BON_01	sand	48.8	0.00
BON_01	sand	50.3	0.00
BON_01	sand	51.8	0.00
BON_01	sand	38.1	0.00
BON_01	sand	30.5	0.02
BON_01	sand	35.1	0.02
BON_01	sand	42.7	0.02
BON_01	sand	24.4	0.02
BON_01	sand	39.6	0.02
BON_01	sand	36.6	0.02
BON_01	sand	33.5	0.04
BON_01	sand	21.3	0.04
BON_01	sand	25.9	0.05
BON_01	sand	10.7	0.05
BON_01	sand	44.2	0.05
BON_01	sand	18.3	0.06
BON_01	sand	29.0	0.07
BON_01	sand	22.9	0.07
BON_01	sand	27.4	0.07
BON_01	sand	32.0	0.08
EKO-01	sand	53.3	0.08
BON_01	sand	19.8	0.08
BON_01	sand	13.7	0.08
BON_01	sand	9.1	0.09
BON_01	sand	16.8	0.12
LAN-01	sand	9.1	0.13
LAN-01	sand	10.7	0.13
LAN-02	sand	27.4	0.14
LAN-01	sand	21.3	0.15
LAN-01	sand	19.8	0.16
LAN-01	sand	15.2	0.17
BON_01	sand	7.6	0.18

LAN-01	sand	12.2	0.18
LAN-01	sand	18.3	0.18
LAN-02	sand	25.9	0.18
LAN-01	sand	16.8	0.19
LAN-02	sand	24.4	0.2
EKO-01	sand	54.9	0.21
LAN-01	sand	4.6	0.23
LAN-01	sand	7.6	0.23
EKO-01	sand	57.9	0.23
LAN-01	sand	3.0	0.24
LAN-01	sand	6.1	0.24
LAN-01	sand	22.9	0.24
LAN-02	sand	39.6	0.24
EKO-01	sand	47.2	0.24
BON_01	sand	12.2	0.26
LAN-01	sand	13.7	0.26
LAN-01	sand	1.5	0.27
EKO-01	sand	56.4	0.31
EKO-01	sand	51.8	0.33
EKO-01	sand	48.8	0.34
LAN-02	sand	29.0	0.37
EKO-01	sand+clay	45.7	0.37
EKO-01	sand	50.3	0.42
LAN-02	sand	38.1	0.48
LAN-02	sand	44.2	0.49
EKO-01	sand	44.2	0.5
EKO-01	sand	4.6	0.52
LAN-02	sand	45.7	0.54
EKO-01	sand	36.6	0.54
LAN-02	sand	42.7	0.56
BON_01	sand	6.1	0.57
EKO-01	sand	42.7	0.57
EKO-01	sand+clay	18.3	0.58
EKO-01	sand	22.9	0.58
EKO-01	sand	19.8	0.6
EKO-01	sand	41.1	0.6
LAN-02	sand	36.6	0.61
LAN-02	sand	41.1	0.62
EKO-01	sand	16.8	0.62
EKO-01	sand	30.5	0.63
LAN-02	sand	32.0	0.64
EKO-01	sand	25.9	0.65
EKO-01	sand	24.4	0.66

EKO-01	sand	38.1	0.66
EKO-01	sand	21.3	0.68
EKO-01	sand	9.1	0.69
EKO-01	sand	15.2	0.7
EKO-01	sand	27.4	0.7
EKO-01	sand	35.1	0.7
EKO-01	sand	7.6	0.71
EKO-01	sand	29.0	0.72
LAN-02	sand	30.5	0.73
LAN-02	sand	33.5	0.73
EKO-01	sand	32.0	0.74
EKO-01	sand	12.2	0.76
EKO-01	sand	13.7	0.76
EKO-01	sand	6.1	0.77
EKO-01	sand	10.7	0.77
LAN-02	sand	35.1	0.81
EKO-01	sand	33.5	0.88
EKO-01	sand	39.6	0.89
BAT-01	sand	19.8	0.02
BAT-01	sand	27.4	0.02
SUM-01	sand	24.4	0.02
SUM-01	sand	29.0	0.03
BAT-01	sand	22.9	0.04
SUM-01	sand	11.6	0.04
SUM-01	sand	16.8	0.04
SUM-01	sand	19.8	0.04
SUM-01	sand	30.5	0.04
SUM-01	sand	33.5	0.04
BAT-01	sand	25.9	0.05
BAT-01	sand	30.5	0.05
SUM-01	sand	15.2	0.05
SUM-01	sand	21.3	0.05
SUM-01	sand	25.9	0.05
SUM-01	sand	27.4	0.05
SUM-01	sand	35.1	0.05
SUM-01	sand	38.1	0.05
MOH_01	sand	21.3	0.05
MOH_01	sand	25.9	0.06
BAT-01	sand	24.4	0.06
SUM-01	sand	32.0	0.06
BAT-01	sand	15.2	0.07
BAT-01	sand	29.0	0.08
BAT-01	sand	32.0	0.08

SUM-01	sand	18.3	0.08
SUM-01	sand	22.9	0.08
MOH_01	sand	27.4	0.08
MOH_01	sand	35.1	0.08
MOH_01	sand	33.5	0.09
BAT-01	sand	16.8	0.09
BAT-01	sand	21.3	0.09
MOH_01	sand	22.9	0.09
MOH_01	sand	30.5	0.09
MOH_01	sand	32.0	0.10
MOH_01	sand	39.6	0.12
MOH_01	sand	38.1	0.12
SUM-01	sand+clay	12.2	0.12
MOH_01	sand	24.4	0.12
MOH_01	sand	36.6	0.13
MOH_01	sand	41.1	0.14
MOH_01	sand	29.0	0.14
MOH_01	sand	45.7	0.14
MOH_01	sand	44.2	0.23
MOH_01	sand	42.7	0.28
SUM-01	sand	13.7	0.32
BOS_01	sand	19.8	0.06
MAD-01	sand+clay	12.2	0.02
MAD-01	sand	32.0	0.1
MAD-01	sand+clay	30.5	0.14
MAD-01	sand+clay	36.6	0.18
MAD-01	sand	56.4	0.21
MAD-01	sand	57.9	0.23
MAD-01	sand+clay	29.0	0.29
MAD-01	sand	39.6	0.3

List of Publications in Peer Reviewed Journals

1. **Choudhury, R.,** Mahanta, C., Verma, S., Mukherjee, A. (2017). Arsenic distribution along different hydrogeomorphic zones in parts of the Brahmaputra River Valley. **Hydrogeology Journal,** 25(4), pp. 1153-1163

2. **Choudhury**; R., Sharma, P., Mahanta, C., Sharmah, H.P. (2015). Evaluation of processes controlling arsenic contamination in parts of the Brahmaputra Floodplains in Assam, India, **Environmental Earth Science**s, 73(8), pp. 4473-4482

3. Baviskar, S., **Choudhury**, R., Mahanta, C. (2015). Dissolved and solid phase arsenic fate in an arsenic enriched aquifer in the River Brahmaputra alluvial plain, **Environmental Monitoring and Assessment,** pp. 187: 93

4. Mahanta, C., Enmark, G., · Nordborg, D., · Sracek, O, Nath, B., · Nickson, R.T., Herbert, R., Jacks, G., Mukherjee, A., Ramanathan, A.L., **Choudhury, R.,** Bhattacharya, P. (2014). Hydrogeochemical controls on mobilization of arsenic in groundwater of a part of Brahmaputra river floodplain, India. **Journal of Hydrology: Regional Studies**, pp.154-171.

5. Mahanta, C., **Choudhury, R**., Basu, S., Hemani, R., Dutta, A. (2015). Preliminary Assessment of Arsenic Distribution in Brahmaputra River Basin of India Based on Examination of 56,180 Public Groundwater Wells in AL Ramanathan, Scott Johnston, Abhijit Mukherjee, Bibhash Nath (Eds.) **Safe and Sustainable Use of Arsenic-Contaminated Aquifers in the Gangetic Plain.**

6. Verma, S., Mukherjee, A., Mahanta, C., **Choudhury, R.,** Mitra, K., (2016). Influence of geology on groundwater-sediment interactions in varied arsenic enriched tectono-morphic aquifers of the Brahmaputra River Basin , **Journal of Hydrology** ,pp.176-195

Manuscript Submitted

1. **Choudhury**, R., Mahanta, C., Nath, B., Khan, M.R., Ellis, T., Geen, A.van (2017). The impact of aquifer flushing on groundwater arsenic across a 35-km transect perpendicular to the upper Brahmaputra River in Assam, India. Submitted in **Water Resources Research.**